High Power Orbit Transfer Vehicle

Frank S. Gulczinski III
Air Force Research Laboratory (AFMC)
AFRL/PRSS
1 Ara Drive
Edwards AFB CA 93524-7013

Christopher D. Hall
Virginia Polytechnic Institute and State University
233 Burruss Hall
Blacksburg, VA 24061

Lyon B. King
Gordon G. Parker
Martin D. Tervo
Aerophysics, Inc.
30981 Woodbush Road
Calumet, MI 49913

July 2003

Final Report

APPROVED FOR PUBLIC RELEASE; DISTRIBUTION UNLIMITED.

AIR FORCE RESEARCH LABORATORY
AIR FORCE MATERIEL COMMAND
EDWARDS AIR FORCE BASE CA 93524-7048

REPORT DOCUMENTATION PAGE

Form Approved
OMB No. 0704-0188

Public reporting burden for this collection of information is estimated to average 1 hour per response, including the time for reviewing instructions, searching existing data sources, gathering and maintaining the data needed, and completing and reviewing this collection of information. Send comments regarding this burden estimate or any other aspect of this collection of information, including suggestions for reducing this burden to Department of Defense, Washington Headquarters Services, Directorate for Information Operations and Reports (0704-0188), 1215 Jefferson Davis Highway, Suite 1204, Arlington, VA 22202-4302. Respondents should be aware that notwithstanding any other provision of law, no person shall be subject to any penalty for failing to comply with a collection of information if it does not display a currently valid OMB control number. **PLEASE DO NOT RETURN YOUR FORM TO THE ABOVE ADDRESS.**

1. REPORT DATE *(DD-MM-YYYY)*	2. REPORT TYPE	3. DATES COVERED *(From - To)*
14-01-2003	Final Report	01 Oct 2000 – 19 June 2002

4. TITLE AND SUBTITLE

High Power Orbit Transfer Vehicle

5a. CONTRACT NUMBER

5b. GRANT NUMBER

5c. PROGRAM ELEMENT NUMBER
63216F

6. AUTHOR(S)
Frank S. Gulczinski III;
Christopher D. Hall[1]; Lyon B. King[2], Gordon G. Parker[2];
Martin D. Tervo[2]

5d. PROJECT NUMBER
6340

5e. TASK NUMBER
0039

5f. WORK UNIT NUMBER
549928

7. PERFORMING ORGANIZATION NAME(S) AND ADDRESS(ES)

[1]Virginia Polytechnic Institute & State University
233 Burruss Hall
Blacksburg, VA 24061

[2]Aerophysics, Inc.
30981 Woodbush Road
Calumet, MI 49913

8. PERFORMING ORGANIZATION REPORT NO.

AFRL-PR-ED-TR-2002-0032

9. SPONSORING / MONITORING AGENCY NAME(S) AND ADDRESS(ES)

Air Force Research Laboratory (AFMC)
AFRL/PRSS
1 Ara Drive
Edwards AFB CA 93524-7013

10. SPONSOR/MONITOR'S ACRONYM(S)

11. SPONSOR/MONITOR'S REPORT NUMBER(S)
AFRL-PR-ED-TR-2002-0032

12. DISTRIBUTION / AVAILABILITY STATEMENT
Approved for public release; distribution unlimited; July 2003. Refer other requests for this document to AFRL/PRSS, 1 Ara Drive, Edwards AFB CA 93524-7013.

13. SUPPLEMENTARY NOTES

14. ABSTRACT

The AFRL Propulsion Directorate's Spacecraft Propulsion Branch has carried out an in-house propulsion trade study and contracted for two other propulsion design studies, from Virginia Tech University and Aerophysics, Inc., to examine propulsion requirements for a high power orbit transfer vehicle using thin-film voltaic solar array technologies under development by the Space Vehicles Directorate, dubbed PowerSail. The in-house study assumed a 100 kkW array and performed the most in-depth analysis of the forces perturbing the array and of propulsion options to counteract these forces. This study recommended a combination of the Busek BHT-200 Hall thruster and the AFRL μPPT for a near-term mission. The Virginia Tech University design study looked at a 50 k@ array and provided a more comprehensive look at the entire spacecraft system. They chose to employ pulsed plasma thrusters to meet their propulsion needs, thus minimizing complexity and integration issues rather than system mass. Aerophysics, Inc. developed a dynamic optimization code to analyze alternatives for propulsion on a 500 kW array. Based on this code, the optimal propulsion system was determined to be a set of notional low power ion engines.

15. SUBJECT TERMS
orbit transfer vehicle; electric propulsion; thin-film photovoltaic solar array; PowerSail; trade study

16. SECURITY CLASSIFICATION OF:			17. LIMITATION OF ABSTRACT	18. NUMBER OF PAGES	19a. NAME OF RESPONSIBLE PERSON
					Frank S. Gulczinski III
a. REPORT	b. ABSTRACT	c. THIS PAGE	A	215	19b. TELEPHONE NO *(include area code)*
Unclassified	**Unclassified**	**Unclassified**			(661) 275-6796

Standard Form 298 (Rev. 8-98)
Prescribed by ANSI Std. 239.18

NOTICE

When U.S. Government drawings, specifications, or other data are used for any purpose other than a definitely related Government procurement operation, the fact that the Government may have formulated, furnished, or in any way supplied the said drawings, specifications, or other data, is not to be regarded by implication or otherwise, or in any way licensing the holder or any other person or corporation, or conveying any rights or permission to manufacture, use or sell any patented invention that may be related thereto.

FOREWORD

This final technical report, entitled "High Power Orbit Transfer Vehicle," presents the results of an in-house study performed under JON 63400039 by AFRL/PRSS, Edwards AFB CA. The Project Manager for the Air Force Research Laboratory was Frank S. Gulczinski III.

This report has been reviewed and is approved for release and distribution in accordance with the distribution statement on the cover and on the SF Form 298.

FRANK S. GULCZINSKI III
Project Manager

RONALD A. SPORES
Chief
Spacecraft Branch

PHILIP A. KESSEL
Technical Advisor
Space & Missile Propulsion Division

RANNEY G. ADAMS III AFRL/CCPAS 03-12;
Director
Public Affairs

This Page Intentionally Left Blank

Table of Contents

List of Figures

List of Tables

Preface

This document serves as the final report for the Air Force Research Laboratory Propulsion Directorate Spacecraft Propulsion Branch (AFRL/PRSS) High Power Orbit Transfer Vehicle (OTV) Demonstration program – JON 63400039. This program was initiated 1 October 2000.

1. Introduction

This document serves as the final report for the Air Force Research Laboratory Propulsion Directorate Spacecraft Propulsion Branch (AFRL/PRSS) High Power Orbit Transfer Vehicle (OTV) Demonstration program – JON 63400039. This program was initiated 1 October 2000. The goal and primary focus of this program was to develop an advanced propulsion package for the PowerSail flight program.[1] PowerSail is an Air Force Research Laboratory Space Vehicles Directorate (AFRL/VS) program intended to develop and demonstrate high power (100 kW to 1 MW) capability in space using a deployable, flexible solar array constructed of thin-film photovoltaics. Use of thin-film photovoltaics in place of conventional solar arrays is projected to decrease mass and cost, while increasing packability. The original AFRL/VS plan was for a two-phased program: the first phase was to be a proof-of-concept demonstration at 50 kW launching in 2006, followed by an operational system at full power. However, slips in schedule and changes in scope have altered the VS program substantially. It is now geared toward a 2008 demonstration, either ground or space, intended primarily to show the deployment and operation of the thin-film photovoltaic solar array at a power level of ~20 kW with no orbit transfer. Thus, the need for the development of a high power propulsion system for PowerSail has dissipated. Therefore, it was decided that this was the proper time to close this advanced technology development (6.3) JON. Should the PowerSail program reorient itself toward the need for high power propulsion, a new 6.3 JON will be opened.

The intent of this program was to develop propulsion to support two facets of the PowerSail mission: orbit transfer and attitude control. The orbit transfer propulsion was envisioned as operating in the 20 – 50 kW range with a mission to transfer the PowerSail spacecraft between orbital locations. Due to their specific impulse and specific power parameters, high power Hall-effect thrusters were baselined for this mission. Attitude control propulsion in the 100 – 500 W power range was needed to maintain the proper orientation of the large, flexible solar array under the influence of external forces such as solar radiation pressure, atmospheric drag, and gravity gradient torque.

Three major tasks were carried out under this project. The first was an in-house trade study to assess the propulsion requirements for PowerSail. This study is summarized in Section 2. The in-house study was followed by a pair of in-depth design studies to further explore the propulsion design space. The first, performed by students at Virginia Tech University, performed a detailed design of the entire PowerSail spacecraft. This study is summarized in Section 3 and is presented in full in Section 5. The second, performed by Aerophysics, Inc., developed a dynamic optimization code to analyze the propulsion options for the maneuvering of the PowerSail system. This study is summarized in Section 4 and presented in full in Section 6.

Based on these studies, the results of this program can be summarized as follows:

- The primary challenge for the PowerSail attitude control propulsion system does not lie in the development of a new propulsion system – there are several technologies at high levels of readiness that meet the PowerSail attitude control

performance requirements with a reasonable propulsion system dry mass. The challenge arises from the fact that this very large solar array will need to be folded for launch and deployed on orbit. Attitude control propulsion will be required on the edges of the array to counter torques that the array will encounter. Thus, any and all leads (power, propellant, and control) running to the thrusters from the central array control bus must be designed to fold with the array. The most difficult of these is propellant feed, leading most investigators to favor electric propulsion devices that utilize solid propellant, as this propellant is co-located with the thruster. Basic research (6.1) and engineering development (6.2) work is ongoing at AFRL/PRSS on several propulsion technologies that could be utilized to meet the attitude control needs of PowerSail,[2] and is performing a 6.3 flight demonstration of one – a 200 W Hall thruster – on the TechSat 21 mission.[3]

- Near-term high power Hall thruster systems in the 20 – 50 kW range would be best facilitated not by constructing monolithic thrusters, but instead by clustering thrusters of the 10 kW class.[2] This approach results in several advantages, including greater reliability, greater operational flexibility, and, most importantly, lower development and qualification cost. There are several 6.2 programs under way at AFRL to investigate and resolve any issues that may arise from the clustering of Hall thrusters and to develop the hardware necessary to implement clustering schemes. To meet higher power needs, NASA Glenn Research Center is currently building and testing a 50 kW Hall thruster.[4] Discussions are underway between NASA and AFRL regarding applying the knowledge gained in the AFRL clustering effort to the 50 kW thruster should the need to provide hundreds of kilowatts of on-board propulsion power become a reality.

AFRL/PRSS remains committed to the development and demonstration of technologies relevant to implementing an electric propulsion orbit transfer vehicle. Ending the 6.3 High Power OTV Demonstration program at this time merely reflects the realities of spacecraft flight demonstration opportunities. Our ongoing 6.1 and 6.2 programs continue to develop relevant technology for an electric propulsion OTV that will be ready for insertion when the next flight opportunity is presented.

1.1 References

[1] Meink, T., et al., "PowerSail – A High Power Solution", AIAA Paper 2000-5081, AIAA Space 2000, Long Beach, California, September 2000.

[2] Spores, R.A., Spanjers, G.G., Birkan, M., and Lawrence, T.J., "Overview of the USAF Electric Propulsion Program," AIAA Paper 2001-3225, 37th AIAA Joint Propulsion Conference, Salt Lake City, Utah, June 2001.

[3] Bromaghim, D.B., et al., "The AFRL TechSat 21 Propulsion System Development Program," IEPC Paper 01-165, 27th International Electric Propulsion Conference, Pasadena, California, October 2001.

[4] Dunning, J.W., Benson, S., Oleson, S., "NASA's Electric Propulsion Program," IEPC Paper 01-002, 27th International Electric Propulsion Conference, Pasadena, California, October 2001.

2 In-House Propulsion Study

2.1 Introduction

PowerSail is a proposed spacecraft whose mission is to generate large amounts (50+ kW) of electric power for delivery to a host spacecraft through a flexible umbilical. By offloading the power generation requirement to a separate spacecraft, many of the problems associated with large solar arrays, such as structural dynamics and deployment, can be minimized. PowerSail is envisioned to be a large thin-film solar array supported by four extendable booms, with a minimal bus to provide necessary support functions such as guidance, navigation, and control (GN&C); attitude determination and control (ACS); and propulsion.

PowerSail will require a dedicated propulsion and attitude control system to perform its mission. Even if the host spacecraft is not expected to maneuver, the large area-to-mass ratio of PowerSail will lead to differential orbital perturbations that will tend to drive the spacecraft into different orbits unless countered by propulsive force. Any maneuvers by the host spacecraft will also need to be matched by the PowerSail vehicle. Attitude control will be needed to maintain the PowerSail in a sun-pointing orientation.

2.2 PowerSail Parameters

The baseline design for the PowerSail spacecraft assumes a 100 kW delivered power requirement. This is satisfied with a 20m x 20m thin-film solar array with a central bus. The estimated total mass of the spacecraft is 210 kg, with 30 kg allocated to propulsion. A rough estimate of the mass distribution gives central moments of inertia $I_{xx} = I_{yy} = 6000$ kg-m^2 and $I_{zz} = 12000$ kg-m^2, with the +Z axis defined perpendicular to the array surface and toward the sun. The proposed structural geometry allows thrusters to be positioned on the central bus or at the corners of the vehicle. Due to the poor ballistic coefficient of the system, PowerSail is not envisioned for use at altitudes of less than 1000 km.

2.3 Propulsion Requirements

The dominant propulsion requirements on PowerSail, barring substantial maneuvers by the host spacecraft, will be to counter the effects of radiation pressure and atmospheric drag. PowerSail has a cross-sectional area of 400 m^2, a solar absorptivity of nearly 1.0, and will be oriented perpendicular to the sun at all times. This leads to a constant radiation pressure of 1.8 mN along the spacecraft –Z axis except during eclipse periods, and a total propulsive impulse of 57 kN-s per year.

Radiated IR and reflected sunlight from the Earth are also concerns in low orbits, though the intensity is lower and the geometry generally more favorable. Examining these effects over the range of expected orbital parameters gives maximum radiation pressures of 0.25 mN in the X and Y directions and 0.45 mN in the Z direction for a 1000 km orbit. Average values are 0.15 mN and 0.25 mN respectively, with a total impulse per year of 17 kN-s per year.

At 1000 km, atmospheric drag is negligible compared to solar radiation pressure except during periods of anomalously high solar activity. However, if ten-year mission lives are considered, the spacecraft must be designed to handle a worst-case solar max scenario. This is found to result in peak drag forces of 0.15 mN in the X and Y directions and 0.30 mN in the Z direction. Average values are less than 0.02 mN, and the expected propulsive impulse is only 1 kN-s per year.

In addition to translational thrust, the PowerSail propulsion system must be able to counter disturbance torques. The substantial moments of inertia of the PowerSail give rise to large gravity gradient torques, and the requirement that the solar array remain oriented towards the sun precludes allowing the spacecraft to come to rest in a gravity-stable orientation. Countering this torque requires a maximum of 8.8 mN-m of control authority with an average value of 4.4 mN-m and a total impulse requirement of 140 kN-m-s per year.

A small additional torque can arise if the host spacecraft casts a shadow onto the array, creating an imbalance in solar radiation pressure. Assuming a 20 m^2 spacecraft separated from the array by a 20 m umbilical results in a torque that requires a maximum of 2 mN-m of control authority to counter, with an average value of 0.15 mN-m and a total impulse requirement of 5 kN-m-s per year.

The combination of these propulsion demands leads to a requirement for up to 0.4 mN of thrust in the +X, -X, +Y, and –Y directions; 2.55 mN in the +Z direction; and an ACS torque authority about the X and Y axis of 8.8 mN-m. The required thrust impulse is 75 kN-s per year and the torque impulse 145 kN-m-s per year.

2.4 Propulsion System Options

The requirement to provide a constant propulsive force to offset radiation pressure will drive the propulsion system mass to excessive levels if conventional chemical rocket systems are used. The thirty kilograms of mass allotted to propulsion would not suffice for even one year of stationkeeping propellant with a conventional system. It will therefore be necessary to use advanced, electric propulsion systems for this application. Electric propulsion provides much higher specific impulse, and thus vastly reduced propellant consumption, compared to chemical thrusters. It can be handicapped by low peak thrust values and substantial power requirements, but those are not factors in this application, where thrust requirements are low and electric power is abundant.

Seven classes of electric propulsion system are considered in this application. Resistojets and arcjets electrically heat a propellant and thermally expand it to provide thrust. While the thrust mechanism is the same as that used in chemical rockets, the specific energy imparted to the propellant is no longer limited by the energy density available from chemical reactions. Ion and Hall-effect thrusters electrostatically accelerate heavy ions to extremely high velocities to produce thrust, by slightly different mechanisms. Both the Field Emission Electrostatic Propulsion (FEEP) and colloid thrusters use electrostatic acceleration of charged liquid droplets, thus avoiding ionization losses associated with

the Hall and ion thrusters. Finally, pulsed plasma thrusters (PPT) use a capacitive discharge to ablate, ionize, and electromagnetically accelerate an inert solid propellant. While inefficient, the simplicity of a solid-propellant system with no moving parts is attractive for low-mass spacecraft applications.

Examples of all of these systems (save the colloidal and FEEP systems) are commercially available today and have flown on operational missions, and a flight-qualified FEEP system has flown on a space shuttle mission as an experiment. Technical maturity should not be an issue for the use of any of these systems on a PowerSail demonstrator mission. Characteristics of suitable examples of each system are given in Table 2-1 below.

Table 2-1: Thruster Options

Thruster	Thrust	Isp	η
100 W Resistojet[1]	100 mN	150s	55%
Low Power Arcjet	100 mN	500s	35%
200 W Hall Thruster[2]	10 mN	1500s	45%
Small Ion Engine[3]	20 mN	2500s	50%
Pulsed Plasma Thruster[4]	1 mN	1000s	10%
AFRL micro-PPT[5]	50 μN	800s	5%
Colloid Thruster[6]	100 μN	1500s	50%
60 W FEEP[7]	1 mN	8000s	50%

In addition to the question of thruster type, thruster location also has to be considered. The spacecraft geometry lends itself to one primary thruster on the central bus providing +Z thrust, with four secondary thrusters on each corner boom for X/Y thrust and ±Z attitude control. The primary thruster would have to provide 2.55 mN of thrust and each secondary thruster 0.2 mN – with some of the thrusters described above, this would clearly require multiple thrusters per axis. This configuration is shown schematically in Figure 2-1.

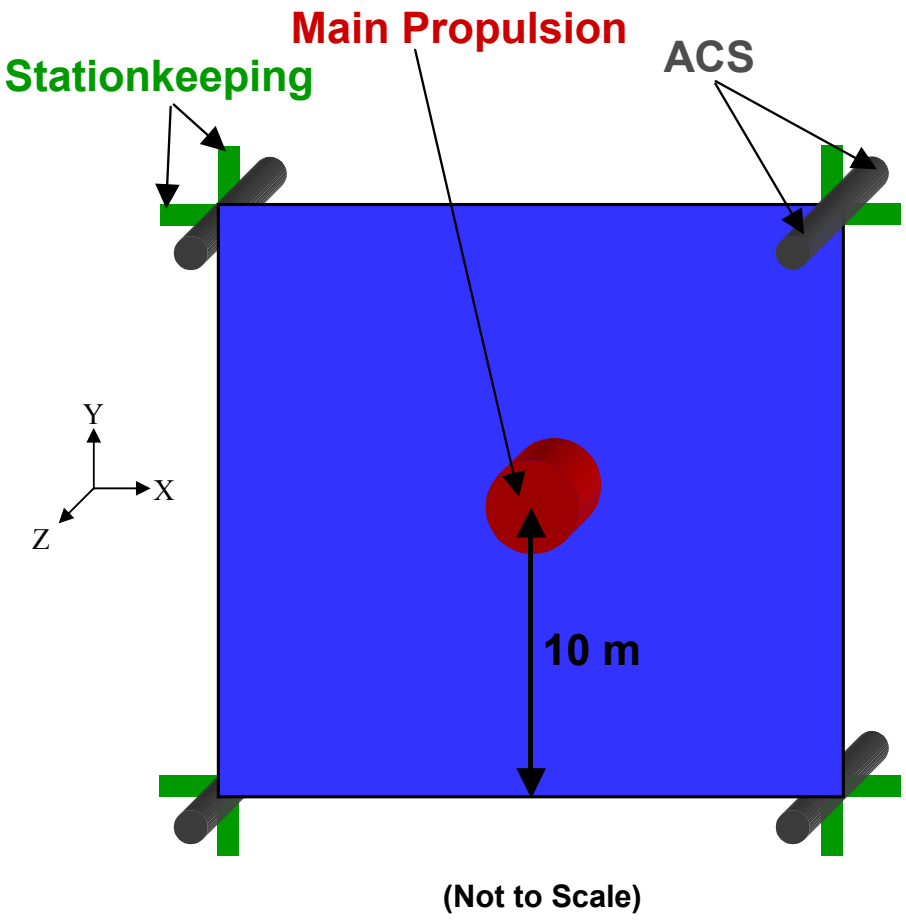

Figure 2-1: Thruster Configuration - Corner Mount

An alternate configuration would be to deploy a short boom, ten meters or less, from the central bus along the Z-axis. Again, a single primary thruster of 2.55 mN would be required, but only two clusters of four secondary thrusters would be needed. This would tend to reduce thruster mass and system complexity, and would eliminate the difficulty of mounting thruster systems at the corners of the deployable solar array. However, the reduction in moment arm for attitude control increases the thrust and propellant requirement for that mission. A 7 m boom (3.5 m moment arm) was selected – no study was conducted of the effects of the length of the boom on the propulsion masses. Additionally, this configuration has limited ability to counter a torque about the Z-axis, though analysis does not indicate that such a torque will be generated under normal operation. This configuration is shown in Figure 2-2.

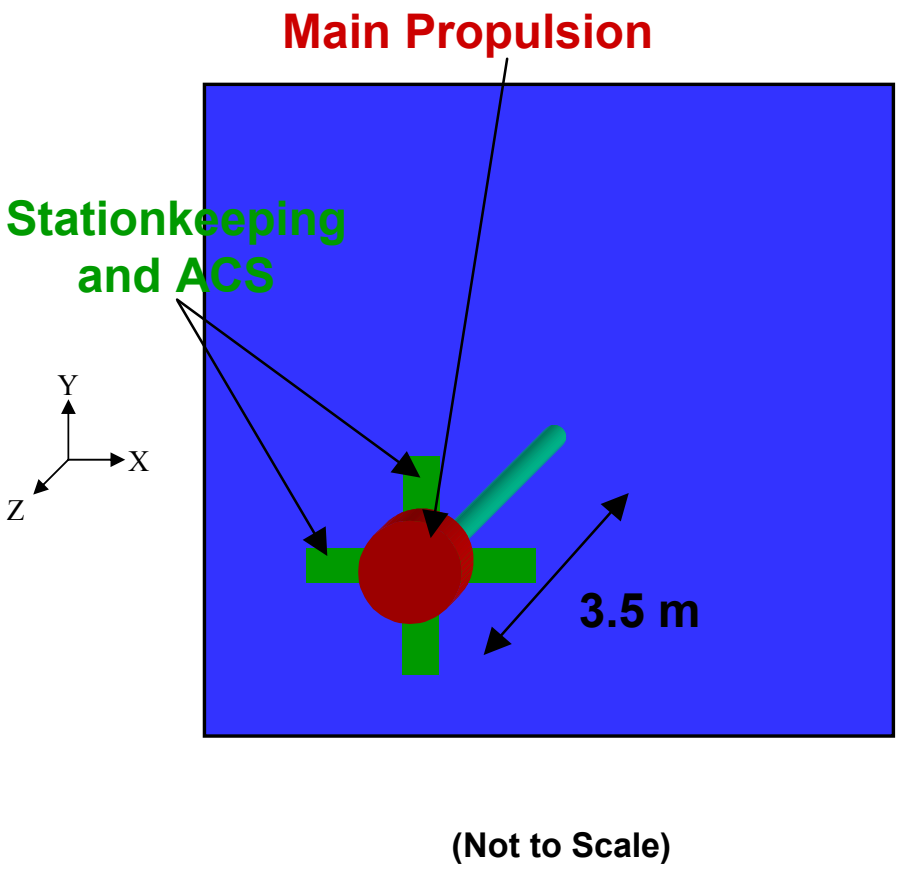

Figure 2-2: Thruster Configuration - Boom Mount

2.5 Propulsion Trade Analysis

Given the extremely tight mass budget set for the PowerSail spacecraft, any comparison of propulsion options must center on predictions of propulsion system mass. To address this issue, detailed mass estimates for propulsion systems using the various proposed technologies were constructed. A number of propulsion options were considered, with each of the potential primary propulsion systems examined for suitability as secondary propulsion as well, and with both center/corner and boom installations considered. Mass estimates for each system were broken down into five categories - thruster, power processing, propellant, propellant feed, and miscellaneous - with one or more line items in each category as appropriate. With central-boom installations, the mass of the boom itself was also charged against the propulsion system.

For each of the necessary items, commercial off-the-shelf hardware was specified whenever possible, preferably space-qualified but in the case of some power processing or propellant feed system components, ground or aviation hardware meeting relevant military specifications was used as a baseline. The intention is to reliably estimate the mass of a flight system rather than to actually design such a system. In some cases,

commercial systems of different power levels were scaled linearly over a modest range to meet specific PowerSail requirements. For experimental thruster concepts, flight-like laboratory test hardware was considered.

Separate evaluations were made for the requirements of 5- and 10-year missions, due to the different ΔV and propellant requirements. The total propulsion system mass requirements are given in Tables 2-2 and 2-3, below.

Table 2-2: Propulsion Mass Estimates – 5-Year Mission

Primary Thruster	Secondary Thruster	5-Year Mission	
		Corner	Boom
Chemical Biprop	Chemical Biprop	241 kg	378 kg
Arcjet	Arcjet	178 kg	231 kg
Ion Engine	Ion Engine	160 kg	115 kg
PPT	PPT	92 kg	106 kg
PPT	AFRL μPPT	87 kg	141 kg
200 W Hall	AFRL μPPT	75 kg	129 kg
FEEP	FEEP	98 kg	66 kg
200 W Hall	200 W Hall	64 kg	84 kg
200 W Hall	Colloidal Thruster	57 kg	92 kg

Table 2-3: Propulsion Mass Estimates – 10-Year Mission

Primary Thruster	Secondary Thruster	10-Year Mission	
		Corner	Boom
Chemical Biprop	Chemical Biprop	470 kg	746 kg
Arcjet	Arcjet	299 kg	430 kg
Ion Engine	Ion Engine	186 kg	157 kg
PPT	PPT	166 kg	229 kg
PPT	AFRL μPPT	161 kg	264 kg
200 W Hall	AFRL μPPT	145 kg	248 kg
FEEP	FEEP	105 kg	78 kg
200 W Hall	200 W Hall	107 kg	154 kg
200 W Hall	Colloidal Thruster	104 kg	173 kg

2.6 Conclusion

Because of the excessive propellant mass, it is clear that chemical propulsion is not appropriate for the PowerSail mission. On examination, the effective delta-V requirement for a 10-year mission is more than 4 km/s, which results in grossly excessive propellant mass. That being the case, the recommended option is the FEEP thruster. Its extremely high specific impulse dramatically reduces propellant mass, with a wet mass of 105 kg for a 10-year corner-mounted configuration and only 78 kg for a boom-mounted

configuration. However, at the power levels required for this mission, the technology is relatively immature and has a high dry mass. If a near-term demonstration is required, it may be more advantageous to utilize propulsion in a more advanced state of engineering development. In this case, we would recommend the use of a 200 W Hall thruster on the central bus for primary propulsion, and four clusters of AFRL micro-PPT thrusters at the corners for lateral stationkeeping and attitude control. At 75 kilograms for a 5-year mission, this is nearly the lightest propulsion option found in the study, and is achievable with mature, near-term technologies. Both a 200 W Hall thruster, the Busek BHT-200, and the AFRL μPPT are scheduled to fly on the TechSat 21 demonstration mission in 2004. Other 200 W class Hall thrusters are at high levels of engineering development. Furthermore, much of the potential integration difficulty associated with placing thrusters at the array corners is reduced by the compact, solid-state nature of the μPPT systems.

2.7 References

[1] Lawrence, T., et al., "Performance Testing of a Resistojet Thruster for Small Satellite Applications," AIAA Paper 1998-3933, 34th Joint Propulsion Conference, Cleveland, Ohio, July 1998.

[2] Hruby, V., et al., "Low Power, Hall Thruster Propulsion System," IEPC Paper 99-092, 26th International Electric Propulsion Conference, Kitakyushu, Japan, October 1999.

[3] Beattie, J.R., Williams, J.D., and Robson, R.R., "Flight Qualification of an 18-mN Xenon Ion Thruster," IEPC Paper 93-106, 23rd International Electric Propulsion Conference, Seattle, Washington, September 1993.

[4] Meckel, N., et al., "Investigation of Pulsed Plasma Thrusters for Spacecraft Attitude Control," IEPC Paper 97-128, 25th International Electric Propulsion Conference, Cleveland, Ohio, August 1997.

[5] Gulczinski, F.S., et al., "Micropropulsion Research at AFRL," AIAA Paper 2000-3255, 36th Joint Propulsion Conference, Huntsville, Alabama, July 2000.

[6] Capelli, M., Stanford University, Palo Alto, California, Personal Correspondence, July 2000.

[7] Gonzalez, J., Saccocia, G., and Von Rhoden, H., "Field Emission Electrostatic Propulsion (FEEP): Experimental Investigation on Microthrust FEEP Thrusters," AIAA Paper 97-3057, July 1997.

3 Executive Summary of Virginia Tech Study

The Virginia Tech University (VTU) design study covered all major spacecraft subsystems; including propulsion, structures, power, thermal control, communications, attitude determination and control (ADCS), command and data handling (C&DH), and umbilical. Only details relevant to the overall spacecraft design and the propulsion subsystem are presented here. It was performed under the auspices of the Aerospace and Ocean Engineering Department's Senior Design (Space) Course (AOE 4065).

3.1 System Synthesis

The objective of system synthesis is to conceptualize possible designs for PowerSail as well as to generate alternatives for components of each subsystem. Each of the alternatives generated in this section are compared using a value system design ranking. From these rankings top configurations are chosen to analyze further. This is a critical step in the design process, which helps identify alternatives while withholding judgment.

3.1.1 PowerSail Configurations

Four array configurations were considered: kite tail, sphere, fan, and flat array.

3.1.1.1 Kite Tail

The kite tail configuration (Figure 3-1) incorporates a formation of solar arrays to complete the mission objectives. Instead of a single large array, a group of smaller arrays provide a total of 50 kW of power. The arrays are strung in a line, each attached by a slack umbilical. There are two types of satellites in this configuration: a command satellite and the power supply arrays. The command satellite is responsible for controlling the formation and attitude of the power supply arrays.

The command satellite is equipped with solar arrays and batteries for its own use. The array on the command satellite also provides some power to the host satellite. Each power satellite generates power for the host and itself. Batteries for the ADCS are located on each power satellite. The power needs of the host satellite determine the number of power satellites.

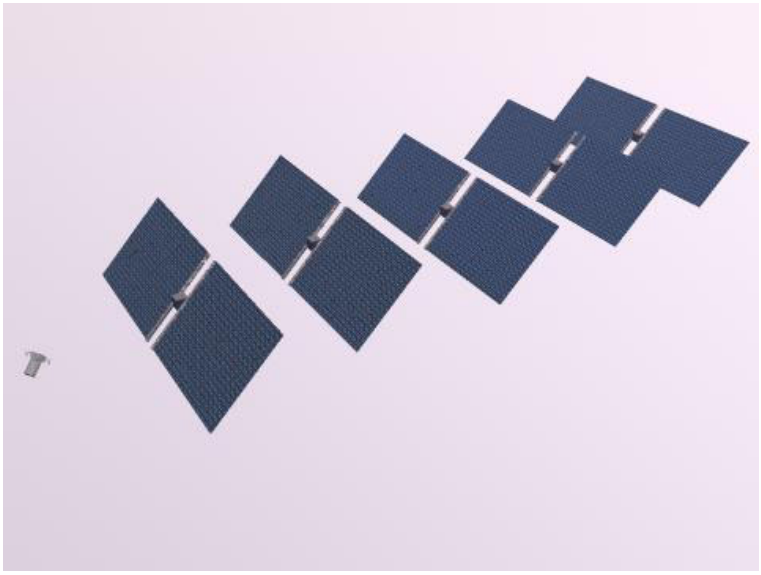

Figure 3-1: Kite Tail Configuration

3.1.1.2 Sphere

The sphere concept (Figure 3-2) is a single solar array. The array is a large sphere, akin to a balloon, covered with flexible solar cells. Filling the balloon with compressed gas inflates the array. The housing for internal components of the system is located at one edge of the array. The slack umbilical is attached to the housing. The thrusters for attitude control are located on the housing and on a mounting opposite the housing. There are supports located in and on the array to maintain the structure of the system. The pointing requirements of this system are decreased since the array is spherical and any orientation collects the same energy from the sun.

Figure 3-2: Sphere Configuration

3.1.1.3 Fan

Figure 3-3 shows the fan design, a structure that deploys in a similar fashion to a folding fan. When deploying, the solar array rotates about the central point creating a circular array. Similar to a Venetian blind, the solar cells will not likely be directly perpendicular to sunlight. The bus of the system is located in the center of the deployed structure. The umbilical is connected to the bus.

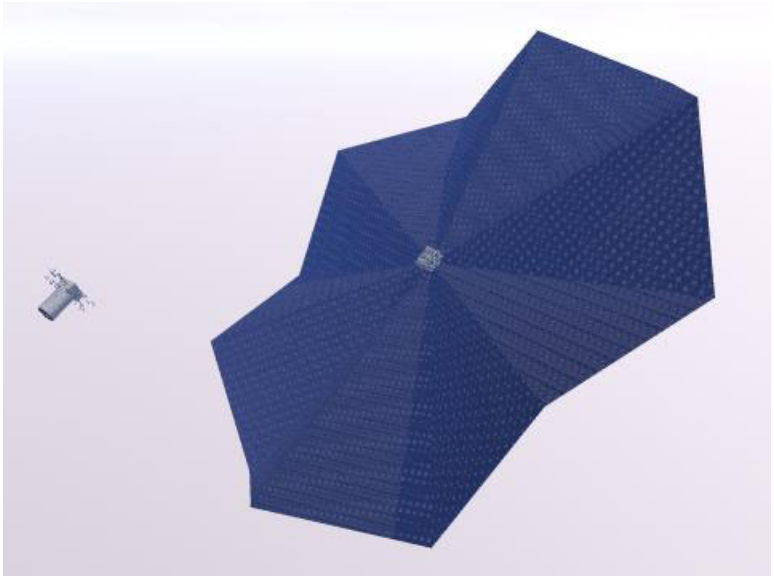

Figure 3-3: Fan Configuration

3.1.1.4 Flat Array

The flat array configuration is comprised of five deployable booms and a main bus. This configuration is a planar array with thin flexible solar arrays, in which the central boom deploys first. The side booms deploy simultaneously, deploying the flexible solar arrays. The bus structure is inherently small compared to the size of the array. The umbilical, thrusters, and attitude sensors are located on any part of this structure. This configuration has a relatively small stowed volume and mass. The booms can also be designed to retract if needed.

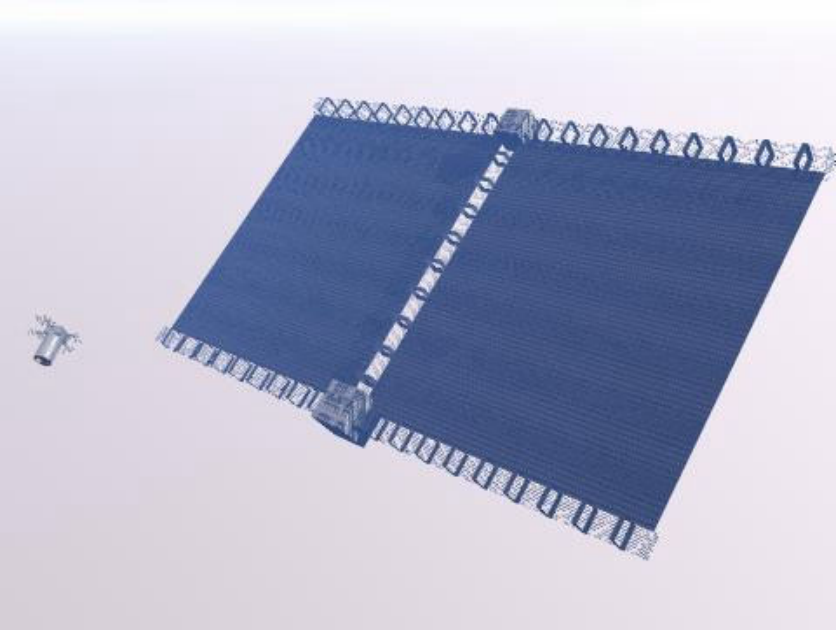

Figure 3-4: Flat Array Configuration

3.1.2 Propulsion Options Considered

The primary purpose of the PowerSail propulsion system is to maintain the proper position of the array in an orbit relative to the host spacecraft. Forces such as solar radiation pressure and atmospheric drag must be countered. These maneuvers must be carried out so that the umbilical does not wrap around the array. The propulsion system must also counteract any dynamics that are induced in the array by the umbilical.

The long lifetime requirements projected for an operational system (10 years) results in a desire to reduce propulsion system propellant mass, making electric propulsion a highly attractive option. There are a growing number of space-rated and production electric propulsion systems. An electric propulsion system accelerates a working fluid to high velocity (in comparison to other propulsion types) to produce thrust. The high velocity, charged particle nature of electric propulsion plumes can present issues in multi-satellite formations. Several types of electric propulsion systems were considered for use in the PowerSail project: resistojets, arcjets, ion engines, Hall thrusters, and pulsed plasma thrusters. The resistojet and arcjet have lower specific impulse than the other systems, leading to higher propellant masses. However, they have neutral plumes, which may be advantageous given the close formation of the array and host. Hall thrusters and ion engines have the highest specific impulses, and thus the lowest propellant masses. However, their large dry masses are a concern and their ionized plumes may cause spacecraft interaction issues. Pulsed plasma thrusters are inefficient, but are simple, reliable, and use a solid propellant (Teflon™); which makes them attractive for positioning at the end of a deployable structure since it avoids the need to run propellant

lines from a centralized tank or, alternatively, carry separate tanks for each thruster location.

3.2 System Analysis

The impact of the array configuration on the propulsion subsystem was analyzed. This information was combined with the impact on other subsystems to select a final design.

3.2.1 Kite Tail

This configuration creates a number of different problems for the propulsion system. Each satellite in the kite tail has its own propulsion system and attitude thrusters, so the mass of the overall system is larger than a centralized configuration. Although each satellite needs a smaller thruster size and propellant mass, the number of thrusters and overall mass of propellant for all satellites offset this advantage.

Since a slack umbilical connects each satellite, wave propagation down each umbilical creates a need for thruster operation. This additional need for thruster operation increases the amount of propellant required as opposed to other configurations. It is assumed that the umbilical between each satellite is long enough that the plume from the thrusters will not interfere with the other satellites in the chain.

The system needs small controlled bursts to maintain the attitude of the kite tail. The best system for this is a Pulsed Plasma Thruster. Ion engines and Hall thrusters create more thrust than is necessary and are too massive for use on the smaller satellites. Arcjets and resistojets also are more massive than the PPTs, and have greater propellant mass. The sizing of the PPTs is dependent on the location of the thrusters and size of each satellite. It will be difficult to integrate the thrusters into the array because of the minimal support structure.

3.2.2 Sphere

The sphere configuration for PowerSail reduces the need for propulsion system operation to maintain attitude control since the spherical array always has an equal amount of surface area facing the sun. The reduced pointing requirements lead to a decrease in thruster operation. However, because the array is spherical, it will experience cosine losses in areas not perpendicular to the sun vector. To make up for these losses, area must be increased, making the sphere configuration the largest of the options considered, thereby increasing both the solar radiation pressure and drag force that the array experiences. The result is an increase in primary propulsion requirements, overwhelming the savings from pointing.

This configuration does not have the stringent impulse bit requirements of the kite tail. It optimizes well for a small Hall thruster or ion engine. A large PPT could also be used, but would suffer from high dry mass and low efficiency. The system would, however, benefit from the simplicity of the PPT. Again, there are expected to be integration issues.

3.2.3 Fan

The fan configuration is akin to a single piece of the kite configuration, although it is much larger than a single piece of the kite tail. Overall, the array area is equivalent, but the mass will be less since it is centralized. Thus, the drag and solar radiation pressure will be comparable to the kite tail and less than the sphere. The pointing requirements are less than the kite tail since there is only one array to point, but more than the sphere which requires virtually no pointing.

This fan does not have as stringent an impulse bit requirement as does the kite tail, but the small impulse bit of the PPT is still very compatible. A small ion engine or Hall thruster are options for the fan because it has a larger mass than the individual kite tail sections.

3.2.4 Flat Array

The flat array configuration is a planar array with booms to support the array. It is similar in area and pointing requirements to the fan. The additional mass of the support booms will increase the propulsion needs of the system. However, the additional stiffness that the booms supply will decrease dynamic interaction within the array from the umbilical or other perturbing forces, thereby partially offsetting the increase due to boom mass. The primary advantage of the flat array from a propulsion standpoint is integration. The booms provide ample thruster mounting locations, making integration much simpler than for the other configurations.

Due to the similar propulsion requirements, the same propulsion options that benefited the fan also work well for the flat array: PPTs, small ion engines, or small Hall thrusters.

3.2.5 System Analysis Conclusions

An objective hierarchy and a value system design were applied qualitatively based on the results of the system analysis. From an overall system perspective, the two most attractive options were the sphere and the flat array. The primary advantages of the sphere were its lack of pointing requirements (which leads to both decreased propulsion mass and operational cost) and ease of deployment. Its disadvantages were that the larger array drove up the mass and volume of the array, thus increasing the impact on the launch vehicle. The three other configurations (kite tail, fan, and flat array) have similar propulsion requirements. The advantages of the flat array were low mass and stowed volume, a reasonable deployment system, and, most importantly, ease of integration of components such as the bus and propulsion system. The disadvantages are its pointing requirement and dynamic interaction issues. Based on these considerations, the flat array appeared to be the most advantageous and was selected for the system.

The resultant array must provide 50 kW to the host in addition to powering its own propulsion system, ADCS, computer, and battery. These components will consume an additional 2.6 kW of power. The array is composed of Copper Indium Diselenide thin-film photovoltaic solar cells.[1] These cells operate at an estimated efficiency of 17%, provide an energy density of 125 W/m^2, and a specific power of 200 W/kg. The final configuration of PowerSail, shown in Figure 3-5, is an array split into 14 panels to allow

for deployment via rigidizable, inflatable booms. Each panel is 3m × 10m (of which 29 m^2 is solar cell, the remainder boom) for a total area of 420 m^2. PowerSail's mass, including propulsion, solar array, umbilical and structure is 796 kg.

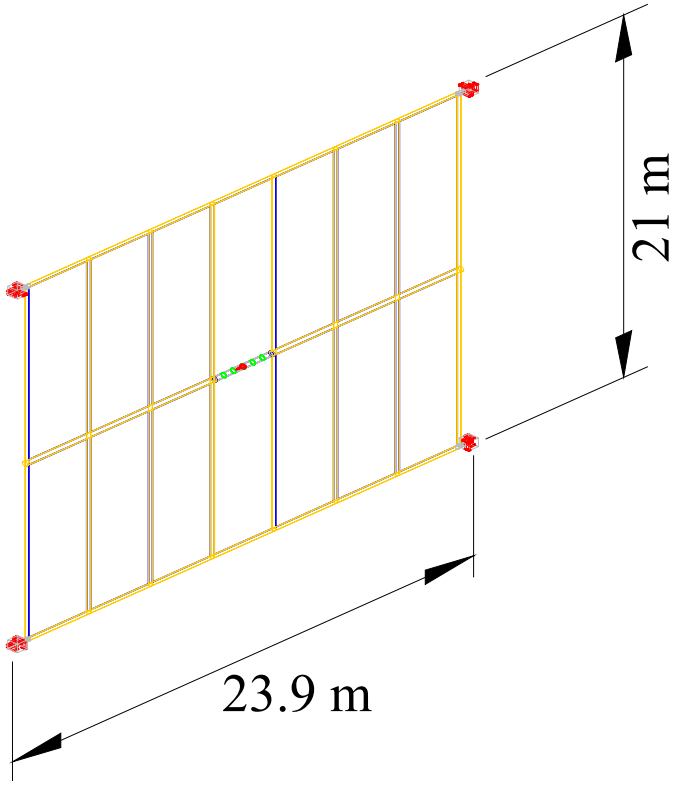

Figure 3-5: PowerSail Array Dimensions

The overall system, separated by major subsystem, is shown schematically in Figure 3-6.

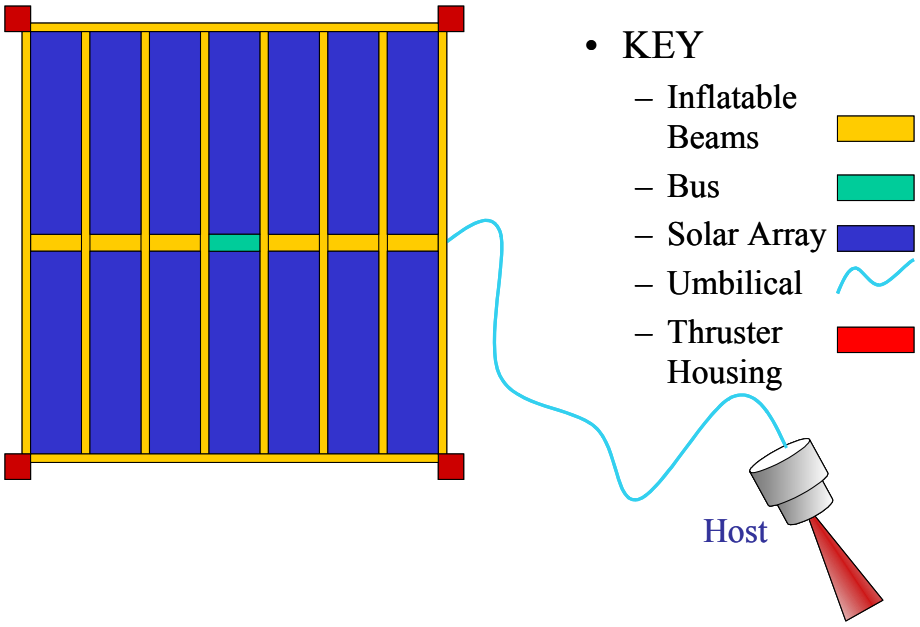

Figure 3-6: PowerSail System Schematic

3.3 Propulsion System Optimization

The propulsion subsystem of PowerSail has two main requirements. The first is maintenance of the formation between PowerSail and the host. The system must be able to maintain the leader-follower formation with the host satellite, while having low mass and power requirements. The umbilical that attaches the two satellites is a fixed length and the distance between the two can't exceed this length. The second requirement of the propulsion system is to keep PowerSail sun pointing as much as possible. In the targeted orbits, above 1000 km, the dominant force acting on the PowerSail array during its orbit is solar radiation pressure. Other forces will be ignored in this analysis.

3.3.1 System Modeling

The effects of solar radiation pressure on the PowerSail orbit are computed based on algorithms that determine whether or not the array is within sight of the sun. If it is, the code applies forces from the solar radiation pressure to alter PowerSail's orbit. The net result is an increase to the eccentricity of PowerSail's orbit.

The host provides its own stationkeeping and orbit maintenance. The data obtained from modeling the leader-follower formation of the host and PowerSail around the earth show that the distance between the host and PowerSail exceeds the umbilical length by several kilometers in less than one orbit when not using a control system. The magnitude of the separation between the host and PowerSail is shown in Figure 3-7, and a planar view is shown in Figure 3-8. To counter this separation, the propulsion system acts to correct the orbit of the PowerSail. A total of 84.9 kN-s per year of impulse from solar radiation pressure must be counteracted to maintain the desired leader-follower formation.

Therefore, over the 10-year lifetime, a total of 849 kN-s must be provided by the propulsion system to counteract solar radiation pressure.

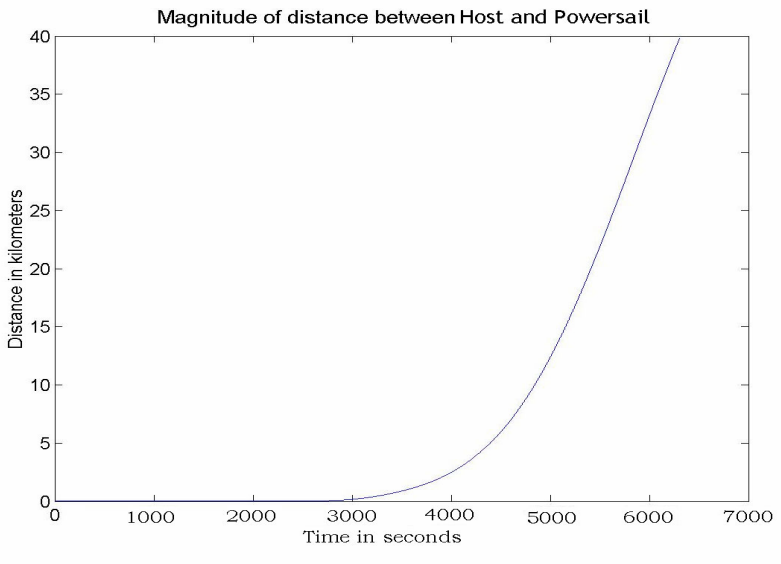

Figure 3-7: Magnitude of the Distance Between the Host and PowerSail vs. Time With an Inactive Control System

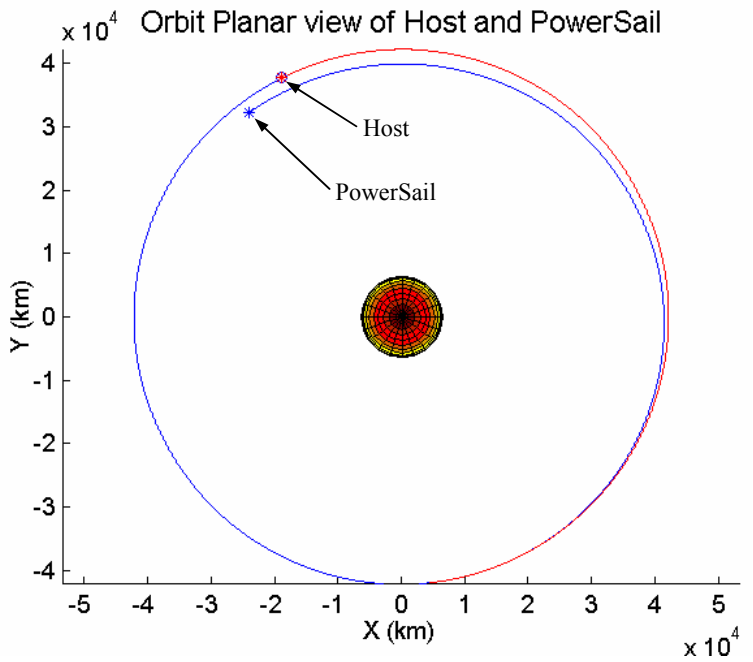

Figure 3-8: Orbit Planar View of the Host and PowerSail in a Geostationary Orbit after One Orbit With an Inactive Control System

3.3.2 Propulsion Subsystem Definition

The PowerSail uses clusters of pulsed plasma thrusters placed in corner modules. The data obtained from the orbit model gave the total impulse needed per year to maintain the formation. The propulsion system has a total of 40 thrusters located in four separate corner modules. An example of a module is shown in Figure 3-9. The overall dimensions of the module are 0.5 m by 0.5 m. The four thrusters oriented in the +Z direction are primarily intended to counter the solar radiation pressure. The thruster pairs pointed along the other axes are intended to counter other torques and provide ACS for the PowerSail. The PPTs chosen for this analysis are manufactured by General Dynamics, who provided information on their operation and mass estimates.[2]

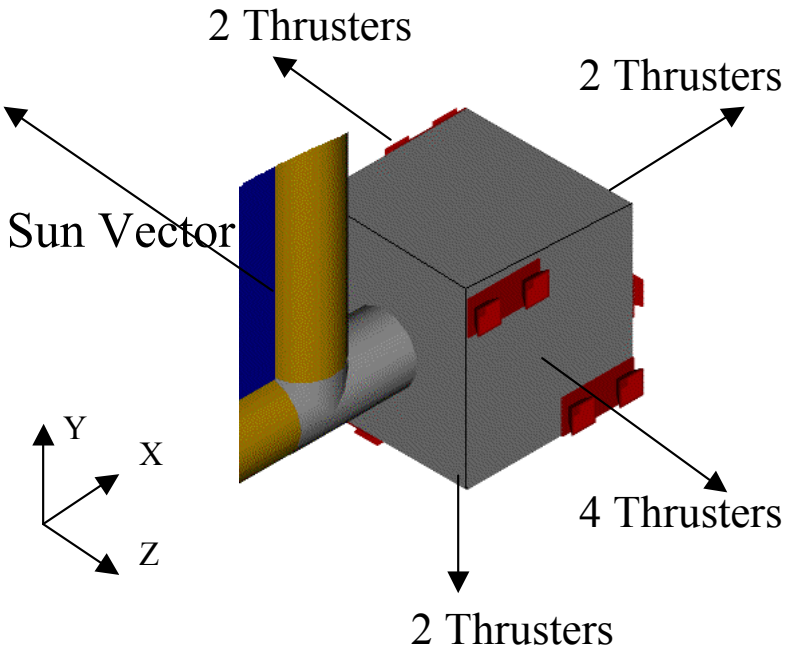

Figure 3-9: Propulsion Module

PPTs were chosen for a number of reasons. They use solid propellant, which eliminates the need for a propellant feed system and avoids the possibility of sloshing a liquid propellant, which could increase the vibration of a thruster module during operation. They have low dry mass and are durable, scaleable, and highly adaptable. They can deliver a precise impulse bit, which could enable them to perform array vibration damping.

PPTs have adaptable power supply systems. The power supply scheme for a cluster of PPTs can include up to four thrusters per capacitor and up to four capacitors per Power Processing Unit (PPU). Thus with a cluster of thrusters in a single small thruster module, the power system can control the whole module while keeping mass at a minimum. The power supply configuration for the PPTs in each module consists of 3 capacitors and 1 PPU for all 10 thrusters. This integration lowers system mass considerably, since

capacitors have the largest amount of dry mass. The thrusters also have extra Discharge Initiation (DI) circuits to increase life. The total impulse capability of a PPT is not based on amount of propellant for the thruster; the limiting factor is the spark plug and DI circuit. Currently, General Dynamics spark plugs and DI circuits are rated at approximately 10 million pulses, corresponding to 0.65 kg of Teflon™ propellant and 8.6 kN-s of total impulse. It is possible to use up to four sets of spark plugs and DI circuits on a single thruster in order to increase its overall total impulse. With four DI circuits, the propellant available to a single thruster is increased to 2.6 kg and the total impulse is increased to 34.4 kN-s. The four thruster groups pointed in the +Z direction for solar radiation pressure counteraction have four DI circuits per cluster, while the thruster pairs pointed in the other directions - which have lower total impulse requirements - have two DI circuits per thruster.

PPTs also have a scaleable firing rate. They fire in pulses, at 100 J per pulse. As long as power is available, the thrusters can fire from 1 Hz to 20 Hz. There is no ramp up in pulse cycling either. Thus, the amount of impulse provided is variable up to a maximum amount. The specific impulse of General Dynamics pulsed plasma thrusters is roughly 1350 seconds. The PowerSail thrusters fire at a nominal rate of 2 Hz; however, this can be increased if an abnormally large or small separation occurs between the host and the PowerSail. The maximum amount of power available in normal operations for the firing of the PPTs is set for 4 thrusters firing in 3 axes at 2 Hz. This worst-case scenario requires 2.4 kW.

Each pulse provides 860 μN-s impulse. With such a low impulse bit, the thrusters can be used as an active damping system to reduce the structural vibrations of the PowerSail. However, operating the thrusters in this manner would increase the propellant mass that the PPTs must carry and consume.

The dimensions of a thruster pair are shown in Figure 3-10 and a photo of the thrusters is shown in Figure 3-11. A schematic of a generic pulsed plasma thruster is Figure 3-12. The mass breakdown of specific components and total system mass is in Table 3-1.

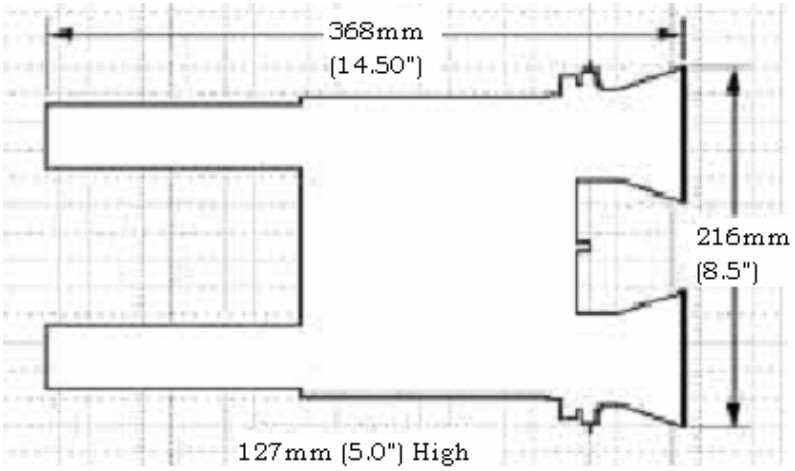

Figure 3-10: Dimensions of a PPT Pair

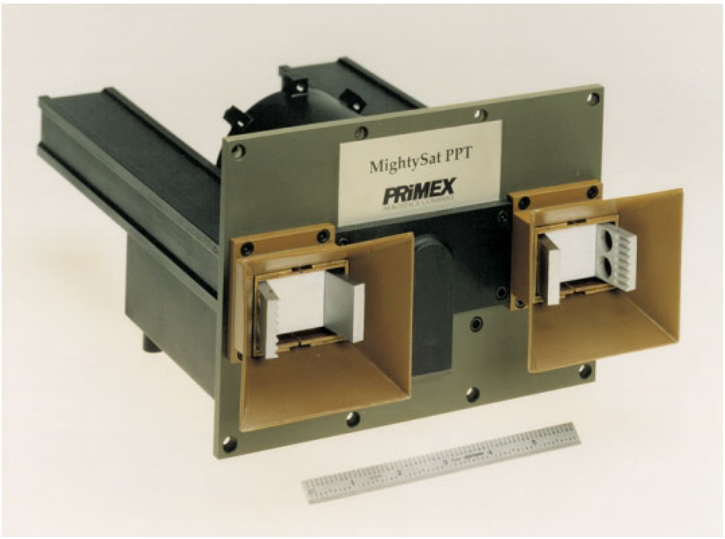

Figure 3-11: Photo of a General Dynamics PPT Pair Developed for the AFRL MightySat Program[3]

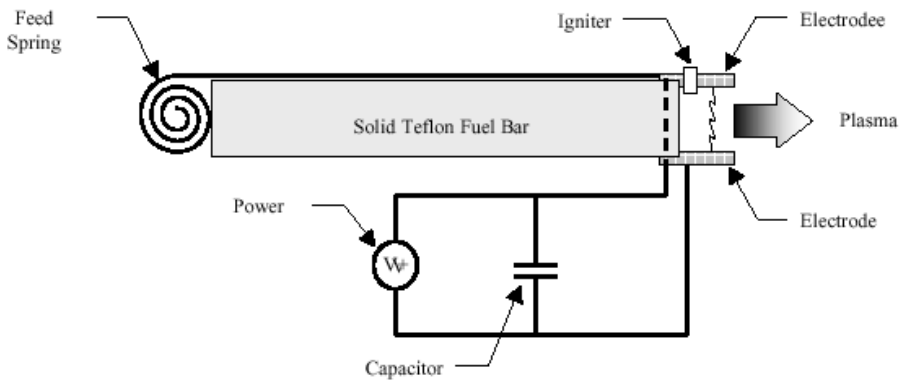

Figure 3-12: Schematic of a Generic Pulsed Plasma Thruster

Table 3-1: PPT Mass Properties

Component	Mass (kg)
Thruster + Housing	0.54
Capacitors	2.32
PPU	0.52
DI Circuit	0.2
Overall System	
Thrusters & Propellant (40)	127
Capacitors (12)	27.8
PPUs (4)	2.2
Total System Mass	157

3.4 Summary

PowerSail needs to provide 50 kW of power to a host spacecraft ranging in orbit from 1000 km to geostationary. It has a lifetime of 10 years, which leads to the need to use electric propulsion to maintain the formation between it and the host. The power is transmitted to the host using a slack umbilical.

The final configuration of PowerSail is a flat array split into 14 panels. Each panel is 3m × 10m for a total area of 420 m^2. PowerSail's mass, including propulsion, solar array, umbilical and structure is 796 kg. This is a fairly low mass considering the size of the solar array when deployed.

The dominant propulsion driver is the need to counteract 84.9 kN-s of solar radiation pressure per year over the 10-year lifetime of the system. The propulsion system chosen is the PPT manufactured by General Dynamics. PPTs are a good choice as a propulsion system for a number of reasons including solid propellant, adaptable power systems, and low dry mass. These thrusters will maintain the formation between PowerSail and the host. They also keep PowerSail pointing toward the sun. There are a total of 40 PPTs,

clustered into four thruster modules. The maximum available power allotted for the PPTs is 2.4 kW.

3.5 References

[1] Tringe, J., Capt., USAF, Air Force Research Laboratory Space Vehicles Directorate, Kirtland AFB, NM, Personal Correspondence, February 2001 through April 2001.

[2] Hoskins, A., Personal Correspondence, General Dynamics (was Primex Aerospace Corporation), October 2000 through December 2000.

[3] LeDuc, J.R., et al., "Mission Planning, Hardware Development, and Ground Testing for the Pulsed Plasma Thruster (PPT) Space Demonstration on MightySat II.1," AIAA Paper 1997-2779, 33rd Joint Propulsion Conference, Seattle, Washington, July 1997.

4 Executive Summary of Aerophysics, Inc. Study

4.1 Introduction

Aerophysics, Inc. performed a design trade study for the PowerSail propulsion system. The target missions were space based laser and radar satellites in a circular 900 km orbit with a 10-year lifetime. For these missions, a flat PowerSail array capable of supplying 500 kW was baselined. Based on projections for 2005 PowerSail capability, the array will have a specific power of 400 W/kg and an efficiency of 15%. The resultant areal density of the array material is 0.53 kg/m^2. It was assumed that the overall density of the array (including structure, deployment, bus, etc.) was 1.75 times the density of the array material (0.93 kg/m^2).

In this investigation, seven canonical electric propulsion technologies were considered: Teflon™ pulsed plasma thruster, hydrazine resistojet, hydrazine arcjet, ammonia arcjet, hydrogen arcjet, xenon Hall thruster, and xenon ion engine. The performance specifications (specific impulse – I_{sp}, thruster power-specific mass – β_T, power processing unit power-specific mass – β_{PPU}, and power conversion efficiency – η) for each technology, based on numerous studies,[1] are given in Table 4-1.

Table 4-1: Performance Characteristics for Canonical EP Technologies Investigated for PowerSail Vehicle Sizing Estimates

	Teflon PPT	N_2H_4 Resistojet	N_2H_4 Arcjet	NH_3 Arcjet	H_2 Arcjet	Xe Hall	Xe Ion
I_{sp} (s)	1000	300	500	600	1000	1600	3000
β_T (kg/W)	0.12	0.002	0.0007	0.0007	0.0005	0.003	0.006
β_{PPU} (kg/W)	0.11	0.001	0.0025	0.003	0.0025	0.01	0.01
η (-)	0.07	0.80	0.35	0.36	0.40	0.50	0.65

4.2 Method

This study developed and utilized a three degree-of-freedom dynamic numeric optimization tool in order to determine the optimal orbital trajectory and corresponding thrust requirements for each propulsion technology considered. The coordinate system used is shown in Figure 4-1. Key assumptions used in the derivation of the dynamic equations were:

- External forces are due to gravity, atmospheric drag, solar pressure, and thrusters
- Propulsion system mass is uniformly distributed over the vehicle
- The sail is rigid and of uniform density
- The sail has only three degrees of freedom (x,y,ψ)
- The distance between the target (host) spacecraft and the PowerSail, $\sqrt{x^2 + y^2}$, is sufficiently small such that they enter the earth's shadow at the same time

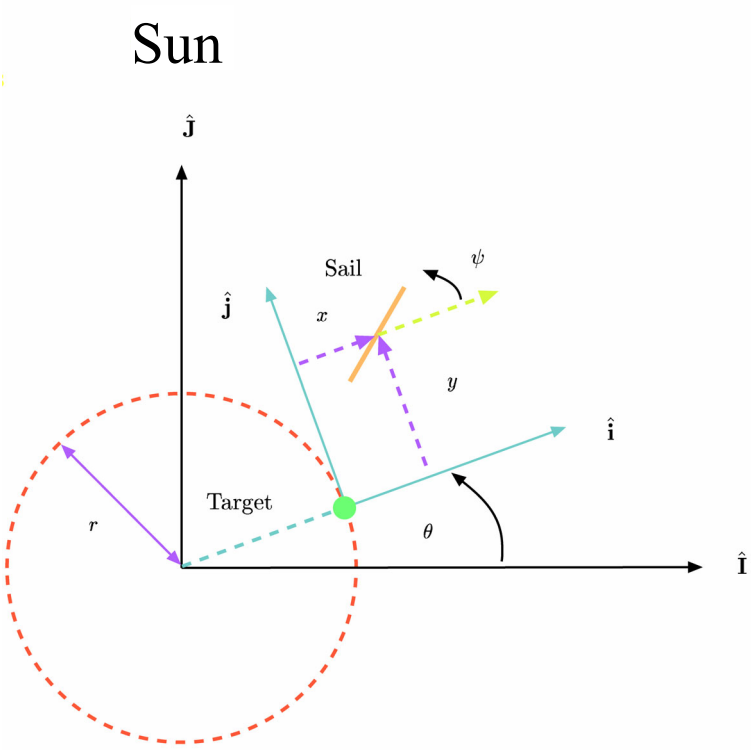

Figure 4-1: Coordinate System for Dynamic Optimization

A set of 16 thrusters was used for this analysis. Eight are on the outside edges of the sail (four on each edge for attitude control), four are oriented to provide in-plane thrust, and four are located at the center for orbit maintenance. However, accounting for all 16 thrusters in the derivation of dynamic equations overcomplicates the process. Instead, as illustrated in Figure 4-2, it was assumed that there is thrust capability at the edges of the PowerSail in the $\hat{j}_b$ direction. Denoted as F_{y1} and F_{y2}, these thrusters provide either attitude control or, by using simultaneous firings, orbit maintenance. There is also thrust capability in the $\hat{i}_b$ direction (in the plane of the PowerSail), denoted F_x. The actual 16 thrusters can be distributed amongst these fundamental thrust magnitudes and directions.

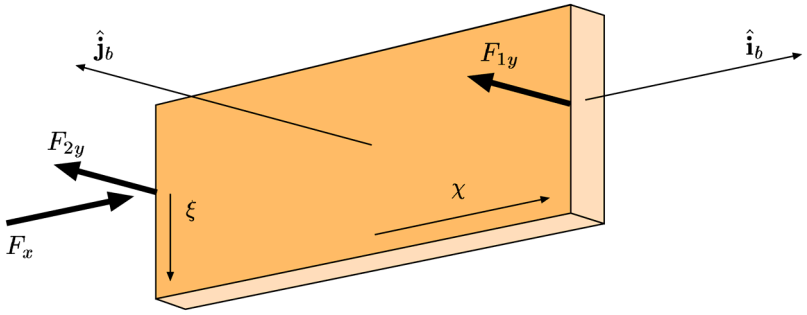

Figure 4-2: Thrust Vectors

4.3 Preliminary Mass Analysis – Continuous Thrust

In order to gain insight before employing the thruster pulse generation optimizer, three cases were run where the thrusters were assumed to be fully throttleable. These cases explored three different spacecraft orientation scenarios. The first, sun pointing, keeps the PowerSail oriented perpendicular to the sun at all times to maximize power generation. The second, minimum drag, keeps the spacecraft oriented such that the sail never encounters atmospheric drag (ignoring shear). The third, minimum gravity gradient, keeps the PowerSail oriented such that no gravity gradient torques are imparted to it. These scenarios are illustrated in Figures 4-3 through 4-5. For each orientation, the thruster force histories are computed analytically and compared.

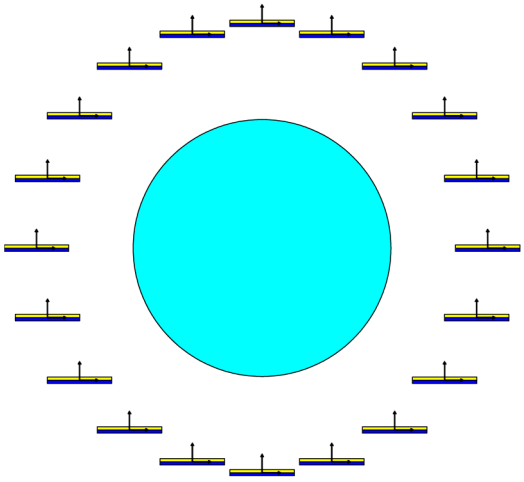

Figure 4-3: Sun Pointing Orientation

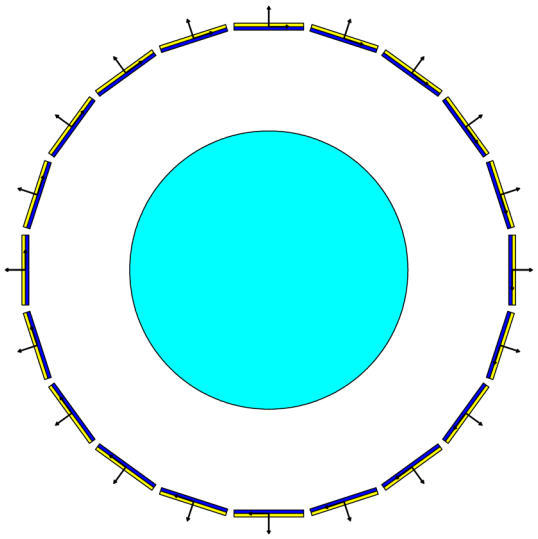

Figure 4-4: Minimum Drag Orientation

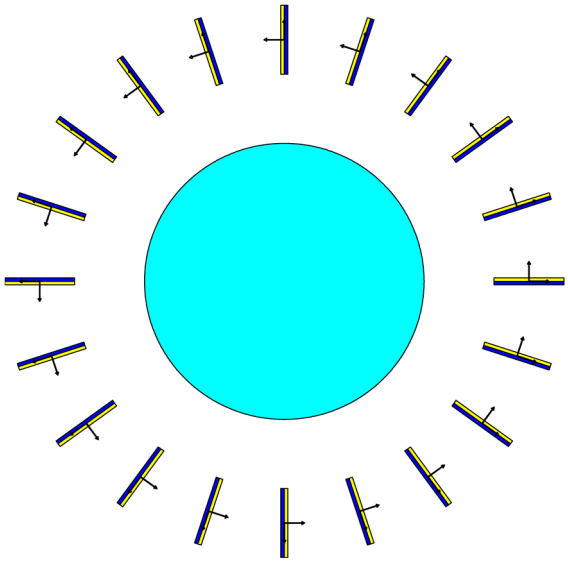

Figure 4-5: Minimum Gravity Gradient Orientation

To perform this basic analysis, the mass of the thrusters was assumed to be small compared to the fuel mass, allowing a canonical case with a specific impulse of 1000 s to be utilized. The mass and size of the PowerSail system were then computed by constraining the system to provide 500 kW, or an average energy of 1545 MJ per orbit. The results are presented in Table 4-2. It is clear that a sun pointing orientation has the smallest area since it maximizes solar energy collection. At 900 km it also has the lowest total mass. However, if the PowerSail is operated at lower altitudes, the atmospheric drag term will eventually dominate and the minimum drag orientation will become the

lowest mass solution. The thrust profiles are given in Figures 4-6 through 4-8 and ensure zero sail/host formation error throughout the orbit.

Table 4-2: Summary of Mass and Impulse Results for the Three Different PowerSail Trajectory Orientations

	Length (m)	Area (m^2)	m_{sail} (kg)	m_{fuel} (kg)	m_{total} (kg)	Impulse (N-s)	Pointing Time (s)
Sun Pointing	42.46	1803	1659	510	2169	98	4080
Minimum Drag	61.16	3741	3441	258	3699	50	1967
Minimum Gravity	71.04	5047	4643	479	5122	92	1458

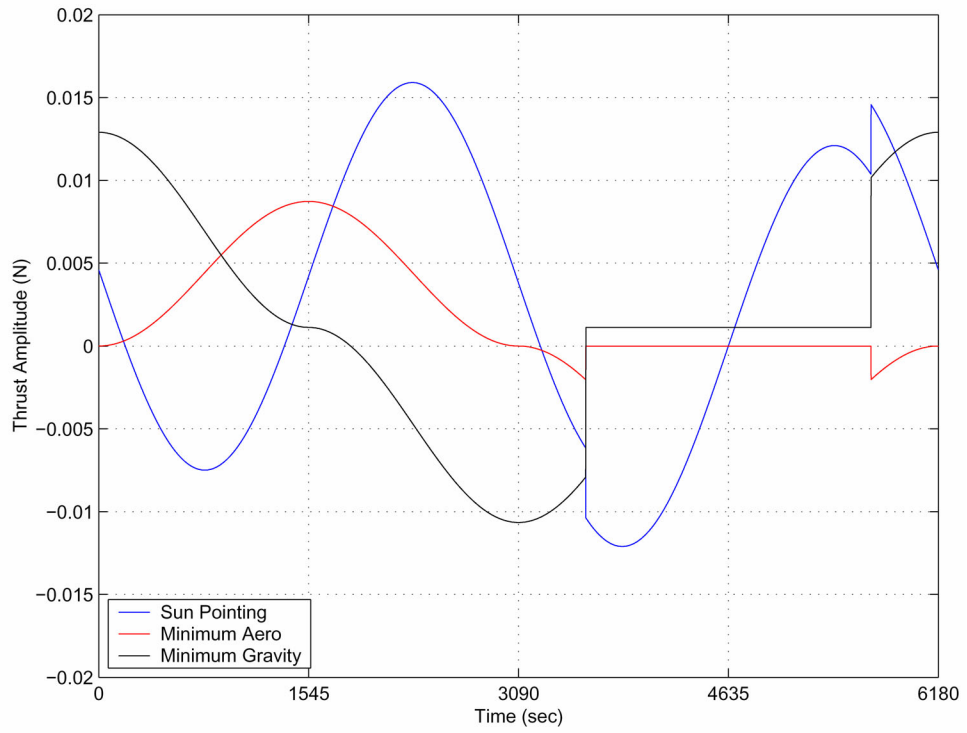

Figure 4-6: Time History of the F_{y1} Thruster

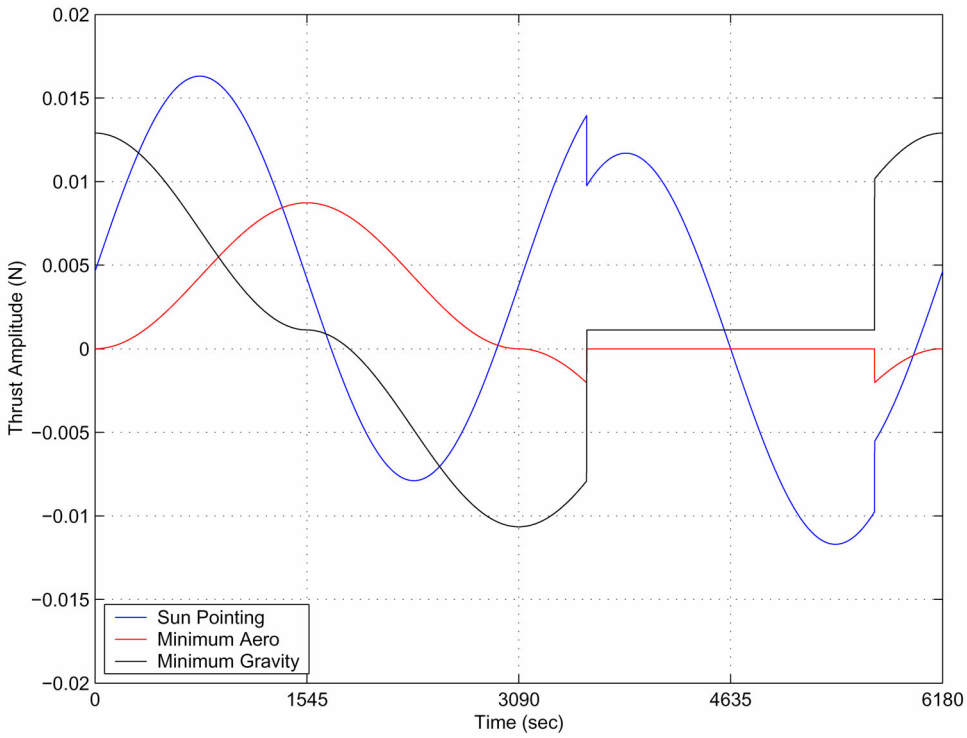

Figure 4-7: Time History of the F_{y2} Thruster

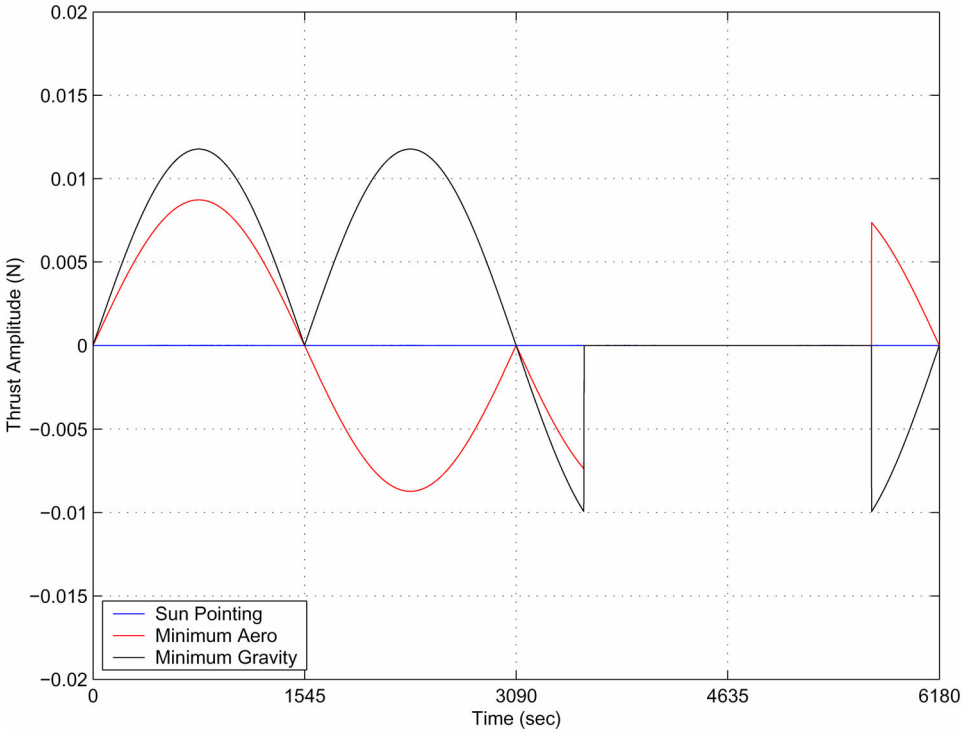

Figure 4-8: Time History of the F_x Thruster

4.4 Electric Propulsion Trajectory Estimates

In the previous section, the use of fully throttleable thrusters was shown to enable perfect formation maintenance. However, real electric propulsion thrusters, while typically having some throttle capability, cannot go smoothly from full power to zero thrust. In order to perform a realistic simulation, each thruster will be constrained to fire only at a single, discreet, thrust level.

As a first attempt, the sun pointing thrust profile shown in Figures 4-6 through 4-8 was decomposed into pure translation and moment producing components. These components were then approximated by constant amplitude pulses and reassembled into thrust profiles as shown in Figure 4-9, which compares the new discreet pulse profile with the original throttleable solution.

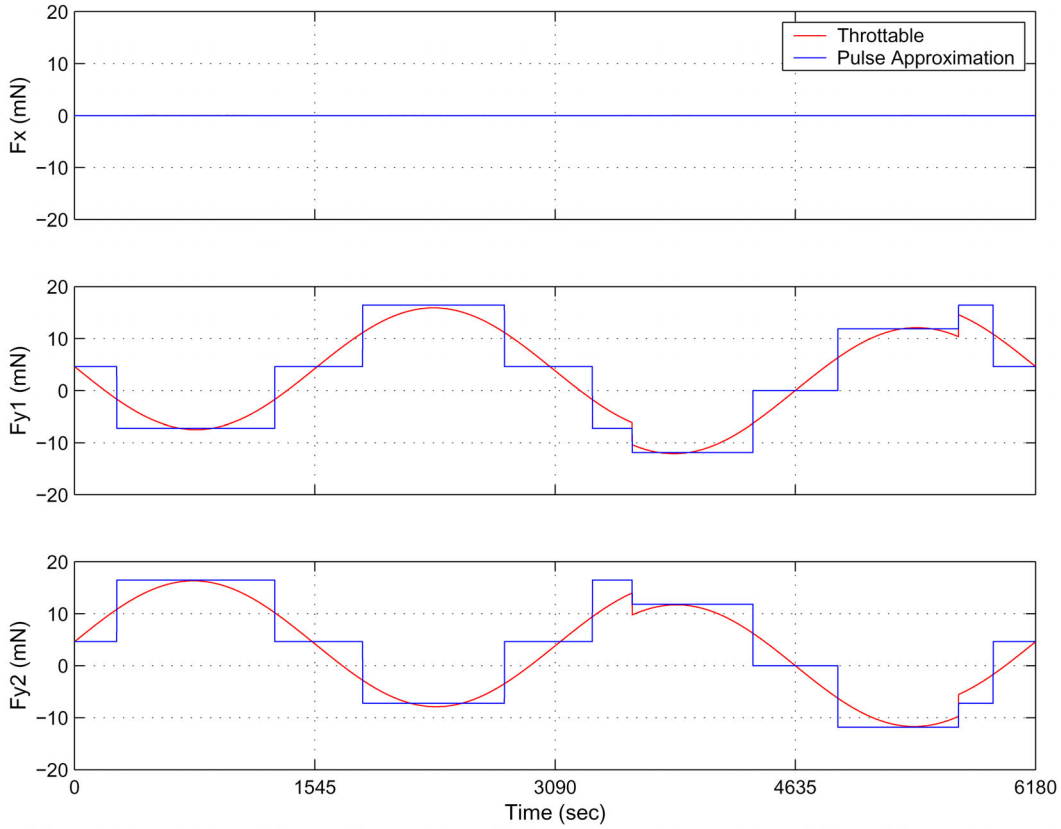

Figure 4-9: Comparison of Discreet Pulse Profile with the Throttleable Solution it is Based Upon

The solution was calculated by setting the system mass at 2169 kg, the same as was found for the throttleable sun pointing case. The resultant trajectory is shown in Figure 4-10, significant errors in stationkeeping and pointing occur in the first orbit.

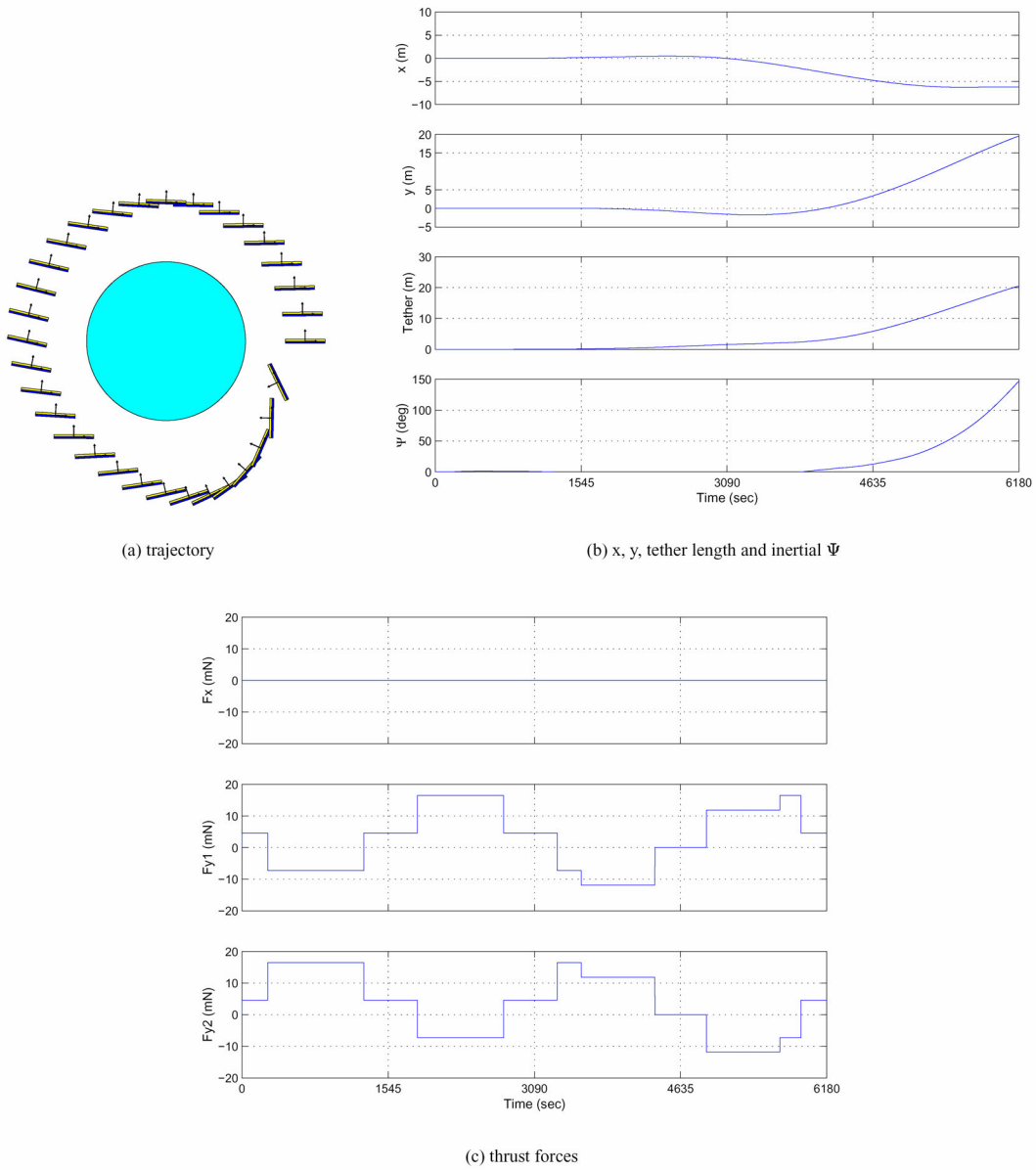

(a) trajectory

(b) x, y, tether length and inertial Ψ

(c) thrust forces

Figure 4-10: Dynamic Simulation Results Using the Pulse Approximation Thrust Profiles Derived From the Throttleable Results

It was decided that a systematic approach was needed for determining thrust profiles. To this end, an optimization capability was developed that generates pulse profiles that achieve mission requirements while minimizing system mass. To do this, each y-axis thruster (F_{y1} and F_{y2}) was allowed to have two positive and two negative pulses, all of the same amplitude. A center thruster was allowed to have a different amplitude and two positive pulses. Finally, the x-axis thruster was allowed to have its own amplitude and two positive and two negative firings. The amplitude and timing of these thruster firings was selected by the optimization code, and the pulses were allowed to overlap to mimic

the effect of two thrusters firing simultaneously. An initial orientation and angular rotation rate were also set by the code. To constrain the problem, the energy generated per orbit had to be within 5% of the 1545 MJ computed earlier and the PowerSail was required to return to within 0.01 m and 0.1º of its initial position.

Results were calculated for the seven thruster technologies under consideration – the computed impulse and thrust requirements are given in Table 4-3. As can be seen, the PowerSail converged to approximately the same size, independent of thruster technology, reflecting a tendency to favor small, and thus light, PowerSails. In each case, the pointing accuracy slipped to the maximum allowable error in power generation, 1468 MJ (-5%). A typical result for the trajectory and thrust profiles is shown in Figure 4-11 for the xenon ion engine. Though the thrust profiles vary, the overall trajectory is nearly identical for all cases, representing a hybrid motion between the sun pointing and minimum drag solutions. By exploiting the trade-off between pointing accuracy and fuel mass, the optimizer determined a solution that required less mass than either true sun pointing or true minimum drag.

Table 4-3: Impulse and Thrust Requirements from the Mass Optimization Results

	Impulse Per Orbit (N-s)	Center Thruster Amplitude (μN)	Outboard Thruster Amplitude (μN)	In-Plane Thruster Amplitude (μN)	Sail Length (m)	Effective Pointing Time (s)
Teflon PPT	37.64	3814.0	18.0	452.3	41.92	3978.1
N_2H_4 Resistojet	33.53	7157.2	1896.6	48.8	41.83	3994.8
N_2H_4 Arcjet	36.67	7604.2	19.5	1003.8	41.91	3979.0
NH_3 Arcjet	33.22	9005.4	14.6	121.0	41.90	3981.6
H_2 Arcjet	37.59	7892.0	766.7	925.0	41.92	3978.3
Xe Hall	40.91	10845.0	21.8	101.3	41.89	3982.8
Xe Ion	36.32	10532.0	66.7	210.4	41.89	3984.0

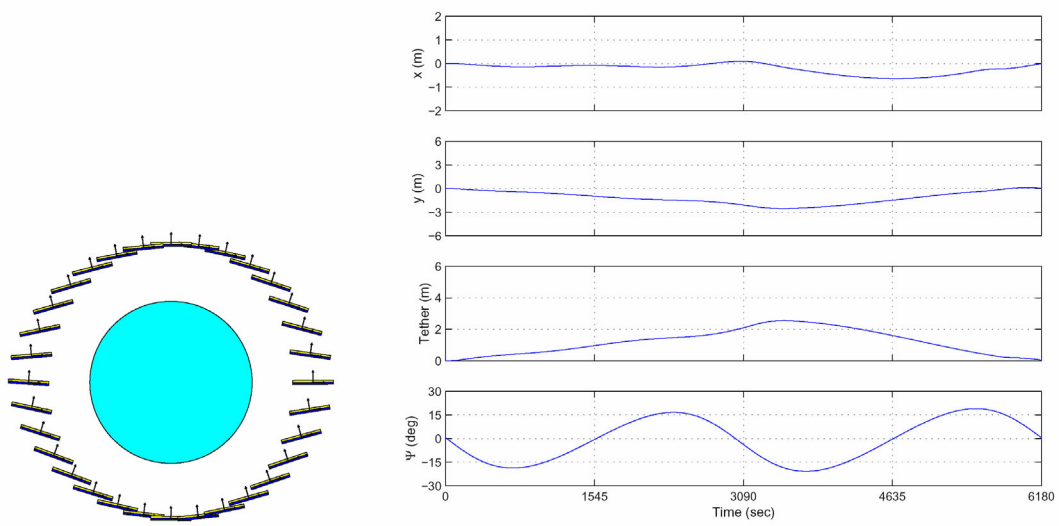

(a) trajectory

(b) x, y, tether length and inertial Ψ

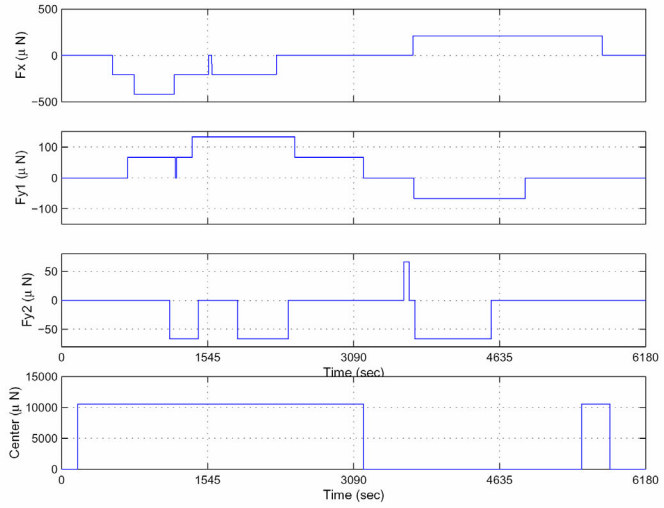

(c) thrust forces

Figure 4-11: Mass Optimal Results Using Xenon Ion Thruster Technology

4.5 Propulsion System Sizing Calculations

Propulsion system sizing calculations can be performed based on the performance requirements presented in Table 4-3. The 16 thrusters are laid out as shown in the following schematic:

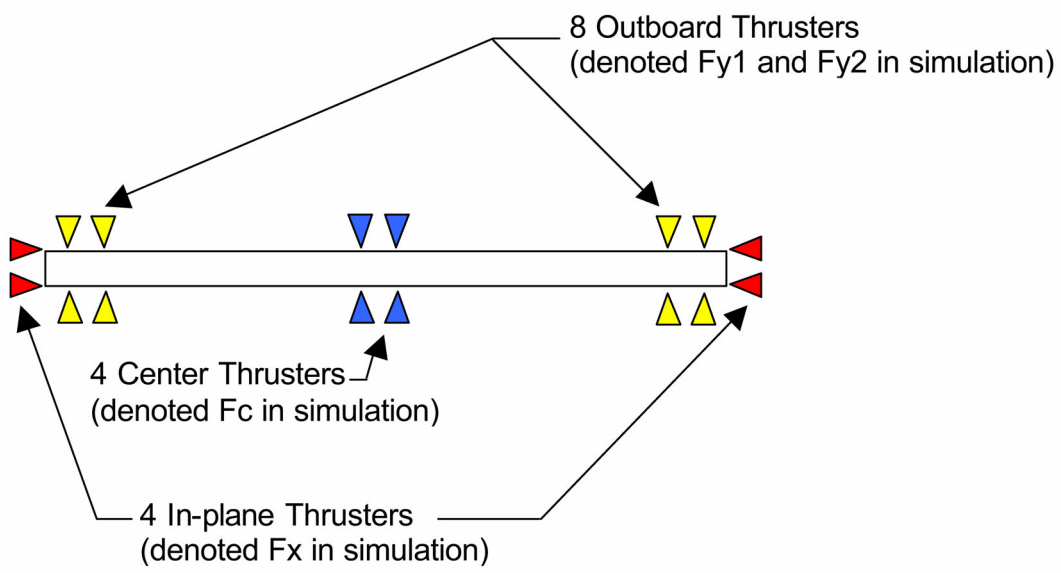

Figure 4-12: Schematic Showing Thruster Layout Implied by Force Constraints Imposed in the Dynamic Simulation/Optimization Routine

All 16 thrusters are the same type, but are allowed to vary in power, size, and thrust as summarized below.

- The eight outboard thrusters all have the same thrust amplitude and, hence, power requirements
- The four center thrusters all have the same thrust amplitude and, hence, power requirements
- The four in-plane thrusters all have the same thrust amplitude and, hence, power requirements
- The on-board power processing system is capable of simultaneously firing all sixteen thrusters

By assuming that all thruster parameters scale linearly with thrust level - system masses, thrust and power levels, and other relevant parameters can be calculated. These are summarized in Table 4-4, and the vehicle mass breakdowns are shown in Figure 4-13.

Table 4-4: Summary of Optimizer Results for Seven Different Thruster Technologies

	Teflon™ PPT	N_2H_4 Resistojet	N_2H_4 Arcjet	NH_3 Arcjet	H_2 Arcjet	Xe Hall	Xe Ion
I_{sp} (s)	1000	300	500	600	1000	1600	3000
β_T (kg/W)	0.12	0.002	0.0007	0.0007	0.0005	0.003	0.006
β_{PPU} (kg/W)	0.11	0.001	0.0025	0.003	0.0025	0.01	0.01
η (-)	0.07	0.80	0.35	0.36	0.40	0.50	0.65
Total Impulse per Orbit (N-s)	37.64	33.53	36.67	33.22	37.59	40.91	36.32
Center Thrust Amplitude (mN)	3.81	7.16	7.60	9.01	7.89	10.8	10.5
Outboard Thrust Amplitude (mN)	.018	1.87	.0195	.0146	.767	.0218	.0667
In-Plane Thrust Amplitude (mN)	.452	.0488	1.00	.121	.925	.101	.210
Center Thruster Power (W)	534.5	26.3	106.6	147.2	193.6	340.4	476.9
Outboard Thruster Power (W)	2.5	6.9	0.3	0.2	18.8	0.7	3.0
In-Plane Thruster Power (W)	63.4	0.2	14.1	2.0	22.7	3.2	9.5
Fuel Mass (kg)	195.8	581.4	381.5	288.0	195.5	133.0	63.0
Inert (PPU + Thruster) Mass (kg)	554.7	0.5	1.6	2.2	3.0	17.9	31.5
Sail Mass (kg)	1616.4	1609.6	1616	1615	1616.3	1615.5	1614.1
Total Vehicle Mass (kg)	2366.9	2191.5	1999.1	1905.2	1814.9	1766.4	1708.6
Sail Edge Length (m)	41.92	41.83	41.91	41.9	41.92	41.89	41.89
Max Formation Error (m)	3.6	1.6	2.4	2.5	1.7	2.9	2.7

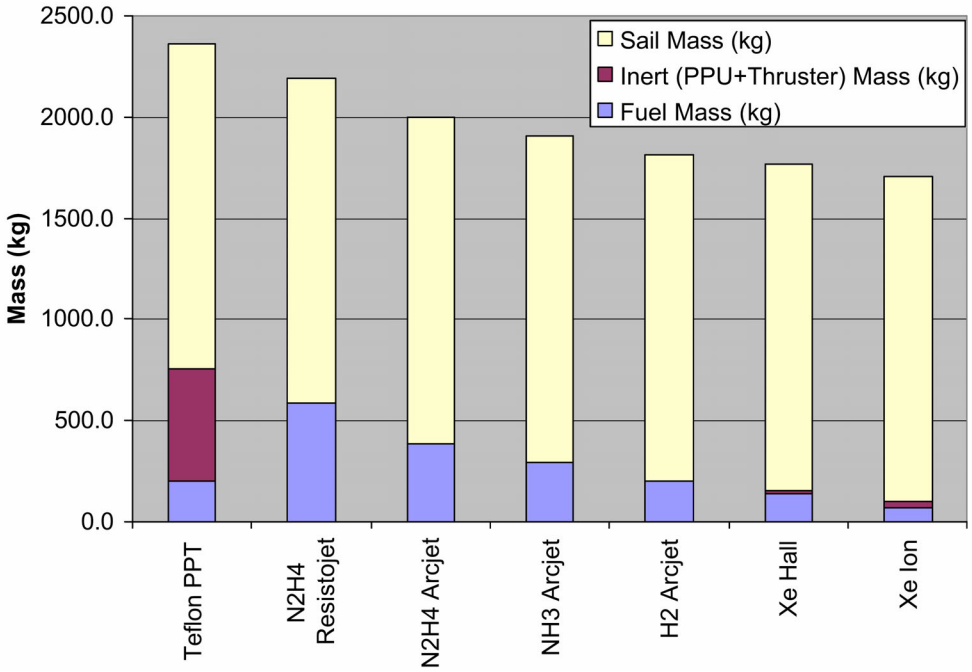

Figure 4-13: Comparison of Total Vehicle Mass for Optimized Trajectories

4.6 Summary

The goal of this work was to investigate practical vehicle sizing and performance requirements for a free-flying 500 kW solar array in orbital formation with a power-consuming host vehicle. To meet these requirements, the sail vehicle must employ propulsion for two functions: formation keeping with host and ACS/Sun-pointing maneuvers. The equations of motion were developed assuming a rigid vehicle subject to gravity, aerodynamic drag, and solar pressure.

For preliminary analyses, investigators calculated the required sail size (mass), and force profiles for three predefined orbital trajectories: 1) minimum aerodynamic drag; 2) minimum gravity gradient torque; and 3) direct sun-pointing. In this analysis, the thrusters were assumed to have unrealistic throttleability and formation-flying constraints. The performance characteristics of a 1000-s specific impulse thruster were assumed as a candidate technology. Results indicated the best performance (lowest vehicle mass) for the direct sun-pointing trajectory, with the minimum gravity-gradient torque as the most massive vehicle. The per-orbit impulse requirements spanned 50 to 98 N-s for the three trajectories studied.

The trajectory study brought to light a design trade-space involving the overall vehicle dimensions (area) and required thruster mass. The trade-space involved balancing propulsion resources with required solar energy absorbed per orbit. The trade is defined by competing effects concerning array sun pointing: 1) if the array normal is allowed to slip from true sun pointing then the propulsion system mass required for attitude control can be reduced; 2) if the array sun-pointing angle deviates from normal, then a larger

(more massive) array area will be necessary to collect the required solar energy per orbit. Based on the competing mass effects an optimal trajectory was pursued. The optimal trajectory depends upon thruster technology, as some thrusters will impose a greater mass expense in order to save a given amount of array area (mass) through attitude control.

Performance characteristics of real EP thrusters necessitated a different approach from the preliminary analysis. Although a generalization, it is prudent to assume that EP thrusters are not throttleable. Thruster hardware is usually designed and optimized for a single performance point (e.g., thrust amplitude, specific impulse) or a narrow range about a fixed point. Thus, the continuously throttleable solution from the preliminary analysis becomes a somewhat unrealistic starting point. Lessons learned from the preliminary analysis were used to estimate realistic EP thrust profiles, employing discrete thrust amplitude pulses, with the goal of achieving desired flight trajectories. It soon became apparent that the relation between the overall vehicle trajectory and the thruster pulse profile was non-intuitive.

A trajectory optimization algorithm and computer code was developed to explore the attitude control/formation flying trade-space for realistic EP technologies. Based on defined orbit parameters, formation constraints, solar energy constraints, and thruster limitations, the optimization routine was capable of calculating the required sail size and mass, thrust amplitude, and thruster firing profile such that the overall vehicle mass was an extremum. The vehicle was configured with eight out-board (moment-producing) thrusters, four center (no moment) thrusters, and four in-plane thrusters of the same technology, but different thrust amplitude. The tool was used to compute the trajectories and associated vehicle sizing parameters for seven canonical EP thruster technologies. The lowest vehicle mass was found to be 1708 kg for a 41.89 m^2 array propelled using xenon ion thrusters in a near-sun-pointing trajectory, with the PPT being the worst performer with a vehicle mass of 2367 kg.

4.7 Conclusions

Although only an exploratory study, the results of this work yield the following conclusions:

- The optimized trajectory found significant propulsion mass savings over analytical design estimates. The optimization tool found a 60% savings on required per-orbit impulse for a hydrogen arcjet when compared with the 1000 second specific impulse canonical case, reflecting an overall vehicle mass savings of 11%
- As propulsive flexibility is made more robust, the optimization tool will exploit the added degrees-of-freedom to provide greater mass savings. The configuration document in this report, that of 16 thrusters distributed as prescribed, likely does not represent a hard minimum vehicle mass. Adding more thrusters, more pulsing repetitions, capability to mix technologies on the same vehicle, thrust vectoring, limited throttleability, etc., are likely to provide improved mass savings.
- Propulsion savings may be possible by relaxing the formation flying constraint. As a starting point, the work reported here constrained the sail vehicle to have a

zero formation error after one orbit. Trajectories calculated according to this constraint displayed a formation position error less than five meters during the orbit for all cases.

- The imposed limitation requiring identical thruster technology was overly restrictive. Examination of the optimized results indicated that the majority of the propulsive work was carried by the center thruster package, while the out-board ACS thrusters were least utilized. As such, the optimized results implied the use of unrealistic technology, such as 700 mW Hall thrusters or 500 W PPTs.
- Although not studied quantitatively, results indicate that an attractive vehicle design could consist of a Hall or ion thruster for the center package, coupled with a PPT as an out-board technology. Such a configuration may be advantageous for a vehicle deployment standpoint: the center of the sail, which will likely consist of the spacecraft bus, can house the xenon technologies and incorporate propellant storage and flow control devices, while the out-board PPTs would require only electric connection. This would make in-space deployment of the stowed vehicle practical and avoid complicated propellant routing.

4.8 Suggestions for Future Work

Results of this preliminary design study naturally led to inspiration for follow-on studies. Aerophyics investigators make the following recommendations for future work:

- At the expense of computation time, an optimization tool could be modified to explore a number of different vehicle configurations with increased flexibility. Specifically, it is recommended to investigate the effects of mixed propulsion technologies on the same vehicle, limited throttleability consistent with thruster state-of-the-art, and limited thrust vectorability. It is reasonable to assume that vehicle mass reductions will arise from such studies.
- The analyses here were performed for a single canonical orbit: 900 km circular in-plane with the sun pointing vector. It is imperative to explore the behavior of different orbital regimes. For instance, as the altitude decreases the effect of atmospheric drag will become more pronounced as will the magnitude of the gravity gradient torque. The resulting optimal trajectory and propulsive needs will differ, as the vehicle must counter different perturbations. Likewise, higher orbits and different inclinations will impact vehicle sizing.
- Flexible vehicle dynamics need to be incorporated into the equations of motion. Distributed mass and modal behavior will influence required per-orbit impulse as well as optimal thrust amplitudes and pulse firing history. The effects of spacecraft flexibility are not readily intuitive.

4.9 References

[1] Martinez-Sanchez, M., and Pollard, J.E., "Spacecraft Electric Propulsion – An Overview," Journal of Propulsion and Power, Vol. 14, No. 5, September – October 1998, pp. 688 – 699.

5 Virginia Tech University Design Study

Final Report

Project Title :	PowerSail High Power Propulsion System
Contract Number:	F04700-01-P-0047
Submitted:	June 1, 2001
Submitted By:	Christopher D. Hall, Associate Professor Department of Aerospace and Ocean Engineering Virginia Polytechnic Institute and State University Blacksburg, VA 24061 (540) 231-2314 (540) 231-9632 (FAX) chall@aoe.vt.edu
Principal Investigator:	Christopher D. Hall, Associate Professor Department of Aerospace and Ocean Engineering
Submitted To:	Dr. Frank S. Gulczinski III AFRL/PRSS 1 Ara Road Edwards AFB, CA 93524-7013
Prepared By:	Brian Borchardt, Elizabeth Cantando, Nicholas DeFazio, Adam Harvey, Coelle Schott, Ann-Marie Townsend, and Jonathan Woodward

Abbreviations

ADCS	Attitude Determination and Control System
C&DH	Command and Data Handling
CIS	Copper Indium Diselinide
CP1	Clear Polymide
DI	Discharge Initiation
GA AS	Gallium Arsenide
GA IN	Gallium Indium
GEO	Geostationary Earth Orbit
GPS	Global Positioning System
IAA	Instantaneous Access Area
IR	Infrared
IVP	Individual Pressure Vessel
LEO	Lower Earth Orbit
LiCF	Lithium Sulfur Dioxide
LiOCI2	Lithium Carbon Monofluoride
LiSO2	Lithium Thionyl Chloride
MLI	Multi-Layer Insulation
NiCd	Nickel Cadmium
NiH	Nickel Hydrogen
PPT	Pulse Plasma Thrusters
PPU	Power Processing Unit
RAAN	Right Ascension of Ascending Node
SPT	Stationary Plasma Thrusters

Symbols

θ	Incidence angle of the sun
a	Albedo
A	Array area
A	Surface area of the satellite
A	Cross sectional area of the conductor
A_c	Area of the solar cell
A_c	Cross sectional area of the component
A_{sa}	Area of the solar array
c	Speed of light
D_r	Distance between the Host and PowerSail
Eff	Efficiency of the solar cell
eff	Efficiency of solar cells
F	View factor
G_s	Solar flux
H	Altitude of PowerSail
I	Current
JD	Julian date
k	Control constant
K_a	Reflection of collimated energy
L	Length of the umbilical
L_d	Lifetime degradation
M_{sun}	Mean anomaly
N	Number of solar cells needed
N_p	Number of solar cells per panel
P_{BOL}	Power at the beginning of life
P_{bus}	Power required by the bus
P_d	Total power required
P_{EOL}	Power at the end of life
P_{Host}	Power required by the Host
P_l	Power loss for umbilical
P_o	Estimate power output
P_{sa}	Power of the solar array
q	Heat transfer
Q_a	Total absorbed energy
Q_{Aa}	Absorbed albedo energy
Q_e	Emitted radiation of array
q_I	Infrared radiation flux
q_{Ia}	Absorbed IR radiation flux
Q_{sa}	Absorbed solar energy
Q_w	Internal energy dissipation
r	Radius vector
R	Resistance
R_E	Radius of Earth
r_{ref}	Position vector of PowerSail

R_{sun}	Distance to the sun
S	Solar flux
t	Time
T_{max}	Maximum temperature
T_{min}	Minimum temperature
T_{uti}	Universal time
U_{lyap}	Acceleration using Lyapunov controller
V	Voltage
V_{bus}	Voltage of the bus
V_r	Relative velocity between Host and PowerSail
α_b	Absorptivity of bottom of solar array
α_t	Absorptivity of top of solar array
ε	Emissivity
ε_b	Emissivity of top of solar array
ε_t	Emissivity of top of solar array
$\lambda_{elliptic}$	Long elliptic plane
λ_{sun}	Mean longitude
μ	Gravity parameter
ρ	Angular radius of Earth
ρ	Resistively of the conductor
σ	Boltzmann's constant
σ	Absorptivity
τ	Placement variable
ϵ	Oblique of the elliptic

5.1 Problem Definition

5.1.1 A Descriptive Scenario

The goal of society has commonly been to make products that are bigger and better. Technology is pushing the limits of space exploration with size frequently defining that limit. But what happens when the requirements of the mission exceed the available power?

Satellites today not only have longer lifetimes, but they are also larger and require more power. As the power requirements of the spacecraft increase, so do volume and mass. For most satellites in Earth orbit, the power subsystem is a large portion of the spacecraft and includes solar arrays and batteries. The power subsystem can limit the capabilities of the spacecraft due to volume and mass constraints. The ability for a spacecraft to power itself has been a design constraint since the beginning of space flight. The cost of launching a satellite into orbit greatly dictates the mass permitted in the payload of a launch vehicle. Imagine the possibilities if one could find a way to eliminate some of that mass and reserve it for other purposes. A satellite could have more scientific equipment, more propellant, or less mass if an alternate power supply were available. The PowerSail concept is a potential solution to this dilemma of balancing a spacecraft's mass with its design needs.

The most common method of collecting power is the use of solar panels to convert solar radiation to electrical energy. Not only are solar panels massive, but also they affect the dynamics and control of a spacecraft. Solar panels change the natural frequency of spacecraft, obstruct the field of view, and occasionally are the focus of repair missions.

PowerSail is a large flexible solar array connected to a Host satellite through a slack umbilical. It will provide up to 50 kW of power with minimal dynamic and structural interference. The use of PowerSail eliminates the aforementioned design constraints imposed on a spacecraft using solar panels by supplying power from a separate source.

Consider the Hubble Space Telescope, a giant observatory telescope in space flanked on both sides by large solar panels. Visualize the telescope without the panels; mobility would improve and there may be fewer hardware interfaces. The goal of this project is to develop the most effective and cost efficient PowerSail to provide energy to high-powered satellites. This semi-autonomous spacecraft will possess the ability to collect and store energy from the sun and deliver the stored power through an umbilical to a Host spacecraft.

5.1.2 Societal Sectors and Disciplines Involved

As with any other satellite, numerous engineering disciplines are needed to design PowerSail. Mechanical engineers are needed to design the structure for PowerSail, including the support structure for the solar array and the complex folding mechanism needed to stow PowerSail during launch. The solar arrays, along with other external components, are susceptible to rapid heating and cooling due to the extreme temperature

variations in space. These extreme temperature variations cause thermal gradients on the solar arrays, which produce severe vibrations. Thermal engineers design a thermal system after studying the effects of the thermal gradients on solar arrays, and the thermal needs for the rest of the spacecraft. Aerospace engineers are needed to determine the orbital attitude and control as well as model the dynamic fluctuations of the solar array to meet the lifetime requirements of the spacecraft. Electrical engineers and computer programmers are needed to collect and transmit data to its ground base through programming and coding. As with any satellite, electrical engineers are required to design the electrical subsystem of PowerSail. This will be complicated since PowerSail needs to transfer power from one satellite to another and possibly share subsystems. Finally, the propulsion experts are tasked with designing an electrical propulsion system.

Utilizing PowerSail will increase the available power for the Host spacecraft, thus expanding the capabilities of the Host satellite. This increase in available power will affect a number of organizations, including defense contractors such as TRW and Lockheed and governmental departments such as the Central Intelligence Agency, National Security Agency, and the Department of Defense. Also government-financed institutions such as the Jet Propulsion Laboratory, Applied Physics Laboratory, and National Aeronautical and Space Administration would be interested in a PowerSail system. Commercial satellites with high power requirements could also benefit from PowerSail.

5.1.3 Assessment of Scope

PowerSail is a free-flying solar array with the capability to accommodate any orbit from 1000 km to geostationary orbit at any inclination. PowerSail collects solar energy in order to supply a satellite with power as high as 100 kW. PowerSail uses electric propulsion for orbital and attitude control. The system has a deployable array of flexible solar cells to collect and convert solar energy to electrical energy and provide power to the Host spacecraft through a slack umbilical. The array must provide a minimum of 50 kW of power to the Host satellite. PowerSail interferes as little as possible with the Host spacecraft and must not block the Host's view of the Earth. Structural and dynamic interference must be minimized. The most efficient launch vehicle will be selected based on mass, the complexity of deploying the solar array, and its connection with the Host satellite. Once in orbit and operational, the satellite will have a minimum lifetime of 10 years with minimal maintenance required.

PowerSail utilizes existing space-rated technology to accomplish the mission requirements. The solar cells and sail material will be bought from off-the-shelf technology, along with the battery. An off-the-shelf communications system will be employed if deemed necessary. Existing propulsion systems for attitude control thrusters and the launch vehicle will be utilized. All structural components of the spacecraft will be from existing technology and will most likely be flexible and possibly inflatable.

5.1.4 Needs, Alterables and Constraints

Spacecraft subsystems interact with other subsystems in order to complete tasks. The design of each subsystem must take into account the level of interaction of the particular

subsystem with the rest of the spacecraft. Table 5-1 charts each subsystem and its interaction with others. Section 5.2 discusses these interactions further.

Table 5-1: Interactions of Needs, Alterables and Constraints

		Constraints							Needs						Alterables		
		50 kW Power to Host Satellite	Any Orbit Between 1000 km to GE	Any Inclination	Slack Umbilical	Electric Propulsion	10 Year Lifetime	New Technology Required	Dynamic Interference	Structural Interference Minimized	Blocking Minimized	Cost Minimized	Stowed Volume Minimized	Mass Minimized	Launch Vehicle	Shape	Length of Umbilical
Alterables	Subsystem Sharing	1	0	0	0	0	0	0	0	0	0	1	1	2	1	0	0
	Length of Umbilical	2	2	0	2	0	0	0	2	2	2	1	1	1	0	1	
	Shape	2	0	0	2	2	0	0	2	2	2	1	2	2	2		
	Launch Vehicle	2	2	2	0	2	0	0	0	0	0	2	2	2			
Needs	Mass Minimized	2	1	0	1	2	1	2	0	2	0	2	2				
	Stowed Volume Minimized	2	0	0	1	1	0	2	0	0	0	2					
	Cost Minimized	2	1	1	1	2	2	2	1	2	1						
	Blocking Minimized	2	2	0	2	2	0	2	2	1							
	Structural Interference Minimize	2	0	0	2	0	0	2	2								
	Dynamic Interference Minimized	2	2	0	2	2	0	2									
Constraints	New Technology Required	2	0	0	1	2	0										
	10 Year Lifetime	0	0	0	1	2											
	Electric Propulsion	1	2	0	2												
	Slack Umbilical	2	0	0													
	Any Inclination	1	0														
	Any Orbit Between 1000 km to	1															

0-no interaction, 1- some interaction, 2 – numerous interactions

5.1.5 Partitioning of the Problem into Relevant Elements

Through astrodynamics and mission analysis, the attitude control system is sized to include the attitude sensors and actuators, and performance predictions. An umbilical is used to transfer power to the Host satellite. The umbilical causes unique dynamics on both the Host and PowerSail. The mission geometry, guidance, and navigation of the Host satellite determine the level of attitude dynamics and control of PowerSail. The method of propulsion affects which electric propulsion unit the PowerSail uses for both orbital and attitude control. The attitude determination and control system involves the advanced guidance navigation and control concepts of PowerSail.

The power, thermal and environment group constitutes the basis of PowerSail's design. The power subsystem includes the solar array design and cell selection, load, and batteries to store the power captured by the solar cells for PowerSail's use. The thermal and environment subsystems work together to ensure that the correct environment exists so the systems of PowerSail operate nominally in and out of the sun. This deals with the

high efficiency flexible thin-film photovoltaic solar cell blankets. Heat flow analysis and thermal management system design are areas of expertise in this field.

The structures and mechanisms team designs the large deployable or inflatable structure to hold the solar cells. This group also develops a mass property spreadsheet, and performs stress analysis. They also pick the ideal launch vehicle interface along with the deployment mechanisms and Host satellite interface. This team determines the appropriate launch vehicle depending on mass, volume, and orbit considerations.

Program management controls all disciplines and brings all areas of work together to a final design. Management also develops mission plans and mission operations along with a detailed schedule of activities for development and deployment of the system. The program manager also controls the budget and analyses success probability of the project. The cost modeling and reliability of PowerSail involves a cost estimate of production, deployment, and operations.

Mission operations and ground systems personnel identify all the major features of the mission architecture and run fly-over details. These people are concerned with economic, political, and legal systems, which determine the end of life disposal procedures and ensure the design of the satellite satisfies all political constraints. They consider all possibilities for their satellite so that other missions might be adapted in case of primary mission failure or change. Mission operators are responsible for the success of the mission from launch to shutdown.

5.1.6 Problem Element Interactions

The different subsystem teams of the PowerSail project work together in order to conceive an effective design. Table 5-2 indicates the subsystem interaction levels. These subsystem teams work closely together throughout the design process to ensure that appropriate consideration is given to subsystem interactions.

Table 5-2: Problem Element Interactions

	Mission Operations, Ground Systems	Structures	Mechanisms	Thermal	Power	Command and Data Handling	Communications	Attitude Determination and Control	Propulsion
Guidance and Navigation	2	0	0	0	2	2	1	2	2
Propulsion	2	1	2	1	2	1	0	2	
Attitude Determination and Control	2	2	1	2	2	1	2		
Communications	2	1	0	1	2	2			
Command and Data Handling	2	1	0	1	2				
Power	2	2	2	2					
Thermal	1	2	2						
Mechanisms	2	2							
Structures	1								

0=no interacion, 1=some interaction, 2=much interaction

5.1.7 Summary

Supporting the missions of PowerSail requires the subsystems between the spacecraft to work together in a process efficiently. There are many different solutions to this problem. The least massive, least interactive and most efficient concept will win approval and move from the conceptual to design phase. To begin, though, subsystem interactions are studied and analyzed.

5.2 Value System Design

5.2.1 Introduction

A method of measuring design parameters is needed to develop the best PowerSail system possible. To design the most efficient PowerSail system, system objectives are created based on the needs, alterables, and constraints described in Section 5.1. Each objective is assigned a design priority. The objective hierarchy in Figure 5-1 relates the different objectives of PowerSail. The weights are odd numbers between 1 and 9: 1 being a crucial objective to an efficient PowerSail design, and 9 being the least crucial. The objective hierarchy is applied to the different conceptual designs discussed in Sections 5.3 and 5.4. After analysis of each concept, a final design is chosen based on the MOE's and the effectiveness of the design in satisfying or exceeding the objectives. The following paragraphs discuss the relationships between the different levels of the hierarchy and the weights assigned to each.

5.2.2 Value System Design

The value of each objective changes depending on the chief decision-maker ensuring the production of the most efficient design leading to a product favorable to customers and mass production. The production cost of PowerSail has a lower priority than its performance characteristics. Therefore, the efficiency of PowerSail is twice as important as cost in selecting the best alternative. The production cost of PowerSail is three times more important than operational costs. It is desirable to have a product capable of mass production. The operational cost is determined to be low due to the simple task of PowerSail and the high autonomy.

Fractional parts of 20 are assigned to design criteria to determine the most efficient design. A greater fraction of 20 indicates a less essential design property. A small fraction of 20 specifies an important property. The primary mission of PowerSail is to supply 50 kW of power to a spacecraft through transferring converted electrical energy through a slack umbilical. The high power requirement of PowerSail mandates the use of high efficiency solar cells on the order of 16 percent efficiency. The solar cells determine the size and shape of the solar array, which contribute to most of the mass and stowed volume of PowerSail. For this reason the weight assigned to high efficiency solar cells is 1/20.

The mass of PowerSail is important to many aspects of the complete mission. The mass of the solar array guides the design of the propulsion system and batteries needed on PowerSail. For example, the area of the array affects the total mass of the solar array which is directly proportional to the size of the propulsion system that is proportional to the size of the batteries. For this reason, minimizing the mass of the solar array is designated a weight of 2/20. Minimizing the total mass is also important because it allows the Host satellite to have a greater mass and volume. Minimizing PowerSail mass is also important to satisfy the need of having PowerSail and its Host spacecraft launch on the same launch vehicle.

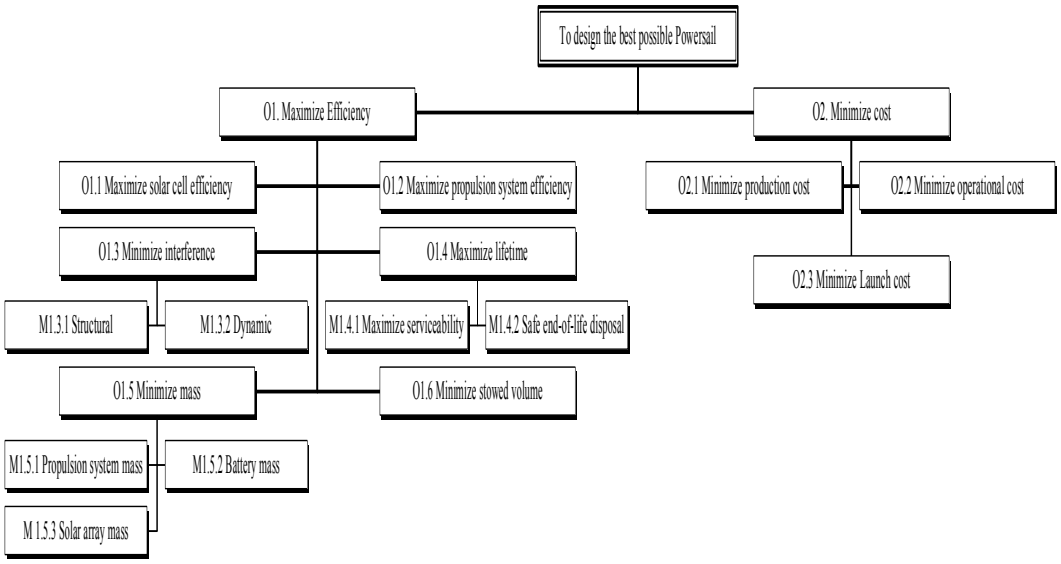

Figure 5-1: Objective Hierarchy

PowerSail is considered a subsystem of the Host spacecraft, meaning most of PowerSail's subsystems are shared with the Host satellite. Although considering PowerSail in this manner simplifies the design and decreases the mass and volume of PowerSail, careful considerations must be taken to limit the interference between the two spacecraft. Interference comes in two forms: either structural or dynamic. Dynamic interference from the vibrations of the umbilical connecting PowerSail to the Host must be minimized in order to allow the Host to accomplish its mission. Structural components of PowerSail blocking the Host's communication and sensor systems cause interference, violating a constraint of PowerSail. A slight amount of interference is possible with the interaction between shared subsystems; however, it must be limited. The total interference of PowerSail on the Host satellite is rated a weight of 4/20 and structural interference is selected as slightly less important than dynamic interference.

PowerSail must be disposed of at the end of its lifetime. The most common method of disposing satellites today is controlled de-orbits to allow them to burn up in the atmosphere. However, depending on the orbit, placing PowerSail in a supersynchronous orbit may be more efficient. In either case, the PowerSail must be disposed without creating orbital debris that will hinder the mission operations of other spacecraft. A

weight of 4/20 is assigned to an efficient end-of-life disposal.

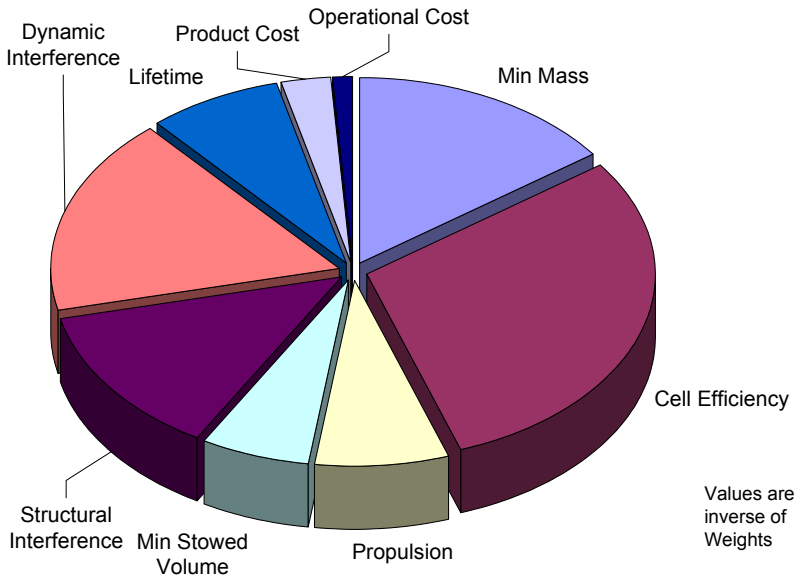

Figure 5-2: Importance of Design Variables

The propulsion subsystem is given a weight of 4/20. The system is important to the design of PowerSail although not an overriding factor. Most electric thrusters can be selected to perform the job satisfactorily. Likewise, the minimum stowed volume is important to the design of PowerSail especially in its launch. For this reason the value of the stowed volume is 5/20.

Using the measures of effectiveness discussed in this chapter, the different conceptual designs generated in the System Synthesis (Section 5.3) are compared and analyzed in System Analysis (Section 5.4) and all but one are eliminated. This design is developed in the preliminary design phase.

5.2.3 Conclusion

The application of the value system design will lead us to the best alternative design to study further. Figure 5-2 is a chart studying the effects of the property weights in the entire selection process. Because desirable properties lead to a smaller number, the inverse of the weights is plotted in the pie chart. It is clear that the solar cell efficiency, mass, and interference are the overriding factors in selecting the best design. Total cost and stowed volume are of lesser importance, as you can see from the figure.

5.3 System Synthesis

5.3.1 Introduction

The objective of the system synthesis chapter is to generate alternatives for components of each subsystem as well as to conceptualize possible designs for PowerSail. Each of the alternatives generated in this section will be ranked according to our value system design. From these rankings we will choose the top one or two configurations to analyze further. This is a critical step in the design process, which helps identify alternatives while withholding judgment.

5.3.2 Configurations

5.3.2.1 Kite Tail

The kite tail configuration incorporates a formation of solar arrays to complete the mission objectives. Instead of a single large array, a group of smaller arrays provide a total of 50 kW of power. The satellites are strung in a line, each attached by a slack umbilical. There are two types of satellites in this configuration: a command satellite and the power supply arrays. The command satellite is responsible for controlling the formation and attitude of the power supply arrays.

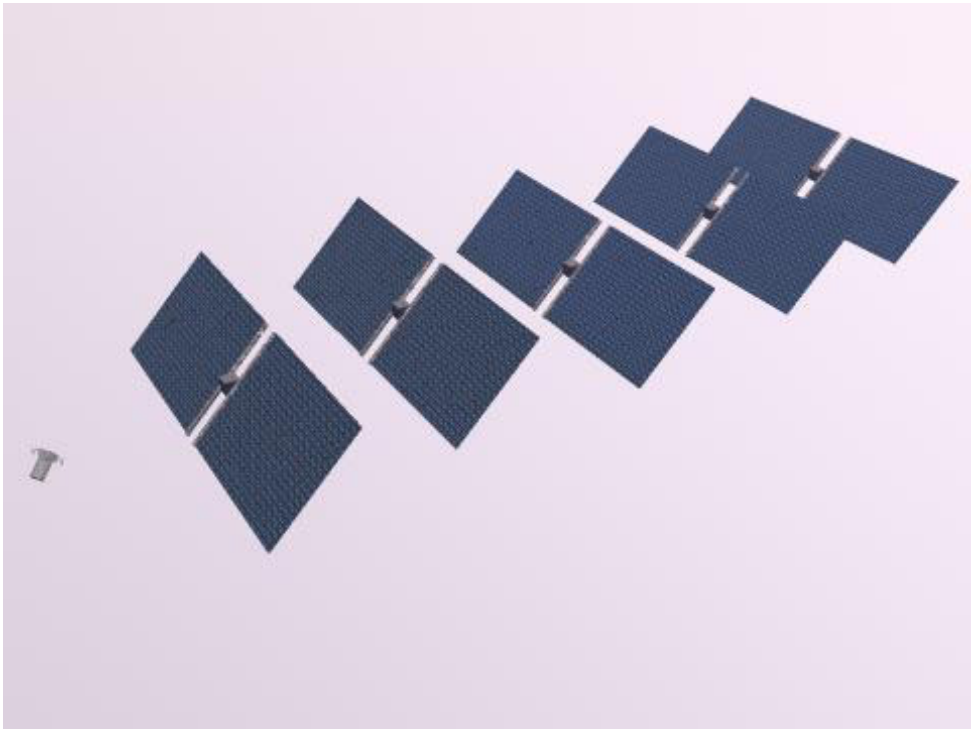

Figure 5-3: Kite Tail Configuration

The command satellite is equipped with solar arrays and batteries for its own use. The array on the command satellite also provides some power to the Host satellite. Each

power satellite generates power for the Host and itself. Batteries for the ADCS are located on each power satellite. The power needs of the Host satellite determine the number of power satellites.

5.3.2.2 Sphere

The sphere concept is a single solar array. The array is a large sphere, akin to a balloon, covered with flexible solar cells. Filling the balloon with compressed gas inflates the array. The housing for internal components of the system is located at one edge of the array. The slack umbilical is attached to the housing. The thrusters for attitude control are located on the housing and on a mounting opposite the housing. There are supports located in and on the array to maintain the structure of the system. The pointing requirements of this system are decreased since the array is spherical and any orientation collects the same energy from the sun.

Figure 5-4: Sphere Configuration

5.3.2.3 Fan

The fan design is a deployable structure that deploys in a similar fashion to a folding fan. When deploying, the solar array rotates about the central point creating a circular array. Similar to a Venetian blind, the solar cells will not likely be directly perpendicular to sunlight. The bus of the system is located in the center of the deployed structure. The umbilical is connected to the bus.

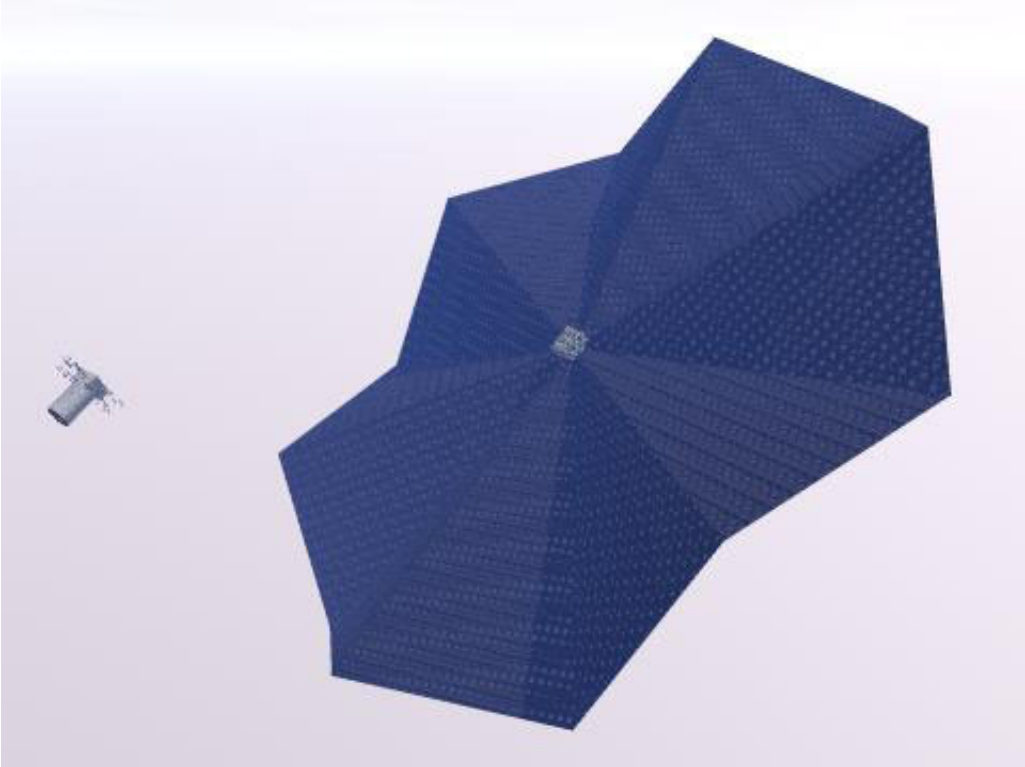

Figure 5-5: Fan Configuration

5.3.2.4 Flat Array

The flat array configuration is comprised of five deployable booms and a main bus. This configuration is a planar array with thin flexible solar arrays, in which the central boom deploys first. The side booms deploy simultaneously, deploying the flexible solar arrays. The bus structure is inherently small compared to the size of the array. The umbilical, thrusters, and attitude sensors are located on any part of this structure. This configuration has a relatively small stowed volume and small mass. The booms can also be designed to retract if needed.

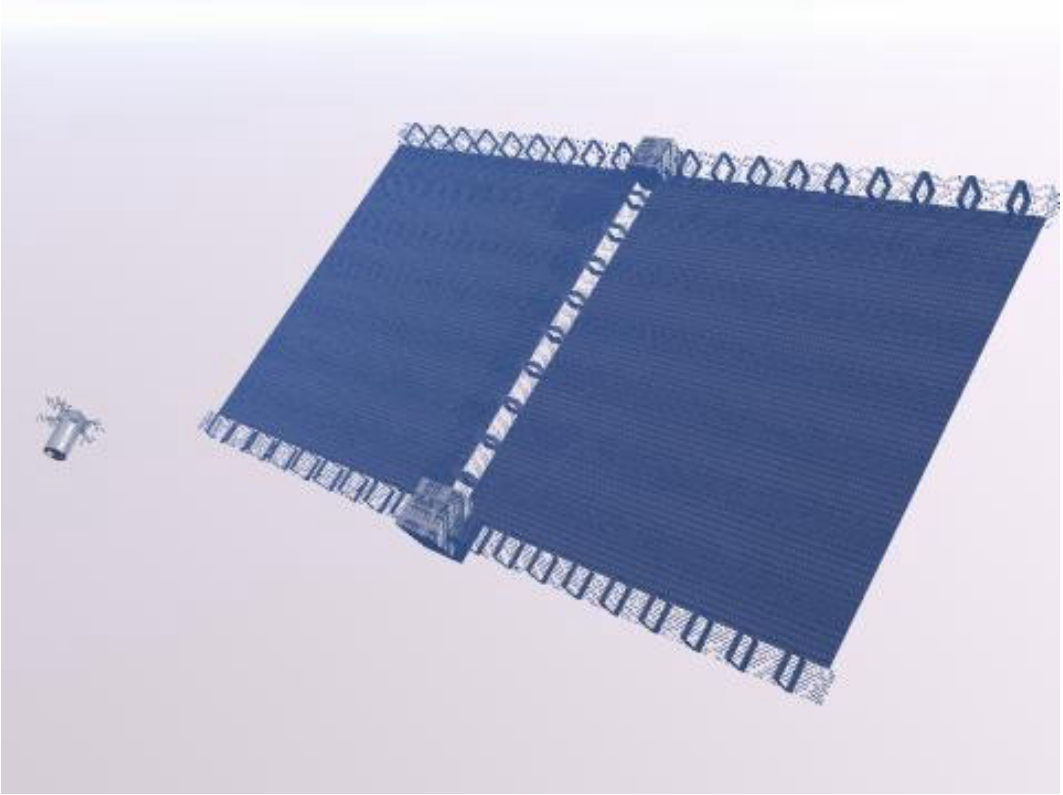

Figure 5-6: Flat Array Configuration

5.3.3 Electrical Power Subsystem

5.3.3.1 Solar Cells

There are many types of space-rated solar cells available. Five types of photovoltaic solar cells are silicon, thin sheet amorphous silicon, gallium arsenide (GaAs), indium phosphide, and multijunction GaIn/GaAs. Each cell has different characteristics that determine which is best for a particular mission.

The first of the photovoltaic solar cells is crystalline silicon, a blue anti-reflective cell with 95% absorption. Crystalline silicon has a planar cell theoretical efficiency of 20.8%, with an achieved efficiency for production of 14.8%. The best laboratory efficiency achieved is 20.8% (Ref 37, p. 414). The electrical output for an open circuit is 0.55 volts (Ref. 37, p. 412). The electrical output for a short circuit is 0.275-0.3 amps. Crystalline silicon cells have a light level of 1000 W/m^2 at a temperature of 25°C, meaning it can create 1000 W for every square meter. The equivalent time in geosynchronous orbit for 15% degradation for 1 MeV electrons is 10 years and 4 years for 10 MeV protons.

A second type of photovoltaic solar cell is a thin sheet of amorphous silicon. This material is useful because the cells are flexible and can roll up, if required. These cells

have a planar-cell theoretical efficiency of 12%, an achieved efficiency for production of 5%, and 10% efficiency for best laboratory tests. The equivalent time in geosynchronous orbit for 15% degradation for 1 MeV electrons is 10 years and 4 years for 10 MeV protons.

Gallium arsenide is a third type of photovoltaic solar cell. These solar cells are unique because they are liquid cooled with a light-conditioning feature that removes unusable wavelengths from the light spectrum. The planar-cell theoretical efficiency is 23.5% with an achieved efficiency for production of 18.5% and a laboratory efficiency of 21.8%. The equivalent time in geosynchronous orbit for 15% degradation for 1 MeV electrons is 33 years and for the 10 MeV protons is 6 years.

A fourth type of photovoltaic solar cell is indium phosphide. These cells along with gallium arsenide resist radiation better than silicon and provide greater end-of-life power for a given area. They have a planar cell theoretical efficiency of 22.8%, an achieved efficiency for production of 18%, and a best laboratory efficiency of 19.9%. The equivalent time in geosynchronous orbit for 15% degradation for 1 MeV electrons is 155 years and 89 years for 10 MeV protons.

The last type of photovoltaic solar cell presented is a multijunction GaIn/GaAs cell. "A multijunction device is a stack of individual single-junction cells in descending order of band gap. The top cell captures the high-energy photons and passes the rest of the photons on to be absorbed by lower-band-gap cells. Multijunction devices achieve a higher total conversion efficiency because they convert more of the energy spectrum of light to electricity" (Ref. 37, p. 415). Their planar cell theoretical efficiency is 25.8%. They also have a production-achieved efficiency of 22.0% and a best laboratory efficiency of 25.7%. Their equivalent time in geosynchronous orbit for 15% degradation for 1 MeV electrons is 33 years and for 10 MeV protons is 6 years.

5.3.3.2 Batteries

There are two main power sources on today's orbiting spacecraft: primary batteries, and solar power. Primary batteries are not rechargeable and are specifically used in short-duration missions. Secondary batteries are used in conjunction with solar cells to provide power to a spacecraft. Since the idea behind PowerSail is to harness the sun's energy to provide 50 kW of power to a Host satellite, secondary batteries will be the source of energy storage. Secondary batteries are for a solar-array-powered system and supply power for the electrical load when in eclipse or when the load exceeds the power supply of the solar array. The different secondary batteries on the space market today are chosen based on the power needs, lifetime, and orbit of the spacecraft. The important properties one looks for when choosing a battery are high lifecycles, high energy density, summarized in Table 5-3, depth of discharge (DOD), and wide-range operating temperature. In the following sections, different types of secondary batteries are discussed for possible use on PowerSail (Ref. 37, p. 417).

5.3.3.2.1 Nickel Cadmium

Nickel cadmium cells (NiCd) have been used on most spacecraft in the past decades of

the space program. Nickel cadmium cells have high lifecycles, high specific energy density, and the simplicity of their power regulation system. Nickel cadmium cells have an average energy density of 25 to 30 W-hr/kg (Ref. 37, p. 420). They generally never discharge a full 100%. The maximum DOD depends on the number of life cycles. After discharging the battery to only 35% for many cycles, the battery develops a memory and will not discharge further than that 35% if more power is needed. This problem is solved by discharging the battery fully to erase the memory and allow any amount of discharge at any time. "Increased cycle life reduces the amount of energy available from the batteries during each cycle – DOD decreases with cycle life" (Ref. 37, p. 421). In summary, the number of lifecycles is considered when sizing a battery so it can store the amount of power needed at the end of life, after battery degradation.

5.3.3.2.2 Nickel Hydrogen

There are three different types of nickel hydrogen batteries: individual pressure vessel, common pressure vessel, and single pressure vessel. Each type has similar operational procedures. The most common of these is the individual pressure vessel (IVP). The IVP NiH battery cell withstands between 400 to 900 PSI of internal pressure during overcharge. It has a longer life than the nickel cadmium batteries. Also, the hydrogen gas does not fade or become coated with metallic oxides, as do the cadmium plates. NiH batteries have a greater overcharge rate tolerance since the hydrogen combines with the oxygen produced in the NiH cells to produce water. These advantages combine to improve the lifetime of the NiH batteries versus the NiCd batteries by at least a factor of four (Ref. 37, p. 421).

5.3.3.2.3 Lithium Ion

As displayed in Table 5-3, lithium ion batteries ($LiSO_2$, LiCF, LiSOCl2) have significantly higher energy densities than their NiCd and NiH counterparts. The lithium ion technology offers a 65% decrease in volume and a 50% mass decrease over the present day spacecraft battery applications. Since this is a fairly new technology, it is not yet qualified for space applications. By 2005-2010 it will be space qualified for applications between low earth orbit and geosynchronous earth orbit.

Table 5-3: Characteristics of Secondary Batteries (Ref. 37, p.420)

SECONDARY BATTERY COUPLES	SPECIFIC ENERGY DENSITY (W-hr/Kg)	STATUS
NiCd	25-30	Space qualified, extensive database
NiH (individual pressure vessel)	35-43	Space qualified, good database
NiH (common pressure vessel)	40-56	Space qualified for GEO and planetary missions
NiH (single pressure vessel)	43-57	Space qualified
$LiSO_2$, LiCF, LiSOCl2	70-110	Under development

5.3.3.3 Power Regulation

The electrical power generated by the solar array must be regulated to prevent battery

overcharging and undesired heating. The two main power regulation subsystems used with photovoltaic solar cells are peak-power trackers or direct-energy-transfer subsystems (DET). There are a variety of power control subsystems, which depends on the regulation system chosen. Table 5-4 shows the steps in the power regulation and control subsystem design.

Table 5-4: Steps in the Power Regulation and Control System Design (Ref. 37, p. 427)

STEP	CONSIDER	POSSIBILITIES
Determine power source	All spacecraft loads, their duty cycles, and special operating modes	Primary batteries Photovoltaic Static power Dynamic power
Design the electrical control subsystem	Power source Battery charging Spacecraft heating	Peak Power Tracker Direct-Energy Transfer
Develop the electrical bus voltage control	How much control each load requires Battery voltage variation from charge to discharge Battery recharge subsystem Battery cycle life Total system mass	Unregulated Quasi-regulated Fully Regulated

5.3.3.3.1 Peak-Power Tracker

A peak power tracker operates in series with the solar array, changing the operating point of the solar array source to the voltage. When the peak power point demand exceeds peak power, the operating point changes to the voltage side of the array, and the tracker tracks the peak-power point. The array voltage increases to its maximum power point, and the converter transforms the input power to equal the output power at a different voltage and current. Shunt-regulation, discussed below, is not needed with the peak power tracker because it backs off the peak power point of the arrays toward the end of the batteries charging period. A peak power tracker has advantages for missions of less than 5 years that require more power at beginning of life than at end of life (Ref. 37, p. 425).

5.3.3.3.2 Direct-Energy-Transfer (DET)

Direct-energy-transfer systems run in series with the solar array and require a shunt regulator to control the array current. The shunt is typically located at the array and shunts the current away from the battery subsystem when power is not needed. Overall, DET systems are more efficient than peak power trackers because they dissipate little energy, have lower mass, and fewer parts.

5.3.3.4 Electrical Bus Voltage Control

5.3.3.4.1 Unregulated System

In an unregulated system the load bus voltage varies. "The bus-voltage regulation derives from battery regulation which varies about 20% from charge to discharge." (Ref. 37, p. 426). The load bus voltage is the voltage of the batteries.

5.3.3.4.2 Quasi-Regulated System

In a quasi-regulated system, the bus voltage is regulated during battery charge only, and a charger is in series with the batteries. This system is inefficient and has electromagnetic interference if used in conjunction with a peak power tracker.

5.3.3.4.3 Fully Regulated System

A fully regulated system uses charge regulators during the charge and discharge cycles of the battery. The only advantage of this type of DET is that it behaves like a low-impedance power supply when connected to loads. This simplifies design integration of the subsystems. Otherwise, fully regulated transfer is inefficient and only works on a spacecraft that requires low power and a highly regulated bus.

5.3.3.5 Propulsion Subsystem

Propulsion systems on space vehicles have many purposes, such as station keeping and attitude correction. Attitude is especially significant in orbit transfer burns to maintain a correct orbit. If an orbit transfer is required, the propulsion system provides thrust to achieve the transfer. Orbit transfers can be a mission requirement or used to correct the vehicle's orbit.

5.3.3.5.1 Propulsion Options

PowerSail must have an electric propulsion system. Currently there are few space-rated and production electric propulsion systems. An electric propulsion system accelerates a working fluid to high velocity (in comparison to other propulsion types) to produce thrust. There is no real design limit to the velocity of the exhaust plume. The thrust of the system reaches a point of diminishing returns for power consumption as velocity of the plume increases. The type of propulsion system determines the level of power required to produce additional thrust efficiently. The optimum exhaust plume velocity determines the optimum specific impulse (Ref. 37, p. 702). The following is a list of possible electric propulsion systems for use in the PowerSail project.

5.3.3.5.2 Ion Thruster (IT)

Ion thrusters are among the highest specific impulse propulsion systems currently available. The propellant of an IT is produced by separating neutral propellant into ions and electrons. The ions pass through a strong electrostatic field and are accelerated to high speeds. The thrust of the rocket is produced by the total reaction of the accelerating forces. (Ref. 37, p. 706) One way of separating the propellant has propellant atoms ionized by electron bombardment. The electrons are emitted by a cathode surface and gain energy from the potential difference between cathode and anode surfaces in a bombardment ionization chamber. Propellant for an IT is generally one of three

elements. Mercury was the original propellant choice for the Kaufman IT (Ref. 21). Though a mercury propellant has the highest potential thruster efficiency, the Kaufman IT has been adapted to use Xenon and argon due to environmental concerns. Xenon has almost as high a thrust efficiency as mercury (Ref. 17, p. 660). This efficiency is on the order of 85-90%. An arcjet or resistojet is more efficient than an IT when specific impulse values are within the range of 1000-2000 seconds. An IT ejects a high velocity charged plume presenting issues in multi-satellite formations.

5.3.3.5.3 Pulsed Plasma Thruster (PPT)

A PPT is an inherently pulsed device that features small impulse bit capability, use of a solid propellant (Teflon™), and the ability to operate at near constant performance over large power ranges (Ref. 37, p. 705). The plasma created in a PPT is an electrically neutral mixture of ions, electrons, and neutral particles flowing at high temperature in a fluid stream (Ref. 17, p. 653). The plasma is created by an electric discharge across the Teflon that produces a fluorpolymer gas. Pressure forces and the interaction of the discharge current and its self-generated magnetic field accelerate the hot gas.

5.3.3.5.4 MagnetoPlasmaDynamic Thruster (MPD)

In an MPD thruster, current-carrying plasma interacts with a magnetic field resulting in a Lorentz acceleration to expel the plasma (Ref. 37, p. 701). Experiments have been done using argon, helium, ammonia, and hydrogen propellants (Ref. 17, p. 680). The magnetic field is created using loops of wire with a running current. The loop induces a magnetic field. The plume of an MPD thruster is highly charged and has high velocity. Currently there are no operational MPD thrusters that are available for use.

5.3.3.5.5 Resistojet

A resistojet is an electrothermal rocket that uses nitrogen, ammonia, or hydrazine as a propellant. The resistojet may have a throat diameter as small as 1 mm (Ref. 17, p.653). A resistojet can operate with a wide variety of propellants. A resistojet can utilize liquid waste and thus are available for use on the space station to produce thrust for orbital maintenance. Electric energy heats the working fluid, which then acts like a standard thruster. A resistojet has a thrust-to-power ratio higher than other electric propulsion systems (Ref. 37, p. 703). The dry mass of the system is less than other systems due to the lack of a power processor. A resistojet also has an uncharged and benign plume.

5.3.3.5.6 Arcjet

An arcjet uses an electric arc discharge to increase the temperature of the propellant. The high temperature propellant is then expanded in a conventional nozzle. Helium is the most attractive propellant due to its low molecular weight and its dissociation properties (Ref. 17, p. 677). Arcjets have about twice the specific impulse of resistojets while maintaining some of the benefits (Ref. 37, p. 704).

5.3.3.5.7 Stationary-Plasma Thruster (SPT)

An SPT uses the Hall effect to create thrust. A Hall electric field is within the plasma when the current flows across a magnetic field. This electric field accelerates the plasma ions axially (Ref. 18, p. 571). The thruster is designed similarly to the IT and MPD.

Relatively low particle densities restrict SPT performance. This restriction implies relatively low thrust density. Scaling up thruster dimensions or using an array of multiple thrusters can overcome this restriction.

5.3.4 Attitude Determination and Control Subsystem

There is a wide array of sensors and actuators that PowerSail can use. Some of these sensors and actuators will work given the constraints in the problem definition, and some may not. This section examines some possible types of sensors and actuators, and examines the feasibility of using such options.

5.3.4.1 Attitude Sensors

There are many different control actuators on the space-rated market. Since the configuration of PowerSail has not been permanently selected, specific sensors cannot be chosen. However, several sensors are described here.

Some sensors for attitude determination include Earth horizon sensors, rate-integrating gyros, sun sensors, GPS receivers, star trackers and magnetometers. Most of these sensors are widely used, or are currently under development.

5.3.4.1.1 Horizon Sensors

The two main types of Earth horizon sensors are visible light cameras and infrared sensors. The infrared cameras have an advantage over the visible light cameras in that they can see the horizon even in eclipse. If visible light cameras are used, there must be some other type of sensor to determine attitude in the eclipse. Horizon sensors typically have errors on the order of 0.25°.

5.3.4.1.2 Rate Gyros

A rate gyro is one way to measure the spin rate about a certain axis. Integrating this spin rate over a period of time leads to an angular displacement. Rate gyros do have problems associated with them. Thermal and radiation environments have a large effect on the accuracy of the gyros by creating drift problems, affecting the lifetime.

5.3.4.1.3 Sun Sensors

Sun sensors are used to acquire a vector from the spacecraft to the sun within 3.0° accuracy. Knowing this vector, the attitude of the spacecraft is easily determined. If the structure were planar in shape like the flat array or fan configurations, PowerSail will be required to point almost directly at the sun. Sun sensors are used to determine the attitude for PowerSail given this configuration.

5.3.4.1.4 GPS receivers

Another method of determining attitude on a spacecraft is the use of GPS receivers. Since PowerSail is a large structure, multiple GPS receivers could be used to determine attitude. Typically, GPS receivers are accurate to within 10 to 15 meters. However, there are some problems associated with this technique of determination. The GPS orbit altitude is approximately 18,600 km, whereas the constraints of this project put PowerSail in an orbit anywhere between 1,000 km and GEO. It is possible to use GPS receivers at a

higher altitude than the GPS orbit, since GPS satellites on the other side of the Earth could possibly see PowerSail, as shown in Figure 5-7.

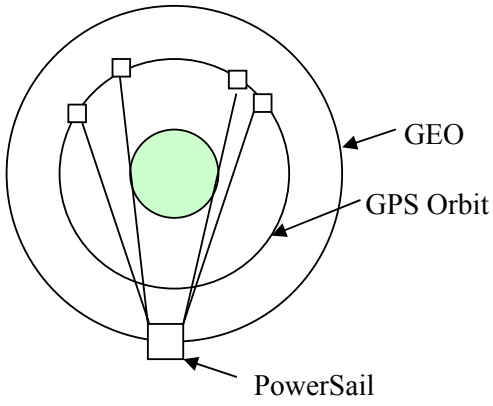

Figure 5-7: GPS Configuration

The orientation of the satellites shown in Figure 5-7 is an ideal case that provides a navigation solution and an attitude measurement to PowerSail. However, this idea is affected by the beam width of the GPS signal and ionospheric effects. Multipath errors occur when GPS signals bounce off surfaces on PowerSail, and arrive at the GPS receiving antenna at a later time than the original signal. Space-rated GPS receivers are not widely available for attitude control, but are under development.

5.3.4.1.5 Star Trackers

Star trackers are a precise way of determining attitude on a spacecraft, with errors on the order of 0.01°. The disadvantage of star trackers is that they are bulky and require complex tracking software and memory in the computer. They also require more power than other attitude sensors.

5.3.4.1.6 Magnetometers

Magnetometers detect the Earth's magnetic field and work best when combined with a horizon sensor or star tracker. The measured magnetic field is compared to the known magnetic field at the spacecraft's position to determine attitude within 3º of accuracy. The advantage of magnetometers is that they are light and reliable. PowerSail's residual magnetic dipole could interfere with the measurement of the magnetometers.

None of the above mentioned attitude sensors violate any constraints in the problem definition. However, the technology required to use a GPS receiver in geostationary orbit may present feasibility issues, though the idea cannot be discarded.

5.3.4.2 Control Actuators

PowerSail has the option of using many types of attitude control actuators. Because the problem definition states electric propulsion must be used for attitude control, these actuators must work with the propulsion system or simply be a backup to the propulsion system.

5.3.4.2.1 Reaction wheels

Reaction wheels are wheels that, while spinning, create an angular momentum providing control to one axis. If control of more than one axis is desired, multiple reaction wheels are used. There are harmonic and secular disturbances that can add to the momentum of reaction wheels.

5.3.4.2.2 Momentum Wheels

Momentum wheels are capable of providing gyroscopic stiffness in more than one axis. These wheels provide a nominally constant angular momentum to provide angular stiffness. The mean disturbance torque typically determines the momentum storage of reaction wheels and momentum wheels over one half an orbit.

5.3.4.2.3 Control Moment Gyros

Control moment gyros are essentially momentum wheels mounted on gimbals. Control moment gyros can be controlled such that large output torques are obtained. Such an output torque is dependent on the momentum of the gyro and rate at which the gimbal is turned.

5.3.4.2.4 Magnetic Torquers

Magnetic torque coils and torque rods are simple control devices. These torquers create magnetic dipole moments, producing a torque perpendicular to the Earth's magnetic field. Magnetic torque coils decrease in performance because of the degradation of Earth's magnetic field with increasing orbits. Degradation of torque coils and rods is an unfavorable attribute since PowerSail might operate in a geostationary orbit.

5.3.4.3 Conclusion

All the above options are technically feasible and work well with the problem definition for PowerSail. However, analysis is needed to show if any of these options are required. The propulsion system may be capable of fulfilling the requirements of attitude control.

5.3.5 Communications Subsystem

PowerSail's main task is to provide power to another spacecraft and thus can be considered a subsystem of that spacecraft. One subsystem that can be removed from the design of PowerSail is the communications network. Utilizing the communications architecture of the Host will simplify the design and decrease the mass of PowerSail. The communication network is routed through the umbilical to the Host. The hazard of information being damaged is minimized if sufficient insulation is used in the umbilical.

5.3.6 Structures Subsystem

5.3.6.1 Materials

Material selection is an important part of the structural design process. Metals and composite materials are the only space-rated materials for satellite structures because of their out-gassing properties. The following materials are commonly used in spacecraft: aluminum, steel, magnesium, titanium, beryllium, and composites. The advantages and disadvantages of these materials are described in the following section.

5.3.6.1.1 Aluminum

Aluminum is the most commonly used metal in aerospace structures. It is relatively strong for its weight, easy to shape and has a low density. However, aluminum does have undesirable properties including low strength-to-volume ratio, a low hardness and a high coefficient of thermal expansion. This material could be used for the main structure but not for the solar array itself.

5.3.6.1.2 Steel

Steel is an uncommon material for aerospace structures because it is a strong metal that has a high range of strength, ductility and hardness. Unfortunately, steel is dense and hard to machine. The electro-magnetic field created by any steel used in the craft must be offset to eliminate any possible field fluctuations.

5.3.6.1.3 Magnesium

Magnesium is a stable material with low density, which is good for maintaining a steady dynamic situation. Magnesium has a low strength-to-volume ratio and is susceptible to corrosion. Corrosion is not a concern due to the vacuum of space since there are no natural electrolytes to corrode the magnesium. However corrosion is a concern while in Earth's atmosphere before launch.

5.3.6.1.4 Titanium

Titanium is a highly desirable but expensive material. It has a high strength-to-weight ratio and a low coefficient of thermal expansion. There are two major disadvantages of titanium: it is hard to machine and has poor fracture toughness if treated and aged. Barring cost, though, titanium is an ideal material.

5.3.6.1.5 Beryllium

Beryllium is a dangerous but useful material. It has a high stiffness to density ratio but this is not much of a benefit compared to the disadvantages. Beryllium has a low ductility and fracture toughness, and has short transverse properties. It is also toxic which makes it difficult to work with in the construction phase. Beryllium could be used as stiffening elements in the structure.

5.3.6.1.6 Composite materials

Composite materials have a wide range of beneficial properties but are still in experimental stages. In general, they have low density and respond favorably in tension. Composites are tailored for high stiffness, high strength and extremely low coefficients of friction as needed.

5.3.7 Conclusion

This chapter focused mainly on generating alternatives for PowerSail. The proposed designs include a kite tail, sphere, fan, and a flat array. Also presented in detail were methods of accomplishing the missions of some of the subsystems that drive the design selection. The most important subsystems are those using significant power. The driving factors are PowerSail's solar cells, batteries, and electric propulsion, attitude dynamics and control, and material selection. In the following chapter the alternatives are

compared and rough estimates applied to subsystem. Finally, the calculated value of the alternatives will determine the best design.

5.4 System Analysis

Section 5.3 discussed possible options for each subsystem and possible array configurations. This chapter combines these two by analyzing the subsystems of each configuration and an educated decision is made of which design to further explore. This section does not lead to the final design, but allows for a starting point.

5.4.1 Electrical Power Subsystem

5.4.1.1 Solar Cells

With PowerSail requiring 50 kW of power, the solar array design is crucial. Different types of arrays gather energy from the sun by different methods determining the size and mass of each array configuration. Each array configuration must be with minimal volume and easy deployment. With each array configuration, certain types of solar cells are the more beneficial. Rigid cells are generally more massive but produce more energy. Flexible cells are less massive but have lower cell efficiency. The decision to use flexible cells over rigid is determined by the array shape and stiffness. If minimizing stowed volume, flexible cells are more beneficial. If the array is rigid and can maintain a rigid support structure, rigid cells are favorable. The following are different configurations with benefits and drawbacks of each design with respect to the solar cells and array.

5.4.1.1.1 Kite Tail

The orientation of the solar cells on kite tail configuration is simple because of the rectangular arrays. The number of sub-satellites depends on the most efficient solar cell. A III-V tandem cell would work the best since the arrays are rigid. In certain formations, the subsatellite arrays can potentially shadow the following satellites. The formation configuration must compensate for the shadowing losses. Stowing the solar arrays on each sub-satellite is a simple process, each sub-satellite stowing and deploying its own arrays.

5.4.1.1.2 Sphere

Flexible solar cells are used on a spherical array. Thin-film silicon solar cells work best in this configuration. Since the spherical array does not require the satellite to orient itself to face the sun, the array must have a large enough area to collect enough energy to fulfill the Host power requirement. Since the spherical array must be large in comparison to the other configurations, the stowed volume of the array is larger. The array is much more massive as well. Deployment, if inflated, is a simple process.

5.4.1.1.3 Fan

Since the fan configuration is a rigid array, rigid III-V tandem solar cells work best. Solar cell orientation on each array section is a triangular layout. The pointing requirements of this configuration are high since the solar array is planer. High-accuracy pointing requirements lead to a larger array to fulfill the power requirements.

5.4.1.1.4 Flat Array

A flexible array is used with a flat array configuration. Thin-film silicon cells are ideal for this configuration. Orientation of the cells on a rectangular array, along with the stowing and deployment, is simple.

5.4.1.2 Power Storage

The battery of PowerSail must store enough energy generated by solar cells to sustain the power needs of PowerSail while in eclipse. The type of battery is not impacted by the different conceptual designs. The overall power requirements combined with the orbit and lifetime of PowerSail determine the type of battery. The propulsion and solar array deployment power requirements of the different designs determine the size of the battery system.

As stated in Section 5.3.3.2, there are a variety of space-rated batteries available on the market today. Since PowerSail must serve in any orbit between 1000 km and geo-stationary with a 10-year lifetime, Nickel Cadmium and Nickel Hydrogen batteries are the probable choices. Lithium Ion and Sodium Sulfur batteries have a higher depth of discharge and a higher specific energy density than NiCd and NiH batteries. However, they cost more and are not yet space-rated. The low power requirements of PowerSail do not justify the increased the cost of Lithium Ion or Sodium Sulfur batteries.

5.4.1.2.1 Kite Tail

Of all of the conceptual designs discussed in Chapter 3, the Kite Tail is the most inefficient with respect to the battery sizing. The cost of PowerSail increases since more batteries are needed to store power for each section of the kite tail. Also, the overall battery power is larger than any other configuration since the propulsion power requirement increases. The number of primary batteries also increases with the Kite Tail configuration to provide power for each satellite's solar array deployment.

5.4.1.2.2 Sphere

The sphere requires a larger primary battery than the other configurations. Opening the valves of the gas canisters requires more power then the traditional solar array deployment mechanisms used in the other configurations. The sphere does not require the pointing accuracy of the other configurations because the cells are collecting the same amount of solar energy no matter what the orientation. Thus, the propulsion system requires less power than the other configurations, which decreases the size of the secondary batteries.

5.4.1.2.3 Fan

The fan configuration requires more overall propulsion system operation than the sphere and less then the kite tail. The primary battery is small since the deployment mechanism does not require much power. The pointing accuracy of the fan requires more propulsion system operation than the sphere, requiring larger secondary batteries.

5.4.1.2.4 Flat Array

The deployment method for the flat array configuration is similar to that of the fan,

requiring approximately the same size primary batteries. There is no significant change in the propulsion system of the flat array in comparison to the fan, implying the same secondary battery size.

5.4.1.2.5 Conclusion

As described in Section 5.3.3.2, the configuration does not impact the size and type of battery chosen on a large scale. The orbit and lifetime dictate the most efficient type of battery. The altitude of PowerSail's orbit is anywhere between 1000 km and geo-stationary. Higher orbits have longer eclipse, meaning the depth of discharge of the battery must be greater to provide power throughout the entire eclipse. NiH batteries have an advantage over NiCd batteries due to the larger depth of discharge at greater lifecycles. Orbits in the range below 1500 km have decreasing eclipse time and more orbits per day with increasing altitude. Orbits above 1500 km altitude have greater eclipse time and more orbits per day corresponding to an increase in charge/discharge cycles. The size of the battery system is dependent on the power requirements of the propulsion system for each configuration, as is discussed in the following sections.

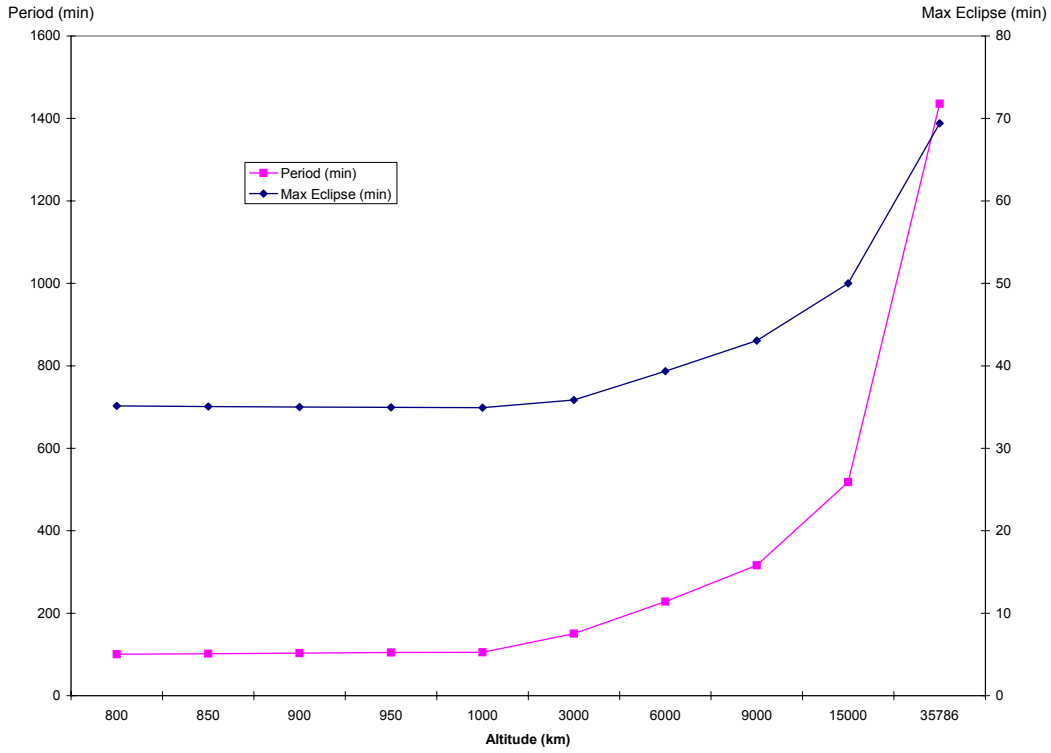

Figure 5-8: Orbit Characteristics (Ref 37)

5.4.2 Propulsion

This section considers the possible configurations of PowerSail with respect to the propulsion system. There is no one propulsion system that is the most efficient for all configurations. PowerSail has the option to accomplish attitude control through electric propulsion system.

5.4.2.1 Kite Tail

This configuration creates a number of different problems for the propulsion system. Each satellite in the Kite tail has its own propulsion system and attitude thrusters. Since each satellite requires a propulsion system, the mass of the system will increase. Each satellite needs a smaller thruster size and propellant mass. The number of thrusters and overall mass of propellant for all satellites offset the benefit of smaller thrusters.

Since a tether connects each satellite, wave propagation down each tether creates a need for thruster operation. This additional need for thruster operation increases the amount of propellant. This additional propellant is not needed for other configurations with only one satellite. There is an assumption that the tether between each satellite is long enough that the plume from the thrusters will not interfere with the other satellites in the chain.

The system needs small controlled bursts to maintain the attitude of the kite tail. The best system for this is a PPT. The Hall Effect Thrusters and the SPT create more thrust than is necessary and are too massive for use on the smaller satellites. Arcjets and resistojets also are more massive than the PPTs, and have greater propellant mass. The sizing of the PPTs is dependent on the location of the thrusters and size of each satellite.

5.4.2.2 Sphere

The sphere configuration for PowerSail reduces the need for propulsion system operation to maintain attitude. The pointing requirements of the system are less than that of other configurations. These pointing requirements lead to a decrease in thruster operation. The system is also the largest of the configurations examined thus the torques produced by the thrusters are the greatest. The same thrusters used for orbit control are also used for attitude control. Using the same thrusters for both functions minimizes mass, reduces complexity, and reduces cost for supplemental systems that are not required. The thrusters must be used to prevent the umbilical from wrapping around the PowerSail, or any possible dynamic interference induced by the umbilical. Any thruster can be used with this system if sized correctly.

5.4.2.3 Fan

The fan configuration is akin to a single piece of the kite configuration. The system is just much larger than a single piece of the kite tail. The satellite must be pointed accurately, thus leading to increased thruster operation. Thruster mountings must provide thrusters with the ability to counteract the disturbance torques on the satellite. Any thruster can be used with this system if sized correctly.

5.4.2.4 Flat array

The flat array configuration is a planar array with booms to support the array. The system is not fully rigid, but there are ample thruster mounting locations on the booms. The pointing requirements of this configuration are akin to the fan configuration. The vibration of the satellite is an issue leading to high impulse, low thrust thrusters to minimize oscillations. The attitude control thrusters are used for both attitude control as well as orbit control.

5.4.3 Attitude Determination and Control Subsystem

The configurations listed in Section 5.3 are analyzed in this section from the viewpoint of the ADCS. Similarities exist in each of the options, which are derived from the problem constraints. For example, magnetometers or magnetic torquers cannot be used since PowerSail may operate above LEO. Rate integrating gyros have drift errors that become too great for a 10-year lifetime if not reset periodically. Therefore, star trackers, sun sensors, and Earth horizon sensors comprise the attitude determination system.

5.4.3.1 Kite Tail

The Kite Tail approach poses many problems to the ADCS. This system has a high complexity compared to the other design configurations described in Section 5.3. The kite tail needs attitude sensors and control actuators on each sub-satellite, reducing efficiency. There is also blocking of earth horizon sensors, sun sensors, and much more multi-path error for possible GPS receivers. Sensors and actuators on all the sub-satellites lead to a much higher mass than is necessary for such a system.

Each sub-satellite requires a sun sensor and a horizon sensor to detect attitude while in the sun and eclipse. The sun sensor could be integrated with the Earth horizon sensors such that cameras could double as Earth horizon and sun sensors. Each sub-satellite is also equipped with a rate gyro.

The mass of the system is easily minimized using this system of Earth horizon and sun sensors. For the sensors to operate in eclipse, they must operate in the infrared spectrum. However, each of the sub-satellites needs one of these systems, which becomes costly.

If the sub-satellites block each other's views to the horizon, they require some other means of determining attitude. Attitude determination is accomplished by using star trackers. Star trackers are being developed less massive and less expensive, but each sub-satellite must be equipped with these components, again increasing cost.

The same electric propulsion system used for orbit control is also used for attitude control. However, there are plume effects that need to be analyzed. Since each sub-satellite needs some orbit and attitude control, each sub-satellite needs a propulsion system. The constraints of this problem state that electric propulsion must be used. Using electric propulsion has some effects such as unwanted spacecraft charging and degradation of solar cells by contamination.

5.4.3.2 Sphere

The sphere approach to the PowerSail problem is a good configuration for a simple ADCS. The sphere is covered in solar cells eliminating any pointing requirements of the system. However, the attitude of the sphere must be known to make any orbital corrections to maneuver relative to the Host spacecraft.

To obtain attitude data, PowerSail uses Earth horizon sensors and sun sensors. There must be different modules containing the sensors placed around the sphere so at least one of the sun sensors could have direct line of sight to the sun. Likewise, for the horizon sensors, there needs to be a suite of sensors located around the sphere so the sensors could have direct line of sight to the horizon. In this configuration, there is no need for the accuracy that a star tracker offers. GPS receivers are also used in this configuration. Rate gyros are used to determine any rate of rotations.

The same thrusters used for orbit control are also used for attitude control minimizing mass, and reducing complexity and cost for supplemental systems that are not required. Considerations are made concerning the position of the umbilical and its dynamics interference with the Host.

5.4.3.3 Fan

The Fan is a simplified model of the kite tail and is a single planar array. PowerSail in this configuration needs to be perpendicular to the direction of sunlight. Some margin of error away from the perpendicular is allowed. Earth horizon sensors, sun sensors, and GPS receivers accomplish the goals of the attitude determination system for this configuration. Star trackers could either complement or replace the Earth horizon sensors because of their accuracy. Rate gyros are used to determine rates of rotations.

Attitude control is accomplished using the electric propulsion system that exists for orbit control. Momentum wheels supplement the electric thrusters to help counteract the gravity gradient disturbance torques. Momentum wheels also lengthen the lifetime of the propulsion system, because less propellant is used onboard PowerSail.

5.4.3.4 Flat array

The flat array option is another planar array that needs to point at the sun for mission success and is similar to the Fan configuration. The Flat array configuration is not an ideal structure, making attitude determination somewhat more difficult during periods of vibration. However, the precise attitude is not important since an approximation is acceptable. The attitude determination system is comprised of Earth sensors, sun sensors, GPS receivers, and rate gyros.

The same thrusters used for orbit control are used to control attitude. Again, momentum wheels could assist the propulsion system in resisting disturbance torques.

5.4.3.5 Disturbance Torques

Disturbance torques are estimated using assumptions on the physical properties of PowerSail. A 400 m^2 planar array is used to estimate the torques as shown in Figure 5-9.

Solar radiation torque clearly dominates any torques applied to PowerSail. This torque will need to be controlled in some manner.

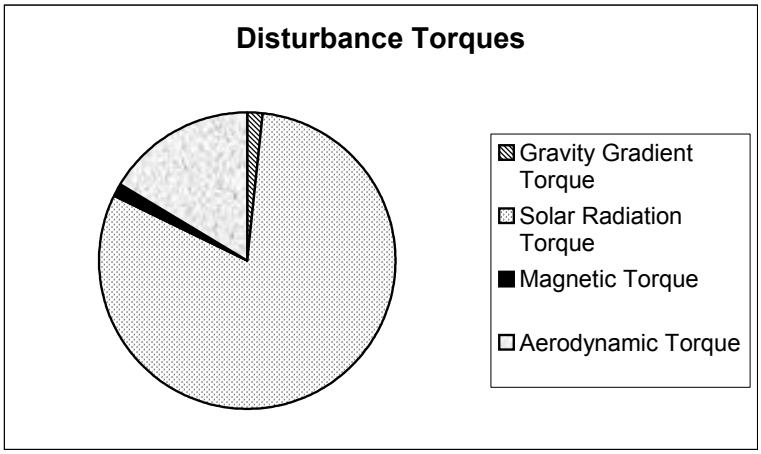

Figure 5-9: Estimated PowerSail Disturbance Torques

5.4.4 Conclusions

The objective hierarchy and the value system design are applied qualitatively. The results of this chapter are mostly educated guesses as to which design will be more desirable over another or which option was more feasible than another. The kite, sphere, flat array and fan are the design options. Table 5-5 summarizes our quantitative predictions of the performance of each alternative. The sphere is the most optimal design. However, there are some major flaws with a sphere design that do not appear in the MOE. Even though the sphere has no pointing requirements, there is still need for a propulsion system to maintain formation of PowerSail with respect to the Host. The main advantage of the sphere over the flat array is the use of inflatable technology. The flat array also needs propulsion to maintain formation with respect to the Host, and the limited pointing requirement of facing the sun. As a result of these considerations, a flat array using inflatable technology for the supporting structure and a fan-like deployment scheme is the chosen configuration for PowerSail to be studied in detail.

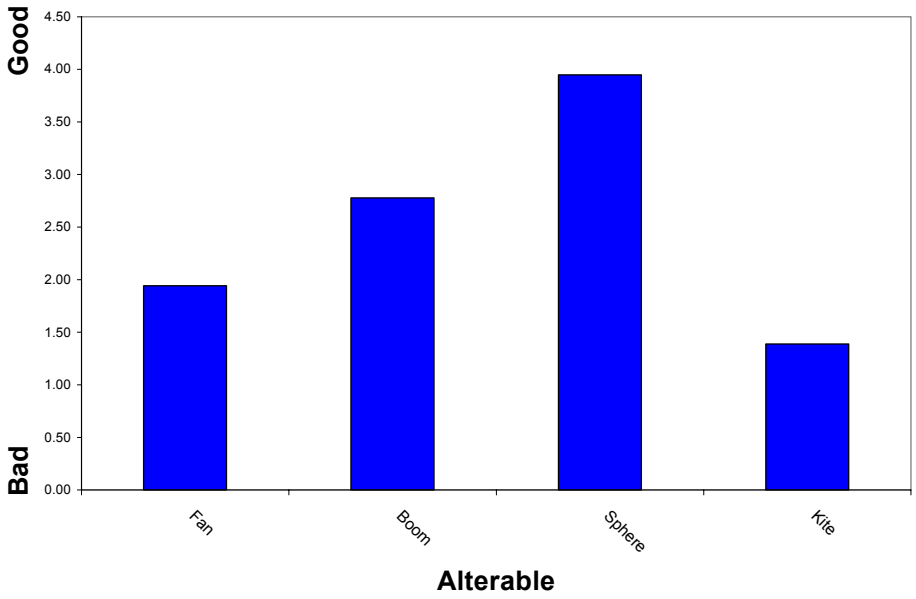

Figure 5-10: Value of Alterables

Table 5-5: Estimated MOEs

	Max Efficiency (1/3)							Min Cost (2/3)	
					Interface (4/20)				
	Min Mass (2/20)	Thin Film Solar Cell Efficiency (1/20)	Propulsion (4/20)	Min Stowed Volume (5/20)	Structural (9/16)	Dynamic (7/16)	Life (4/20)	Product Cost (1/4)	Operational Cost (3/4)
Fan	5	1	5	5	7	3	3	7	5
Boom	3	1	5	5	3	3	3	5	3
Sphere	7	1	3	3	9	1	7	3	1
Kite	9	1	7	7	3	9	7	3	9
*high numbers indicate a low priority									

5.5 System Modeling

In the previous chapter, we justified the selection of a flat array using inflatable technology as the supporting structure and a fan-like deployment scheme for further in-depth study. The next step is modeling the different subsystems of the spacecraft. PowerSail is considered to be a subsystem of the Host. Subsystem sharing between PowerSail and the Host simplifies the analysis and limits the mass and volume of PowerSail. This chapter discusses the equations that model the power, thermal, structure, propulsion, and attitude determination and control systems. It also includes basic modeling of the umbilical that connects PowerSail to the Host.

5.5.1 Power Subsystem

The power subsystem for PowerSail is a large solar array that must provide 50 kW of power to the Host spacecraft as well as meet the power needs of the components on PowerSail. Power loss through the umbilical is also a factor. There are two types of solar cells that are available, rigid and thin-film flexible photovoltaic solar cells. Once the decision is made on which type to use, a specific cell is chosen by their desired characteristics. In this section, particular types of solar cell layouts are determined along with their voltage and current output.

Modeling PowerSail's power system correctly requires the specifications of the chosen solar cell. Two options of cells are rigid photovoltaic and thin film photovoltaic solar cells. From the Table 5-6, we can see that the high specific energy density and thinness of thin film solar cells outweighs the higher efficiency of the rigid solar cells. Thin-films are also easily stored in small areas. The requirements of the solar cell dictate the mass and size and stowage ability of the array. Since PowerSail is launched with the Host conserving volume and mass for the launch vehicle is essential.

We selected Copper Indium Diselenide, or CIS thin film photovoltaic solar cells for PowerSail. These cells are a new technology and are constantly changing and improving. The estimated cell sizes we used are 2.5 cm × 2.5 cm cell and 4 cm × 4 cm cells (Ref. 33). The small cells are needed to produce a reasonable voltage. These cells produce an estimated efficiency of 17% and a specific energy density of 200 W/kg. They have a degradation of 0.25% per year. All of this information along with cell layout and the power losses through the umbilical are taken into consideration while modeling the solar array.

Table 5-6: Rigid vs. Flexible Solar Cells (Ref. 3)

	Rigid Photovoltaic (GaAs)	Thin Film Photovoltaic (CIS)
Specific Energy	40 W/kg	200 W/kg
Cost	High	Low
Thickness	15 mils	1 mils

The first steps in modeling the solar cell area is accounting for all of the factors that decrease the efficiency of the solar cells. Such factors include the lifetime degradation, cell degradation, and sun incidence angle. With an initial size of the array, the structure and propulsion systems can do preliminary calculations on the mass and power requirements. An iterative process occurs between the various subsystems' power requirements and the required solar cell area to produce the final array size.

Modeling the solar array is accomplished using a series of equations as described below. With consideration of power loss through the umbilical, the Host requires 50 kW at the end. The initial power loss is assumed to be 1.34 kW. The thrusters, main computer, and attitude determination are the components of PowerSail needing power. These values are shown in Table 5-7.

Table 5-7: Power Requirements for PowerSail

Component	Power Required (Watts)
Thrusters	2400
Attitude, Determination and Control	40
Computer	18
Primary Battery	55

Batteries add extra mass and need power for charging. Obtaining power from the Host outweighs the use of an onboard battery during eclipse. Therefore, PowerSail will not generate power in eclipse. Power during eclipse is routed back the umbilical from the Host power bus.

The total power requirement of the solar array is:

$$P_d = P_{host} + P_{losses} + P_{bus} \tag{1}$$

where P_{Host} = 50 kW, P_{losses} is the power lost through the umbilical, and P_{bus} is the power needed for PowerSail. This total power is then used to calculate the power that the solar array needs to generate with a 15 % design margin:

$$P_{sa} = \frac{P_d}{0.85} \tag{2}$$

The following equation determines the power output, P_o, in Watts:

$$P_o = 0.9\eta \times S \tag{3}$$

where 0.9 provides additional margin, η is the efficiency of the solar cell and S is the minimum solar flux of 1350 W/m^2. Using P_o, equation 4 calculates the beginning of life power, P_{BOL}:

$$P_{BOL} = 0.9Cos(\theta)P_o \tag{4}$$

Here θ is the worst-case sun incidence angle of 23.5˚ degrees. In order to determine the power at the end of the 10-year lifetime, P_{EOL}, we need to calculate the lifetime degradation, L_d, using:

$$L_d = (1 - degradation)^{lifetime} \tag{5}$$

Where degradation is the degradation of the solar cell and lifetime is the lifetime of the satellite in years. P_{EOL} is now calculated using:

$$P_{EOL} = P_{BOL} L_d \tag{6}$$

These equations produce the required area in m^2 using the equation below:

$$A_{sa} = \frac{P_{sa}}{P_{EOL}} \tag{7}$$

The solar cell area determines the number of cells needed to produce P_{sa}. The equation to determine the total number of cells needed is:

$$N = \frac{A_{sa}}{A_c} \tag{8}$$

Where A_c is the area of the solar cell using either the 2.5^2 cm^2 or 4^2 cm^2 cells. This relationship then leads to the number of cells needed per panel:

$$N_p = \frac{N}{number\_of\_panels} \tag{9}$$

There are many possibilities in the layout of the solar cell strings and the number of cells per string. These two factors affect the voltage and current through the umbilical. An iterative process is used to determine the optimal cell layout to minimize the power lost through the umbilical.

Determining the number of cells needed on a panel requires analysis of the string layout. Each string must have the same amount of cells per string. Each string can be placed in series or parallel. When the strings are placed in series, the total voltage is the voltage output of one string. We consider two string layouts to illustrate the string design tradeoffs. Figure 5-11 illustrates both options. Option one has strings mounted parallel to the 10 m edge with one string being the length of the panel. Option two has the same layout as option one, but each string contains two "rows" of cells. If a string is damaged due to a design fault or orbital debris, it will not generate power. The power loss of damaging shorter strings is minimal compared to that of losing larger strings. Thus shorter strings are favorable from the reliability viewpoint.

The cell voltage and the number of cells in a string determine the total voltage:

$$V_{bus} = \frac{N_p V_{cell}}{N_{cell/string}} \tag{10}$$

The voltage of one CIS solar cell is 0.4 V and the number of cells per string varies depending on the string layout. The current of each string is:

$$I = \frac{P_{sa}}{V_{bus}} \tag{11}$$

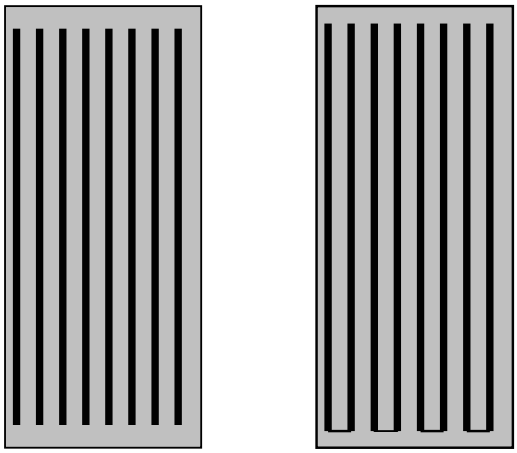

Option One Option Two

Figure 5-11: Solar Cell String Layout

5.5.2 Thermal Subsystem

5.5.2.1 Introduction

The thermal analysis of the final configuration of PowerSail is important in order to maintain the operational temperatures of the individual components. This includes calculating the heat absorption and emission of the solar array and the maximum and minimum temperatures of the thruster modules and main bus. This section discusses the procedures and calculations involved in the thermal analysis of PowerSail.

5.5.2.2 Thermal Modeling

In analyzing the thermal characteristics, PowerSail is split into different sections for simplicity. The solar array is the first section analyzed. As stated earlier, PowerSail is a large array covered with CIS thin film solar cells. These cells absorb and emit solar radiation from various sources. Figure 5-12 depicts the general radiation environment imposed on PowerSail. (Ref. 37, 428)

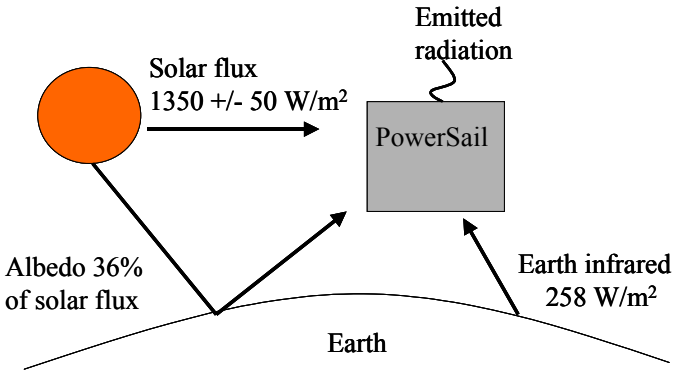

Figure 5-12: Radiation Environment

PowerSail absorbs radiation directly from the sun, reflected solar energy from Earth's albedo, and the Earth's infrared emission. The albedo reflects 36% of the total solar flux and decreases with altitude, as does the Earth's infrared radiation. The thermal emittance of the solar cells causes the emitted radiation depicted in Figure 5-12.

Before equations can model the thermal properties of the solar array, the properties of the cells themselves must be known. Table 5-8 displays all of the thermal properties of the CIS solar cells.

Table 5-8 Thin Film Thermal Properties

Property	Front and Back of Solar Cells
Emissivity	0.39
Absorptivity	0.82
Maximum Temperature	90 °C
Minimum Temperature	No minimum temperature

Table 5-8 lists the high absorptivity and low emissivity of CIS cells. These properties raise some concerns as to how hot the solar cells run during sunlight. Since they have a maximum temperature of 90°C, there is potential for the cells to run too hot due to their low thermal emissivity.

Since we know the properties of the solar cells and understand the radiation environmental effects on PowerSail, numerical calculations are added to the analysis.

The first assumption made in calculating the thermal properties is that PowerSail is a large, rigid, flat plate. The calculations also assume the worst-case solar flux at a 0° sun-incidence angle. Maximum albedo and IR emission are also assumed at 0° incidence angle. Figure 5-13, similar to Figure 5-12 shows these assumptions in detail. Values of emissivity and absorptivity of the solar array are not defined since these properties may change depending on thermal materials added to the top and bottom of the solar array.

All of the variables and the values used in the thermal analysis equations are shown in Table 5-9 below.

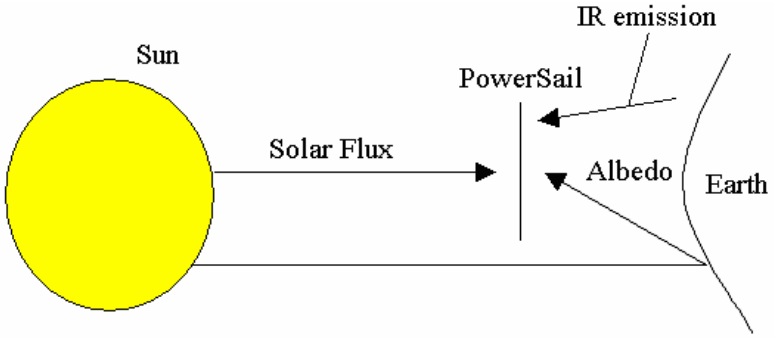

Figure 5-13: Thermal Environment Model

Table 5-9: Variables for Thermal Analysis

Variable	Significance	Assumptions
Q_{sa}	Absorbed solar energy	Varies
G_s	Solar flux	1418 W/m^2
A	Array area	420 m^2
α_t	Absorptivity of top of solar array	Varies
α_b	Absorptivity of bottom of solar array	Varies
q_I	Infrared radiation flux	258 W/m^2
ρ	Angular radius of Earth	$R_E/(H+R_E)$
R_E	Radius of Earth	6378 km
H	Altitude of PowerSail	1000-Geo-stationary
ε_t	Emissivity of top of solar array	Varies
ε_b	Emissivity of top of solar array	Varies
q_{Ia}	Absorbed IR radiation flux	Varies
Q_{Aa}	Absorbed albedo energy	Varies
a	Albedo	$.36 \times G_s$
K_a	Reflection of collimated energy	$0.664+0.521 \times \rho-0.203 \times \rho^2$
Q_a	Total absorbed energy	$Q_{sa}+Q_{Aa}+q_{Ia}$
σ	Boltzmann's constant	5.670×10^{-8} W/(m^2 $\times$K^2)
eff	Efficiency of solar cells	17%
T_{min}	Minimum temperature	Varies
T_{max}	Maximum temperature	Varies
Q_e	Emitted radiation of array	Varies

The direct solar radiation energy absorbed by the solar array is calculated using Equation 12. This energy depends on the absorptivity of the material normal to the sun vector and the area of the array.

$$Q_{sa} = G_s A \alpha \tag{12}$$

Equation 13 calculates the absorbed radiation from the Earth. This energy is absorbed on the side opposite of the absorbed solar radiation energy. The front side of PowerSail refers to the side that is sun vector pointing. Note that the infrared radiation absorbed by the backside of the array is inversely proportional to the altitude. As the altitude of PowerSail's orbit approaches GEO, the IR absorbed energy diminishes.

$$q_{Ia} = q_I \sin^2(\rho) A \varepsilon_b \tag{13}$$

The albedo energy also affects the amount of total radiation on the backside of the solar array. Equation 14 calculates the total absorbed albedo energy. This is inversely proportional to the altitude of PowerSail, so its effects diminish with altitude.

$$Q_{Aa} = aA\alpha_b K_a \sin^2 \rho \tag{14}$$

The sum of all the absorbed solar energies is shown in the following equation.

$$Q_e = Q_{sa} + q_{Ia} + Q_{Aa} \tag{15}$$

The radiation absorbed by the solar array determines the maximum and minimum temperatures of the solar array. As seen in Table 5-8, the maximum temperature of the solar cells cannot exceed 90°C. Equations 16 and 17 determine the maximum and minimum temperatures of the solar array, respectively. The maximum temperature incorporates the total absorbed radiation on the solar array. The equation for the minimum temperature does not include any solar, albedo, or electric power generation. Only the IR radiation emission is incorporated into the minimum temperature equation.

$$T_{max} = \left[\frac{G_s \alpha_t + q_I \varepsilon_b \sin^2 \rho + a\alpha_b K_a \sin^2 \rho - effG_s}{\sigma(\varepsilon_b + \varepsilon_t)} \right]^{(1/4)} \tag{16}$$

$$T_{min} = \left[\frac{q_I \varepsilon_b \sin^2 \rho}{\sigma(\varepsilon_b + \varepsilon_t)} \right]^{(1/4)} \tag{17}$$

As stated earlier, changing the absorptivities and emissivities of the front and backsides of the array change the maximum and minimum temperatures. The analysis to find the optimal absorptivity and emissivity in order to keep the cells under 90°C is performed in next chapter.

The second round of thermal analysis equations models the thermal properties of the thruster modules and the main bus. These equations differ from those previously discussed since the modules and main bus are not flat plates. The first step is defining the operating temperatures of the components found in the modules and bus. Table 5-10 illustrates these parameters.

Table 5-10: Operating Temperatures

Component	Minimum Operating Temperature (°C)	Maximum Operating Temperature (°C)
PPT capacitors	-20	50
Computer	-10	40
Star Trackers	-20	50
Beacon	-20	50
Accelerometers	-20	60
Global Positioning System	-20	50

The modeling equations use the cross sectional areas and surface areas of the modules and the bus. Table 5-11 illustrates these additional variables.

Table 5-11: Additional Thermal Modeling Variables

Variable	Significance
A_c	Cross sectional area of the component
Q_w	Internal energy dissipation
A	Surface area of the satellite

The method used to calculate the maximum and minimum temperature of the solar array is also used in modeling the temperatures of the module and bus. Refer to the previous equations to calculate the absorbed energies. Equation 18 calculates the maximum temperature of the thruster module or computer housing. This equation takes into account maximum solar radiation energy, albedo, and Earth IR emission. Equation 19 calculates the minimum temperature of the components of PowerSail. This includes minimal heat dissipation by the internal components, no solar radiation energy, and minimal Earth IR emission.

$$T_{max} = \left[\frac{A_c G_s \alpha + AFq_I \varepsilon + AFa\alpha K_a + Q_w}{A\sigma\varepsilon} \right]^{(1/4)} \tag{18}$$

$$T_{min} = \left[\frac{AFq_I \varepsilon + Q_w}{A\sigma\varepsilon} \right]^{(1/4)} \tag{19}$$

(Equations 12-19 Ref. 37, page 445-447).

5.5.2.3 Conclusion

Calculating the maximum and minimum temperatures while varying important values such as the emissivity, absorptivity, and internal heat dissipation is the next step in the analytical process. This results in a large range of maximum and minimum temperatures. Finally, the thermal materials to insulate or radiate heat are selected based on the analytical results.

5.5.3 Structures Subsystem

5.5.3.1 Introduction

The required area for the photovoltaic solar array is 420 m^2 that incorporates inflatable structure technology. The normal modes of vibration are of importance in this design since PowerSail is a large flexible structure. We must identify low frequency modes of vibration since they can cause large stresses and deflections. Inflatable structures are emerging are a developing technology for the space structures industry. They possess low mass and are packaged in small containers. This makes inflatable structures an attractive alternative to standard deployable structures. PowerSail's primary structure utilizes these advantages. The system that is needed to inflate the structure is designed with similar methods to that of a cold gas propulsion system. Modeling of the inflation system turns out to be simple, but non-trivial. This section discusses the method used to analyze the normal mode vibrations, inflatable materials, and the inflation system.

5.5.3.2 Inflatable Materials

Table 5-12 shows available materials for inflatable space structures.

Table 5-12: Inflatable Material Properties

	CP1&2	Kapton	Mylar	TOR	Upilex-R	Upilex-S
Polymer	Polyamide	Polyamide	Polyester	Polyamide	Polyamide	Polyamide
E [Gpa]	2.6	3	3.8	3.4	3.7	8.8
Density [g/cm^3]	1.4	1.42	1.38	1.4	1.39	1.47
Strength [MPa]	124	172	172	138	248	393

Because inflatable space structures are a relatively new technology, there are only a few types of materials being currently reviewed for flight use. With a value system design of low cost and favorable material properties, Kapton emerges as the optimal material.

5.5.3.3 Finite Element Modeling

The following section discussed the approach to finite element method modeling for PowerSail. PowerSail's 420 m^2 area is divided into 14 sections, each being a 3 m by 10 m rectangle. At the corners are modules housing 10 thrusters and an accelerometer. These components are included when modeling the structural dynamics of PowerSail. Mass distribution is also a consideration since it has a major effect on modal vibrations.

We used I-DEAS software to produce a finite element model and examine the structural dynamics of PowerSail. There are 223 beam elements and 140 shell elements in the model shown in Figure 5-14. This model is optimized and discussed further in the next chapter.

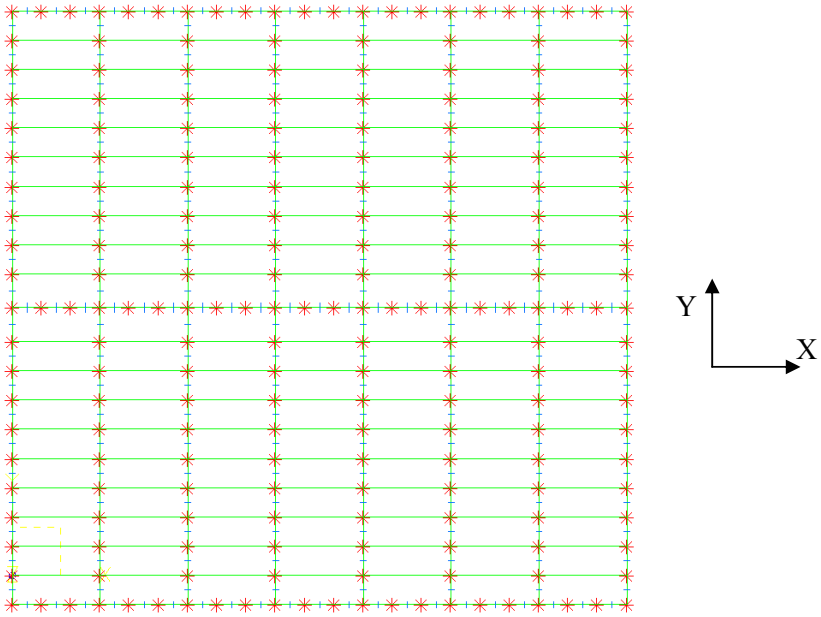

Figure 5-14: Finite Element Model

The beam elements were used to model the behavior of a beam under any loading condition or boundary condition. Nodes connect the structural elements. Table 5-13 describes the two beam elements used. The ribs are smaller beams used in the 'Y' direction and the main spar in the center of PowerSail runs in the 'X' direction.

Table 5-13: Beam Elements

	Diameter [m]	Thickness [m]	Density [kg/m^3]
Rib and End Beam	0.2	0.0001	1400
Main Spar	0.3	0.0001	1400

A shell element models the solar array as a thin plate. It has a density of 1.2 kg/m^2 and the material properties of Kapton. The shell elements are each 1 m × 3 m. The elements can be broken into smaller pieces for a higher resolution.

This section examines the lump masses of the thruster modules and the main bus. The thruster modules are 50 kg lump masses placed at the corners of PowerSail. The bus is a 25 kg lump mass distributed across the central section of the main spar.

5.5.3.4 Inflation System

Typically, low pressures are needed to deploy inflatable space structures. The structure is inflated to a pressure that removes the wrinkles in the material. The rigidization method determines the inflation pressure.

The inflation system deploying PowerSail uses a cold gas propulsion system that operates with a perfect gas pressurant. The system is shown in Figure 5-15.

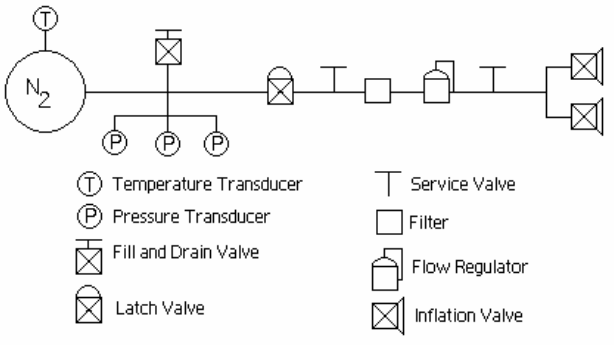

Figure 5-15: Inflation System Model

The pressurant is a perfect gas with a fixed inflated volume of 8.1 m^3 and a fixed pressure. The inflation tanks must fit inside the 0.3 diameter bus. The required tank pressure and volume are computed using these parameters.

5.5.4 Propulsion and Formation Flying Modeling

5.5.4.1 Introduction

The propulsion system of PowerSail has two main requirements. The first and most important is maintenance of the formation between PowerSail and the Host. The umbilical that attaches the two satellites is a fixed length and the distance between the two must never exceed this length. The second requirement of the propulsion system is to keep PowerSail sun pointing as much as possible. The modeled factors include the effects of solar radiation pressure and the forces applied by the propulsion system. The solar radiation pressure is the dominant force above 1000 km. Atmospheric drag is the dominant force under 1000 km altitude. This section discusses the equations used in the propulsion modeling.

5.5.4.2 Modeled State

The effects of solar radiation pressure on the PowerSail orbit are computed as described below. The algorithm incorporates control forces applied to PowerSail and propagates the Host-PowerSail formation around the earth with Runge-Kutta numerical integration. The algorithm begins with the equations of Keplerian two-body motion:

$$\ddot{\vec{r}} + \frac{\mu}{r^3}\vec{r} = \vec{f} \tag{20}$$

$$\vec{r} = x\vec{i} + y\vec{j} + z\vec{k} \tag{21}$$

Here, μ is the gravitational parameter of the earth and $\vec{r}$ is the radius vector of the satellite in the geocentric reference frame. (Ref. 2)

Solar radiation pressure only affects orbits when a satellite with a large cross-sectional area is in the view of the sun. The following three algorithms integrated together determine if PowerSail is in sunlight. The first calculates the current Julian time based on user-defined inputs for the exact time and date. This is algorithm 2 Fundamentals of Astrodynamics and Applications (Ref. 35).

$$JD = 367 \times Year - \left(\frac{7 \times \left(Year + \frac{(Month + 9)}{12} \right)}{4} \right) + 275 \times \frac{Month}{9} + Day + 1721013.5 + \frac{\left(\frac{\left(\frac{Second}{60} + Minute \right)}{60} + Hour \right)}{24} \quad (22)$$

The following algorithm, using the current Julian date, gives the current sun vector in geocentric coordinates. These equations came from algorithm 18 in Fundamentals of Astrodynamics and Applications (Ref. 35):

$$T_{uti} = \frac{(JD - 2451545)}{36525} \quad \textbf{[Min]} \quad (23)$$

$$\lambda_{sun} = 280.4606184 + 36000.77005361 \times T_{uti} \quad \textbf{[Deg]} \quad (24)$$

$$M_{sun} = 357.5277233 + 35999.05034 \times T_{uti} \quad \textbf{[Deg]} \quad (25)$$

$$\lambda_{ecliptic} = \lambda_{sun} + 1.914666471 \times sin(M_{sun}) + 0.019994643 \times sin(2 \times M_{sun}) \quad \textbf{[Deg]} \quad (26)$$

$$R_{sun} = 1.000140612 - .016708617 \times cos(M_{sun}) - 0.000139589 \times cos(2 \times M_{sun}) \quad \textbf{[AU]} \quad (27)$$

$$\varepsilon = (23.439290 - 0.013004 \times T_{uti}) \quad \textbf{[Deg]} \quad (28)$$

$$\overrightarrow{R_{sun}} = \left(R_{sun} \times cos(\lambda_{ecliptic})\right)\vec{i} + \left(R_{sun} \times cos(\varepsilon) \times sin(\lambda_{ecliptic})\right)\vec{j} + \left(R_{sun} \times sin(\varepsilon) \times sin(\lambda_{ecliptic})\right)\vec{k} \quad \textbf{[AU]} \quad (29)$$

This algorithm determines the current sun vector by calculating the current universal time (T_{uti}) leading to the mean longitude (λ_{sun}) and mean anomaly (M_{sun}) of the sun (Equations 23-25). From these values, Equation 26 calculates the mean longitude of the ecliptic plane ($\lambda_{ecliptic}$). Once the mean anomaly of the sun is known, the distance to the sun can be found (R_{sun}, Equation 27). R_{sun} requires two more calculations to obtain the

sun vector. The first, using the current universal time (T_{uti}), calculates the obliquity of the ecliptic (ε, Equation 28). This value is used in Equation 29 to determine the current sun vector ($\overrightarrow{R_{sun}}$) in astronomical units.

After obtaining the current sun vector, another algorithm is run to determine if PowerSail is in sunlight. This is algorithm 22 from Fundamentals of Astrodynamics and Applications (Ref. 35). Note the importance of maintaining unit similarity. The algorithm is Equations 30 and 31.

$$\tau = \left(\frac{\left(\left| \overrightarrow{R_{PS}} \right|^2 - \left(\overrightarrow{R_{ps}} \bullet \overrightarrow{R_{sun}} \right) \right)}{\left| \overrightarrow{R_{PS}} \right|^2 + \left| \overrightarrow{R_{Sun}} \right|^2 - 2 \times \left(\overrightarrow{R_{ps}} \bullet \overrightarrow{R_{sun}} \right)} \right) \tag{30}$$

If τ is less than 0 or greater than one, PowerSail is in view of the sun. Also, when the Equation 31 is true, PowerSail is in sunlight.

$$(1-\tau) \times \left| \overrightarrow{R_{PS}} \right|^2 + \left(\overrightarrow{R_{ps}} \bullet \overrightarrow{R_{sun}} \right) \times \tau \geq 1.0 \tag{31}$$

The code then applies forces from the solar radiation pressure to alter PowerSail's orbit.

Figure 5-16 is a diagram describing the modeled state. PowerSail and the Host are in an orbit around the earth, with the solar radiation pressure acting on PowerSail, and changing its orbit.

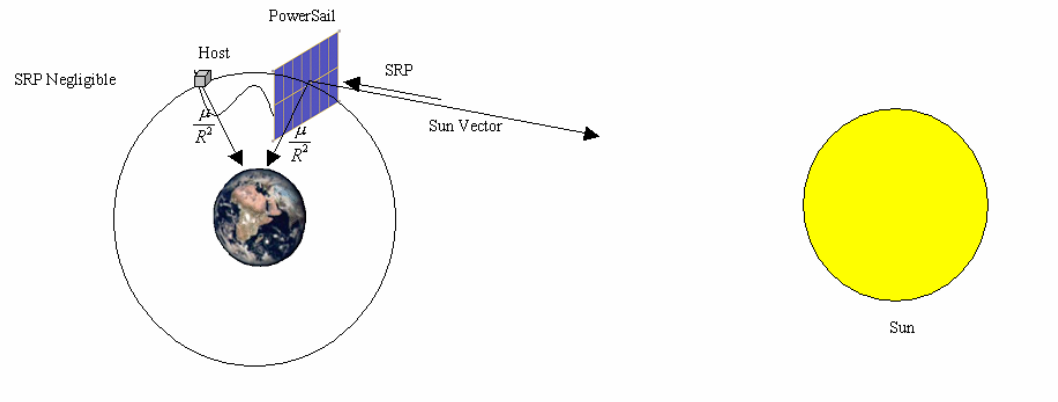

Figure 5-16: Orbital Forces Model

The Host provides its own station keeping and orbit maintenance. If the Host requires an alteration in its orbit, the effects are not difficult to place in the model, and PowerSail can maintain the formation with the Host if possible. This is due to the addition of a reference state vector for PowerSail's location. The changes made to the code must be applied to the reference state vector. This reference position is directly behind the Host at a specified distance. In tests with this code, the distance is half the length of the

umbilical. The reference position follows the Host in the same orbit with a slightly smaller true anomaly.

The need for a reference state vector comes from the control system that maintains the leader-follower formation. A Lyapunov nonlinear control theory maintains the formation. This control theory uses the difference in state vectors between the reference position and PowerSail. The control theory creates an accelerative $\vec{U}$ that PowerSail must apply. Equation 32 calculates the control vector.

$$\vec{U}_{lyap} = \mu\left(\frac{\vec{r}_{ps}}{r_{ps}^{\ 3}} - \frac{\vec{r}_{ref}}{r_{ref}^{\ 3}}\right) - \frac{k_1}{k_2}\delta\vec{r} - k_3\delta\vec{v} \qquad \textbf{[kg/sec}^2\textbf{]} \qquad (32)$$

Where μ is the gravitational parameter of the earth, $\vec{r}_{ps}$ and $\vec{r}_{ref}$ are the position vectors of PowerSail and the reference point, $\delta\vec{r}$ is the difference between $\vec{r}_{ps}$ and $\vec{r}_{ref}$, $\delta\vec{v}$ is the difference between $\vec{v}_{ps}$ and $\vec{v}_{ref}$, and k_1, k_2, and k_3 are control constants. The control constants vary between spacecraft, and are optimized for specific spacecraft properties. The constants vary widely based on propulsion system, mass of the spacecraft, and the forces acting upon it. The control vector correlates the difference in radius and velocity vectors to correct PowerSail's position and velocity vectors.

5.5.4.3 Conclusions

The data obtained from modeling the leader-follower formation of the Host and PowerSail around the earth shows that the distance between the Host and PowerSail far exceeds the umbilical length in less than one orbit. The largest force acting on PowerSail during its orbit is solar radiation pressure. If PowerSail is in sunlight then this perturbation force affects the orbit. This effect increases the eccentricity of PowerSail's orbit. The application of a Lyapunov nonlinear control system maintains the formation. The analysis can be found in Section 5.6.

5.5.5 Umbilical Subsystem

5.5.5.1 Introduction

An essential component of PowerSail is the umbilical. The umbilical connects the Host with PowerSail, allows for the transfer of power and telemetry, and minimizes interactions between the two spacecraft. The design is closely linked with the construction and layout of the cells on the solar array. Many factors contribute to an efficient design of an umbilical. The umbilical must have as little interaction with the Host as possible, but still maintain some flexibility. It must be capable of transferring power to the Host without excessive loss through the conductor. The umbilical must not affect the mission of the Host by either blocking or dynamic interactions. Using basic laws of electrical theory, the design of the conductor is studied.

5.5.5.2 Umbilical Modeling

Ultimately, the umbilical must be capable of transferring 50 kW of power. Due to the power requirements of PowerSail and power loss through the umbilical, PowerSail needs

to generate more than 50 kW of power. Total power generated by PowerSail is the sum of 50 kW, the power needed for the safe operation of PowerSail, and the loss due to the umbilical. The loss of power due to the conductor is in the form of

$$P_l = I^2 R \qquad \textbf{(Ref. 1, page115)} \tag{33}$$

where P_l is the power loss in Watts, I is the current through the conductor measured in Amps, and R is the resistance of the conductor in Ohms.

The design of the array determines the power generated by PowerSail. The power generated by solar cells follow the common law:

$$P = VI \tag{34}$$

where P is the power in Watts, V is the voltage, and I is the current. As the voltage of the cell increases, the power will increase. The same is true for current, concluding that the balance of voltage and current is a major contributor to an efficient design.

Material for the conductor is selected based on density and electrical conductivity (Ref. 22). Density is important because the desired mass of the conductor should not exceed design mandates. Conductivity is the measure of how well a material conducts electricity. High conductivity reduces the resistance making for a more efficient PowerSail. The resistance of the conductor is modeled with the relation:

$$R = \frac{\rho L}{A} \tag{35}$$

In this equation, R is the resistance, ρ is the resistivity of the conductor is Ω·m, L is the length of the umbilical in meters, and the cross-sectional area, A, is in meters^2. Combining Equations 33-35 gives the relationship between the power loss in the umbilical due to the conductor to the voltage and cross-sectional area of the conducting wire.

$$P_l = \left(P^2 \rho L\right)\frac{1}{V^2}\frac{1}{A} \tag{36}$$

The power loss in the umbilical is inversely proportional to the voltage through the umbilical and the area of the conducting wire. P is the total power generated minus the power required for PowerSail.

The design of the conductor is essential to minimize mass and maximize the performance of the umbilical. Cables are modeled in two classifications; stranded and solid. "Because of the additional length due to stranding, the dc resistance of stranded conductors is larger than that of solid conductors of equal area" (Ref. 1). The resistance in a stranded conductor is approximately 1.02 times greater than a solid conductor, though its effects are not exactly modeled (Ref. 1).

It is common practice to design a conductor according to the current it is required to carry. The cross-sectional area of a circular conducting wire is measured in units of circular mils, which is the area of a circle with a diameter of 0.001 inch (Figure 5-17). Considering no other factors, "a good rule to follow for copper conductors is to allow

1000 cir mils per amp" (Ref. 22). The design of the umbilical for PowerSail involves much more than a simple conducting wire. Kinetic and kinematic interactions, insulation, and string layout of the solar array all contribute to the design process of the umbilical.

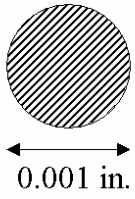

Figure 5-17: Conductor cross section

Kinetic coupling of the Host and PowerSail involves transmission forces and torques through the umbilical. These interactions depend on the physical properties of the umbilical (Ref. 13). A completely slack umbilical allows wave propagation and creates high resistance due to the small conducting wire area. Therefore, a completely slack umbilical is not the optimal design. Kinetic coupling through an umbilical is difficult to model due to its unknown characteristics and limited flight heritage.

On the other hand, kinematic coupling is easily analyzed with the aid of the equations defining Keplerian motion. The study of kinematic coupling of PowerSail and the Host describes blocking and shadowing. Blocking occurs when PowerSail moves between the Host and its target. Shadowing is the loss of generated power due to the Host moving between PowerSail and the Sun. Several orbital properties of PowerSail are varied to study their effect on blocking and shadowing including inclination, true anomaly, right ascension of the ascending node (RAAN), and argument of perigee (Ref. 13). An American Institute of Aeronautics and Astronautics study showed that an umbilical length of 100 m is sufficient to keep the satellites from colliding (Ref. 25).

Equation 36 states that a conductor with a greater cross-sectional area has less resistance than one with a smaller area. This area is dependant on the current flowing through the conductor, which depends on the voltage of the solar array. Table 5-14summarizes the voltage and current of the cells used in equations to model the power loss.

Table 5-14 Cell Electrical Properties

Cell Size [cm^2]	Voltage [Volts]	Current [Amps]
2.5×2.5	0.4	0.3607
4.0×4.0	0.4	0.9234

In all electrical circuits, the electrical loop must be grounded and closed. Several possibilities exist to close the electrical loop through the umbilical. One option is a wire mesh around the outer portion of the umbilical. The mess will provide variable flexibility

of the umbilical and protects the umbilical from space debris. A second option is a conducting cable stranded in the umbilical embedded in the insulation.

The umbilical also provides a data link with the Host. PowerSail will not have any antennas or data transmitters to communicate with a ground station. PowerSail will use the communication system of the Host since it requires a small amount of telemetry and commands. There is unnecessary redundancy in both systems having ground communication capability. To establish this data connection, a data wire is implanted in the insulation of the umbilical. Positioning of the cable must minimize the risk of current interfering with the data transfer.

5.5.5.3 Conclusion

With these modeling concepts in mind, the process of optimizing the design of the umbilical begins. An efficient design consists of an umbilical with little interaction with the Host. Conductor size and kinetic and kinematic interactions drive the design of the umbilical. The Host's communications system is used to send telemetry and receive commands from the ground station via the umbilical. The next chapter discusses the design of the umbilical accounting for all of these considerations.

5.5.6 Attitude Determination and Control Subsystem

5.5.6.1 Introduction

The attitude determination and control system for PowerSail is a trivial system that has several major components. Orbit and attitude determination is complicated because PowerSail is not a rigid panel. In actuality, it is a large, flexible structure that is difficult to model. Several types of measuring devices are used to determine PowerSail's position relative to the Earth and Sun, and relative velocity and separation from the Host (Ref. 13).

5.5.6.2 Accelerometers

One characteristic being measured is the frequency of the entire structure. This is accomplished by positioning accelerometers at each of the four thruster modules. Accelerometers measure the acceleration of a point relative to another fixed point. The acceleration is integrated once to calculate the relative velocities of each component and again to find the relative position of a point (Ref. 13).

The reference plane used for the relative position is the plane of PowerSail experiencing no deformation. Reference velocity and acceleration are each zero. Once the frequency at each corner is known the frequency can be estimated for the entire structure.

5.5.6.3 Global Positioning System and Orbit Propagation

Orbit determination is another aspect of ADCS. This is determined by GPS and orbit propagation theory. GPS satellites send signals to a receiver, and each of those satellites knows their position. Based on the triangulation of these signals, the orbit of PowerSail is determined. The only major flaw with GPS is that it is not reliable at or near the GPS satellite altitude (Ref. 13).

Above the GPS constellation, an alternative needs to be found. One alternative to using GPS is a store and forward method of orbit propagation. Orbit propagation works by receiving a two-line element set describing PowerSail's orbital parameters, and using these parameters to determine position. These two line element sets are sent to the Host when PowerSail in is view of the ground station (Ref. 13).

5.5.6.4 Star Tracker

Attitude determination is an essential part of PowerSail's operations. PowerSail generates the greatest amount of power when it is perpendicular to the sun vector. There are many options available to establish this attitude but a low power, relatively quick and highly accurate system is the most desirable. A star tracker is an accurate and quick method of attitude determination (Ref. 13).

A star tracker works by determining stars positions in the body frame to a data bank of star locations in the inertial frame. This is an accurate and fast measure of attitude. Since PowerSail is highly flexible, a quick series of measurements gives an accurate average attitude.

5.5.6.5 Signal Transmission

The final part of the ADCS system is a signal transmitter. This is used to determine the relative distance and velocity between PowerSail and the Host. This is an important aspect of the control system because should never collide with the Host. This is accomplished through a simple transmitter (Ref. 13).

This transmitter will be located on the end of the umbilical that is attached to the Host. It will transmit two signals to PowerSail, one through the umbilical and one directly to the receiver. The signals both travel at the speed of light. The umbilical signal will travel the length of the umbilical while the other signal travels a direct route to the receiver. This information is used to calculate position and velocity. Equations 37 and 38 describe the relations between the relative distance and relative velocity of PowerSail and the Host.

$$D_R = c \times t \tag{37}$$

$$V_r = \frac{D_{R1}}{t_1} - \frac{D_{R2}}{t_2} \tag{38}$$

Here, D_R is the relative distance between PowerSail and the Host, and V_R is the relative velocity. C is the speed of light (3.00×10^8 m/s), and t is the time it takes for the signal to reach the receiver. D_{R1}/t_1 is the relative velocity at time one, and D_{R2}/t_2 is the relative velocity at time two. The difference between these two is the relative velocity between the two spacecraft. The difference between t_1 and t_2 will be a set interval of about 5 seconds, so there are continual updates on the status of the distance and velocity between spacecraft.

5.5.6.6 ADCS Conclusion

The ADCS is important because it keeps PowerSail from interfering with the Host while at the same time providing the Host with power. Position relative to the Earth, Sun and Host is determined by these systems acting together as a whole.

5.5.7 Command and Data Handling

The command and data handling system is an important part of spacecraft because it handles all of the functions onboard. This is an integral system on PowerSail because of PowerSail's need for autonomous attitude and orbit control. The word length, operating frequency, sizes spacecraft computer systems and the number of operations required per second. The analysis for PowerSail's computer is based on Chapter 16 of Ref. 37. Table 5-15 summarizes the computer requirements for PowerSail's mission.

Table 5-15 Computer Properties

Function	Software Estimations Size Code	Size Data	Throughput KIPS	Frequency Hz	Number
Communications	Kwords	Kwords			
Command Processing	1	4	7	10	
Telemetry Processing	1	2.5	3	10	
Attitude Sensors					
Accelerometers	3.2	2	36	10	4
Star Tracker	2	15	2	0.01	
GPS	1.5	0.8	12	10	
ADCS					
Error Determination	1	0.1	12	10	
Thruster Control	2.4	1.6	20	2	4
Orbit Propagation	13	4	20	1	
Autonomy					
Complex Autonomy	15	10	20	10	
Fault Detection					
Monitors	4	1	15	5	
Fault Correction	2	10	5	5	
Other Functions					
Power Management	1.2	0.5	5	1	
Thermal Control	0.8	1.5	3	0.1	
Function					
Executive	3.5	2	60	10	
Run-Time Kernel	8	4		10	
I/O Device Handlers	2	0.7		10	
Built-In Test and Diagnostics	0.7	0.4	0.5	10	
Math Utilities	1.2	0.2		10	
Totals	63.5	60.3	220.5		
Error Margins	6.35	6.03	22.05		
Adjusted Total	69.85	66.33	242.55		
Total		136.18			

In order to account for possible errors or averages, a margin of 10% is added to the total computing requirements. The computer for this project will be chosen from previously designed and tested computers (Ref. 37).

5.5.8 Conclusion

PowerSail design involves integrating all the subsystem designs. For example, the design of the solar array affects the properties of the current in the umbilical, and the support structure. The support structure affects the propulsion system. Changing the propulsion systems changes the total power requirements and the area of the solar array. The PowerSail design is optimized through many iterations of each subsystem. The next phase in the design process is the iteration and optimization of each subsystem to finalize PowerSail's configuration.

5.6 Optimization

5.6.1 Introduction

Optimizing the design of a subsystem involves defining the best option that achieves set goals. Each subsystem attempts to create an efficient and effective design based on the modeling equations presented in the previous chapter. Subsystem interaction often requires cooperation between subsystems due to design constraints. In this section, each subsystem is optimized while accounting for all of the factors that may affect other subsystems. The final product achieves all criteria defining the mission.

5.6.2 Power Subsystem

5.6.2.1 Introduction

Optimization of PowerSail's power configuration involves several models. Several graphs are used below to illustrate the relationships between variables. Power loss is a major concern since it affects the array, the array size, and sizing of components. Another factor is the exact number of strings that is placed on a single panel and how many cells there are in that string. This affects the voltage and current that the strings produce. All of these are considerations when optimizing the power for PowerSail.

5.6.2.2 Subsystem Optimization

Optimizing the solar array requires minimizing the power loss. The power transferred to the Host must be a constant 50 kW. PowerSail's power requirement is 2.6 kW. Power loss changes with cell area and number of cells per panel. The relations between these factors and power loss are seen in Figure 5-18. The optimal power loss between the array voltage and the umbilical size is 1.34 kW.

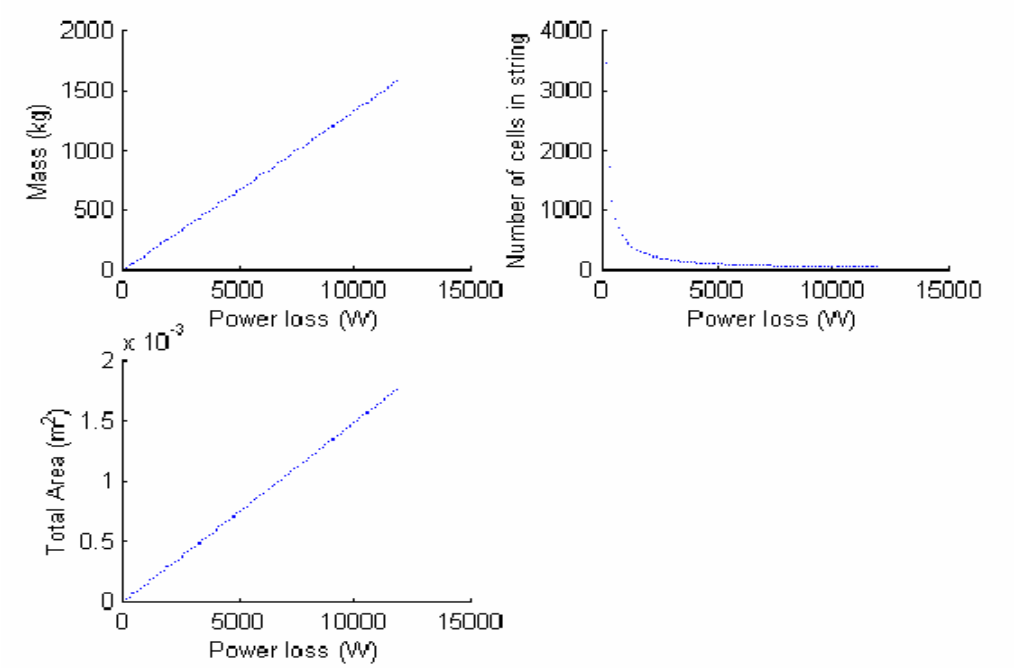

Figure 5-18: Power Loss Modeling

When varying the number of cells in a string, voltage and current change. Fewer strings on a panel create a higher bus voltage, which reduces power loss through the umbilical. Fewer strings on a panel result in more cells on a string, lower current, and a smaller conductor cross-sectional area. These relations are shown below in Figure 5-19. For the 4 cm solar cell, the number of cells in a string verses the number of strings on a panel is seen in Figure 5-20.

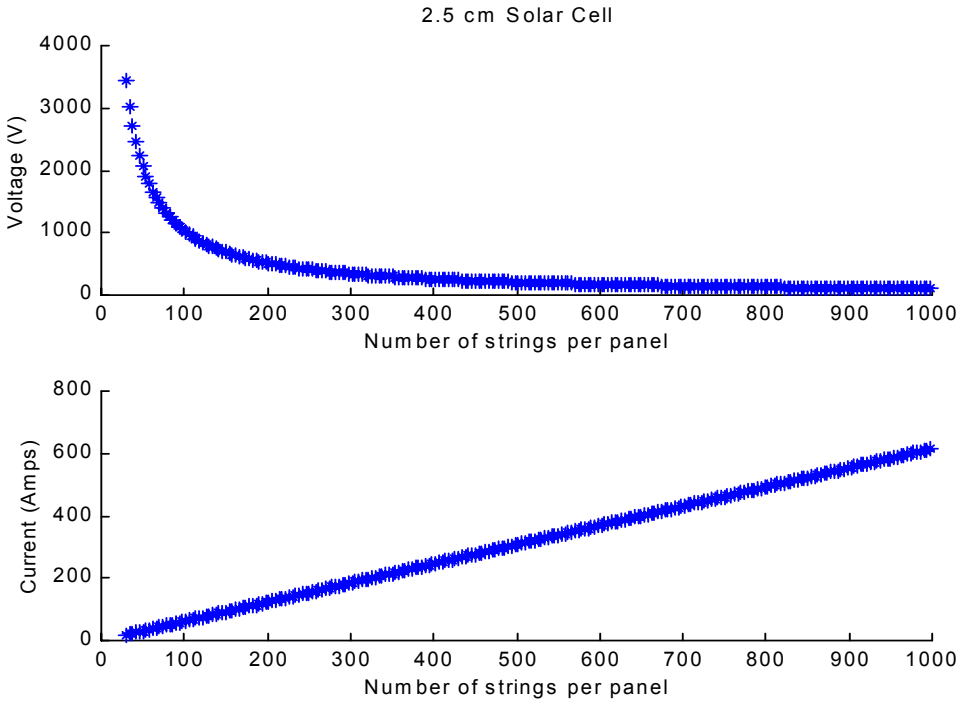

Figure 5-19: Voltage and Current versus Number of Strings

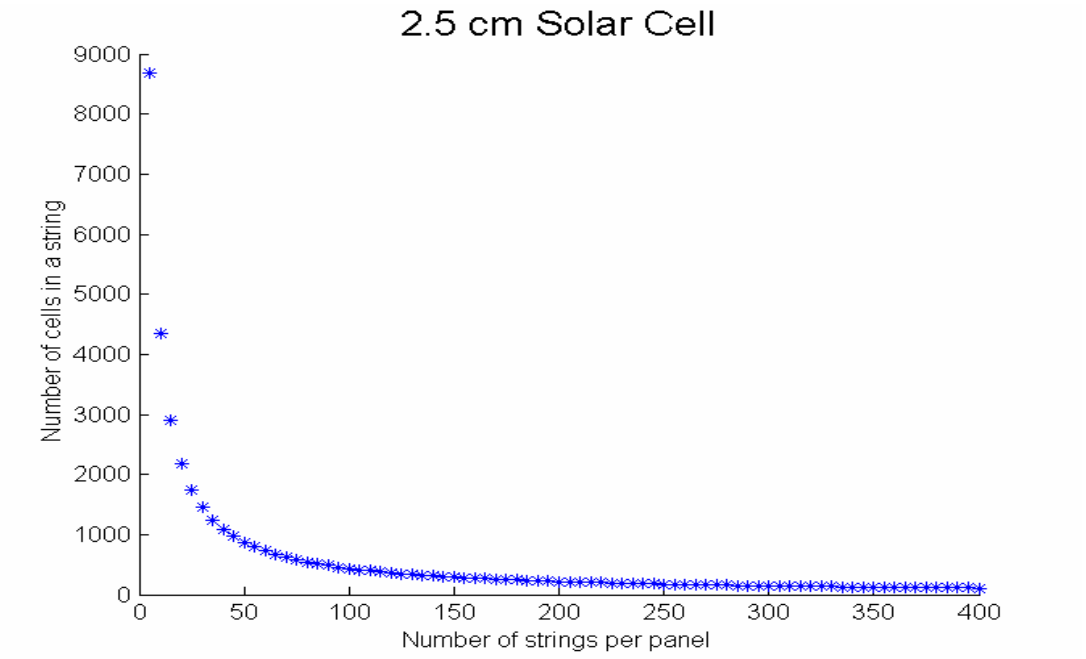

Figure 5-20: String Layout Optimization

For the 2.5 cm solar cell, two string layouts are analyzed. Layout one, shown in Figure 5-21, has 118 strings on a panel with 349 cells in a string. Using this configuration creates 140 Volts and 450 Amps. The voltage for this layout is sufficient, but another layout is analyzed for comparison.

Layout two cuts the number of strings in half and doubles the number of cells in a string, which increases the voltage. With 59 strings on a panel and 698 cells in a string, 280 Volts and 230 Amps are produced. This string layout is more beneficial then the first option because it balances voltage with current. The optimal cell layout is found factoring the power losses through the umbilical, array area, solar cell harnessing, and bus power.

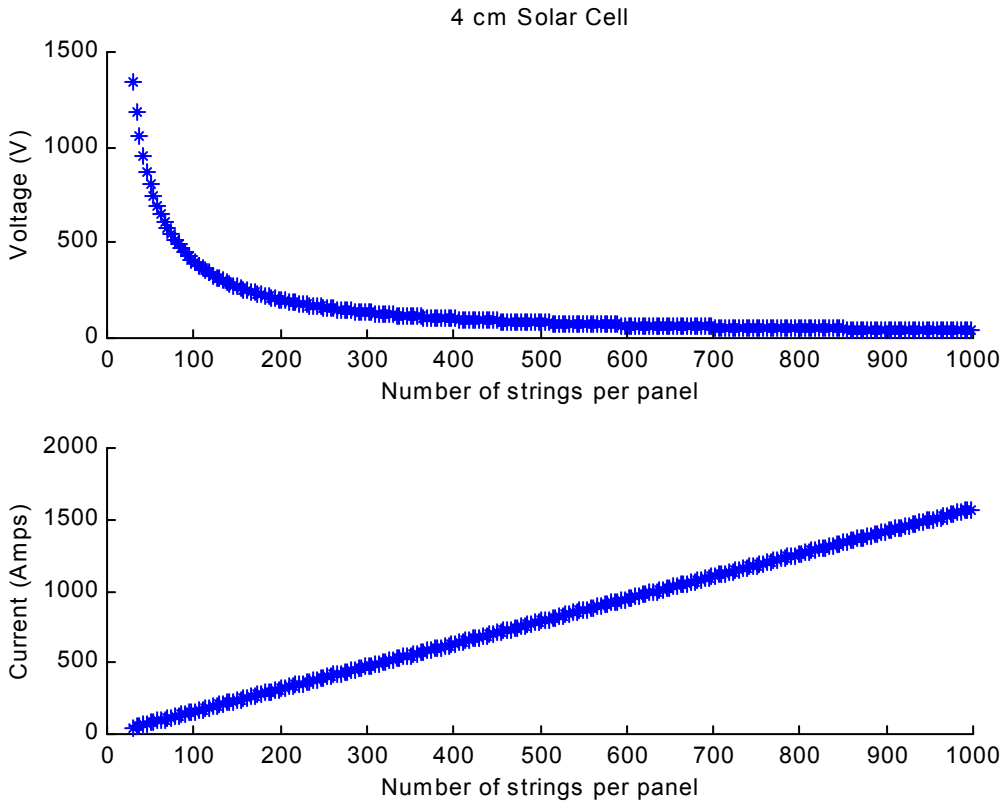

Figure 5-21: Voltage and Current versus Number of Strings

The same two string layouts are analyzed for the 4 cm solar cell. For the 4 cm solar cell, the number of cells in a string verses the number of strings on a panel is seen in Figure 5-22. Using the first layout, there are 74 strings on a panel. This gives 218 cells in a string, and produces 90 Volts and 730 Amps. Constraints on the umbilical design rule out this option because with a lower voltage, the area and power loss of the conductor are large. The second analysis completed using 37 strings on a panel with 435 cells in a string. This produces 180 Volts and 370 Amps. These numbers are better then the first option, but still are not ideal.

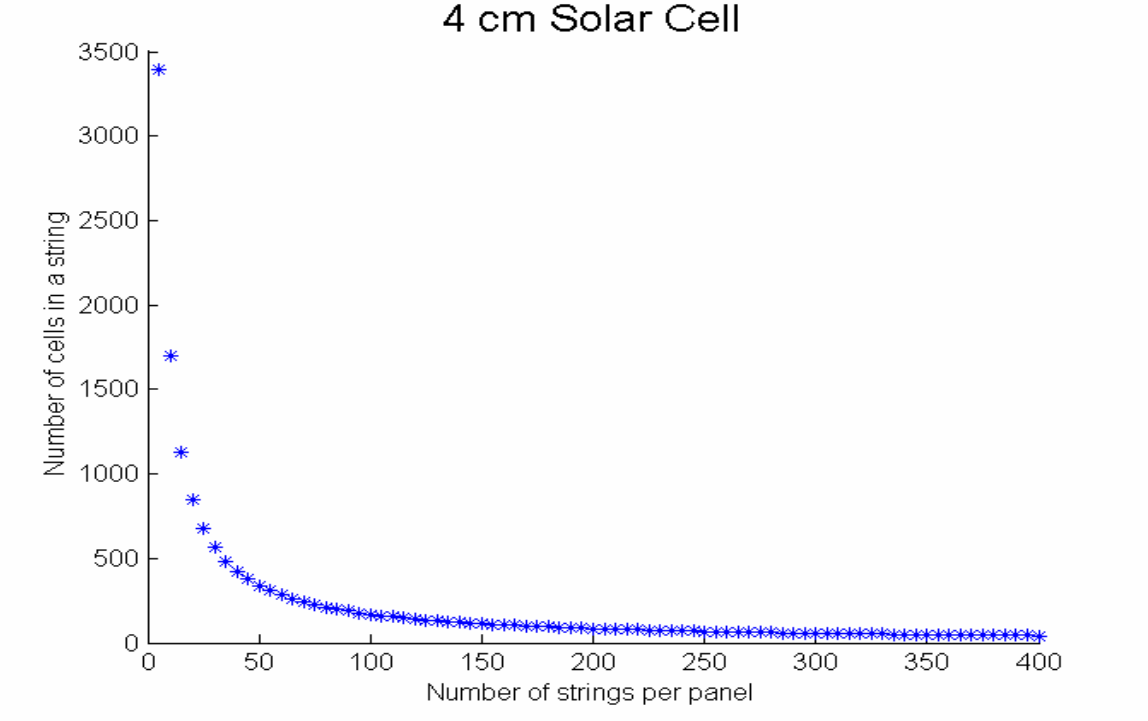

Figure 5-22: String Layout Optimization

5.6.2.3 Conclusion

Optimization is necessary to fully understand the power subsystem. Determining the power loss through the umbilical is iterative, and is dependant between the number of strings per panel and the number of cells per string. The voltage and current of the array is related to the number of cells per string. From the analysis of the two string layout options using the 2.5 cm cell, the second configuration is more efficient than that of Figure 5-21.

5.6.3 Thermal Subsystem Optimization

5.6.3.1 Introduction

The next step in the thermal design of PowerSail is to analyze and optimize the thermal design. This includes studying the effects of thermal properties such as absorptivity and emissivity of thermal coatings. If these properties are not favorable, the temperatures will not be within operating limits. The object of this section is to take into account the different factors affecting the thermal design and find a thermal design that maintains the operational temperatures.

5.6.3.2 Solar Array Optimization

The CIS cells used on PowerSail have a maximum operating temperature of 90°C. By changing emissivity, and absorptivity, we find the properties needed to operate the cells within this limitation. Emissivity and absorptivity are thermal properties of materials that depict how well the material emits or absorbs heat respectively (Ref. 22). If a material,

such as a solar cell, has a high absorptivity, it absorbs most of the heat and therefore increases in temperature. Increasing the emissivity of the solar cell counteracts this effect and maintains the material within the maximum operating temperature. The following figures display the changes that occur in the maximum and minimum temperatures by changing the thermal properties of the front and backside of the solar array. The operating altitude of PowerSail is between 1000km and geostationary, so Earth albedo and IR change with altitude.

Figures 5-23 and 5-24 vary the top emissivity for both 1000 km and geostationary orbit. The top emissivity must be at least 0.5 to maintain the temperature below 90°C for 1000 km. While in geostationary orbit, PowerSail never approaches the maximum operating temperature. This is due to the lowered albedo and Earth IR emission hitting the solar array caused by high altitude. The minimum temperature during eclipse decreases to nearly 200°C in geostationary orbit also causes the lower maximum temperature.

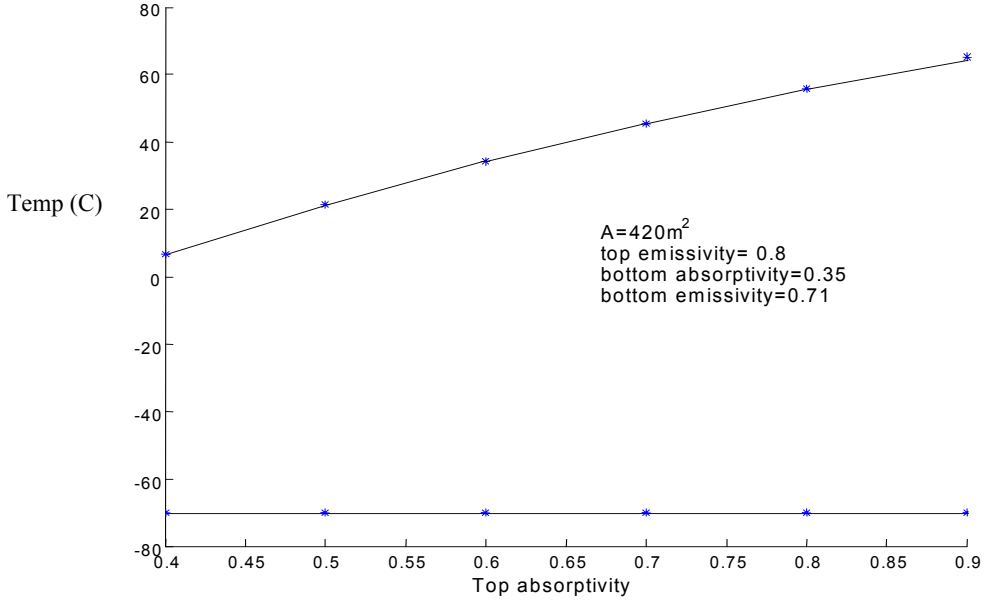

Figure 5-23: Changes in Absorptivity for 1000 km

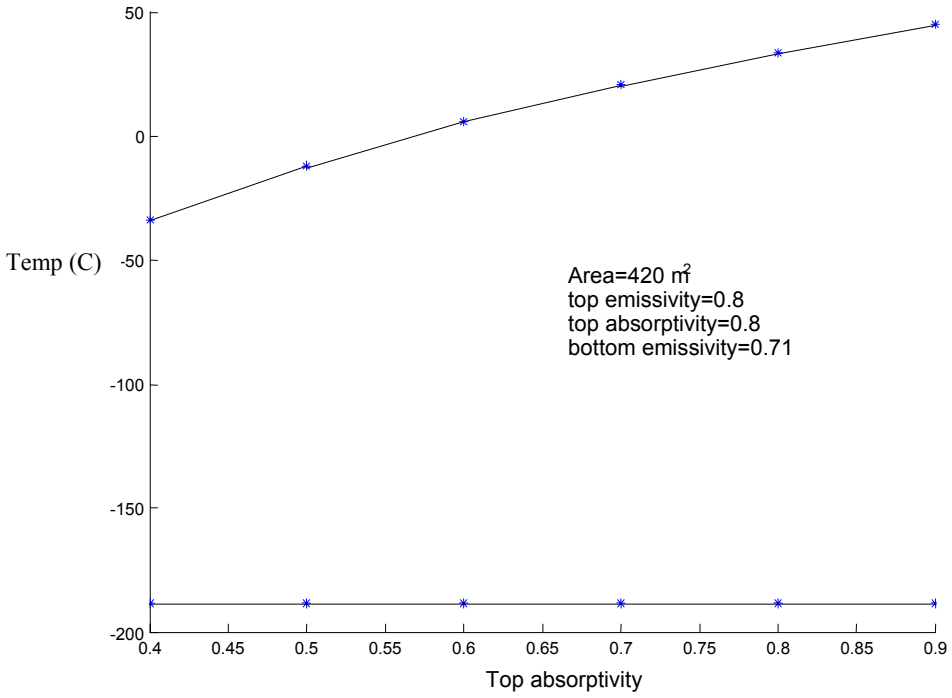

Figure 5-24: Changes in Absorptivity for Geostationary Orbit

Figures 5-25 through 5-28 show that change the thermal parameters of the front and backside of the solar array at both 1000 km and geostationary orbit. Only the top emissivity has a significant effect on the temperature resulting in a required emissivity of 0.5.

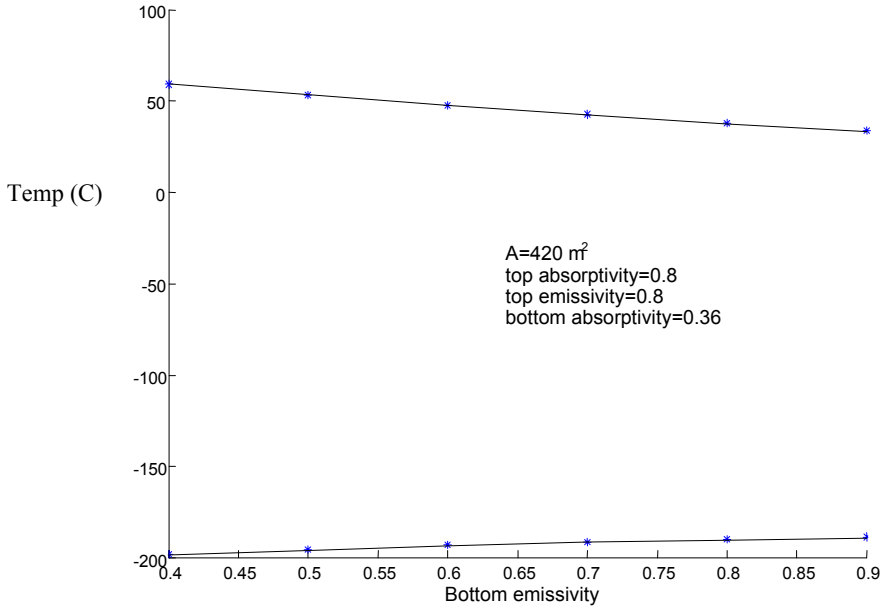

Figure 5-25: Changes in Emissivity for Geostationary Orbit

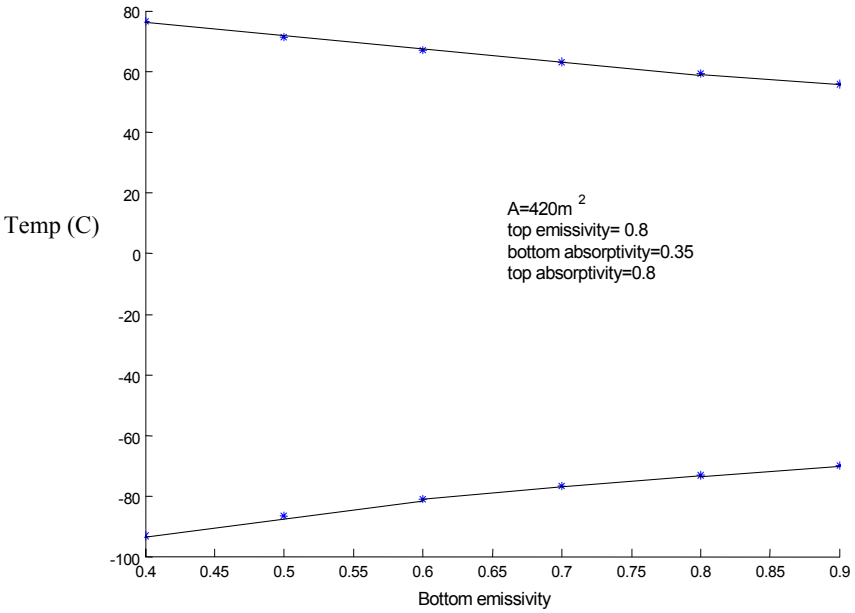

Figure 5-26: Changes in Emissivity for 1000 km

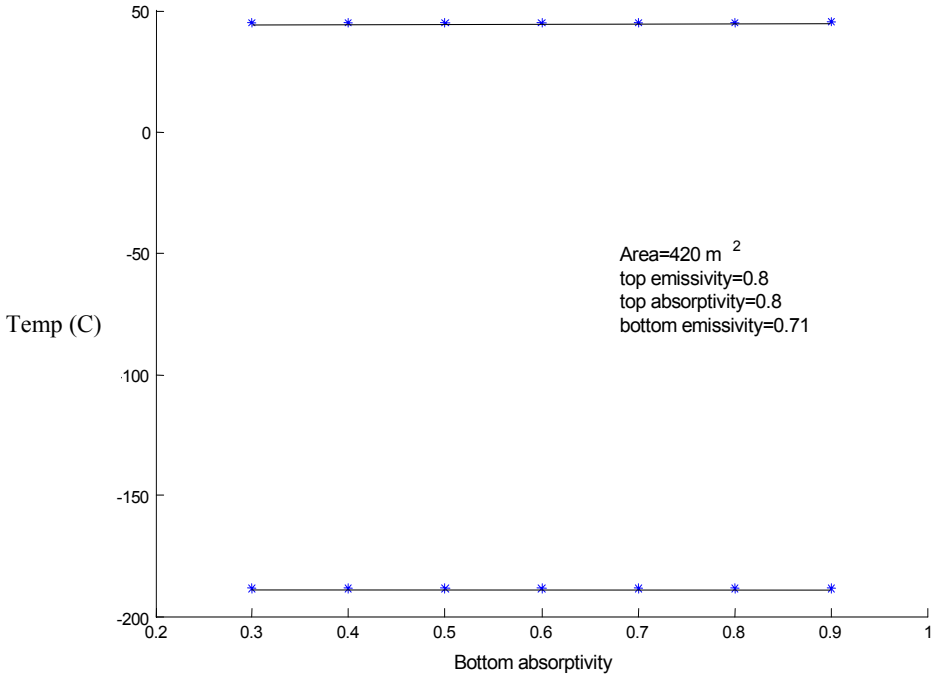

Figure 5-27: Changes in Bottom Absorptivity for Geostationary Orbit

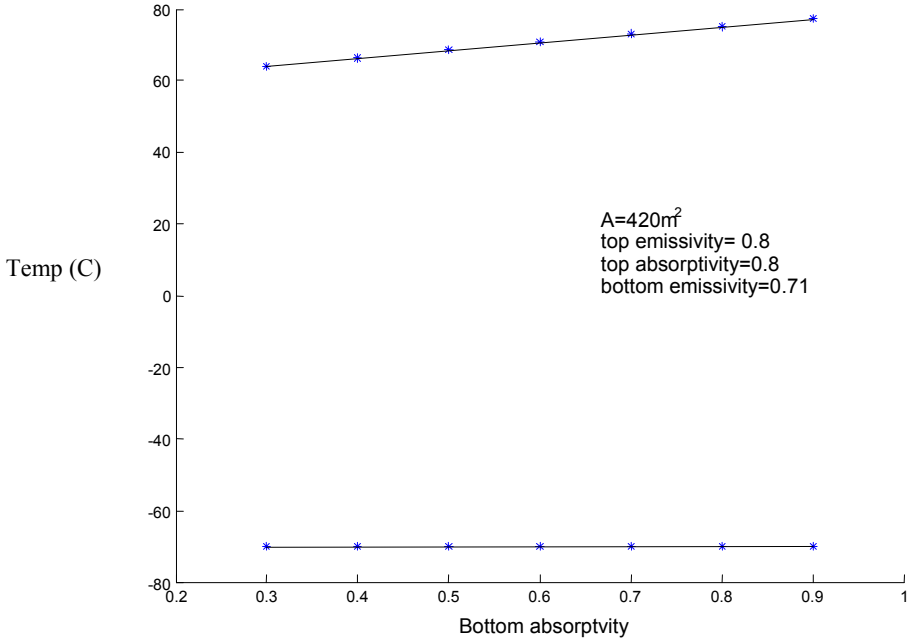

Figure 5-28: Changes in Bottom Absorptivity for 1000 km

The temperature of the solar cells increase at both altitudes as the top absorptivity increases. The solar cells require a high absorptivity to absorb solar energy, so we are limited in how we change that property on the front side of the array. However, we can change the absorptivity of the backside of the array. Lower absorptivities on the backside of the array yield lower maximum temperatures at 1000 km (see Figure 5-28). The only energy impacting the backside of the array is the Earth's albedo and IR emission resulting in lower maximum temperatures in geo-stationary orbit.

Now that the thermal properties required to maintain the operating temperatures of the solar cells are known, materials to coat the front and back of the array are selected. The top absorptivity is at least 0.8 since the absorptivity of the solar cells cannot change. To counteract that value, the emissivity of the front side of the array must be at least 0.5. Tefzel™ or Clear Polyamide 1 (CP1) are the two possibilities considered for coating the front side of the cells (Ref. 28). Both of these materials do not affect the absorptivity of the solar cell. Tefzel™ is a flexible cover glass bonded to the solar cell using a pressure sensitive adhesive that will provide the thermal emissivity needed for the solar cells. CP1 is cast directly onto the solar cells, eliminating the adhesive layer. Both of these materials are under development and there is no significant advantage over the other as of yet. The Tefzel™ has a higher emissivity, but CP1 eliminates the adhesive layer. In either case, the thermal emissivity is greater than 0.5, which satisfies the thermal requirements. Kapton is the polyamide web supporting the solar cells along with increasing the thermal absorption of the backside of the solar array to 0.71.

Since the thermal properties of the solar array are known, the radiation energies absorbed and emitted by the solar array verses altitude are calculated using the equations discussed in Thermal Modeling section. Figure 5-29 illustrates how the solar radiation absorbed by the array remains constant verses altitude and the IR radiation and absorbed albedo decrease with altitude.

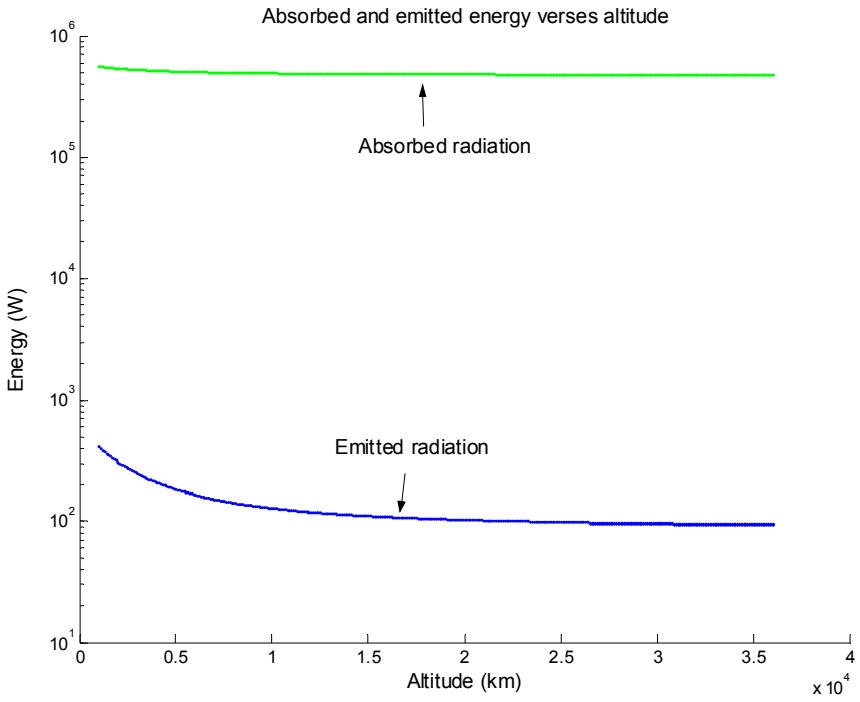

Figure 5-29: Energy Balance *vs.* Altitude

Figure 5-30 shows the total energy absorbed and emitted by the solar array. The emitted radiation decreases with altitude since it depends on the temperature. The temperature decreases with altitude since the absorbed energies from the albedo and IR emission decrease with altitude (see Figure 5-31). The radiation emitted from the array is important to analyze to see if there is enough to significantly heat the thruster modules or center bus.

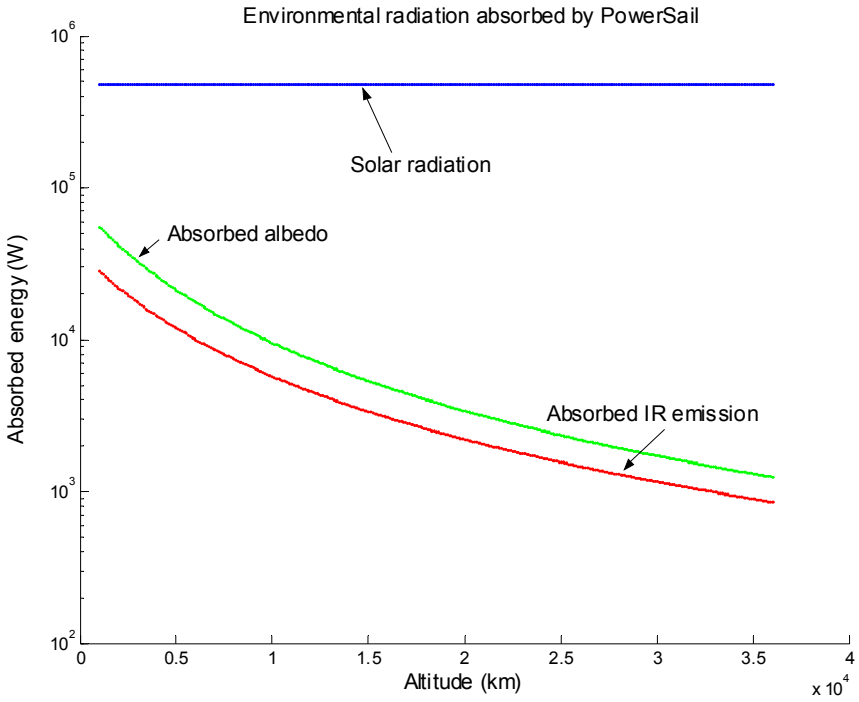

Figure 5-30: Energy Absorption versus Altitude

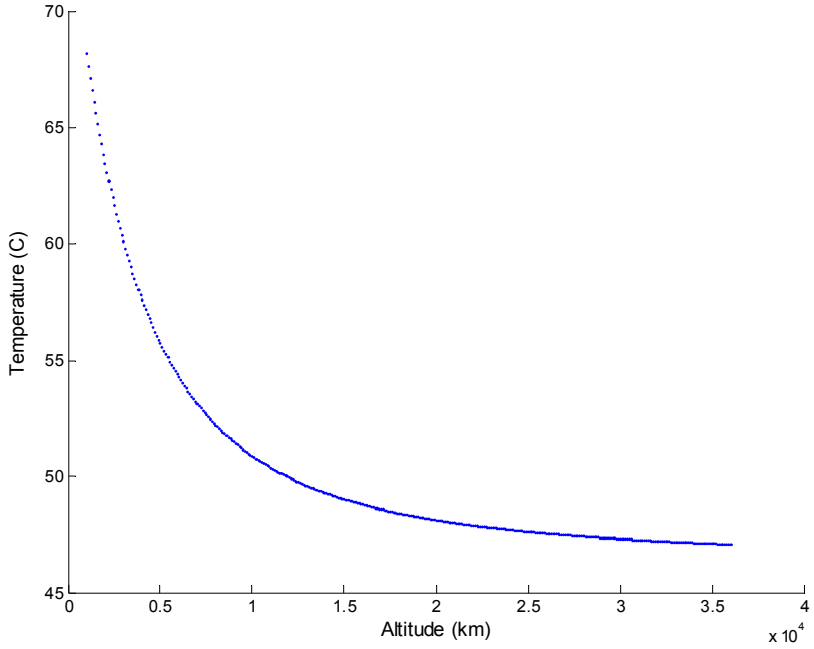

Figure 5-31: Maximum Temperature at Altitude

Once the radiation emitted by the solar array is known, we calculate the maximum and minimum temperatures on the thruster modules and main bus. In the MATLAB code for these calculations, maximum and minimum temperatures are plotted against changing emissivity and absorptivity. This allows for adequate selection of the materials needed to coat these components to maintain operating temperatures. In performing these calculations, the thruster modules are assumed to be cubes of 0.5 m X 0.5 m. The center bus is a cylinder with a radius of 0.13m.

The maximum heat transferred from the solar array to the main bus and the thruster modules is predicted to be around 160 W using the equation below.

$$q = \sigma \varepsilon_1 \varepsilon_2 A_1 F_{1-2} (T^4{}_1 - T^4{}_2) \tag{39}$$

$F_{1\text{-}2}$ is the view factor that is a function of size, geometry, relative position, and orientation of the two bodies. The view factor between the thruster modules and main bus and the solar array is 0.5 (Ref. 26 page 414). The value of the heat transfer is so small compared to the overall absorbed energy that it is disregarded.

Figures 5-32 and 5-33 illustrate the maximum and minimum temperatures at 1000 km for the thruster modules and the central bus, respectively. The red lines are the maximum temperatures while the blue lines are minimum temperatures. The different lines represent different internal heat dissipation starting at 150 W and increasing by 50 up to 300 W for the thruster modules. The lines on the figure for the central bus represent heat dissipation at 0, 25, and 50 W. The average heat dissipation inside the thruster modules will be around 150 W, 12% for the thrusters and capacitors, and 20% for the PPU. The power dissipation in the bus is much lower since the components in the bus do not produce much heat. From these graphs we can see how changes in the heat dissipation affect the temperature of the component. Obviously the higher heat dissipation means higher temperatures. The absorptivity in for both components must be as low as possible to maintain the operating temperatures. For the thruster modules, the absorptivity must be at least 0.2. This will keep the modules from getting too hot for a heat dissipation of around 175 W. The bus must also have absorptivity around 0.2. This protects the bus for heat dissipation up to 25W.

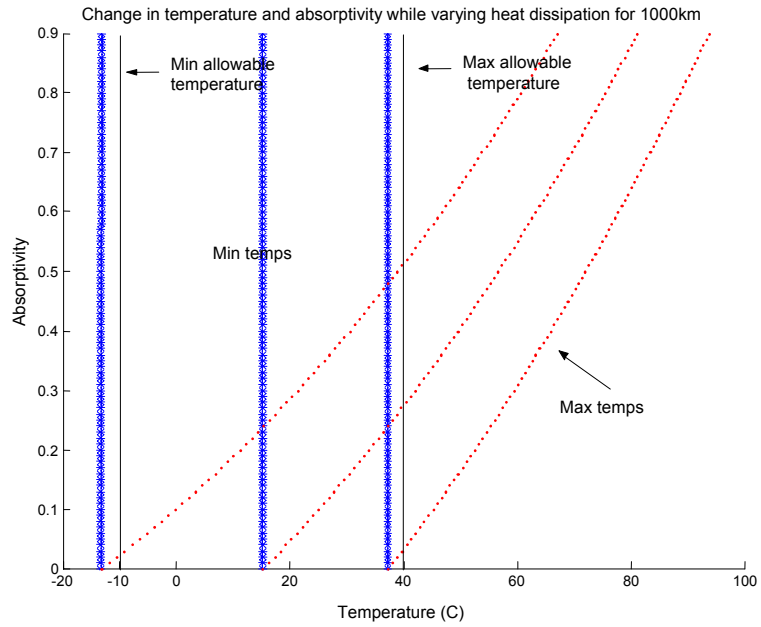

Figure 5-32: Absorptivity versus Temperature of Thruster Modules at 1000 km

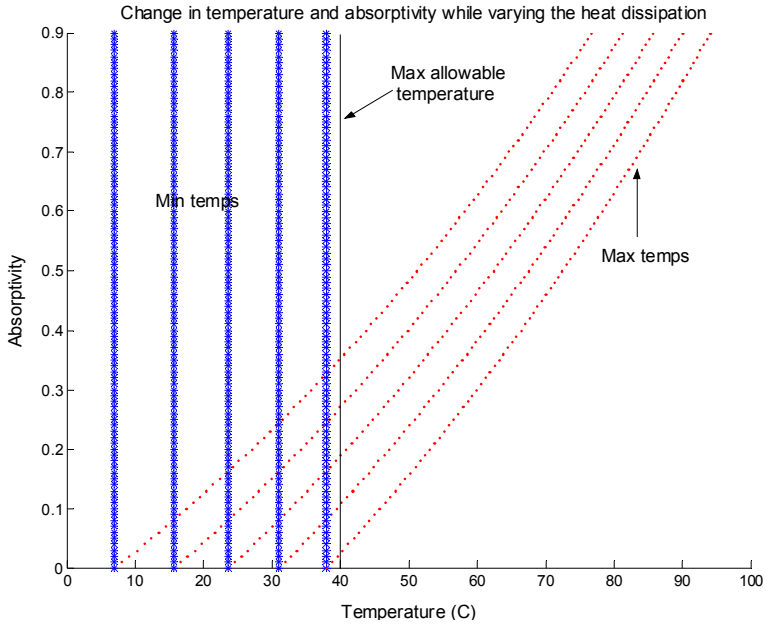

Figure 5-33: Absorptivity versus Temperature of Bus at 1000 km

The same analysis was performed at geo-stationary orbit as well. The temperatures change as the absorptivity increases. Therefore the difference in temperatures between the altitudes is not significant as can be seen in Figures 5-34 and 5-35.

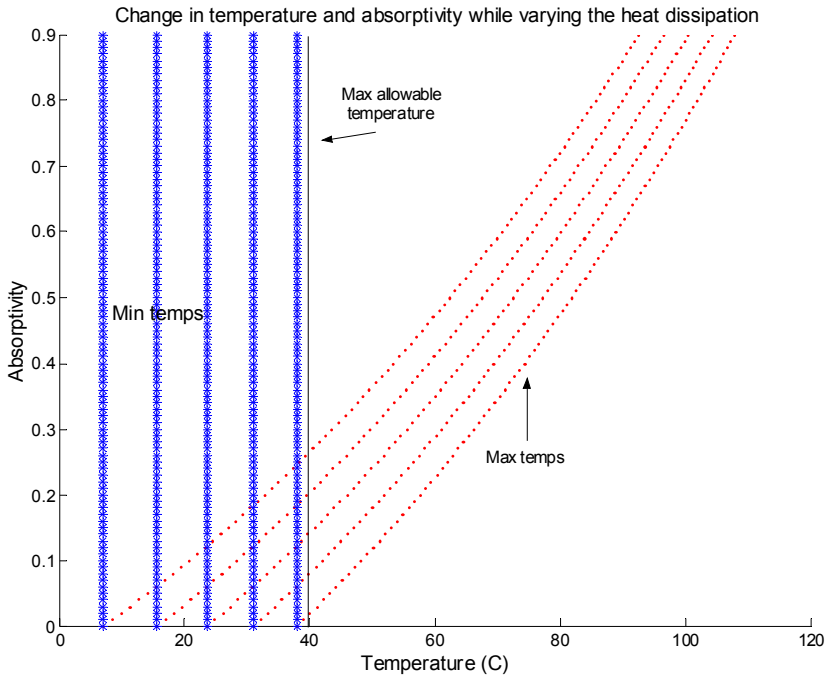

Figure 5-34: Absorptivity versus Temperature of Thruster Modules in Geostationary Orbit

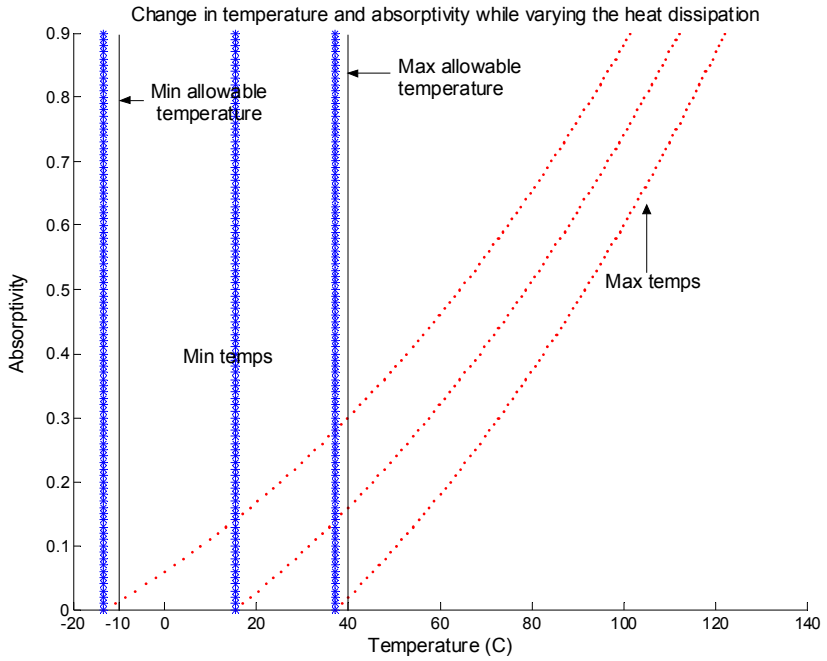

Figure 5-35: Absorptivity versus Temperature of Bus in Geostationary Orbit

Material selection is the next step in the thermal analysis of the thruster modules and the central bus. Passive materials that require no power to dissipate heat are preferred over active thermal control devices. Some common radiators considered for the modules and bus are included in Table 5-16.

Table 5-16 Thermal Material Properties (Ref. 20, page 158)

Material	Absorptivity	Emissivity
YB71 white paint	0.18	.88
S-13G-LO white paint	0.2	0.84
Silvered Teflon	0.10	0.77

From observation, the silvered Teflon™ appears to be the best choice for the PowerSail components. However, the affects of the Teflon™ plume from the PPTs on the Teflon™ coating of the modules has not been analyzed. This is something to be looked into further. In the mean time, the YB71 white paint is the chosen material to cover the thruster modules and the main bus, which are aluminum. The white paint has acceptable absorptivities, and also leaves room for lifetime degradation of the absorptivity. The absorptivity will degrade to 0.25 after 10 years, which still maintains operational temperatures. The white paint will cover 1.25 m^2 leaving room for the PPT nozzles sticking out of the modules. The paint also covers about 75% of the central bus, leaving margin for insulation to maintain the minimum temperature during eclipse.

5.6.3.3 Conclusion

The thermal subsystem maintains the operating temperatures of all the components as well as analyzes the heat radiated from the solar array. This is a simplified version of the thermal analysis required for PowerSail. The next steps required in thermal analysis are discussed in Section 5.8.

5.6.4 Structures Subsystem

5.6.4.1 Introduction

Now that we have an accurate model for both the structure and inflation system, it must be optimized. By optimizing the structural model, mass is reduced, modal frequencies are kept away from the thruster firing frequency of 2 Hz, and stowed volume is minimized. Through optimizing the design of the inflation system, different sections may be inflated, and tank pressures are kept low for safety reasons. This section discusses the process and results of optimizing both systems.

5.6.4.2 Finite Element Model

The finite element model can be optimized numerous ways. Material properties are altered to reflect differences in materials and rigidization methods. Component placement is altered, which changes the dynamic characteristics of the structure. Multiple inflation sections are used to minimize the effects of micrometeor impacts during inflation and before rigidization. Beam sections are also added to raise the natural frequencies.

5.6.4.3 End Beam

A basic PowerSail configuration, shown in Figure 5-36 with eight ribs and one spar, has mode shapes that are shown in Figures 5-37 through 5-39. The color bar on the figures obtained from the finite element model shows the magnitude of deformation, which has a maximum value of 1 m for all modes.

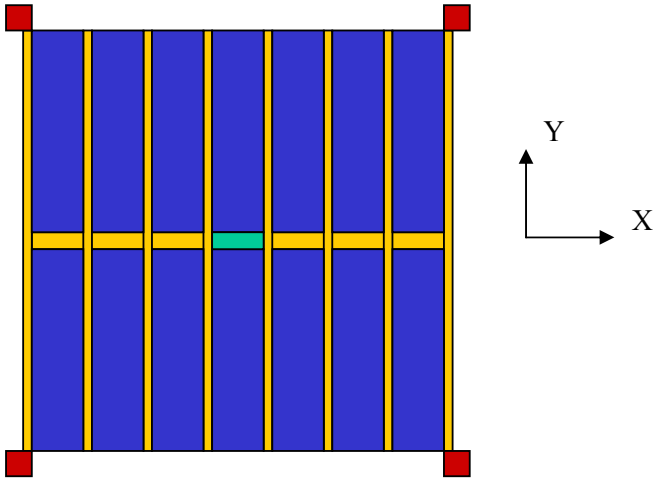

Figure 5-36: PowerSail With No End Beams

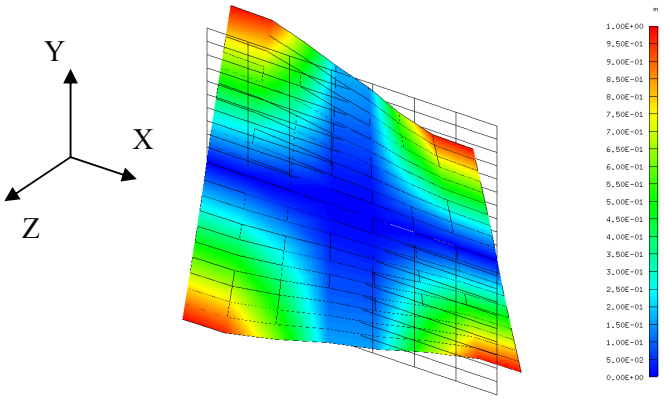

Figure 5-37: First Mode, No Beams

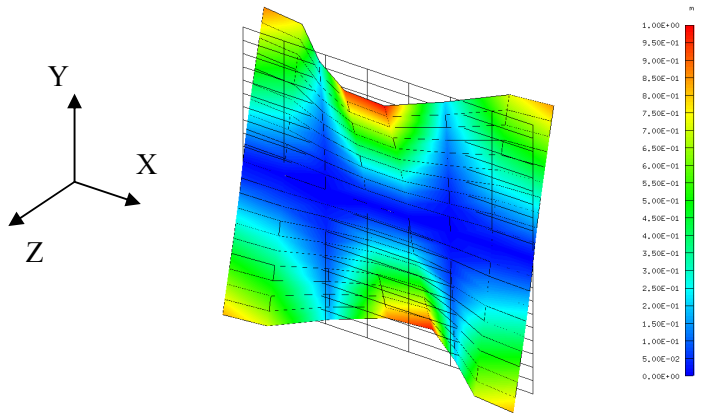

Figure 5-38: Second Mode, No Beams

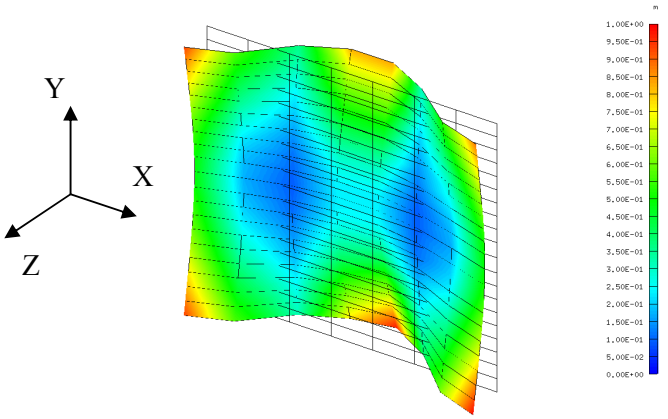

Figure 5-39: Third Mode, No Beams

Results from the finite element model of PowerSail without end beams show that significant deformation gradients exist in the second and third mode of vibration. These modes occur at low natural frequencies. High deformation gradients cause unfavorably high stresses in the solar array. Placing an end beam on the structure produces the mode shapes shown in Figures 5-40 through 5-42.

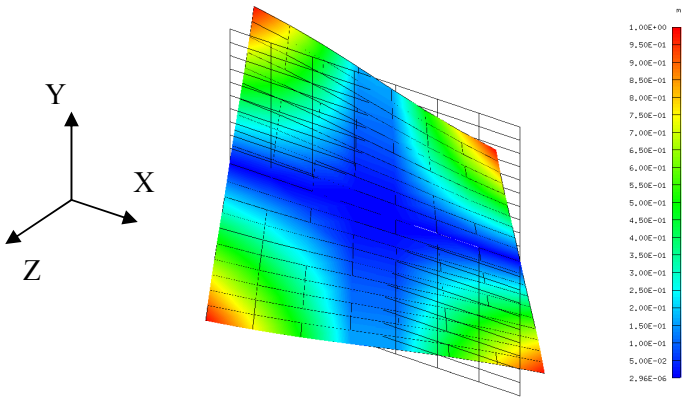

Figure 5-40: First Mode– Structure Alone

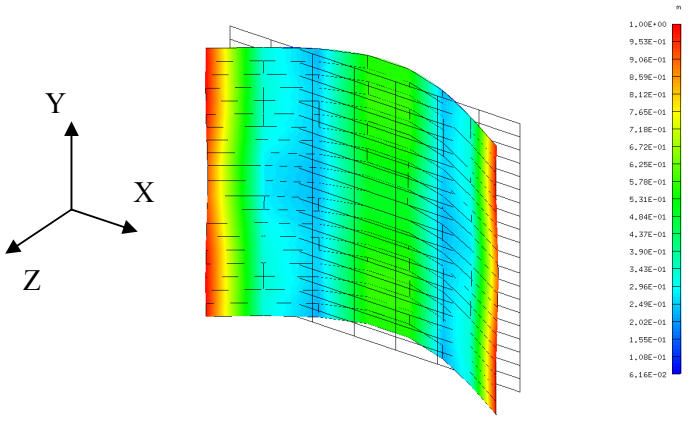

Figure 5-41: Second Mode– Structure Alone

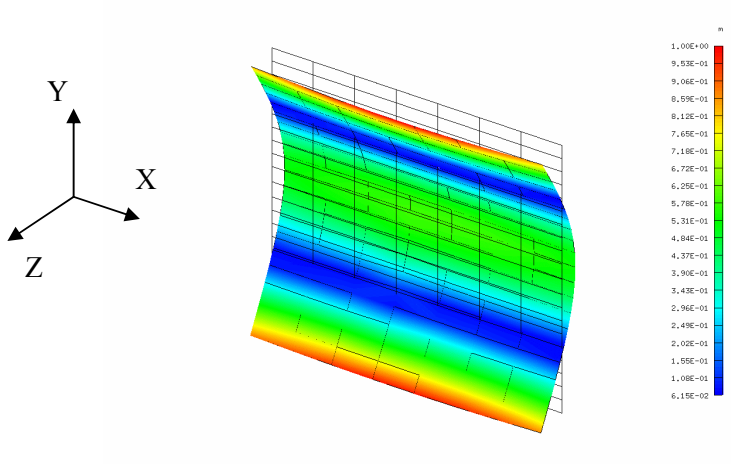

Figure 5-42: Third Mode– Structure Alone

Using the end beams the structure has smaller deformation gradients and higher modal frequencies as shown in Table 5-17. By adding this beam, mass is added and more requirements are placed on the inflation system. However, the inflatable beams and pressurant have low mass. Since the inflation pressure is so low, only a small addition to the pressurant tank is required.

Table 5-17: Effect of Adding End Beam

	First Mode [Hz]	Second Mode [Hz]	Third Mode [Hz]
With End Beam	0.21	0.29	0.38
Without End Beam	0.01	0.17	0.19

5.6.4.4 Modal Dependence on Material Properties

When rigidizing method is considered, the modulus of elasticity changes from the original material. In the case of an aluminized laminate on Kapton, the modulus ranges from 5 to 12 MPsi (Ref. 6), and is primarily dependent upon the thickness of the aluminized laminate layer.

Table 5-18 shows how the mode frequencies are proportional to Young's Modulus. By decreasing an average modulus for aluminized Kapton by an order of magnitude, the first mode frequency decreased by 70 %. Doubling the same modulus gave a 50 % increase to the first modal frequency. Mass density variations have little effect on modal frequencies, as shown in Table 5-19.

Table 5-18: Modal Dependence on Young's Modulus

E [GPa]	First Mode [Hz]	Second Mode [Hz]	Third Mode [Hz]
3	0.06	0.09	0.11
34.5	0.21	0.29	0.38
72	0.30	0.40	0.55

Table 5-19: Modal Dependence on Beam Density

Corner Mass [kg]	Bus Mass [kg]	Beam Density [kg/m^3]	First Mode [Hz]	Second Mode [Hz]	Third Mode [Hz]
50	50	1400	0.14	0.21	0.34
50	50	1470	0.14	0.21	0.34

5.6.4.5 Modal Dependence on Mass Distribution

Changing component mass distribution is a major factor that alters the dynamic characteristics of the structure. Table 5-20 shows the affect of incorporating the bus and corner modules into the finite element model. This table shows that when a tip mass is added, the first mode frequency drops by 33%.

Table 5-20: Modal Dependence on Component Mass Distribution

Corner Mass [kg]	Bus Mass [kg]	First Mode [Hz]	Second Mode [Hz]	Third Mode [Hz]
0	0	0.21	0.29	0.38
0	50	0.21	0.29	0.37
50	0	0.14	0.22	0.34
50	50	0.14	0.21	0.34

Figures 5-43 through 5-45 show the dynamic response when a 50 kg bus is added to the structural model. By adding the bus mass, the mode shapes change only slightly from the case when only the structure is considered, but modal frequencies stay relatively constant.

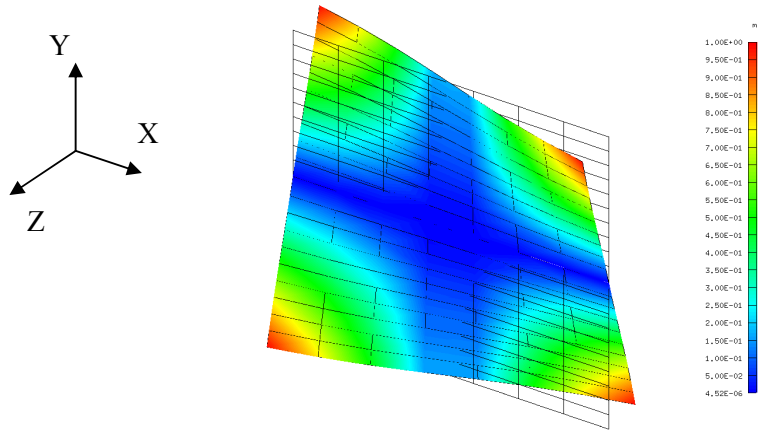

Figure 5-43: First Mode– 50kg Bus Included

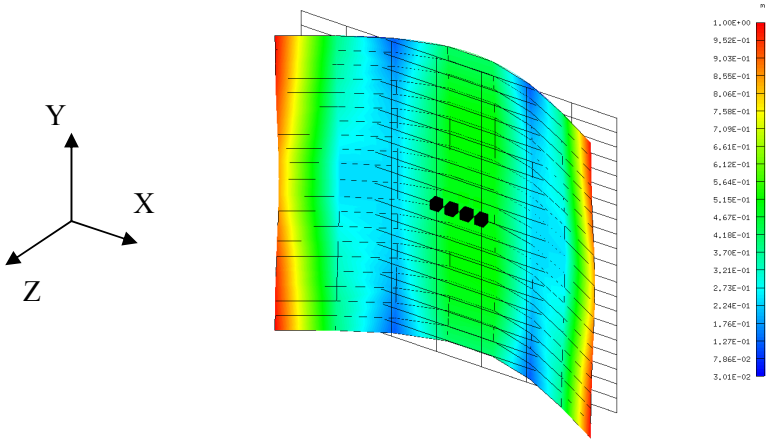

Figure 5-44: Second Mode, 50kg Bus Included

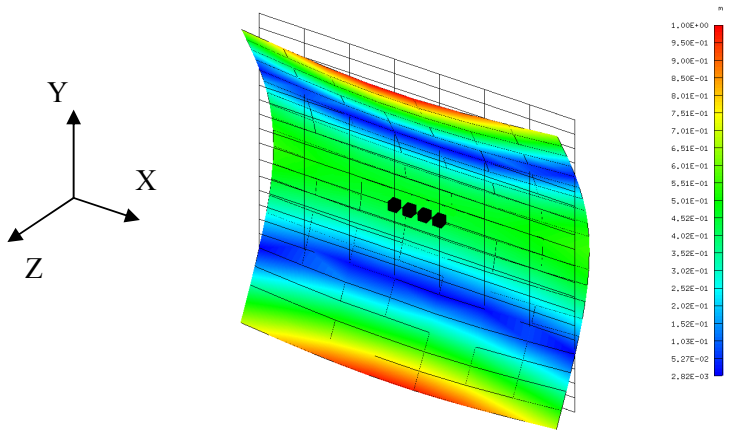

Figure 5-45: Third Mode– 50kg Bus Included

Figures 5-46 through 5-48 show the mode shapes when 50 kg tip masses are added to the model. Adding corner masses change the mode shapes from when the structure alone and the bus mass are modeled.

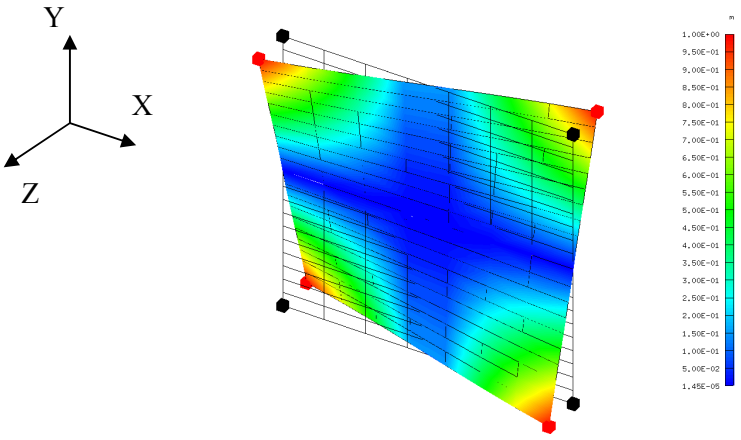

Figure 5-46: First Mode, 50kg Bus and 50kg Corner Mass Included

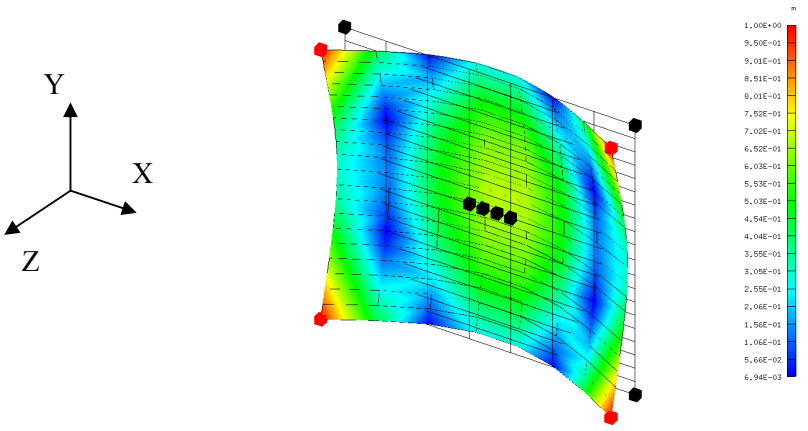

Figure 5-47: Second Mode, 50kg Bus and 50kg Corner Mass Included

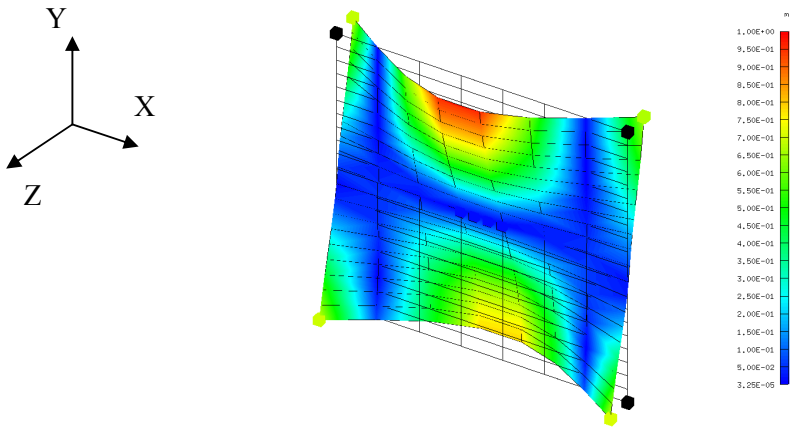

Figure 5-48: Third Mode, 50kg Bus and 50kg Corner Mass Included

5.6.4.6 Inflation System

Optimizing the design of the inflation system requires developing a tank that has low mass and fits inside the bus. The system schematic is shown again in Figure 5-49. An inflation pressure of 2.1 Pa is sufficient to inflate the structure, and rigidize an aluminum laminate (Ref. 7). Knowing this inflation pressure, the tank size is picked to be a 13.5 cm radius sphere leading to a tank pressure of 8 kPa.

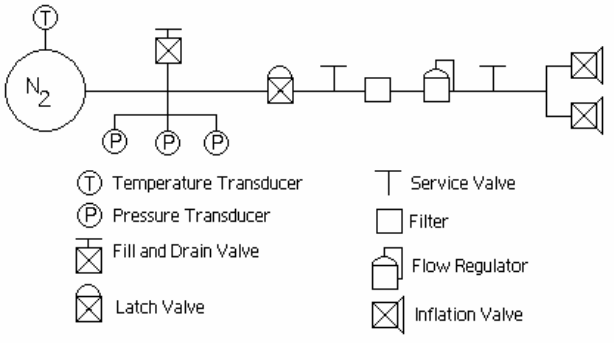

Figure 5-49: Inflation System

Temperature and pressure transducers are located on the pressurant tank so that ground controllers may monitor tank pressure and vent the tank if pressure is near the operating limits of the system. There are two service valves located on the inflation system plumbing. A filter is used such that no foreign objects are vented into the inflatable beams of PowerSail that could puncture the wall material. A flow regulator is included so that PowerSail does not deploy too rapidly and cause any failures in the inflatable beams or solar arrays. The inflation system mass is minimized by having the capability to inflate both sections using system.

5.6.4.7 Final Structural Configuration

The deployed configuration of PowerSail is shown in Figure 5-50, and is driven by the requirement to generate 50 kW of power. The solar arrays dominate the structure, with a total area of 420 m^2. This array is divided into 14 pieces, each being 3 m × 10 m.

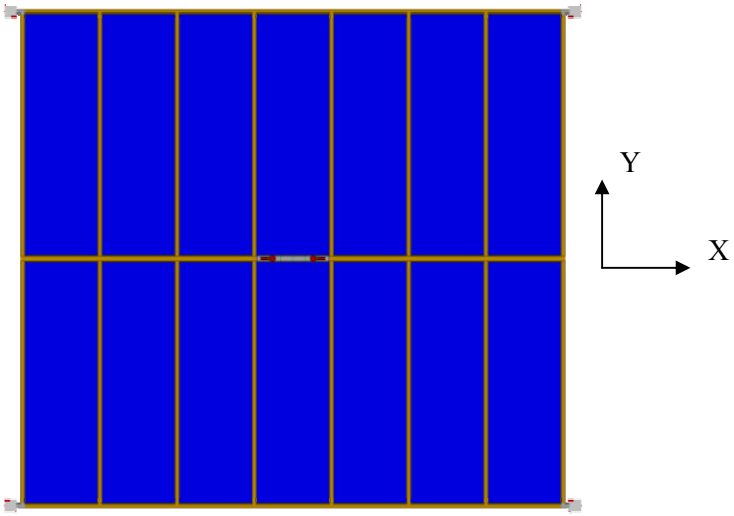

Figure 5-50: PowerSail Configuration

The ribs and end beams are 0.2 m in diameter and the spar is 0.3 m in diameter. There are a total of eight ribs, two end beams, and one spar. Thruster modules are located at each of the four corners, each containing ten thrusters and one accelerometer. Aluminum isogrid is used as the secondary structure for the corner modules. This is done to reduce mass without losing strength when compared with a typical stiffened shell structure. This structure is not analyzed or described further because it is beyond the scope of this project as it is secondary structure. Located in the center section of PowerSail is the main bus housing the command and data handling system, the inflation system, and a star tracker. The secondary structure of the bus is a stiffened, thin shell aluminum structure. Figure 5-51 shows the dimensions of the thruster mounts, and Figure 5-52 shows the dimensions of the solar array sections.

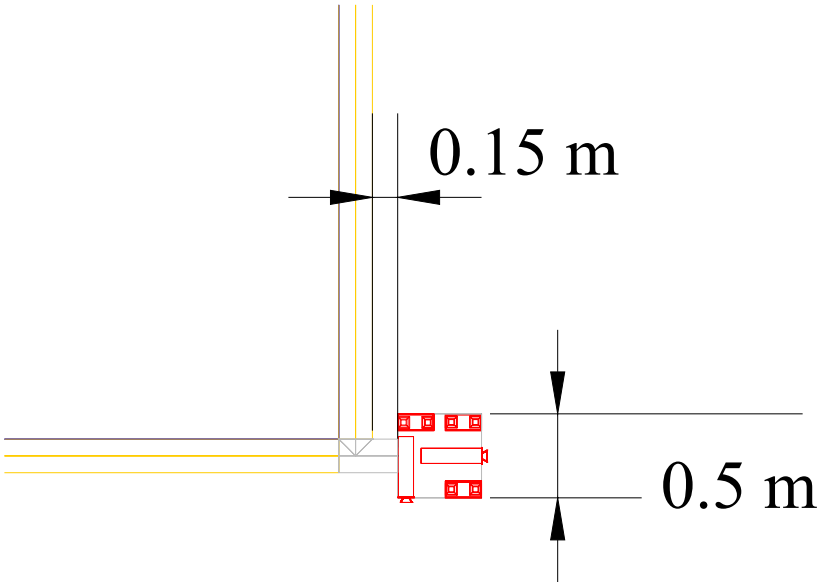

Figure 5-51: Thruster Module Dimensions

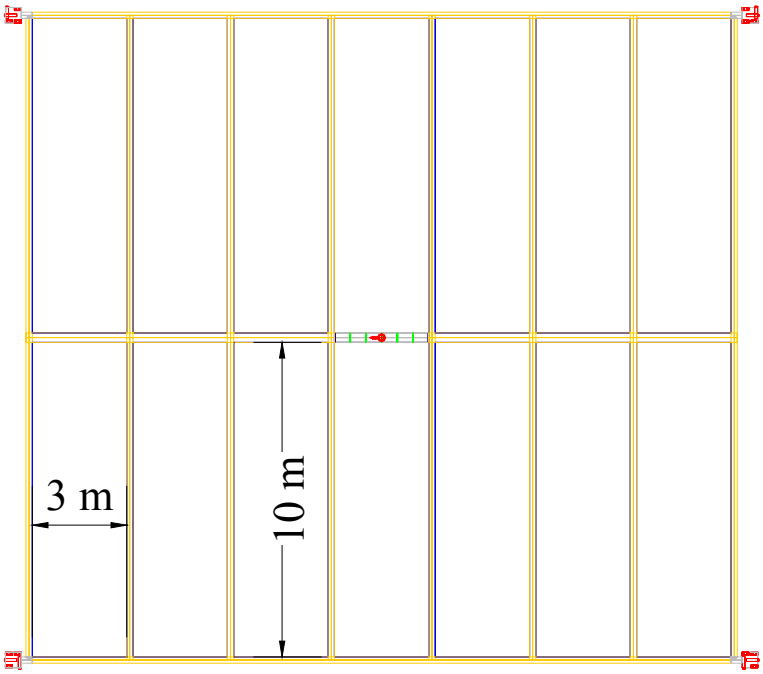

Figure 5-52: Solar Array Dimensions

5.6.4.8 Beam Description

A cross section of the beams of PowerSail is shown in Figure 5-53. The beams consist of a layer of multi-layer insulation (MLI) and the support laminate. The MLI layer is comprised of two layers of Kapton® and one layer of Mylar®. The support laminate is made of a thin layer of aluminum between two layers of Kapton®.

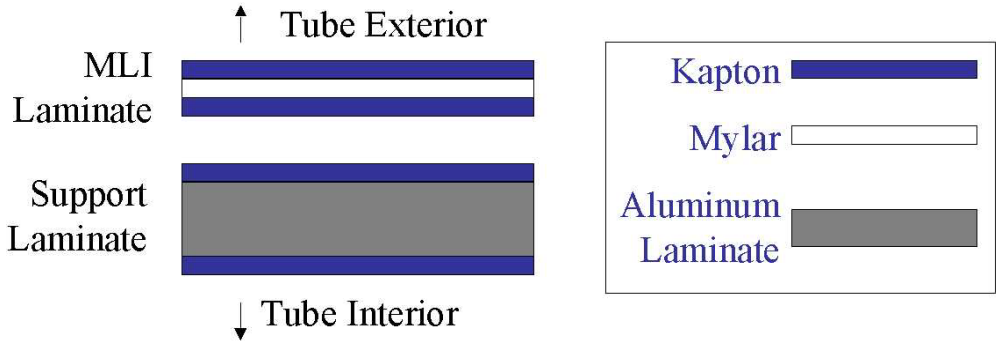

Figure 5-53: Beam Cross Section

Typically, the aluminum laminate layer is no more than 0.13 mm thick. A thickness greater than 0.13 mm leads to wrinkling of the aluminum when the structure is stowed (Ref. 6).

The beams are inflated to a pressure at which the aluminum laminate layer yields. This yielding produces cold work to occur in the aluminum leaving it rigidized.

5.6.4.9 Deployment Sequence

The deployment sequence of PowerSail shown in Figure 5-54 is simple, but requires a feedback control system. Figure 5-54 (A) shows PowerSail in the stowed configuration. The ribs, which are the beams lying in the y-axis direction, inflate first bringing PowerSail to the configuration shown in Figure 5-54 (B). Once the ribs are fully inflated the control system starts inflation of the spar and end beams, bringing PowerSail to the fully inflated and deployed configuration as shown in Figure 5-54 (C).

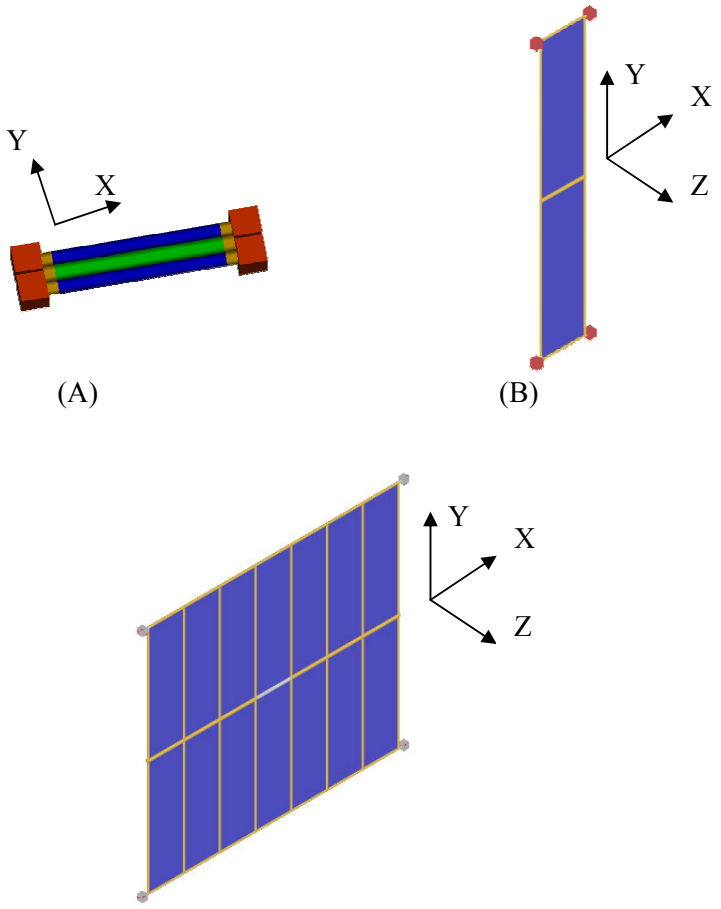

Figure 5-54: Deployment Sequence

5.6.4.10 Mass Breakdowns

When component masses are considered, the modal frequencies are determined to be well below the operating frequency of the PPT's. The mass breakdown of the structure subsystem is shown in Table 5-21.

Table 5-21: Mass Breakdown

Inflatables	21.8 kg
Thruster Module	28.0 kg
Latch Valve	0.5 kg
Relief Valves	0.1 kg
Service Valves	0.7 kg
Solenoid Valves	0.6 kg
Tank	7.0 kg
Bus	20.0 kg
Total Structure Mass	78.6 kg

Figure 5-55 shows another breakdown of the system mass. Note that the primary structure accounts for only 28% of the total structural mass, and the secondary structure of the corner modules has the most mass of any components.

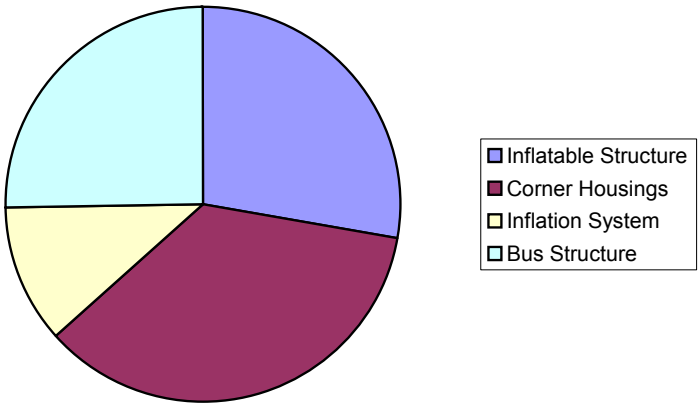

Figure 5-55: Mass Breakdown of Structures Subsystem

5.6.4.11 Conclusion

The PowerSail structural configuration is optimized using different structural and component configurations. Mass and stowed volume are minimized, while still allowing PowerSail to meet its requirements. Modal frequencies are kept away from the thruster firing frequency. The inflation system is also optimized to minimize mass, while maintaining reliability.

5.6.5 Propulsion Subsystem

5.6.5.1 Introduction

The propulsion system is a critical part of PowerSail's design. The system must be able to maintain the leader-follower formation with the Host satellite, while having low mass and power requirements. Thus, the configuration and optimization of the propulsion system is important.

5.6.5.2 Propulsion System

The results obtained from the code show that the distance between the Host and PowerSail exceed the umbilical length by several kilometers in less than one orbit when not using a control system. In all figures in this section the Host's orbit is green, PowerSail's orbit is blue and the reference point is in red. The circle is the original location, while the star is the final location after one orbit. The magnitude between the Host and PowerSail is shown in Figure 5-56.

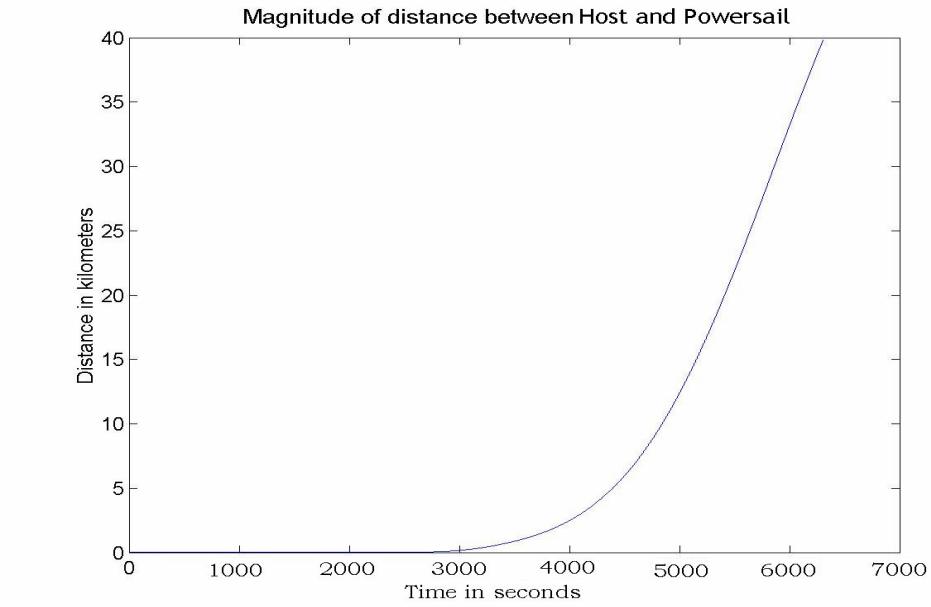

Figure 5-56: Magnitude of the Distance Between the Host and PowerSail vs. Time With an Inactive Control System

A planar view of the orbit viewing down the angular momentum vector is in Figure 5-57.

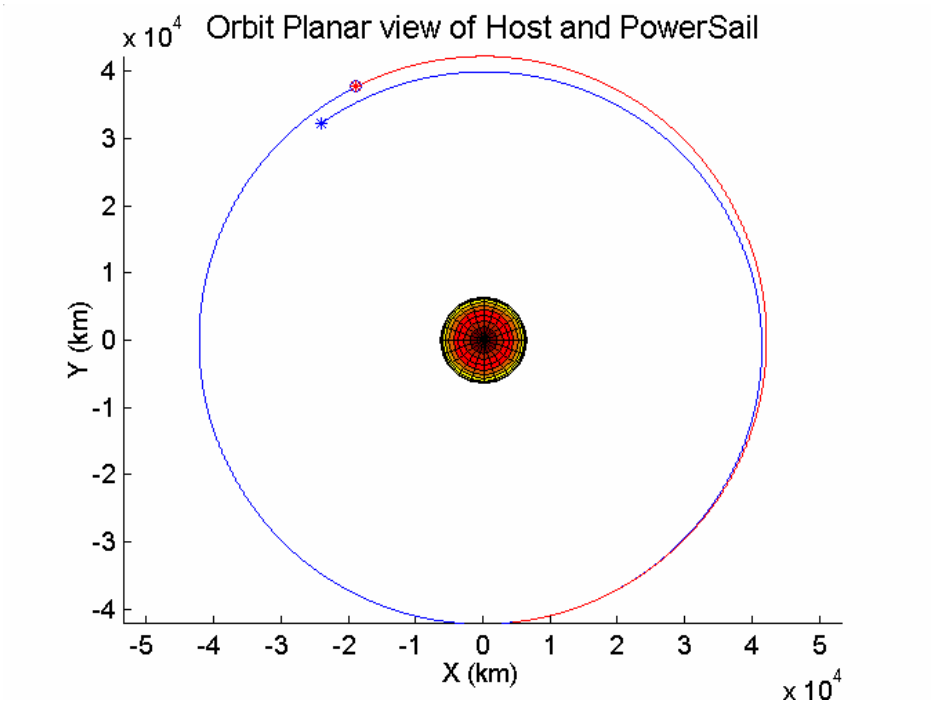

Figure 5-57: Orbit Planar View of the Host and PowerSail in a Geostationary Orbit after One Orbit With an Inactive Control System

PowerSail uses clusters of PPTs placed in corner modules. PPTs were selected for a number of reasons. The data obtained from the orbit model mentioned in Section 5.5.4 gave amounts of system impulse needed per year to maintain the formation. The propulsion system has a total of 40 thrusters located in 4 separate corner modules. An example of a module is shown in Figure 5-58.

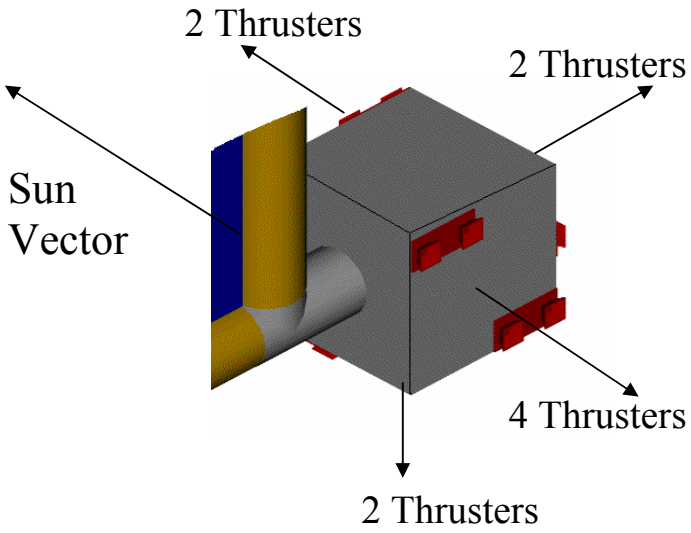

Figure 5-58: Thruster Module Diagram

The propellant for a PPT is a solid block of Teflon™. Solid propellant is desirable to avoid sloshing effects of liquid propellant. The thruster modules translate from their original locations when the thrusters are firing, as well as during the normal course of PowerSail's operation. If there were liquid propellant tanks in the modules, the vibration could be greater due to sloshing in the tanks.

PPTs have adaptable power supply systems. The power supply scheme for a cluster of PPTs can include up to four thrusters per capacitor and up to four capacitors per PPU. Thus with a cluster of thrusters in a single small thruster module, the power system can control the whole module while keeping mass at a minimum. The power supply configuration for the PPTs in each module consists of three capacitors and one PPU for all ten thrusters. This integration lowers system mass considerably, since capacitors have the largest amount of dry mass.

The thrusters also have extra Discharge Initiation (DI) circuits. The total impulse of a PPT is not based on amount of propellant for the thruster; the limiting factor is the spark plug and DI circuit. Currently, Primex Aerospace Company spark plugs are rated at a lifetime of approximately 10 million pulses. This cycle life corresponds to 0.65 kg of Teflon propellant. It is possible to add additional spark plugs and DI circuits so that a single thruster has a higher overall lifetime impulse. It is also possible to have up to 4 DI circuits in a single thruster. With four DI circuits, the propellant available to a single thruster is increased to 2.6 kg. The thruster group of 4 has thrusters with four DI circuits, while the thruster pairs have two DI circuits per thruster (see Figure 5-58). With a single DI circuit, the total impulse for a single thruster is 8.6 kN-sec. With four DI circuits, the total impulse of a single thruster is increased to 34.4 kN-sec.

Pulsed plasma thrusters also have a scaleable firing rate. They fire in pulses, at 100 J per pulse. As long as power is available the thrusters can fire from 1 Hz to 20 Hz. There is no ramp up in pulse cycling either. Thus, the amount of impulse provided is variable up to a maximum amount. The specific impulse of Primex pulsed plasma thrusters is roughly 1350 seconds. The PowerSail thrusters fire at a rate of 2 Hz; however, this can be increased if an abnormally large or small separation occurs between the Host and PowerSail. The maximum amount of power available in normal operations for the firing of the PPTs is set for 4 thrusters firing in 3 axes at 2 Hz. This worst-case scenario requires 2.4 kW.

Each pulse provides 860 μN-sec impulse. With such a low impulse bit the thrusters can be used as an active damping system to reduce the structural vibrations of PowerSail. This application is not investigated further in this report.

The dimensions of a thruster pair are shown in Figure 5-59 and a photo of the thrusters is shown in Figure 5-60. A schematic of a generic pulsed plasma thruster is Figure 5-61. The mass breakdown of specific components and total system mass is in Table 5-22.

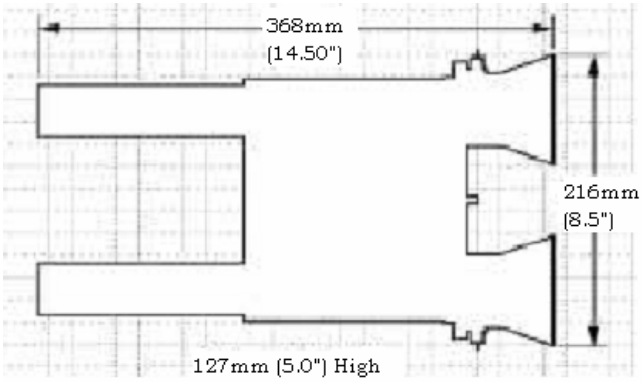

Figure 5-59: Dimensions of a Pulsed Plasma Thruster Pair

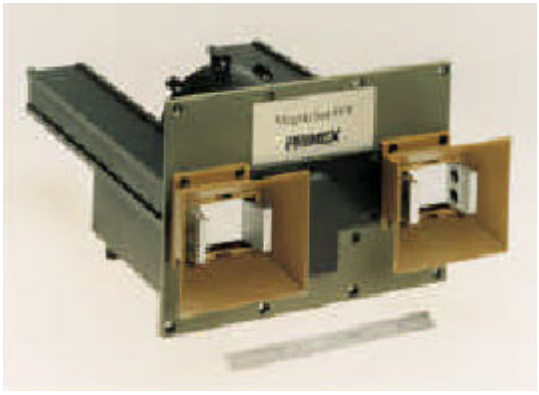

Figure 5-60: Photo of a Primex Pulsed Plasma Thruster Pair

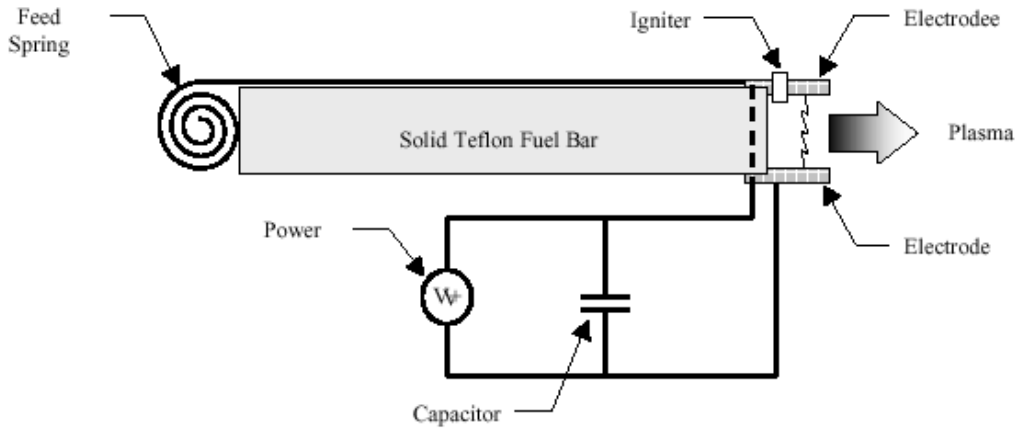

Figure 5-61: Schematic of a Generic Pulsed Plasma Thruster

Table 5-22: PPT Mass Properties (Ref. 16)

Component	Mass (kg)
Thruster+housing	0.54
Capacitors	2.32
PPUs	0.52
DI circuit	0.2
40 Thrusters & propellant	127
Capacitors & PPUs	30
Total System mass	157

5.6.5.3 Conclusions

The propulsion system on PowerSail uses clusters of pulsed plasma thrusters mounted in four thruster modules. There are a total of 40 thrusters, with 10 in each module. The maximum available power allotted for the PPTs is 2.4 kW. PPTs are a good choice as a propulsion system for a number of reasons; including solid propellant, adaptable power systems, and low dry mass.

5.6.6 Formation flying

5.6.6.1 Introduction

Without an effective control system with optimal control constants, the formation between the Host and PowerSail is either not possible or has a propellant requirement far greater than necessary. A Lyapunov nonlinear control system creates an acceleration vector that maintains the formation with a minimum amount of propellant. The control constants vary and must be determined to have an optimal propulsion system.

5.6.6.2 Formation Flying Optimization

The system to maintain the leader-follower formation of the Host and PowerSail uses Lyapunov nonlinear control theory. The control theory has three constants that are varied to create optimal thruster firing. The direction and magnitude of thruster firing is given in Equation 32. The total magnitude of the control vector is limited by the available thrust. For more information, see Ref. 14. With the control system active, the magnitude of the distance between the Host and PowerSail is almost constant, as shown in Figure 5-62.

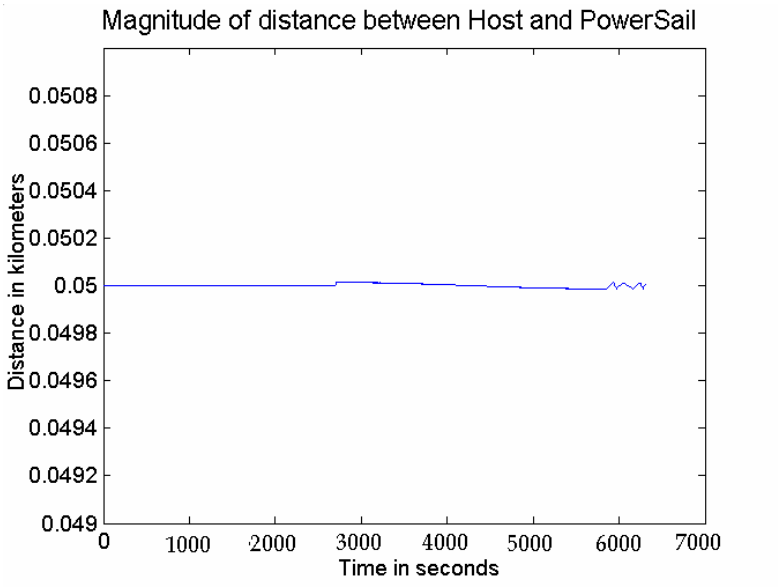

Figure 5-62: Separation Distance Using Lyapunov Controller

To maintain the formation, choosing control constants k_1, k_2, and k_3 is an iterative process. There is not a group of constants that works best in all scenarios for all satellites. The control constants found to work best with this configuration of PowerSail are in Table 5-23.

Table 5-23: Optimal Lyapunov Control Constants

Control Constant	Value
k_1	0.9 [1/sec]
k_2	1 [sec]
k_3	1 [1/sec]

Since the three control constants are arbitrary, varying k_1 while holding k_2, k_3 constant yields the constants above. The number of thrusters required to maintain the orbit of PowerSail varies from 15 with k_1 = 5 [1/sec] to more than 100 with k_1 = 0.005 [1/sec]. These thrusters face in the negative sun vector direction, which has the greatest need for

thrusters. With k_1 = 0.9 [1/sec], the number of thrusters required to maintain the formation is approximately 10. Do note, however, these thrusters are only being used to counteract the solar radiation pressure effects on PowerSail's orbit, and the relative distance between PowerSail and the reference point. Applied torques create a need for additional thrusters on the negative sun vector face to maintain the sun pointing requirements of PowerSail. These control constants are for 4 thrusters firing in each direction, firing at 2 Hz.

5.6.6.3 Conclusions

The formation flying control system uses Lyapunov nonlinear control theory. Control constants must be optimized in order to have an optimal and efficient propulsion system. The optimal control constants found are in Table 5-23. Without optimized control constants, the propulsion system is not efficient.

5.6.7 Umbilical

5.6.7.1 Introduction

Optimizing the design of the umbilical for PowerSail requires many fields of study working together for a common goal. The study involves aerospace and electrical engineering as well as research into material science. The umbilical design has the most favorable flexibility that provides for efficient transfer of power, and does not interfere with the operation of either the Host or PowerSail.

5.6.7.2 Umbilical Optimization

The material selected for the conductor needs to have favorable resistivity and be light enough for space application. Other attributes include material degradation and workability. Three materials are evaluated for this function: silver, copper, and aluminum. The relative properties of the three materials are summarized in Table 5-24.

Table 5-24: Conductor Material Properties (Ref. 34)

Material	Density [kg/m^3]	Electrical Resistivity $\cdot 10^{-8}$ [Ω·m]
Silver	10492	1.47
Copper	8933	1.7241
Aluminum	2702	2.8264

Copper is the most favorable material. "It conducts electric current very readily, ranking next to silver. It is very plentiful in nature, and therefore, its cost is comparatively low. Aluminum on the other hand has a conductivity of only about two thirds that of copper. To achieve the same power transfer of copper, an aluminum wire must have a cross-section 1.66 times greater than a copper wire but would have 55 % of the weight" (Ref. 4). These characteristics lead to the selection of copper as the conducting wire in the umbilical.

The kinetic coupling of PowerSail and the Host is complicated, not thoroughly understood, and not in the scope of this project. To analyze the kinematic coupling of the Host and PowerSail, a Matlab function is used to study the effects of varying the eccentricity, inclination, RAAN, and true anomaly. The functions search for favorable combinations of these elements to find orbits that provide for little blocking of the instantaneous access area (IAA) of the Host and shadowing of the Host on PowerSail. To analyze the blocking effects, the Host is assumed to be nadir-pointing and the umbilical 100 m in length. Eccentricity changes alone cause blocking directly through the middle of the Host's IAA. A sole inclination change causes collisions and thus requires a change in another orbital element. A slight decrease in true anomaly of $2.5° \times 10^{-4}$ and an inclination increase of $2.5° \times 10^{-4}$ leads to a total separation of 59 – 68 m with no blocking of the Host's IAA throughout the orbit (Ref. 11). Results from the study draw several conclusions:

a. There are pairs of orbits for the Host and PowerSail that are unfavorable and pairs which have the correct combination of orbital elements providing for minimal blocking and encouraging satellite separation.
b. The most promising orbits are those in which PowerSail follows the Host in almost the same orbit as the Host several thousandths of a second later.
c. Solely an eccentricity change causes the orbit of PowerSail to move directly in front of the Host's view of the Earth.

The orbit and materials are now analyzed with respect to the umbilical design. The next step in the design of the umbilical is to size the copper conducting wire. Many aspects of the design of PowerSail are affected through this design. This process relies heavily on the string layout. The number of cells in a string sets the voltage of the current generated by the array. The current in turn drives the size of the conductor. During this design loop, concern is placed on the limits of the conductor, harness, and slip ring, which are mentioned later.

The solar cell area is fixed at 395 m^2. Figure 5-63 below shows possible string layouts on this fixed area for different conducting wire sizes. This analysis studies the 4.0×4.0 cm^2. The curve in red is the upper limit of placing cells on the array with the area of the array as the constraint. Any curve above this line produces a total area of cells too large for the array. The curves below illustrate the number of strings required to meet the power requirements with resistances of 0.01 – 0.25 Ohms.

Though not studied, the mass of the wire harnesses for the solar cells needs to be minimized. This leads to a desire to utilize the size of the 4.0×4.0 cm^2 solar cell. Using the larger cell results in the least number of cells to wire, creating a total harness of less mass than would be needed for the smaller cell.

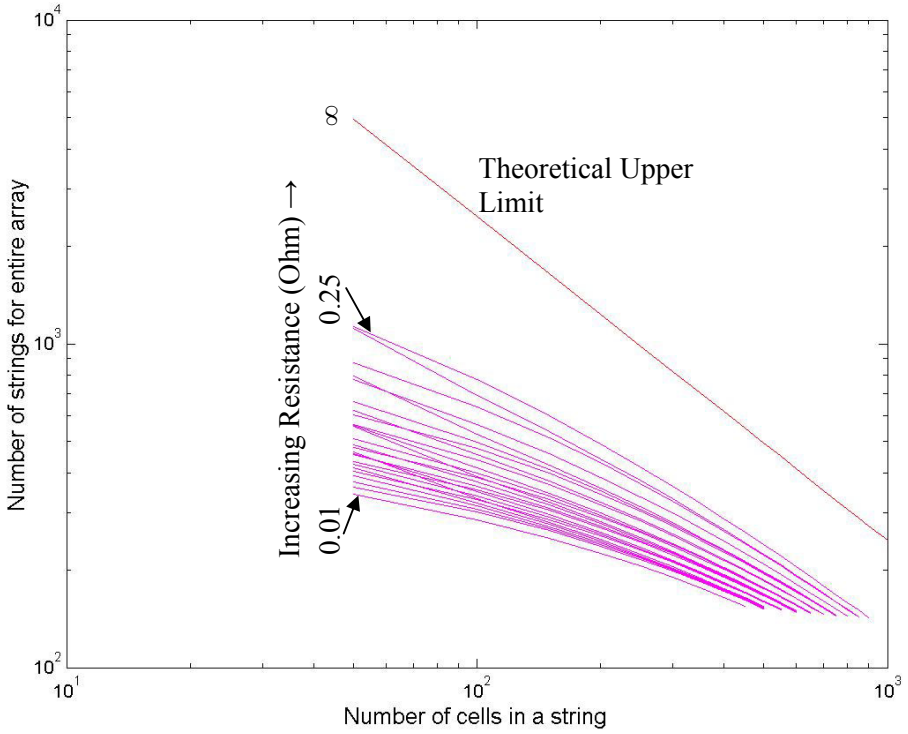

Figure 5-63: Feasible String Layouts

One problem needing attention is the threat of the umbilical tangling with PowerSail. This is a serious concern with any orbit. One solution to this problem is to utilize a slip ring and arm extension. A slip ring with an arm extension stretches the umbilical just beyond the thruster modules. Rotating at 360º per orbit, the slip ring and arm can prevent entanglements. A design constraint of a slip ring is the amount of current. IEC Corporation manufactures custom slip rings (Ref. 32). Two slip rings with ratings of 90 A each can be used together for a total current rating of 180 amps. A copper conductor size of 1.2 cm (0.46 in.) diameter is sufficient for this application, resulting in a 1.3 kW power loss due to the conductor (Ref. 22). This option has 295 V for a power rating of 53 kW.

5.6.7.3 Conclusions

Shown here are the extreme interactions between PowerSail's umbilical and several of its other subsystems. The design of the umbilical relies heavily on the current passing through it. A conductor diameter of 1.2 cm (0.46 in.) and length of 100 m is a reasonable size. The mass of one copper conducting wire of these dimensions is 95 kg. To complete the circuit, another conducting wire is in the umbilical and has the same mass. Thus, the total mass of the conductor in the umbilical is 190 kg.

5.6.8 Attitude Determination and Control Subsystem

5.6.8.1 Introduction

The ADCS of PowerSail consists of accelerometers, a star tracker, a GPS receiver, and a transmitter/receiver package. Working together these components give the attitude relative to the Sun, orbit relative to the Earth, frequency and displacement relative to the normal plane (flat PowerSail), and relative distances and velocities to the Host.

5.6.8.2 Accelerometers

The accelerometers chosen for PowerSail's vibration measurements are the Silicon Designs G-Logger Model 3310. Silicon Designs, Inc. is one of the leaders in accelerometer design. Their products are widely used on both aircraft and spacecraft. This particular model was used on STS-93 for vibration measurement. Figure 5-64 shows a battery-powered version of this model, which is the primary means of powering an accelerometer (Ref. 31).

Figure 5-64: Silicon Designs G-Logger Model 3310 (Silicon)

PowerSail's accelerometers take power directly the solar array. Table 5-25 shows the important characteristics of the G-Logger Model 3310 (Ref. 31).

Table 5-25: Silicon Designs G-Logger Model 3310 Characteristics (Ref. 31)

G-Logger 3310 Characteristics	
Temperature Range	-20 to +60 C
Size	3.5" × 4.5" × 2.2"
Weight	29 oz.
Acceleration Rates	1/sec to 4000/sec
Velocity Rates	1/sec to 4000/sec
Power	1.5 to 5.5 watts

5.6.8.3 GPS/Orbit Propagation

GPS receivers are not easy to select because they are a secret technology for space-based systems. A company can give information that it makes GPS receivers and some basic characteristics but gives no additional information without signing a strict contract. Any GPS receiver is acceptable for PowerSail so we chose the Honeywell basic receiver recommended by Reference 37. Table 5-26 describes the satellite as much as possible.

Table 5-26: Honeywell GPS Receiver Information

Honeywell GPS Receiver	
Size	4000 cm^3
Mass	4 kg
Power	35 Watts

5.6.8.4 Star Tracker

The star tracker on PowerSail is the Caltrac designed by the Cal Corporation. This star tracker is new technology recently developed by the Cal corporation, and is awaiting space testing. Figures 5-65 and 5-66 show two different types of Caltrac sensors, a swivel mounted and non swivel mounted design (Ref. 5).

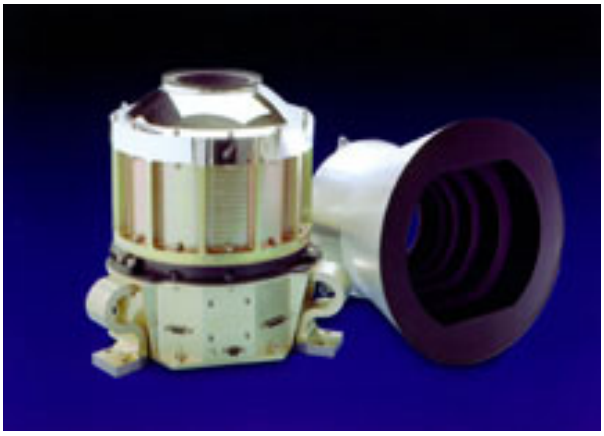

Figure 5-65: Swivel Mounted Caltrac Star Tracker (Ref. 5)

Figure 5-66: Caltrac Star Tracker (Ref. 5)

Table 5-27 describes the important characteristics of these trackers (Ref. 5).

Table 5-27: Caltrac Star Tracker Characteristics

Caltrac Star Tracker	
Temperature Range	-20 to +50 C
Size	330mm high, 225 mm diameter
Mass	3.4 kg
Acquisition Time	< 500 ms
Power	11 - 14 watts
Error	+/- 0.013 deg in pitch/yaw +/- 0.035 deg in roll

"Integrated Caltrac sensors combine the accuracy of star trackers with the speed of control moment gyros or sun sensors" (Ref. 5). PowerSail is limited on possible changes in orbit. These sensors help determine where PowerSail is in order to keep necessary movements to a minimum.

5.6.8.5 Transmitter/Receiver

The only communications device on PowerSail is a receiver mounted on the end of umbilical. This device will receive the signals from the transmitter at the end of the umbilical for relative distance and velocity measurements. This receiver will also receive the two line element sets from the ground via the Host for the orbit propagation calculation corrections.

This system will work as described in the modeling section, with difference in signal times being used to measure relative velocities and distances between PowerSail and the

Host (Ref. 13). This is an important subsystem because relative distances need to be achieved and maintained throughout the orbits of PowerSail and the Host. The optimal distance is 50 m, which is maintained by the attitude thrusters throughout the mission lifetime.

5.6.8.6 Conclusion

The ADCS system of PowerSail is a combination of several components working together. A Caltrac star tracker determine the attitude, a Honeywell GPS receiver determines the orbit, a G-Logger 3310 calculates the vibration modes of the of PowerSail and a transmitter/receiver package determines relative distances and velocities.

5.6.9 Command and Data Handling System

The computer selected for PowerSail C&DH needs is the Southwest Research Institutes model SC-1750A. MSTI-1, 2, 3, New Millennium and DS-1 used this computer previously. A summary of the operating capabilities of the SC-1750A is in Table 5-28 (Ref. 37).

Table 5-28: SWRI SC-1750 Computer Characteristics

SWRI SC-1750A Computer		
	Available	Required
Word Length	16 Bit	16 Bit
Memory	512 KB	137 KB
Performance	1 MIPS	0.25 MIPS

This computer gives an approximate factor of safety of 4, assuming all subsystems are operating at maximum capacity at all times. These numbers are based on the approximations and averages given in Reference 37 and the known factual data from the various components.

5.7 Trade Study

5.7.1 Introduction

Throughout this paper, we show that it is possible to generate 50 kW of power with a free-flying solar array. There is potential to scale PowerSail from 50 kW to 100 kW. The estimated area of a 100 kW PowerSail is 748 m^2. Problems may arise in each subsystem due to the large increase in area. This section discusses the problems and potential of each subsystem in scaling to 100 kW.

5.7.2 Structures Subsystem

The structural configuration developed for the 100 kW PowerSail is shown in Figure 5-67. The array is divided into nine rows and three columns of arrays, each measuring 3 m × 9.3 m. There are four spars, and ten ribs, each measuring 0.3 m in diameter.

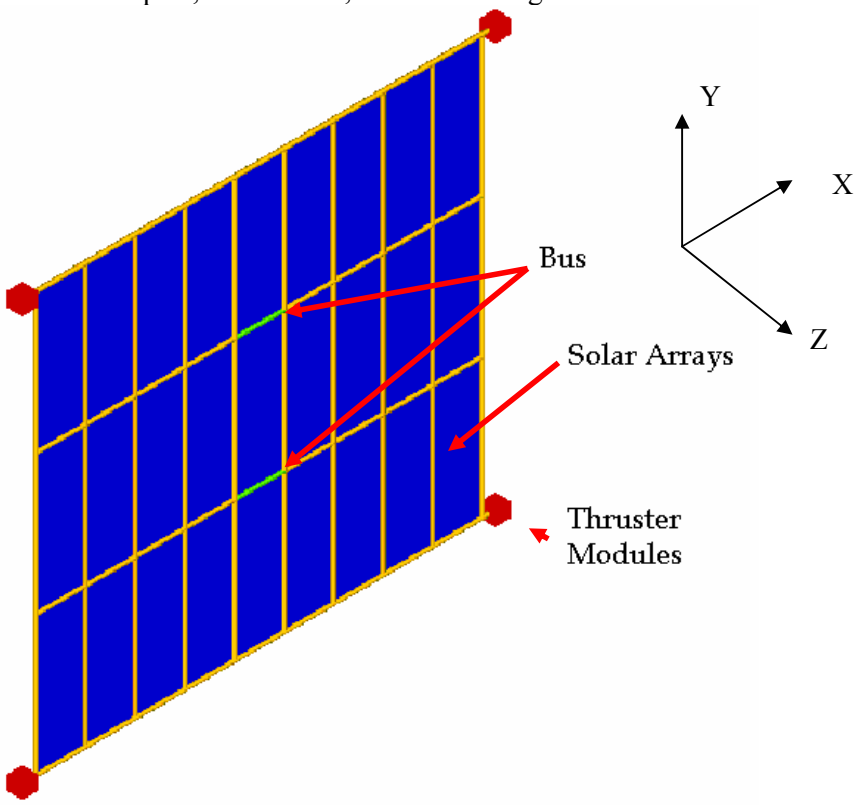

Figure 5-67: Final PowerSail Configuration

The required thruster mass and volume increase from the 50 kW PowerSail scales each corner housing to a cubic meter having a 100 kg mass. The bus mass remains constant, since the command and data handling system remains unchanged. The center of the 100 kW PowerSail is a solar array, so the bus is distributed between the adjacent spars. One bus houses the inflation system, and the other bus houses any computers and power hardware.

The modes of vibration also change with the increase area and mass. Table 5-29 illustrates the different modes of vibration. These are lower than the 50 kW PowerSail vibration modes. The only concern is the thrusters firing at these natural frequencies.

Table 5-29: Modes of Vibration

. Corner Mass [kg]	Bus Mass [kg]	1st Mode [Hz]	2nd Mode [Hz]	3rd Mode [Hz]
0	0	0.18	0.24	0.29
100	0	0.12	0.18	0.28
100	50	0.12	0.18	0.28
0	50	0.18	0.24	0.29

5.7.3 Propulsion Subsystem

The propulsion system for a 100 kW PowerSail has the same basic needs that the system has for the 50 kW PowerSail. However, with a larger PowerSail the forces from solar radiation pressure increase and the overall system mass increases. The mass of the system does not increase linearly like the area of solar array. The mass of PowerSail plays a more important role than the solar array area with regards to the orbit of PowerSail.

With the model used earlier, the 100 kW PowerSail propulsion system requires more power, additional thrusters and a different firing method. The control thrusters that only have two DI circuits require additional propellant, and since there is room for additional DI circuits and thus propellant, additional thrusters for control are not needed. Therefore, these thrusters include an additional DI circuit and 0.65 kg of propellant. There also needs to be an increase in the number of thrusters (those facing in the negative sun vector direction). The number of orbit correction thrusters is increased from 16 to 24. Each of these additional thrusters has 4 DI circuits and 2.6 kg of propellant. The thrusters fire 12 at once to maintain the orbit, at 4 Hz. This increases the maximum power needs of the propulsion system from 2.4 kW in the 50 kW PowerSail to 6.4 kW. The total mass of the system increases from 157 kg to 210 kg. The propulsion system does not increase in mass linearly since the overall mass of PowerSail does not increase proportionally to the array size. The force applied on PowerSail depends on array size, while the acceleration in any direction depends on force and overall mass. This leads to an increase in the propulsion system requirements, but the number of thrusters does not double because PowerSail's power requirements double. In fact, only additional propellant is needed in the thrusters with two DI circuits. Additional propellant is added with additional DI circuits. Eight thrusters are added to the modules, facing in the negative sun vector direction. These thrusters are split among the thruster modules, with six thrusters in each module. Since each capacitor in the thruster modules can handle four thrusters, no additional capacitors are added to the propulsion power system. An additional capacitor can be added to create redundancy incase a capacitor fails, but this additional capacitor is probably not needed.

5.7.4 Power Subsystem

For this trade study, the new requirement is to provide the Host with 100 kW of power doubling the initial requirement. This increases the amount of power that PowerSail needs because of an increase of the solar array area. Increasing the amount of power the Host requires also increases the amount of power loss through the umbilical.

With the given 100 kW to the Host, the new power requirements are 6.4 kW for propulsion, and about 600 W for ADCS and the computer, totaling 7 kW of power. Since the loss through the umbilical is linearly proportional to the size of the array, we double the power loss to 3 kW. With the increased power requirements, the array size required to produce 110 kW is 735 m^2. This array fits comfortably on the structural area of 753 m^2. With 27 panels, an area of 27 m^2 is needed which fits on the 28 m^2 panels.

The number of cells needed to produce 110 kW is approximately 460,000 cells. This gives 1700 cells on a panel. The possible ways of laying the strings on a panel using the 2.5 cm cell is in Figure 5-68. The possible voltages and current flow through these string layouts is in Figure 5-69. For the 4 cm cell, the possible string layouts are in Figure 5-70. The possible voltages and current flowing through these layouts for the 4 cm cell are shown in Figure 5-71.

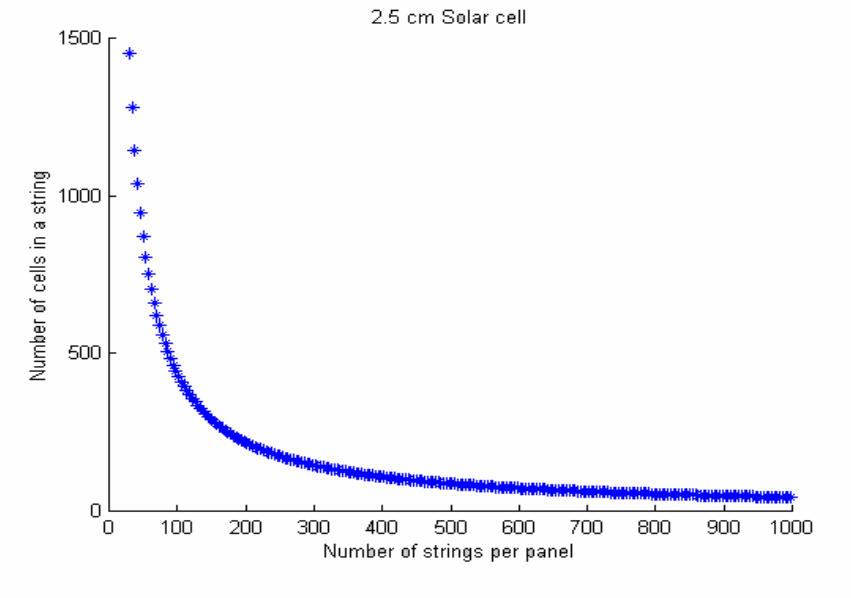

Figure 5-68: String Layout Optimization

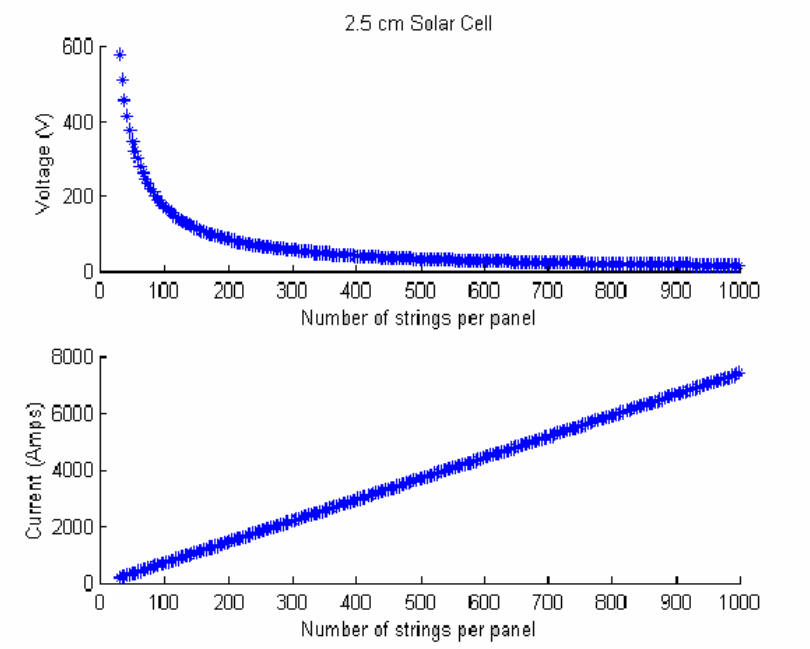

Figure 5-69: Voltage And Current versus Number Of String Per Panel

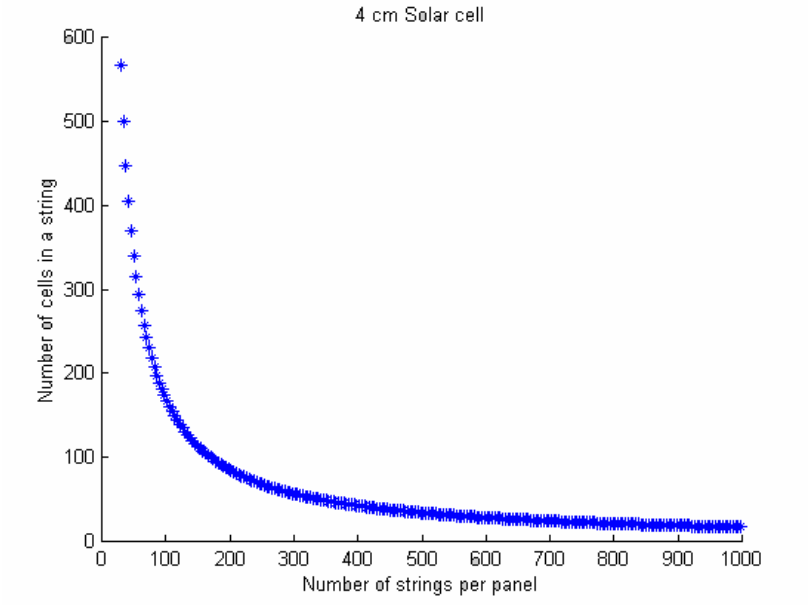

Figure 5-70: String Layout Optimization

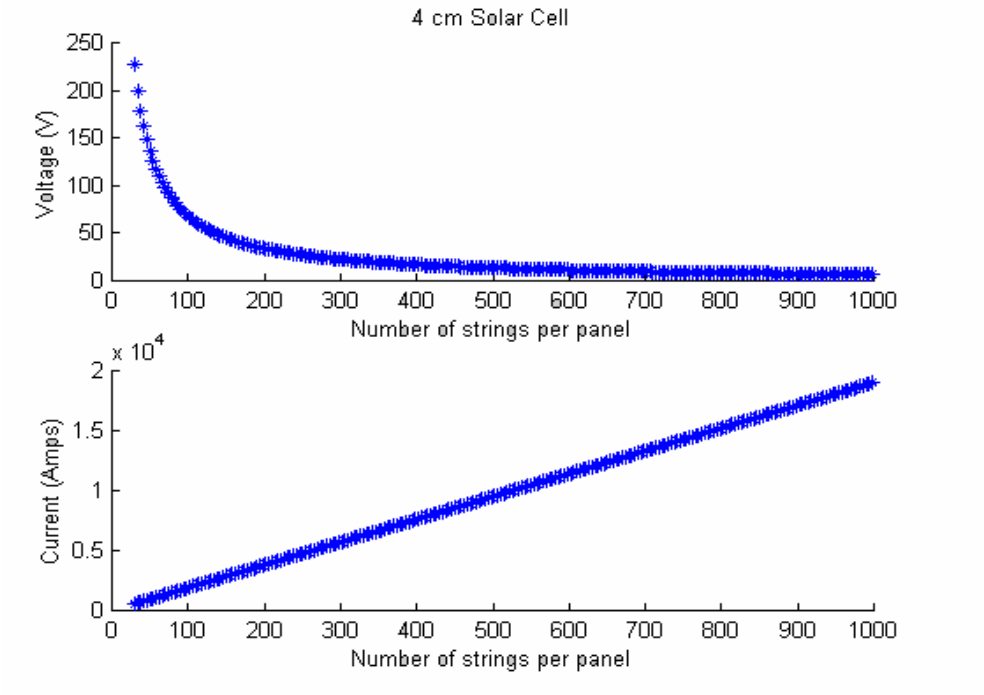

Figure 5-71: Voltage And Current versus Number Of String Per Panel

In order to produce 110 kW of power, the solar array size increases by 334 m^2, adding another row of solar panels. The total solar cell area needed to produce this power is 735 m^2, which fits onto the 754 m^2 solar array. There are a total of 27 solar panels with each needing an area of 27 m^2. The possible string layouts for both cells are seen in Figures 5-68 and 5-70, respectively. The related voltages and current for the possible string layouts for both cells are seen in Figures 5-69 and 5-71, respectively. From these conclusions it is possible to size PowerSail to 100 kW.

5.7.5 Thermal Subsystem

Scalability of the thermal subsystem is straightforward. The components themselves inside the thruster modules and the central bus do not change at all, so the maximum and minimum operating temperatures are the same as a 50 kW PowerSail. The increase in the number of thrusters on the corner modules increases the heat dissipation within the modules. With this increased dissipation, the radiative white paint coating the modules is not thermally effective for a 100 kW PowerSail. Adding a combination of radiators, heat pumps, and cold plates dissipates enough heat to keep the modules within operating temperatures. The capacitors and PPUs are mounted to cold plates, which route the heat through heat pumps to a radiator. Multi-layer insulation may also be added to the modules to maintain the operating temperature while in eclipse. The internal hardware in the central bus remains the same with the 100 kW PowerSail, so the thermal coatings applied for 50 kW will suffice for a 100 kW.

The properties of the solar cells do not change, so the top and bottom coatings of the array do not change in array size. However, the increase in array size will increase the amount of heat absorbed and emitted. The amount of heat dissipation increases from about 500 kW to 1,000 kW. This increases the heating of the modules and the center bus from the solar array. Multi-layer insulation placed on these components will provide protection from this additional heat.

The thermal subsystem is probably the easiest to scale to a 100 kW PowerSail. There are many thermal materials besides those discussed in this section to maintain the operational temperatures of PowerSail. The main concern is avoiding active thermal devices. Active devices have higher mass and volume and require more power. Passive devices should suffice for a 100 kW PowerSail.

5.7.6 Conclusion

This section shows that the 100 kW version of PowerSail is feasible with modifications to the 50 kW PowerSail. The solar array increases in size, changing the structural and propulsion configurations. The thermal properties of the solar array remain the same since the solar cells do not change. The attitude determination systems remain the same as the 50 kW PowerSail. Much more analysis is needed for a 100 kW conceptual design.

5.8 Recommendations for Further Study

5.8.1 Introduction

This report describes a conceptual design of a free-flying solar array capable of providing 50 kW of power through a slack umbilical to a Host spacecraft. In the future, there may be a need for higher power solutions. This chapter summarizes the study, and provides an exploration of scaling the current PowerSail to provide 100 kW of power.

5.8.2 Final Configurations

PowerSail is a fairly simple design when compared to other satellites. PowerSail needs to provide 50 kW of power to a Host spacecraft ranging in orbit from 1000 km to geostationary. PowerSail must also use electric propulsion to maintain the formation between it and the Host. The power is transmitted to the Host using a slack umbilical. No information is known about the size or mission of the Host. Many assumptions were made concerning the Host in modeling PowerSail. This section summarizes the final configuration we chose for PowerSail considering all of the requirements and assumptions about the Host.

Defining PowerSail as either its own spacecraft or a subsystem of the Host was a vital part of the design process. Keeping PowerSail as its own system complicates the spacecraft. By thinking of PowerSail as a subsystem, we eliminate a complicated command and data handling system, communications to the ground, and batteries. Reverse flow through the umbilical during eclipse eliminates the batteries on PowerSail. Telemetry and commands are also communicated through the umbilical.

The structure subsystem uses inflatable, rigidizable materials. This technology provides stiffness and raises the frequency of the lowest vibration modes. The inflatable technology has a smaller stowed volume complemented by a low mass.

The selection of the solar cells is also an integral part of minimizing the mass and volume of PowerSail. CIS solar cells are chosen for PowerSail because they provide high specific energy density, low mass, and small stowage volume. The low stowage volume is a result of their thinness and flexibility. The cells can be rolled to a diameter of 10 in before they experience electrical difficulty (Ref. 33).

The electric propulsion system chosen is the PPT manufactured by Primex. These thrusters will maintain the formation between PowerSail and the Host. They also keep PowerSail pointing toward the sun. The thrusters also have a low mass and small volume. Ten thrusters fit in each corner housing that is 0.5m x 0.5m.

Figure 5-72 illustrates the final configuration of PowerSail.

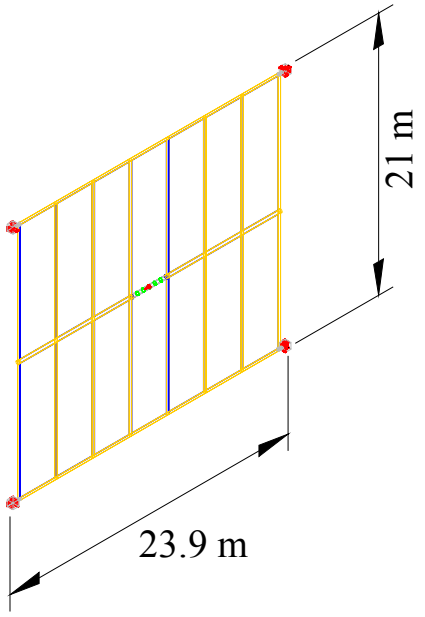

Figure 5-72: Final Configuration of PowerSail

The final configuration of PowerSail is an array split into 14 panels. Each panel is 3m × 10m for a total area of 420 m^2. PowerSail's mass, including propulsion, solar array, umbilical and structure is approximately 800 kg. This is a fairly low mass considering the size of the solar array when deployed.

There are still more details needing further consideration, and the following sections describe these details for each subsystem.

5.8.3 Power Subsystem

Although some analysis of the string layout and solar cell selection is addressed, further analysis is required for a complete design. The PowerSail design and configuration depends highly upon the solar cells. Thin-film flexible solar cell characteristics are changing rapidly since it is a new technology. PowerSail harness layout is not addressed in this design although additional area is included for them.

Only two solar cell string layouts are analyzed in this design, leaving many other options yet to be studied. More analysis is needed to determine which layout is needed to produce a low amount of power loss through the umbilical.

Harness of the solar cells is not considered with this design project. Room is left on each panel for harness layout, but exact dimensions and placement is unknown. The wiring must be chosen and optimized. This affects the solar cell selection and layout.

To achieve an optimal power subsystem, further analysis is required for string layout and cell selection. Placement of the harness and harness specifications also is required.

5.8.4 **Thermal Subsystem**

A basic thermal analysis of PowerSail is performed in this design; however, there are still many details left to be determined. First is the use of heat pumps, or other suitable passive device to radiate the heat from the individual components in the modules and the bus to the radiator. In particular, the heat dissipated from the capacitors, PPUs, and thrusters must be deflected from each other and away from the accelerometers housed in the thruster modules. Passive devices are recommended for this purpose since power usage during eclipse must be limited as well as limiting mass and area of thermal devices.

A more in depth analysis of the heating and cooling of the solar cells and structural effects of the thermal gradients in and out of eclipse must be done. I-DEAS is the recommended program for this more detailed analysis. Also, the rate of thermal expansion of the coatings of the solar array must be analyzed to ensure that no harm will come to the array as these materials heat up or cool down.

Finally, the excess Teflon™ from the PPTs may affect the coating on the solar arrays near the modules and the modules themselves. An analysis of the amount of propellant lost and its effect on the components must be analyzed to ensure operating conditions.

The thermal requirements are made simple by thinking of PowerSail as a subsystem rather than its own spacecraft. The decreased instrumentation onboard PowerSail and the use of the electric propulsion for attitude control electric propulsion is generally hotter than some other propulsion systems also simplifies the thermal subsystem. The only complications are the heat dissipation of the PPTs and the thermal gradients imposed on the large solar array traveling in and out of eclipse.

5.8.5 Structure Subsystem

To make a flight ready PowerSail structure, more analysis is needed. Thruster induced vibrations, secondary structure, and deployment modeling are some major concerns.

Thruster induced structural vibrations must be examined because they cause cyclical loading that decreases the lifetime of the structure. It is possible to damp out any structural vibrations using the PPTs, since they have a low impulse bit.

The secondary structure must be analyzed and designed such that mass is minimized and loads are distributed properly to other structural members. We include a liberal mass margin for secondary structures, since they are only conceptualized. The structural interface of components must also be determined.

Deployment of PowerSail must also be modeled such that dynamic interactions between the Host and PowerSail are minimized during deployment. Modeling the deployment of

inflatable space structures is currently being researched, and is a difficult problem (Ref. 7).

5.8.6 Umbilical Subsystem

Several considerations for extending the 50 kW PowerSail to 100 kW arise in the design of the umbilical. The high level of voltage is unique to space application. There exists a threat of damage to hardware on either the Host or PowerSail due to this current traveling the long distance between spacecrafts. The kinematic and kinetic coupling between both spacecraft needs to be modeled. Also, an accurate model is needed for the insulation of the conducting wire and data wire. The insulation reduces power loss and protects flight hardware. Materials with better conductivity and density may be found with hybrid materials for the conductor.

Alternatives to the slack umbilical are needed to weigh its feasibility. The umbilical could wrap around the Host or PowerSail. If either the Host or PowerSail goes into a "safe" mode, one end of the system would then be in free drift. This creates a completely uncontrolled system, threatening the mission and safety of both spacecraft. An inflatable boom may be used to stiffen the umbilical should safe mode occur, reducing the chance of collision.

Lastly, the extension arm must have a slip ring with a high enough voltage rating to be feasible. The slip ring allows for the transfer of power between rotating bodies. Research into the lifetime of slip rings operating at high voltages is necessary for if this aspect of the design is considered. The extension arm also may be angled away from the PowerSail. This angle moves the end of the arm away from any thrusters and farther away from PowerSail reducing any possibility of entanglement.

5.8.7 Propulsion Subsystem

To fully complete an operational PowerSail propulsion system, a more in-depth study of subsystem interactions is required. The effects of thruster firing and structural dynamics need to be explored.

Since PowerSail is a flexible structure, the thruster modules vibrate with the array. This vibration creates a need to determine degree of the displacement and the relative angle the thrusters make with the original orientation. When PowerSail is oscillating, the thrusters no longer point in the correct direction. When the thrusters fire, the thrust direction is not necessarily in the correct direction. This pointing error leads to a less efficient propulsion system unless the variation in thruster angle is taken into account with formation control software. A need exists for the propulsion system to act as an active damping system if the vibration of PowerSail is severe. This function leads to a need for additional propellant that must be added to the current propulsion system.

In addition, the effects of lost propellant need consideration: PPTs lose roughly 40% of the propellant through losses in the system from the melting of the Teflon™ block. The operation of a PPT creates an electric arc across the surface of the Teflon™ propellant block that ionizes the Teflon™. These ions are then ejected out the nozzle using the

Lorentz force. However, this process also generates enough heat to create gaseous Teflon™ that is not ionized. This Teflon™ floats out the thruster nozzle and is unusable for thrust. The gaseous cloud either floats away or is attracted to any nearby surface. The effect of this extra Teflon™ needs examination.

PPTs can be fired in different modes. Since there are so many thrusters on PowerSail, it is possible to fire the thrusters in different size groups. The current firing method uses the thrusters evenly and simultaneously. It is possible to alternate the thruster firings by firing one pair of thrusters, and then the alternate set. This creates an oscillation in PowerSail. The effects need to be studied to see if the additional thrust created outweighs the increase in oscillation. The thrusters can also fire at different frequencies. This creates an additional power requirement, and increases the size of PowerSail. A more in depth study of different firing methods is needed.

5.8.8 Attitude Determination and Control Subsystem

5.8.8.1 Introduction

The ADCS is an important element of the PowerSail system; however, this subsystem is not complete and recommendations for further work in each area of the ADCS systems are described below. Further work on this subsystem was accomplished in Summer 2001.

5.8.8.2 GPS/Orbit Propagation

This element needs further analysis in terms of orbit propagation theory. Most spacecraft that use GPS and are above the GPS constellation use an orbit propagation technique (Ref. 13). Thus the acquisition of an accurate code that performs the necessary requirements is needed in order to complete this analysis. This technique takes an initial position from the ground and models spacecraft position as a function of time. Periodic updates are received from the ground so that PowerSail can make any necessary orbit corrections. In this manner PowerSail will be able to accurately determine its location relative to the Earth.

5.8.8.3 Star Tracker

Performance of this system needs to be modeled with a vibrating PowerSail. Whereas the central bus has less vibration than corner modules or the ends of the main beam, there is still some vibration that must be taken into account. There should not be a significant increase in error due to the fast acquisition time of the Caltrac star tracker (500 ms).

5.8.8.4 Accelerometers

The actual vibration equations that interpret the data from the accelerometers need to be developed and tested. This modeling should not be too difficult because these accelerometers were used on STS-93 for vibration measurement. The PowerSail program should obtain and use these mathematical models.

5.8.8.5 Transmitter/Receiver

This system needs to be further developed in conjunction with the communications system. The actual signal transmission is easy to measure, but the way the signals are sent out and received needs to be further studied.

5.8.8.6 Command and Data Handling System

This system needs further analysis in order to give the complete C&DH needs for PowerSail. The numbers used in calculations here are based on the analysis in Ref. 37 below, which uses average values from many different systems (Ref. 37 below, page 645). Once more detailed command and data handling numbers are known a more in-depth study on the computer can be made. The selected computer should be adequate for PowerSail's needs; however, due to the design margins included in this analysis.

5.8.9 Conclusions

There are many tasks left to complete for a detailed PowerSail design. The effects of thruster firing on structural response must be evaluated. The thermal system needs a more in-depth analysis using lumped parameter thermal modeling tools. Design of the solar cell harness, and optimizing the string layout to minimize the power lost through the umbilical must also be completed. The umbilical will cause the greatest disturbance between PowerSail and the Host. Wave propagation down the umbilical and its effects on the Host and PowerSail must be analyzed and modeled. Once finalized, the PowerSail concept will prove to be useful in the satellite market by providing large amounts of power to spacecraft. It will do this with minimal interference to the spacecraft. It will also allow for freedom in design constraints since the satellite will not have to worry about providing its own power.

5.9 References

[1.] Anders, George J. *Rating of Electric Power Cables: Capacity Computations for Transmission, Distribution, and Industrial Applications.* New York: IEEE Press, 1997

[2.] Bate, Mueller, & White, *Fundamentals of Astrodynamic*s. New York, Dover Publications, 1971

[3.] Bube, Richard H. *Photovoltaic Materials.* London: Imperial College, 1998

[4.] Boyd, Iain D; Michael Keidar; William McKeon, "Modeling of a Pulsed Plasma Thruster from Plasma Generation to Plume Far Field," *Journal of Spacecraft and Rockets*, Vol. 37, No. 3, May – June 2000

[5.] Cal Corporation Webmaster, Cal Corporation http://www.calcorp.com/Caltrac.htm

[6.] Cassapakis, Constantine. "Personal Correspondence," January – May 2001

[7.] Chmielewski, A.B., and C. H. Jenkins. "Gossamer Space Membranes, Inflatables, and Other Expandables." *Progress in Astronautics and Aeronautics, Structures Technology for Future Aerospace Systems*. Ed. Ahmed Knoor. Virginia: American Institute of Aeronautics and Astronautics, 2000. 201

[8.] Derbes, Billy, *Case Studies in Inflatable Rigidizable Structural Concepts for Space Power.* L'Garde, Inc., Tustin California, 1999

[9.] Freeland, R.E., et al. *Inflatable Deployable Space Structures Technology Summary.* Jet Propulsion Laboratory, California Institute of Technology, 1998

[10.] Hall, Chris, "Request For Proposal: PowerSail System and Propulsion Subsystem Design," AOE 4065 Design (Space), Projects. Available: http://www.aoe.vt.edu/~chall/courses/aoe4065/, Dec. 6, 2000

[11.] Hall, Christopher H. *C.6 Umbilical Coupling.* Virginia Polytechnic Institute and State University, Blacksburg, 2001

[12.] Hall, Chris, "Example VSD and OH," AOE 4065 Class Notes, Aug. 20, 2000. Available: http://www.aoe.vt.edu/~chall/courses/aoe4065/examplevsd-oh.pdf, Sept. 27, 2000

[13.] Hall, Chris. "Personal Correspondence," Virginia Polytechnic Institute and State University, Blacksburg, 2001

[14.] Hall, Chris, Chris Karlgaard and Bo Naasz, *ION-F: A Space-Based Testbed for Distributed Formation Control using the HokieSat Nanosatellite.* Technical Report, Virginia Tech, Blacksburg, VA, March 2001

[15.] Honeywell Corporation Webmaster, Honeywell Aerospace Pages http://www.honeywell.com/en/aerospace/index.jsp

[16.] Hoskins, Andrew "Personal correspondence," Primex Aerospace Company, October 2000 through December 2000

[17.] Hill, Philip; Peterson, Carl. *Mechanics and Thermodynamics of Propulsion.* 2nd Ed. Addison-Wesley, 1992

[18.] Humble, Ronald W. *Space Propulsion and Design*. revised, McGraw-Hill, 1995

[19.] Jenkins, Christopher. "Personal Correspondence," January – May 2001

[20.] Karam, Robert D. *Satellite Thermal Control for Systems Engineers.* Vol. 181. Ed. Paul Zarchan. Cambridge: AIAA, 1998

[21.] Kaufman, H.R. *An Ion Rocket with an Electron-Bombardment Ion Source*. NASA TN D-585, Jan. 1961

[22.] Kurtz, Edwin B., and Thomas M. Shoemaker. *The Lineman's and Cableman's Handbook.* 6th ed. New York: Library of Congress, 1981

[23.] Malone, Patrick, Larry Crawford, Geoffrey Williams, *Developing and Inflatable Solar Array.* L'Garde, Inc., Tustin California

[24.] Meink, Troy, Kitt Reinhardt, Kim Luu ,Ross Blankinship, Steve Huybrechts, Alok Das. *PowerSail – A High Power Solution: AIAA-2000-5081*. Kirtland AFB, New Mexico, 2000

[25.] Meink, T. "PowerSail: The High Power Solution," AIAA Space 2000, Long Beach, California, September 19–21, 2000

[26.] Mills, A. F. *Basic Heat and Mass Transfer.* Chicago: Irwin, 1995

[27.] "Power Products," Communications and Power Center, Lockheed-Martin Commercial Space Systems, Mar 10, 1999. Available: http://www.payloads.com/power.htm, Oct. 1, 2000

[28.] Simburger, Edward J. *Advancements in the Development of Thin Film Amorphous Silicon Space Solar Cell for the PowerSphere Concept.* Los Angeles: The Aerospace Corporation, 2001

[29.] Simburger, Edward J. *PowerSphere Concept.* Los Angeles: The Aerospace Corporation, 2001

[30.] Simburger, Edward J. *Thermal Design Aspects of the PowerSphere Concept.* Los Angeles: The Aerospace Corporation, 2001

[31.] Tauscher, Jason, Silicon Designs, INC. http://www.silicondesigns.com/index.htm

[32.] Technical Department, "Personal Correspondence," ICE, April 2001

[33.] Tringe, J. Capt, USAF, "Personal Correspondence," Kirtland AFB, February – April 2001

[34.] Tslaf, Avaham. *Combined Properties of Conductors.* Amsterdam: Elsevier, 1981.

[35.] Vallado, David A. *Fundamentals of Astrodynamics and Applications.* McGraw Hill publishing, 1997

[36.] Wang, Joseph, "Personal correspondence," Virginia Polytechnic Institute and State University, 2001

[37.] Wertz, James R. and Wiley J. Larson. *Space Mission Analysis and Design.* 3rd Ed. Microcosm Press, 1999

6 Aerophysics, Inc. Design Study

Final Report for AFRL Contract No. F04700-01-P-0048
Entitled

POWERSAIL
Propulsion System Design Trade Study

By

Lyon B. King
Gordon G. Parker
Martin D. Tervo

Aerophysics, Inc.
30981 Woodbush Road
Calumet, MI 49913

Submitted September 11, 2001

ABSTRACT

The goal of this work was to investigate practical vehicle sizing and performance requirements for a free-flying 500-kW solar array in orbital formation with a power-consuming host vehicle. To meet these requirements, the sail vehicle required independent propulsion for two functions: formation-keeping with host and ACS/Sun-pointing maneuvers. The equations of motion were developed assuming a rigid vehicle subject to gravity, aerodynamic drag, and solar pressure. A numerical optimization tool was developed to select the optimum orbital trajectory for seven canonical electric propulsion technologies: Teflon™ PPT, hydrazine resistojet, hydrazine arcjet, ammonia arcjet, xenon Hall thruster, and xenon ion thruster. Subject to orbital and formation-flying constraints, the optimizer selected the thrust amplitude, thruster firing sequence, and total impulse such that the total vehicle mass was minimized. The best performance (lowest vehicle total mass) was found using a xenon ion propulsion system; the total mass was 1708 kg for the xenon ion vehicle. The worst performance (highest vehicle total mass) was found using Teflon™ PPT's; the total mass was 2367 kg for the PPT vehicle.

6.1 Mission Introduction

The PowerSail mission operation regime was specified in the program solicitation and through post-award discussion between Aerophysics, Inc. and AFRL staff. These criteria were used to specify the design space for the proposed vehicle. The purpose of this section is to define mission parameters and introduce assumed physical characteristics of the PowerSail vehicle.

6.1.1 Mission Identification

The overall PowerSail mission requirements were defined in Solicitation F04700-01-T-0002 titled, "PowerSail – High Power Propulsion System," published in the Commerce Business Daily edition of November 3, 2000. The requirements were brief and open-ended. Specifically, the solicitation stated, "The PowerSail High Power Propulsion System is a two -phased program to demonstrate high power (100 kW – 1 MW) capability in space using a deployable, flexible solar-array connected to the host craft using a slack umbilical." This statement encompasses the entire mission definition specified in the program solicitation. Thus, the solicitation effectively stipulated two criteria: 1) solar electric power produced must be between 100 kW and 1 MW, and 2) the PowerSail vehicle must have an independent propulsion system allowing the sail to fly in formation with the host vehicle (slack umbilical).

In follow-on conversations with AFRL personnel, two other key mission constraints were identified.[1] 1) The target orbit for the PowerSail vehicle was chosen as a 900-km circular LEO, and 2) A ten-year mission lifetime was defined. At this altitude, the total mission comprises approximately n=51030 orbits. To further narrow the open-ended mission definition, Aerophysics investigators have selected a middle-of-the-road target solar energy of 500 kW as the design point.

6.1.2 Physical Parameter Estimation

As with any conceptual vehicle design analysis, estimation of the PowerSail mass properties relied upon assumptions based on existing materials and future predictions. The vehicle mass characteristics used in this study are based largely on performance estimates of the thin-film photovoltaic material which will comprise the bulk of the PowerSail.

According to an AFRL presentation by Dr. Troy Meink,[2] the extrapolated far-term performance of the thin-film PV material will likely be

- Specific Power = 400 W/kg
- Energy Efficiency = 15%

With these parameters, and estimating the solar constant $\kappa = 1.4$ kW/m^2, the areal density of the thin-film PV material is $\rho_{film} = 0.53$ kg/m^2. The complete vehicle will require some undetermined structural mass to support and deploy the thin-film blanket. Exact knowledge of the mass properties of the deployed vehicle are impossible to specify at the time of this study. In order to provide an estimate, we have assumed that the required

deployment/structural mass will be somewhat less than the mass of the thin-film material. As an arbitrary estimate, we have assumed that the areal density of the entire PowerSail vehicle, ρ_{pv}, to be:

$$\rho_{pv} = 1.75 \times \rho_{film} \tag{40}$$

Thus, the vehicle areal density assumed for this study is $\rho_{pv} = 0.92$ kg/m^2. We have assumed that the PowerSail vehicle mass is uniformly distributed across the surface.

The structural rigidity and other flexible dynamic properties of the PowerSail vehicle will be strongly dependent upon the configuration of the support and deployment assembly. Since these properties were not possible to estimate for this initial study, the vehicle was assumed to be rigid in all dynamic simulations.

6.1.3 Candidate Thruster Technologies

The propulsion system mass necessary to perform a given mission depends upon the thruster technology employed. The investigation reported here was limited to seven canonical electric propulsion (EP) technologies. Numerous studies have established the performance specifications of each technology, namely, specific impulse (I_{sp}), thruster power-specific mass (β_T), power processing unit power-specific mass (β_{PPU}), and power conversion efficiency (η). The thruster operational characteristics assumed in this study are summarized in Table 6-1.

Table 6-1: Performance characteristics for seven canonical EP technologies investigated for PowerSail[3]

	Teflon™ PPT	N_2H_4 Resistojet	N_2H_4 Arcjet	NH_3 Arcjet	H_2 Arcjet	Xe Hall	Xe Ion
I_{sp} (s)	1000	300	500	600	1000	1600	3000
β_T (kg/W)	0.12	0.002	0.0007	0.0007	0.0005	0.003	0.006
β_{PPU} (kg/W)	0.11	0.001	0.0025	0.003	0.0025	0.01	0.01
η (-)	0.07	0.80	0.35	0.36	0.40	0.50	0.65

6.2 Dynamic Equations

In this section, the dynamic equations of the PowerSail are listed based on the assumptions below with a detailed derivation provided in Section 6.3.

1. External forces are due to gravity, atmospheric drag, solar pressure, and thrusters.
2. Propulsion system mass is uniformly distributed over the vehicle.
3. The sail is rigid and of uniform density.
4. The sail has only three degrees of freedom (x, y, ψ)
5. The distance between the target spacecraft and the PowerSail, $\sqrt{(x^2+y^2)}$, is sufficiently small such that they enter the earth's shadow at the same time.

The three PowerSail dynamic equations (x, y, ψ respectively) are

$$M\ddot{x} - M(x+r)\dot{\theta}^2 - 2M\dot{\theta}\dot{y} = Q_x \tag{41}$$

$$M\ddot{y} - My\dot{\theta}^2 + 2M\dot{\theta}\dot{x} = Q_y \tag{42}$$

$$\frac{1}{12}ML^2\ddot{\psi} = Q_\psi \tag{43}$$

where M is the sail mass, and L is it's length. Each of the generalized forces, Q_x, Q_y, and Q_ψ can be decomposed into components due to gravity, solar pressure, atmospheric, and the thrusters, that is

$$Q_x = Q_{x,grav} + Q_{x,aero} + Q_{x,solar} + Q_{x,thrust} \tag{44}$$

$$Q_y = Q_{y,grav} + Q_{y,aero} + Q_{y,solar} + Q_{y,thrust} \tag{45}$$

$$Q_\psi = Q_{\psi,grav} + Q_{\psi,aero} + Q_{\psi,solar} + Q_{\psi,thrust} \tag{46}$$

These components, for each of the degrees of freedom are listed below.

6.2.1 Q_x Components

$$Q_{x,grav} = -\frac{\mu M}{r^2}\left(1 - \frac{2x}{r}\right) \tag{47}$$

$$Q_{x.aero} = \left\{\dot{\theta}(y\sin\psi + [r+x]\cos\psi) - \dot{x}\sin\psi + \dot{y}\cos\psi\right\} Z\sin\psi \tag{48}$$

$$Z = \frac{\sqrt{2}}{2}A\rho C_d\left|-(\dot{x} - y\dot{\theta})\sin\psi + (\dot{y} + [r+x]\dot{\theta})\cos\psi\right|$$

$$Q_{x,solar} = -\left|\cos(\theta+\psi)\right| AP_{solar}\sin\theta \tag{49}$$

$$Q_{x,thrust} = -(F_{y1} + F_{y2})\sin\psi + F_x\cos\psi \tag{50}$$

6.2.2 Q_y Components

$$Q_{y,grav} = -\frac{\mu M}{r^2}\left(\frac{y}{r}\right) \tag{51}$$

$$Q_{y.aero} = \left\{-\dot{\theta}\left[r + x\right]\cos\psi + y\sin\psi\right) + \dot{x}\sin\psi - \dot{y}\cos\psi\right\} Z\cos\psi \tag{52}$$

$$Z = \frac{\sqrt{2}}{2} A\rho C_d \left| -\left(\dot{x} - y\dot{\theta}\right)\sin\psi + \left(\dot{y} + \left[r + x\right]\dot{\theta}\right)\cos\psi \right|$$

$$Q_{y,solar} = -\left|\cos\left(\theta + \psi\right)\right| AP_{solar}\cos\theta \tag{53}$$

$$Q_{y,thrust} = \left(F_{y1} + F_{y2}\right)\cos\psi + F_x\sin\psi \tag{54}$$

6.2.3 Q_ψ Components

$$Q_{\psi,grav} = -\frac{\mu M}{r^2}\left(\frac{L^2\sin\psi\cos\psi}{4r}\right) \tag{55}$$

$$Q_{\psi.aero} = 0 \tag{56}$$

$$Q_{\psi,solar} = 0 \tag{57}$$

$$Q_{\psi,thrust} = \frac{L}{2}\left(F_{y1} - F_{y2}\right) \tag{58}$$

6.3 Equation of Motion Derivation

Figure 6-1 illustrates the various coordinate frames and degrees of freedom used in the equation of motion development. It is assumed that the orbital plane of both the target (or host) vehicle and the PowerSail contain the sun-pointing vector. Furthermore, the target vehicle has radius r and true anomaly θ. The PowerSail translational degrees of freedom are measured relative to the target vehicle and are x and y. Its single rotational degree of freedom is ψ. The coordinate frames will be denoted using brackets. For example the inertial frame whose center is at the earth's center is denoted {I}. Many of the calculations use vector quantities represented in a rotating frame whose center is at the earth's center, but its x-axis tracks the target vehicle. This frame is denoted as {1}. Finally, a PowerSail body fixed frame is also used to describe locations of thrusters and is denoted {b}.

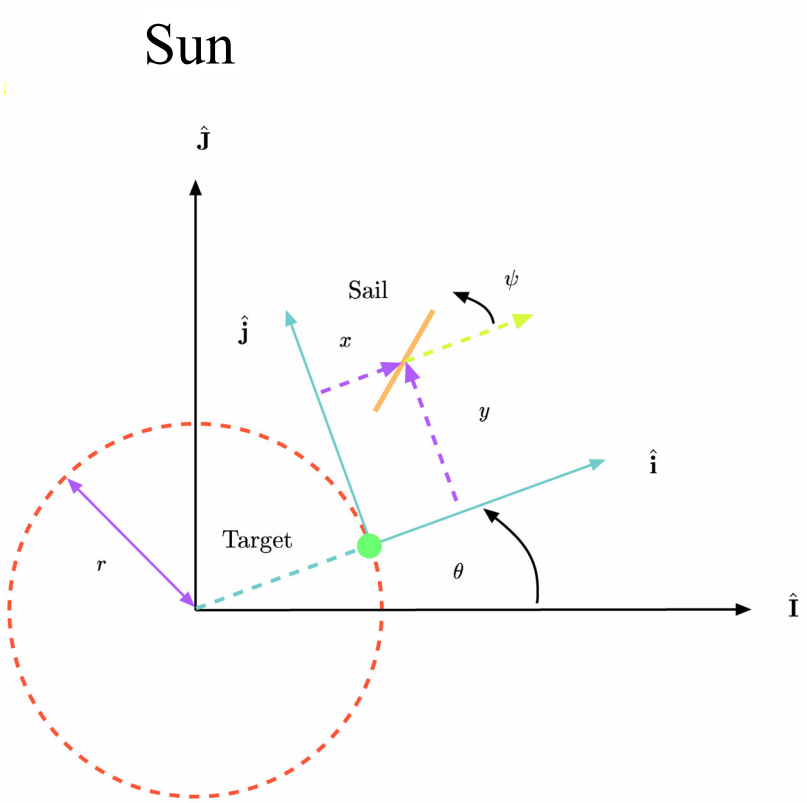

Figure 6-1: Illustration of Target and PowerSail Degrees of Freedom and Coordinate Frames

Later in the study a set of 16 thrusters will be described. Eight are used on the outside edges of the sail (four on each edge for attitude control), four are oriented to provide in-plane thrust, and four are located at the center for orbit maintenance. Accounting for all 16 thrusters during the dynamic equation derivation over complicates the process. Instead it is assumed that there is thrust capability at the edges of the PowerSail (see

Figure 6-2) in the $\hat{x}_b$ direction, denoted F_{y1} and F_{y2}. These can be used for either attitude control or, by using simultaneous firings, orbit maintenance. There is also thrust capability in the $\hat{y}_b$ direction (in the plane of the PowerSail), denoted F_x. The actual 16 thrusters can be distributed amongst these fundamental thrust magnitudes and directions.

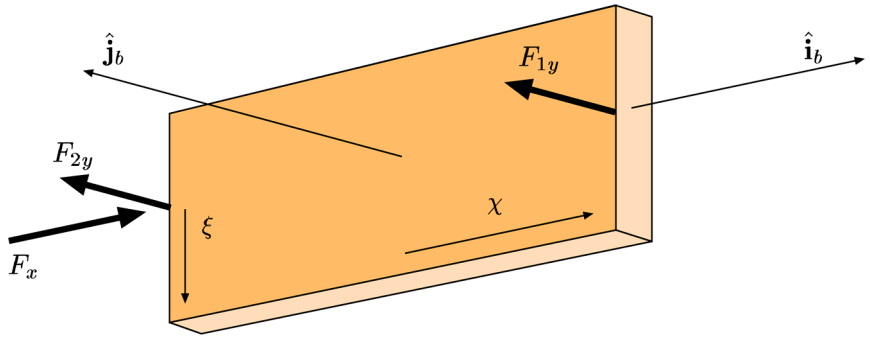

Figure 6-2: Thruster Locations, Body Frame Location, and Definition of the χ and ξ Spatial Variables

Lagranges equations

$$\frac{d}{dt}\left(\frac{\partial T}{\partial q_i}\right)-\frac{\partial T}{\partial q_i}=Q_i \tag{59}$$

were used to derive Equations 41 through 43 where is the spacecraft kinetic energy, are the generalized coordinates ($q_1 = x$, $q_2 = y$, and $q_3 = \psi$), and Q_i are the generalized forces due to gravity, the atmosphere, solar pressure, and thrusters.

The kinetic energy is,

$$T=\frac{1}{2}m\int_{-h/2}^{h/2}\int_{-L/2}^{L/2}v^T v\,d\chi\,d\xi \tag{60}$$

where m is the mass per unit area of the spacecraft, h is the height of the sail along its x_b axis, L is the length of the sail along its y_b axis, **v** is the absolute velocity of any point along the sail located at (χ, ξ).

The absolute position vector from the origin of the earth centered inertial coordinate system to any point on the spacecraft is:

$${}^1p=\begin{Bmatrix} r+x+\chi\cos(\psi) \\ y+\chi\sin(\psi) \\ \xi \end{Bmatrix} \tag{61}$$

where the superscript is used to indicate the coordinate frame used to represent any vector. The absolute velocity vector is then:

$$ {}^{1}v = \begin{Bmatrix} \dot{x} - \chi\left(\dot{\theta} + \dot{\psi}\right)\sin(\psi) - y\dot{\theta} \\ \dot{y} + \chi\left(\dot{\theta} + \dot{\psi}\right)\cos(\psi) + (r + x)\dot{\theta} \\ 0 \end{Bmatrix} \tag{62} $$

Substituting Eq. 62 into Eq. 60, and noting that odd order terms in χ become zero upon integration, gives

$$ \begin{aligned} T &= \frac{1}{2} m \int_{-h/2}^{h/2} \int_{-L/2}^{L/2} \left\{ \left[(r + x)\dot{\theta} + \dot{y} \right]^2 + \chi^2 \left(\dot{\psi} + \dot{\theta} \right)^2 \right\} d\chi\, d\xi \\ &= \frac{1}{2} M \left\{ \left[(r + x)\dot{\theta} + \dot{y} \right]^2 + \left(\dot{x} - y\dot{\theta} \right)^2 + \frac{1}{12} L^2 \left(\dot{\psi} + \dot{\theta} \right)^2 \right\} \end{aligned} \tag{63} $$

where M is the total mass of the spacecraft, M = mhL = mA.

Applying Lagrange's equations to Eq. 63 gives the three dynamic equations for x, y, and ψ,

$$ \begin{aligned} M\ddot{x} - M(x + r)\dot{\theta}^2 - 2M\dot{\theta}\dot{y} &= Q_x \\ M\ddot{y} - My\dot{\theta}^2 + 2M\dot{\theta}\dot{x} &= Q_y \\ \frac{1}{12} ML^2 \ddot{\psi} &= Q_\psi \end{aligned} \tag{64} $$

6.3.1 Gravitational Force – $Q_{i,grav}$

The virtual work for the gravitational force is

$$ \delta W_{grav} = -\mu m \int_{-h/2}^{h/2} \int_{-L/2}^{L/2} \frac{p}{|p|^3} \cdot \delta p\, d\chi\, d\xi \tag{65} $$

where μ is the gravitational constant. The absolute position vector, **p**, represented in the {1} frame will be used in the following development. The denominator of Eq. 65 is then

$$ \begin{aligned} \left| {}^{1}p \right|^3 &= \left[\sqrt{(r + x + \chi\cos\psi)^2 + (y + \chi\sin\psi)^2 + \xi^2} \right]^3 \\ &= \left\{ r \sqrt{1 + \frac{2}{r}(x + \chi\cos\psi) + \frac{1}{r^2}\left[(x + \chi\sin\psi)^2 + (y + \chi\sin\psi)^2 + \xi^2 \right]} \right\}^3 \end{aligned} \tag{66} $$

Assuming that

$$ \frac{1}{r^2} << 1 \tag{67} $$

the last term of Eq. 66 is neglected, and we can write a simplified version of its reciprocal, for use later in Eq. 65, as

$$\frac{1}{\left|{}^{1}\mathrm{p}\right|^{3}} = \frac{1}{\mathrm{r}^{3}}\left[1+\frac{2}{\mathrm{r}}\left(\mathrm{x}+\chi\cos\psi\right)\right]^{-3/2} \tag{68}$$

which can be further simplified using the binomial expansion to give

$$\frac{1}{\left|{}^{1}\mathrm{p}\right|^{3}} = \frac{1}{\mathrm{r}^{3}}\left[1-\frac{3}{\mathrm{r}}\left(\mathrm{x}+\chi\cos\psi\right)\right] \tag{69}$$

where again, Eq. 67 has been exploited to neglect higher order terms. To complete Eq. 65 we need to also define $\delta\mathbf{p}$. As stated earlier, we will use a representation of all quantities in the {1} frame, resulting in

$$\delta\,{}^{1}\mathrm{p} = \begin{Bmatrix} \delta\mathrm{x} - \chi\sin\left(\psi\right)\delta\psi \\ \delta\mathrm{y} + \chi\cos\left(\psi\right)\delta\psi \\ 0 \end{Bmatrix} \tag{70}$$

Substituting Eq. 69, Eq. 61, and Eq. 70 into Eq. 65 gives the double integral

$$\delta\mathrm{W}_{\mathrm{grav}} = -\mu\mathrm{m}\int_{-\mathrm{h}/2}^{\mathrm{h}/2}\int_{-\mathrm{L}/2}^{\mathrm{L}/2}\frac{1}{\mathrm{r}^{3}}\left[1-\frac{3}{\mathrm{r}}\left(\mathrm{x}+\chi\cos\psi\right)\right]\begin{Bmatrix} \mathrm{r}+\mathrm{x}+\chi\cos\psi \\ \mathrm{y}+\chi\sin\psi \\ \xi \end{Bmatrix}\cdot\begin{Bmatrix} \delta\mathrm{x}-\chi\sin\left(\psi\right)\delta\psi \\ \delta\mathrm{y}+\chi\cos\left(\psi\right)\delta\psi \\ 0 \end{Bmatrix}\mathrm{d}\chi\mathrm{d}\xi \tag{71}$$

Evaluating Eq. 71 gives the virtual work expression

$$\begin{aligned}\delta\mathrm{W}_{\mathrm{grav}} = -\frac{\mu\mathrm{M}}{\mathrm{r}^{2}}\Bigg\{&\left[1-\frac{2\mathrm{x}}{\mathrm{r}}-\frac{1}{4\mathrm{r}^{2}}\left(12\mathrm{x}^{2}+\mathrm{L}^{2}\cos\left(\psi\right)^{2}\right)\right]\delta\mathrm{x}+\\ &\left[\frac{\mathrm{y}}{\mathrm{r}}-\frac{1}{4\mathrm{r}^{2}}\left(12\mathrm{xy}+\mathrm{L}^{2}\sin\psi\cos\psi\right)\right]\delta\mathrm{y}+\\ &\left[\frac{\mathrm{L}^{2}}{4\mathrm{r}}\sin\psi\cos\psi+\frac{\mathrm{L}^{2}}{4\mathrm{r}^{2}}\cos\psi\left(\mathrm{x}\sin\psi-\mathrm{y}\cos\psi\right)\right]\delta\psi\Bigg\}\end{aligned} \tag{72}$$

Again, higher order terms are neglected consistent with Eq. 67 yielding

$$\delta\mathrm{W}_{\mathrm{grav}} = -\frac{\mu\mathrm{M}}{\mathrm{r}^{2}}\left\{\left[1-\frac{2\mathrm{x}}{\mathrm{r}}\right]\delta\mathrm{x}+\frac{\mathrm{y}}{\mathrm{r}}\delta\mathrm{y}+\frac{\mathrm{L}^{2}}{4\mathrm{r}}\sin\psi\cos\psi\delta\psi\right\} \tag{73}$$

from which we can easily extract the generalized forces due to gravity as

$$Q_{x,grav} = -\frac{\mu M}{r^2}\left(1 - \frac{2x}{r}\right) \tag{74}$$

$$Q_{y,grav} = -\frac{\mu M y}{r^3} \tag{75}$$

$$Q_{\psi,grav} = -\frac{\mu M L^2}{4r^3}\left(\sin\psi\cos\psi\right) \tag{76}$$

6.3.2 Aerodynamic Drag Force – $Q_{i,aero}$

The aerodynamic pressure, $\mathbf{P}_{aero}$, is assumed to have equal lift ($\mathbf{P}_l$) and drag ($\mathbf{P}_d$) components acting at any point along the spacecraft (χ, ξ),

$$P_{aero} = P_l + P_d \tag{77}$$

normal to the surface of the spacecraft. Its unit vector, indicating the direction of action of $\mathbf{P}_{aero}$, is

$$\hat{P}_{aero} = \hat{i}_b \times \left(\hat{i}_b \times \hat{v}\right) \tag{78}$$

as can be seen from examining Figure 6-2, the quantity $\hat{v}$ is the unit vector in the direction of the velocity of any point along the spacecraft, $v(\chi, \xi)$, or

$$\hat{v} = \frac{v}{|v|} \tag{79}$$

The magnitudes of the lift and drag components are

$$P_l = P_d = \frac{1}{2}\rho C_d\left(v \cdot v\right)S_{aero} \tag{80}$$

where ρ is the density of the atmosphere (assumed constant over the length of the spacecraft), C_d is the drag coefficient, and S_{aero} is the surface area of the spacecraft normal to the velocity,

$$S_{aero} = A\left|\hat{v} \cdot \hat{j}_b\right| \tag{81}$$

where A is the total spacecraft area. Using Eq. 80 the magnitude of the total aerodynamic pressure is

$$P_{aero} = \frac{\sqrt{2}}{2}\rho C_d\left(v \cdot v\right)S_{aero} \tag{82}$$

and together with Eq. 78, Eq. 81, and Eq. 79 results in the aerodynamic pressure vector

$$P_{aero} = \frac{\sqrt{2}}{2}\rho C_d (v \cdot v) A \left| \frac{v}{|v|} \cdot \hat{j}_b \right| \cdot \hat{i}_b \times \left(\hat{i}_b \times \frac{v}{|v|} \right) \tag{83}$$

Since $|v|$ is a positive scalar, it can be factored out and cancelled with the term $v \cdot v$, resulting in a simpler expression for the pressure vector:

$$P_{aero} = \frac{\sqrt{2}}{2}\rho C_d A \left| v \cdot \hat{j}_b \right| \cdot \hat{i}_b \times \left(\hat{i}_b \times v \right) \tag{84}$$

Using the vector triple product identity a slight improvement in the simplicity of the vector is achieved by noting that:

$$\hat{i}_b \times \left(\hat{i}_b \times v \right) = \left(\hat{i}_b \cdot v \right) \hat{i}_b - v \tag{85}$$

In this form it easily observed that there is no component of the aerodynamic pressure in the $\hat{i}_b$ direction. Representing these quantities in the $\{1\}$ frame we first note that the $\hat{i}_b$ vector is

$${}^1\hat{i}_b = \begin{Bmatrix} \cos\psi \\ \sin\psi \\ 0 \end{Bmatrix} \tag{86}$$

which results in:

$${}^1\hat{i}_b \times \left({}^1\hat{i}_b \times {}^1 v \right) = \begin{Bmatrix} \sin\psi \left[-\left(\dot{x} - y\dot{\theta} \right) \sin\psi + \left(\dot{y} + \dot{\theta}[r + x] \right) \cos\psi \right] \\ \cos\psi \left[\left(\dot{x} - y\dot{\theta} \right) \sin\psi - \left(\dot{y} + \dot{\theta}[r + x] \right) \cos\psi \right] \end{Bmatrix} \tag{87}$$

The virtual work due to the aerodynamic pressure is:

$$\delta W_{aero} = \int_{-h/2}^{h/2} \int_{-L/2}^{L/2} P_{aero} \cdot \delta p \, d\chi \, d\xi \tag{88}$$

At this point, we will assume that the aerodynamic pressure is concentrated at the geometric center of the spacecraft. A brief explanation of the motivation for this approximation is given by considering the absolute value term

$$\left| v \cdot \hat{j}_b \right|$$

in the virtual work expression Eq. 88 and Eq. 83. It will be evaluated using all vector quantities represented in the {1} frame, that is,

$$ {}^1\hat{j}_b = \begin{Bmatrix} -\sin\psi \\ \cos\psi \\ 0 \end{Bmatrix} \tag{89} $$

Using Eq. 89 and Eq. 62 we have

$$ \left| {}^1v \cdot {}^1\hat{j}_b \right| = \chi\left(\dot{\theta} + \dot{\psi}\right) + \left[\dot{y} + (r + x)\dot{\theta}\right]\cos\psi - \left(\dot{x} - y\dot{\theta}\right)\sin\psi \tag{90} $$

Since the argument to the absolute value operation changes sign over the range of χ, complications in the integral arise. Specifically, the result will have several conditional statements in the dynamic equations. This problem can be avoided if the net aerodynamic pressure, acting at the spacecraft center of mass, is used instead of a distributed pressure representation. Taking this approach, Eq. 84 becomes:

$$ P_{aero} = \frac{\sqrt{2}}{2}\rho C_d A \left| v_{cm} \cdot \hat{j}_b \right| \cdot \hat{i}_b \times \left(\hat{i}_b \times v_{cm}\right)\delta(\chi, \xi) \tag{91} $$

where the $\delta(\chi, \xi)$ is the Dirac function used to indicate that the pressure is centered at a single point ($\chi = 0$, $\xi = 0$). The absolute value expression which formerly contained the spatial variable χ becomes:

$$ \left| {}^1v_{cm} \cdot {}^1\hat{j}_b \right| = \left[\dot{y} + (r + x)\dot{\theta}\right]\cos\psi - \left(\dot{x} - y\dot{\theta}\right)\sin\psi \tag{92} $$

and can be easily moved outside the integral. This term will be denoted as Z for short, that is,

$$ Z \equiv \frac{\sqrt{2}}{2}\rho C_d A \left| {}^1v_{cm} \cdot {}^1\hat{j}_b \right| = \frac{\sqrt{2}}{2}\rho C_d A \left| \left[\dot{y} + (r + x)\dot{\theta}\right]\cos\psi - \left(\dot{x} - y\dot{\theta}\right)\sin\psi \right| $$

The virtual work becomes:

$$ \delta W_{aero} = \begin{Bmatrix} \sin\psi\left[-\left(\dot{x} - y\dot{\theta}\right)\sin\psi + \left(\dot{y} + \dot{\theta}[r + x]\right)\cos\psi\right] \\ \cos\psi\left[\left(\dot{x} - y\dot{\theta}\right)\sin\psi - \left(\dot{y} + \dot{\theta}[r + x]\right)\cos\psi\right] \end{Bmatrix} \cdot \begin{Bmatrix} \delta x - \chi\sin(\psi)\delta\psi \\ \delta y + \chi\cos(\psi)\delta\psi \\ 0 \end{Bmatrix} \tag{93} $$

where the double integral has been performed, eliminating the Dirac function, replacing all occurrences of χ with zero. Performing the inner product, and grouping coefficients of the virtual displacements:

$$ \begin{aligned} \delta W_{aero} = Z\{ & \delta x\left[\dot{\theta}(y\sin\psi + [r + x]\cos\psi) - \dot{x}\sin\psi + \dot{y}\cos\psi\right]\sin\psi + \\ & \delta y\left[-\dot{\theta}(y\sin\psi + [r + x]\cos\psi) + \dot{x}\sin\psi - \dot{y}\cos\psi\right]\cos\psi \} \end{aligned} \tag{94} $$

from which we can easily extract the generalized forces due to the aerodynamic pressure as:

$$Q_{x.aero} = \left\{\dot{\theta}\left(y\sin\psi + \left[r + x\right]\cos\psi\right) - \dot{x}\sin\psi + \dot{y}\cos\psi\right\}Z\sin\psi \tag{95}$$

$$Q_{y.aero} = \left\{-\dot{\theta}\left(\left[r + x\right]\cos\psi + y\sin\psi\right) + \dot{x}\sin\psi - \dot{y}\cos\psi\right\}Z\cos\psi \tag{96}$$

$$Q_{\psi.aero} = 0 \tag{97}$$

6.3.3 Solar Pressure – $Q_{i,solar}$

The solar pressure acts in the negative $\hat{J}$ direction

$$^{I}P_{solar} = \begin{Bmatrix} 0 \\ -P_{solar} \\ 0 \end{Bmatrix} \tag{98}$$

or represented in the {1} frame

$$^{1}P_{solar} = \begin{Bmatrix} -P_{solar}\sin\theta \\ -P_{solar}\cos\theta \\ 0 \end{Bmatrix} \tag{99}$$

and acts on the sail area incident with the inertial sun direction ($\hat{J}$). This fractional area can be found by forming the dot product of the spacecraft fixed $\hat{y}_b$ body axis with the inertial $\hat{J}$ unit vector. The solar pressure incident area is then the product of the total area A and the absolute value of the fractional area S_{solar} indicating that the solar pressure applies to either side of the sail. Performing this operation using quantities represented in the {I} frame yields

$$S_{solar} = A\left|^{I}y_b \cdot \hat{J}\right| = A\left|\begin{Bmatrix} -\sin(\theta+\psi) \\ \cos(\theta+\psi) \\ 0 \end{Bmatrix} \cdot \hat{J}\right| = A\left|\cos(\theta+\psi)\right| \tag{100}$$

The virtual work due to solar pressure is formed in the usual manner, representing all quantities in the {1} frame

$$\delta W_{solar} = S_{solar}\int_{-h/2}^{h/2}\int_{-L/2}^{L/2} {}^{1}P_{solar}\cdot\delta^{1}p\,d\chi\,d\xi \tag{101}$$

where the virtual displacement is given by Eq. 70 and the solar pressure is from Eq. 99. Integrating Eq. 101 gives

$$\delta W_{solar} = -\left|\cos(\theta+\psi)\right|AP_{solar}\left\{\sin\theta\,\delta x + \cos\theta\,\delta y\right\} \tag{102}$$

The solar pressure force components in the r and θ directions are easily extracted from Eq. 102 as the coefficients of δx and δy respectively, that is,

$$Q_{x,solar} = -AP_{solar}\left|\cos(\theta+\psi)\right|\sin\theta \tag{103}$$

$$Q_{y,solar} = -AP_{solar}\left|\cos(\theta+\psi)\right|\cos\theta \tag{104}$$

$$Q_{\psi,solar} = 0 \tag{105}$$

6.3.4 Thrust Forces – $Q_{i,thrust}$

The PowerSail spacecraft is assumed to have three bidirectional thrusters, two are in body fixed y direction (out of the plane of the sail) and one is in the body fixed x direction (in the plane of the sail). One y-axis thruster is located along the x-axis at a distance of L/2 from the center of mass. The second y-axis thruster is also along the x-axis, but at a distance of –L/2 from the center of mass. The x-axis thruster is collocated with the first y-axis thruster. In the following sections, the thruster force vectors, and virtual displacement vectors are derived and used to generate the virtual work of each thruster.

6.3.4.1 Y-Axis Thruster 1

The thrust vector is simply

$${}^1F_{y1} = \begin{Bmatrix} -F_{y1}\sin\psi \\ F_{y1}\cos\psi \\ 0 \end{Bmatrix} \tag{106}$$

The virtual displacement is found from Eq. 70 by setting $\chi = L/2$, that is

$$\delta^1 P_{F_{y1}} = \delta^1 p\Big|_{\chi=\frac{L}{2}} = \begin{Bmatrix} \delta x - \frac{L}{2}\sin\psi\delta\psi \\ \delta y + \frac{L}{2}\cos\psi\delta\psi \\ 0 \end{Bmatrix} \tag{107}$$

The virtual work of the thruster is then

$$\begin{aligned} \delta W_{F_{y1}} &= {}^1F_{y1}\cdot\delta^1 P_{F_{y1}} \\ &= -F_{y1}\sin\psi\delta x + F_{y1}\cos\psi\delta y + \frac{L}{2}F_{y1}\delta\psi \end{aligned} \tag{108}$$

6.3.4.2 Y-Axis Thruster 2

The thrust vector is simply

$$ {}^1F_{y2} = \begin{Bmatrix} -F_{y2}\sin\psi \\ F_{y2}\cos\psi \\ 0 \end{Bmatrix} \tag{109} $$

The virtual displacement is found from Eq. 70 by setting $\chi = -L/2$, that is

$$ \delta^1 P_{F_{y2}} = \delta^1 p\Big|_{\chi=-\frac{L}{2}} = \begin{Bmatrix} \delta x + \frac{L}{2}\sin\psi\delta\psi \\ \delta y - \frac{L}{2}\cos\psi\delta\psi \\ 0 \end{Bmatrix} \tag{110} $$

The virtual work of the thruster is then

$$ \begin{aligned} \delta W_{F_{y2}} &= {}^1F_{y2}\cdot\delta^1 P_{F_{y2}} \\ &= -F_{y2}\sin\psi\delta x + F_{y2}\cos\psi\delta y - \frac{L}{2}F_{y2}\delta\psi \end{aligned} \tag{111} $$

6.3.4.3 X-Axis Thruster

The thrust vector is simply

$$ {}^1F_x = \begin{Bmatrix} F_x\cos\psi \\ F_x\sin\psi \\ 0 \end{Bmatrix} \tag{112} $$

Since this thruster is located at the same place as the Y-axis thruster one, the virtual displacement is the same as Eq. 107 resulting in the virtual work

$$ \delta W_{F_x} = F_x\cos\psi\delta x + F_x\sin\psi\delta y \tag{113} $$

6.3.4.4 Combined Thrust Force

The net force of all three thrusters is found by summing the coefficients of the virtual displacements from Eq. 108, Eq. 111, and Eq. 113, that is

$$ Q_{x,thrust} = -\left(F_{y1} + F_{y2}\right)\sin\psi + F_x\cos\psi \tag{114} $$

$$ Q_{y,thrust} = \left(F_{y1} + F_{y2}\right)\cos\psi + F_x\sin\psi \tag{115} $$

$$ Q_{\psi,thrust} = \frac{L}{2}\left(F_{y1} - F_{y2}\right) \tag{116} $$

6.4 Preliminary Mass Analysis – Continuous Thrust

This section investigates three different spacecraft orientation scenarios where the three thrusters are assumed to be throttle-able. This will lend insight into the case where the thrusters have fixed amplitude, addressed in Section 6.5.

The first orientation, called sun pointing, keeps the spacecraft oriented such that the solar power absorption material is always pointing directly at the sun as shown in Figure 6-3. The second orientation, called minimum drag, keeps the spacecraft oriented such that the sail never encounters atmospheric drag (neglecting shear) and is shown in Figure 6-4. The third configuration called minimum gravity gradient, results in no gravity gradient torques and is shown in Figure 6-5.

For each orientation the three thruster force histories are computed analytically and compared.

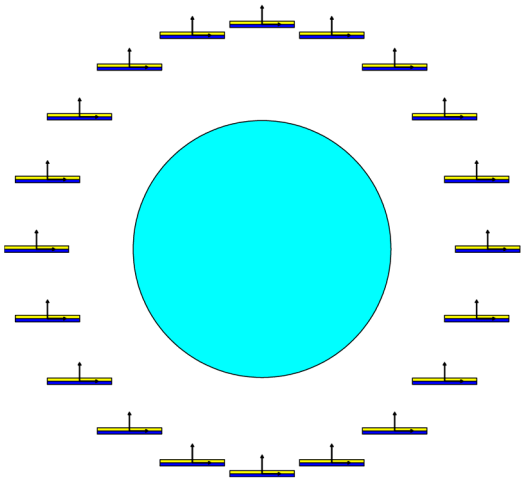

Figure 6-3: Sun Pointing Orientation

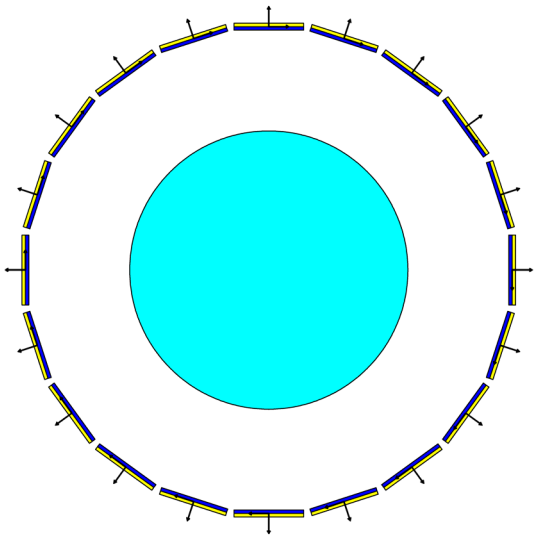

Figure 6-4: Minimum Drag Orientation

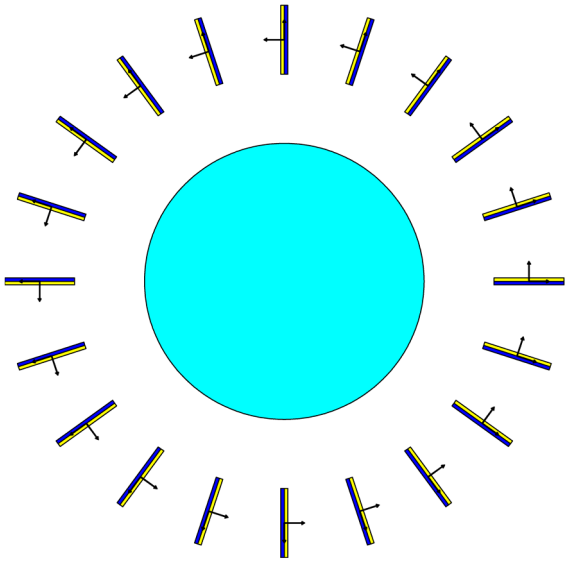

Figure 6-5: Minimum Gravity-Gradient Orientation

6.4.1 Assumptions

In addition to the assumptions employed during the equation of motion development, mission specific assumptions are listed in Table 6-2. Thruster and solar sail constants are listed in Table 6-3. As a canonical case, a thruster I_{sp} = 1000 seconds (representative of an H_2 arcjet or PPT) was chosen.

Table 6-2: Mission Specific Parameters

Description	Symbol	Units	Value
Orbital period	τ	sec	6180
Orbital radius	r	m	7277759
Atmospheric Density	ρ	kg/m^3	5.76e-15
Drag Coefficient	C_d	n.d.	2.0
Nominal Solar Pressure	P_o	N/m^2	4.667e-6
Total number of orbits	n	n.d.	51030

Table 6-3: Thruster and Sail Parameters

Description	Symbol	Units	Value
Thruster specific impulse	I_{sp}	sec	1000
Solar power density	K_{pv}	W/m^2	1400
Sail areal mass	ρ_{pv}	kg/m^2	0.92
Sail efficiency	ε_{pv}	n.d.	0.15

Finally, the PowerSail is assumed to be sufficiently close to the host such that both the host and PowerSail enter (and exit) the earth's shadow at the same time, or more generally, that their true anomalies are equal. The angle α

$$\alpha = \cos^{-1}\left(\mathrm{Re}/\mathrm{r}\right) = 28.835° \tag{117}$$

will be used to define the earth shadow as shown in Figure 6-6. The solar pressure is modeled with a step discontinuity at the shadow transitions, and is defined as

$$P_{solar} = \begin{cases} 0 & : \ \pi + \alpha \le \theta \le -\alpha \\ P_O & : \ \pi + \alpha > \theta > -\alpha \end{cases} \tag{118}$$

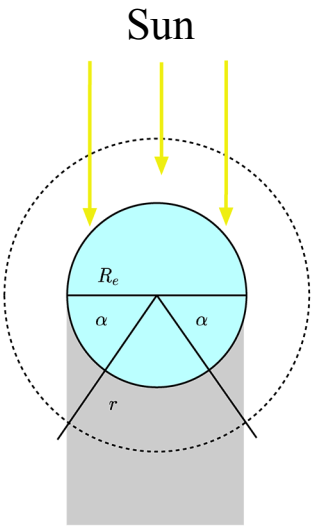

Figure 6-6: Geometry of the Earth's Shadow

The mission requirement of P_O watts is translated into an average energy per orbit, denoted E_O, and is,

$$E_O = \frac{1}{2}\tau P_O = \frac{1}{2}(6180)(500000) = 1545 \text{ MJ} \tag{119}$$

This can also be related to the solar sail energy absorption properties, and an effective pointing angle, γ

$$E_O = \frac{AK_{pv}\varepsilon_{pv}\gamma}{\dot{\theta}} \tag{120}$$

which will be used to determine the sail area , A, for each orientation using an analytical expression for γ.

The mass of the vehicle will be denoted M and for this analysis consists of only the mass of the sail (including support structure), and the fuel. For each case, this will be denoted

$$M = m_{sail} + m_{fuel} \tag{121}$$

The mass of the sail is simply the product of the area and the effective area density.

$$m_{sail} = A\rho_{pv}$$

The mass of the fuel is

$$m_{fuel} = \frac{n\sum\left|\hat{F}\right|}{gI_{sp}} \tag{122}$$

where $\sum\left|\hat{F}\right|$ is the total thruster impulse per orbit

6.4.2 Sun Pointing

The sun pointing trajectory of Figure 6-3, is defined by

$$\begin{aligned} x &= \dot{x} = \ddot{x} = 0 \\ y &= \dot{y} = \ddot{y} = 0 \\ \psi &= -\theta \\ \dot{\psi} &= -\dot{\theta} \\ \ddot{\psi} &= -\ddot{\theta} = 0 \end{aligned} \tag{123}$$

Applying these conditions to the dynamic equations of Eq. 41 through Eq. 43 gives

$$\begin{aligned} \left(F_{y1}+F_{y2}\right)\sin\theta + F_x\cos\theta &= \frac{\sqrt{2}}{2}A\rho C_d r^2\dot{\theta}^2\left|\cos\theta\right|\sin\theta\cos\theta + AP_{solar}\sin\theta \\ \left(F_{y1}+F_{y2}\right)\cos\theta - F_x\sin\theta &= \frac{\sqrt{2}}{2}A\rho C_d r^2\dot{\theta}^2\left|\cos\theta\right|\cos\theta^2 + AP_{solar}\cos\theta \\ \frac{L}{2}\left(F_{y1}-F_{y2}\right) &= \frac{\mu M}{4r^3}L^2\sin\theta\cos\theta \end{aligned} \tag{124}$$

Solving these for the three forces yields force time histories that maintain the PowerSail as shown in Figure 6-3, that is

$$\begin{aligned} F_{y1} &= \frac{\sqrt{2}}{4}A\rho C_d r^2\dot{\theta}^2\left|\cos\theta\right|\cos\theta + \frac{1}{2}AP_{solar} - \frac{\mu M}{4r^3}L\sin\theta\cos\theta \\ F_{y2} &= \frac{\sqrt{2}}{4}A\rho C_d r^2\dot{\theta}^2\left|\cos\theta\right|\cos\theta + \frac{1}{2}AP_{solar} + \frac{\mu M}{4r^3}L\sin\theta\cos\theta \\ F_x &= 0 \end{aligned} \tag{125}$$

The effective pointing angle, γ_{sp}, is

$$\gamma_{sp} = \int_{\theta_1}^{\theta_2} d\theta \tag{126}$$

where for this case, $\theta_1 = -\alpha$ and $\theta_2 = \pi+\alpha$. Solving the integral gives

$$\gamma_{sp} = \pi + 2\alpha = 4.1481 \tag{127}$$

The sail area can then be computed using Eq. 120 and the values of Table 6-3 as

$$A_{sp} = \frac{E_O\dot{\theta}}{K_{pv}\varepsilon_{pv}\gamma_{sp}} = 1803\,m^2 \tag{128}$$

Assuming a sail material (with structure) area density as given in Table 6-3, the mass of the sail, not including propellant, is

$$m_{sp,sail} = A_{sp}\rho_{pv} = 1659\,kg \tag{129}$$

The mass of the fuel is not readily computed using Eq. 122 since the mass of the PowerSail is needed to compute the thruster forces, and the impulse $\hat{F}$. Instead, the fuel mass was calculated by iterating the force equations on the total mass M until the required fuel mass equaled the difference between the total mass, and $m_{sp,sail}$. In this way the fuel mass was found to be

$$m_{sp,fuel} = 510\,kg \tag{130}$$

The time histories of the force profiles are shown in Figures 6-7 through 6-9 using the blue lines.

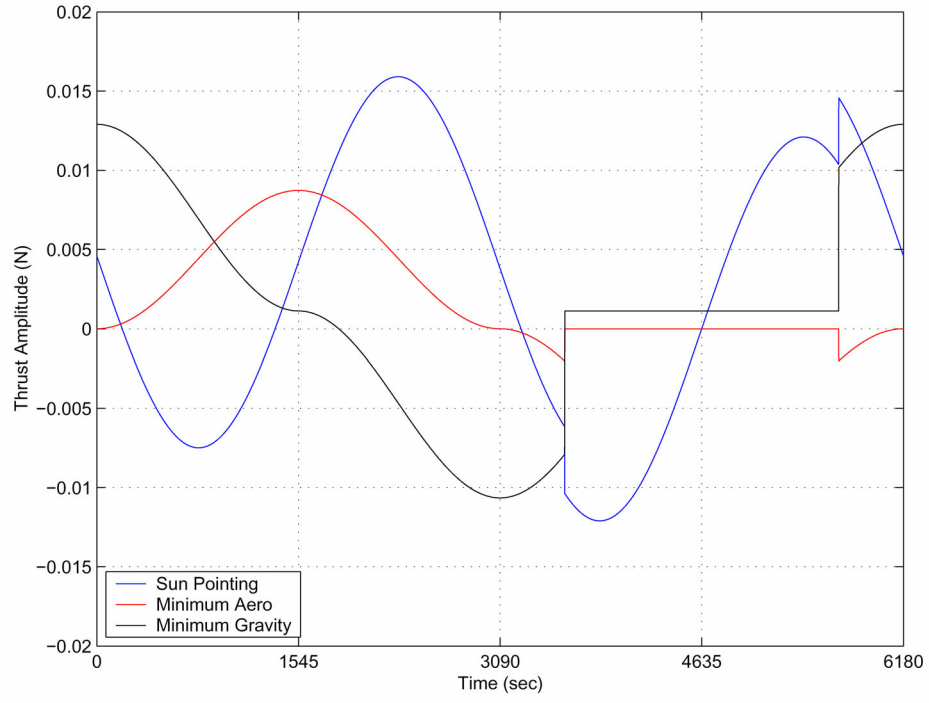

Figure 6-7: Time History of the F_{y1} Thruster

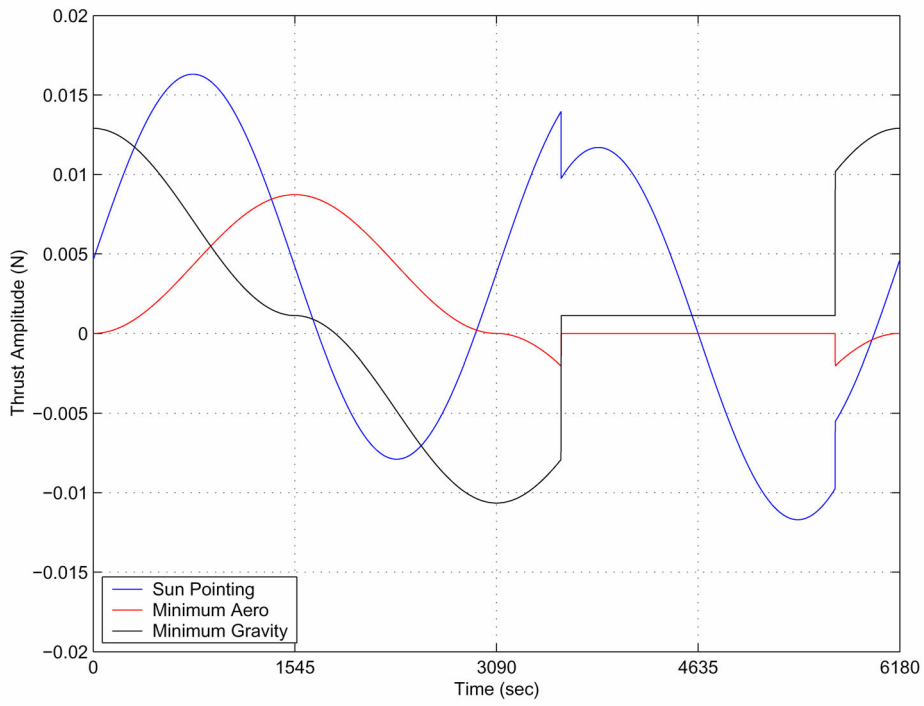

Figure 6-8: Time History of the F_{y2} Thruster

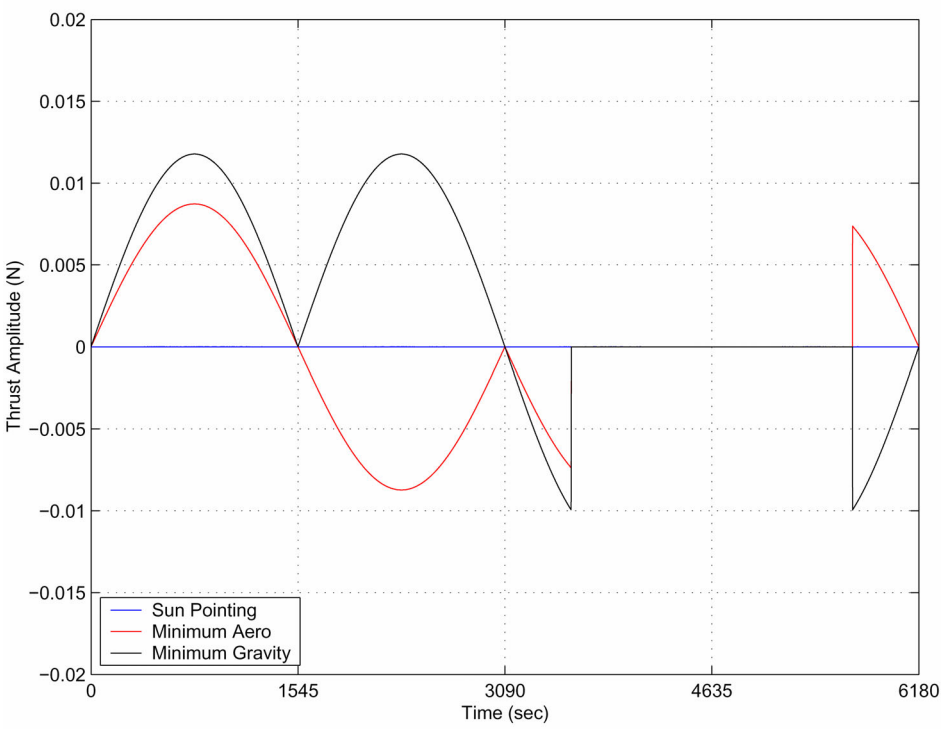

Figure 6-9: Time History of the F_x Thruster

6.4.3 Minimum Drag

The minimum drag trajectory of Figure 6-4, is defined by

$$\begin{aligned} x &= \dot{x} = \ddot{x} = 0 \\ y &= \dot{y} = \ddot{y} = 0 \\ \psi &= -\frac{\pi}{2} \\ \dot{\psi} &= \ddot{\psi} = 0 \end{aligned} \tag{130}$$

Applying these conditions to the dynamic equations of Eq.41 through Eq.43 gives

$$\begin{aligned} F_{y1} + F_{y2} &= -AP_{solar} \sin\theta \left| \cos\left(\theta - \frac{\pi}{2}\right) \right| \\ F_x &= AP_{solar} \cos\theta \left| \cos\left(\theta - \frac{\pi}{2}\right) \right| \\ 0 &= \frac{L}{2}\left(F_{y1} - F_{y2}\right) \end{aligned} \tag{131}$$

Solving these for the three forces yields force time histories that maintain the PowerSail as shown in Figure 6-4, that is

$$\begin{aligned} F_{y1} = F_{y2} &= -\frac{1}{2} AP_{solar} \sin\theta |\sin\theta| \\ F_x &= AP_{solar} \cos\theta |\sin\theta| \end{aligned} \tag{132}$$

The effective pointing angle, γ_{md}, is

$$\gamma_{md} = \int_{\theta_1}^{\theta_2} sin\,\theta d\theta \tag{133}$$

where for this case, $\theta_1 = 0$ and $\theta_2 = \pi$. Solving the integral gives

$$\gamma_{md} = 2$$

The sail area can then be computed using Eq. 120 and the values of Table 6-3 as

$$A_{md} = \frac{E_O \ddot{\theta}}{K_{pv} \varepsilon_{pv} \gamma_{md}} = 3740\, m^2 \tag{134}$$

Assuming a sail material (with structure) area density as given in Table 6-3, the mass of the sail, not including propellant, is

$$m_{md,sail} = A_{md}\rho_{pv} = 3441kg \tag{135}$$

Unlike the sun pointing case, for minimum drag the force balance of Eq. 132 does not depend on the sail mass. Therefore, the fuel is computed directly from Eq. 122.

$$m_{md,fuel} = 258\,kg \tag{136}$$

The time histories of the force profiles are shown in Figures 6-7 through 6-9 using the red lines.

6.4.4 Minimum Gravity Gradient

The minimum gravity gradient trajectory is defined by

$$\begin{aligned} x &= \dot{x} = \ddot{x} = 0 \\ y &= \dot{y} = \ddot{y} = 0 \\ \psi &= \dot{\psi} = \ddot{\psi} = 0 \end{aligned} \tag{137}$$

Applying these conditions to the dynamic equations of Eq.1 through Eq.3 gives

$$\begin{aligned} F_{y1} = F_{y2} &= \frac{1}{2}AP_{solar}\cos\theta|\cos\theta| + \frac{\sqrt{2}}{4}A\rho C_d r^2\dot{\theta}^2 \\ F_x &= AP_{solar}\sin\theta|\cos\theta| \end{aligned} \tag{138}$$

which yields the thruster histories that maintain the PowerSail as shown in Figure 6-5.

The effective pointing angle, γ_{mg}, is

$$\gamma_{mg} = \int_{\theta_1}^{\theta_2} cos\,\theta d\theta \tag{139}$$

where for this case, $\theta_1 = -\alpha$ and $\theta_2 = 0$. Solving the integral gives

$$\gamma_{mg} = 1 + sin\,\alpha = 1.4823 \tag{140}$$

The sail area can then be computed using Eq. 120 and the values of Table 6-3 as

$$A_{mg} = \frac{E_O\dot{\theta}}{K_{pv}\varepsilon_{pv}\gamma_{mg}} = 5047\,m^2 \tag{141}$$

Assuming a sail material (with structure) area density as given in Table 6-3, the mass of the sail, not including propellant, is

$$m_{mg,sail} = A_{mg}\rho_{pv} = 4643\,kg \tag{142}$$

Just like the minimum drag case, the fuel is computed directly from Eq. 122 as

$$m_{mg,fuel} = 479\,kg$$

The time histories of the force profiles are shown in Figures 6-7 through 6-9 using the black lines.

6.4.5 Summary

Table 6-4 summarizes the results of the previous sections, including extracting the total impulse from the plots of Figures 6-7 through 6-9. For the 6180 second period orbit considered (approximately 900 kilometer altitude), it is clear that a sun pointing configuration has the smallest area, and smallest total mass. It should be noted that for lower orbits the atmospheric drag term in the sun pointing equations will eventually dominate. When this occurs the minimum drag orientation will become the lower mass solution. There are two entries for the sun pointing case using different E_O requirements. The second one has an E_O that is 5% lower than the rest. This will be used for comparison and discussion with the fuel optimal results of Section 6.5.2. It should be noted that the force profiles as summarized in Figures 6-7 through 6-9, ensure zero sail/host formation error throughout the orbit.

Although the analysis for the mission with continually throttle-able thrusters is fairly straightforward, this is not the case when using electric propulsion thrusters having fixed amplitudes as considered in the next section.

Table 6-4: Summary of mass and impulse results for the three different PowerSail trajectory orientations

	Length (m)	Area (m^2)	m_{sail} (kg)	m_{fuel} (kg)	m_{total} (kg)	Impulse (N-s)	Pointing Time (s)	Energy/Orbit (MJ)
Sun Pointing	42.46	1803	1659	510	2169	98	4080	1545
Sun Pointing	41.40	1713	1576	471	2047	91	4080	1468
Minimum Drag	61.16	3741	3441	258	3699	50	1967	1545
Minimum Gravity	71.04	5047	4643	479	5122	92	1458	1545

6.5 Electric Propulsion Trajectory Estimates

Several different propulsion technologies are available for use on the PowerSail (e.g. Teflon™ PPT, hydrazine arcjet, and xenon ion). Although some EP systems allow limited throttling, this study conservatively assumed that the thrusters were capable of only discrete thrust amplitudes. Since the goal of this study was to determine the PowerSail configuration (size and thruster technology) with smallest total mass, it was necessary to determine the fuel requirements for various thruster technologies. In addition, the PowerSail was to satisfy power and station keeping requirements. That is, the PowerSail must return to its starting position and orientation after one orbit.

A simple approach would be to use the information learned from Section 6.4 using PowerSail configurations and their throttle-able thrust profiles to set the pulse amplitudes and durations. Unfortunately, this leads to large PowerSail pointing inaccuracies effecting both power generation and station keeping as will be shown in Section 6.5.1.

Another approach is to use a numerical optimization code to determine the thrust durations and PowerSail size such that the system mass is minimized while ensuring that power generation and station keeping constraints are satisfied. This has the added benefit of generating optimal PowerSail trajectories, different from the ones shown in the throttle-able section. This method is described in detail in Section 6.5.2 where it is shown that the best PowerSail trajectory is somewhere between the sun pointing and aero optimal described earlier. This allows the PowerSail system mass to be less than that of the throttle-able solution by trading off pointing accuracy for fuel mass.

6.5.1 Pulse Approximation Based on Throttleable Results

Using the results of Figures 6-7 through 6-9 an approximate pulse profile was constructed as shown in Figure 6-10. The goal of this profile was to exploit the benefit of true sun-pointing to reduce vehicle mass. The amplitudes and pulse durations were selected by decomposing the throttle-able thrust profile into a constant thrust portion (zero moment), and the moment producing portion as shown, for F_{y1}, in Figure 6-11.

The constant thrust portion was approximated as having an amplitude of 4.6 mN between 0 and 3585 s, and again between 5685 s to the end of the maneuver. After applying this approximation to the throttle-able solution, constant amplitude pulses were selected to generate an average amplitude. The decomposition of the approximate pulse profile is shown in Figure 6-12.

The resulting approximate pulse profiles are shown in Figure 6-10 for all three thrusters. They use more impulse, and thus result in larger PowerSail system mass, as compared to the true sun pointing solution of the previous section. However, they represent a reasonable first cut.

The dynamic simulation of the PowerSail was run using the pulse profiles described above, with the resulting trajectories shown in Figure 6-13. The system mass was fixed

to be the same as the throttle-able solution of 2169 kg. It is clear that the approximations lead to significant power generation and station keeping errors after one orbit.

Due to the severity of the pointing and station keeping errors associated with approximate thrust profiles, it was decided that they would not be sufficient for determining meaningful system mass estimates. Furthermore, it is not readily apparent how the profiles should be modified to improve performance. Instead an optimization capability was developed that generates pulse profiles that achieve the mission requirements, while minimizing system mass.

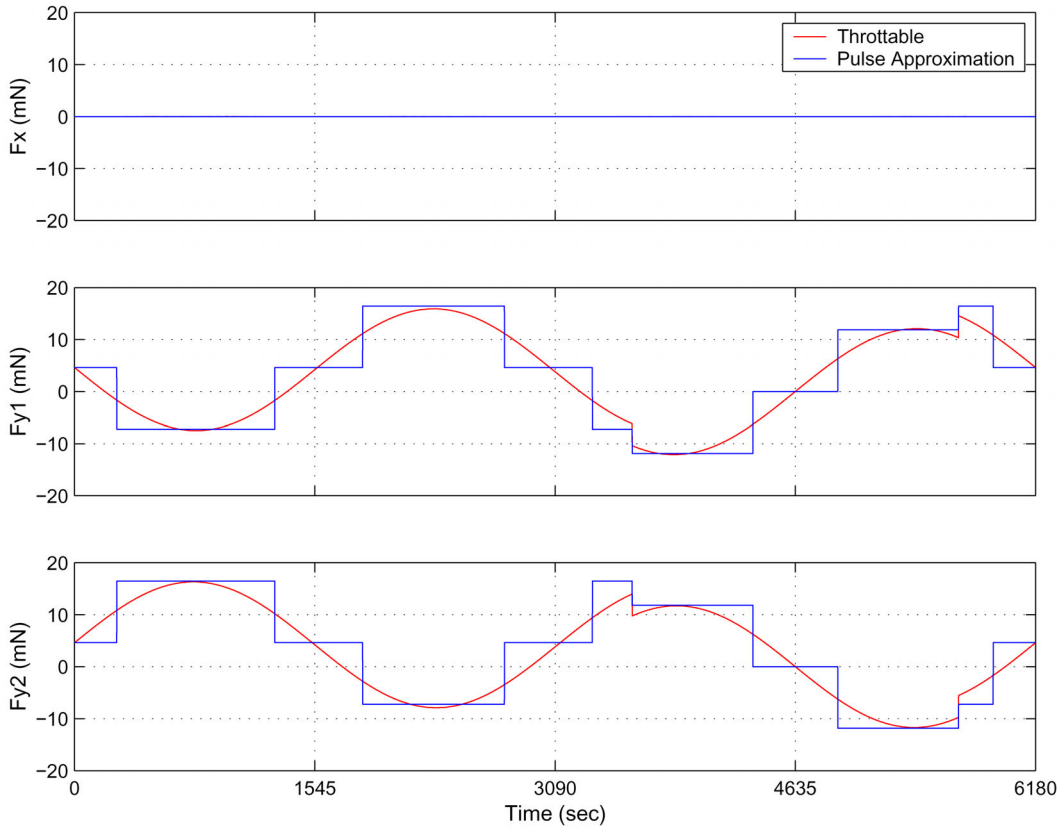

Figure 6-10: Comparison of an approximate pulse profile with the throttle-able solution that it is based on

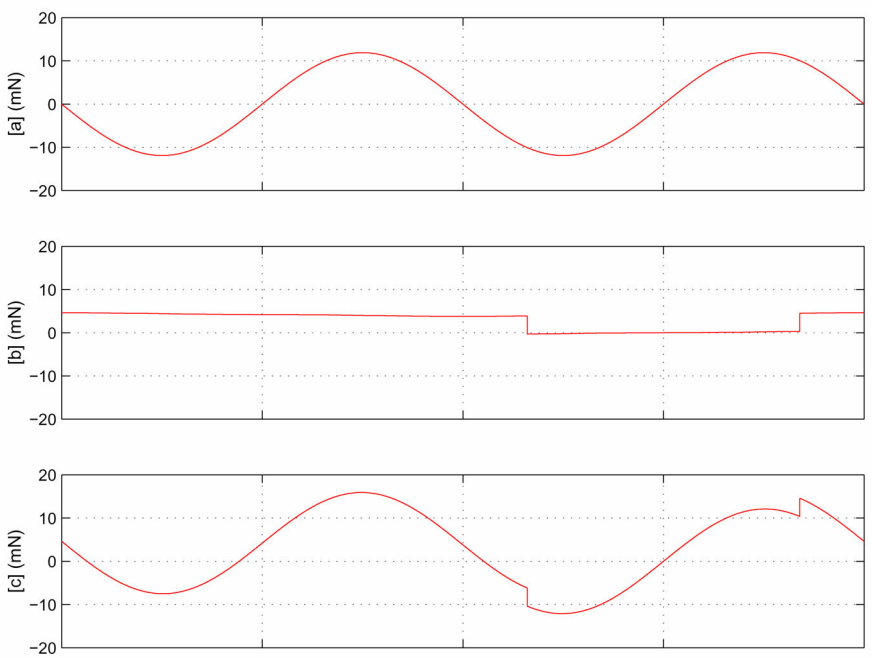

Figure 6-11: Decomposition of the throttle-able force F_{y1} (see the blue line in Figure 6-7) into a component that generates a net PowerSail moment (a), a component that generates no moment (b), and the total force (c)

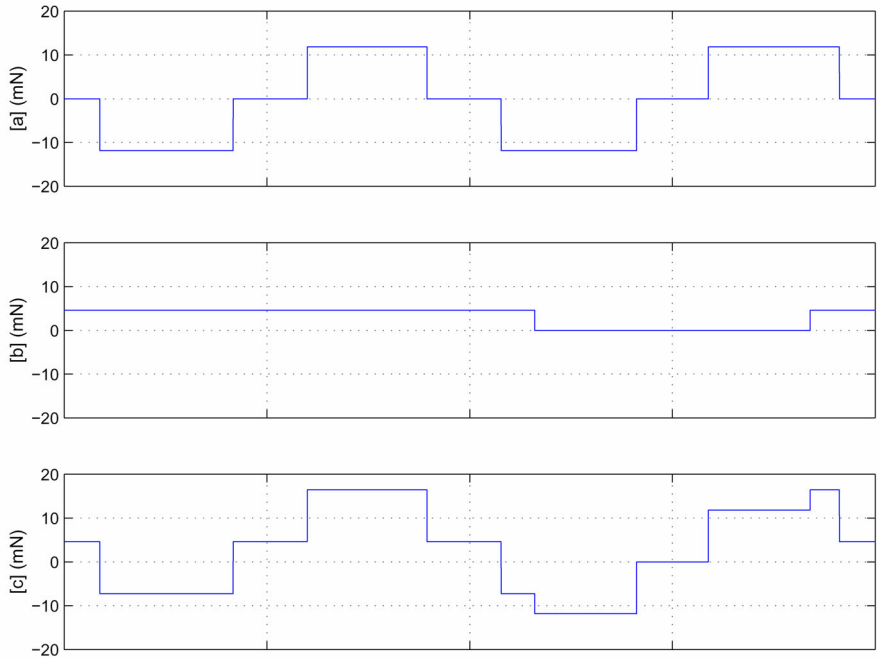

Figure 6-12: Decomposition of the approximate pulse force F_{y1} into a component that generates a net PowerSail moment (a), a component that generates only force (b), and the total force (c).

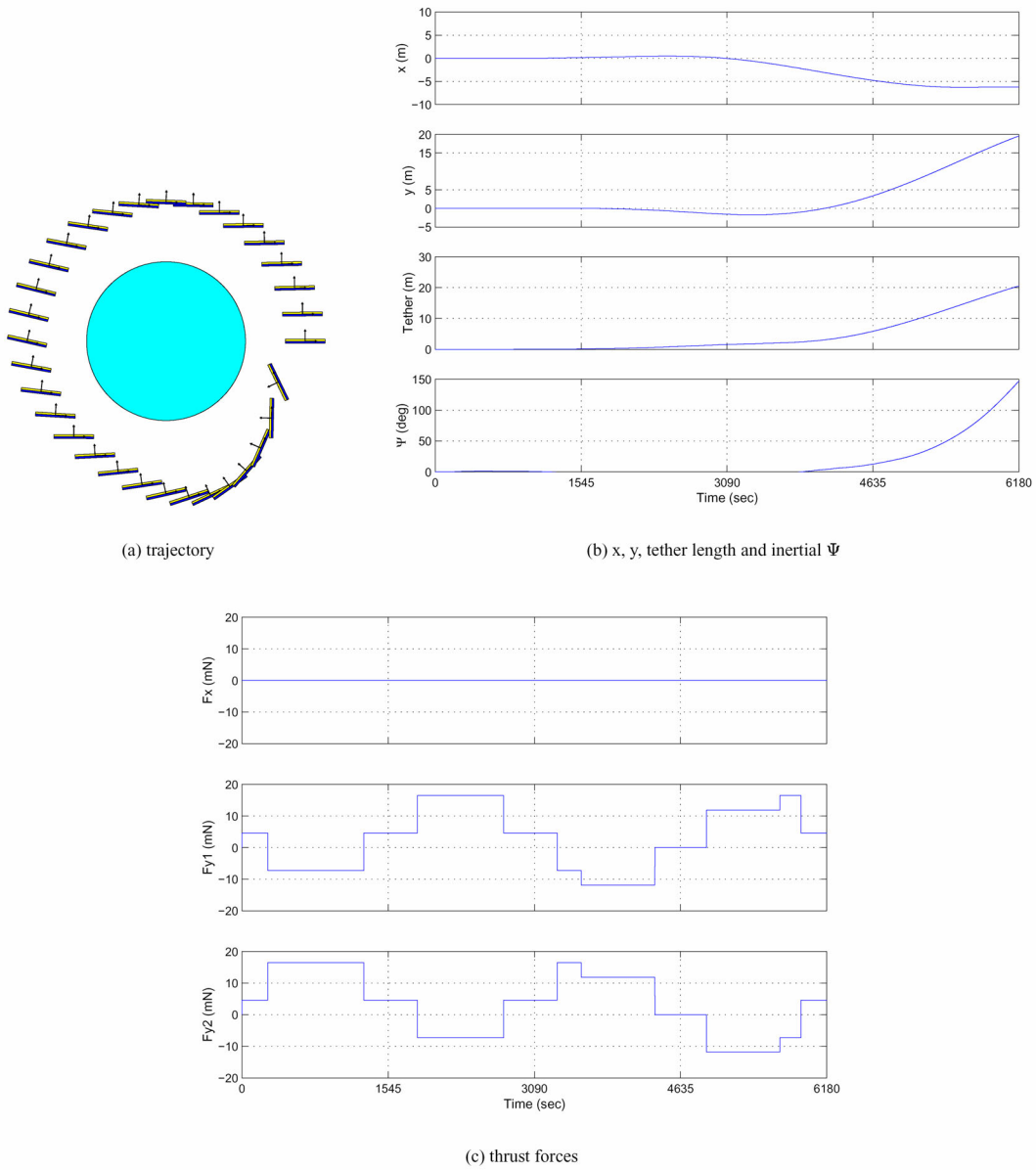

(a) trajectory

(b) x, y, tether length and inertial Ψ

(c) thrust forces

Figure 6-13: Dynamic simulation results using the pulse approximation thrust profiles derived from the throttle-able results

6.5.2 Optimal Thruster Pulse Generation

Each y-axis thruster (F_{y1} and F_{y2}) was allowed to have two positive and two negative pulses, all of the same amplitude. In addition, a center thruster was allowed to have a different amplitude and two positive pulses. Finally, the x-axis thruster was allowed to have its own amplitude, and again, two positive and two negative firings. The optimization code was allowed to select all the amplitudes and thrust times. The pulses were allowed to overlap, mimicking the effect of two thrusters firing simultaneously to

double the force. In addition, it could give the PowerSail an initial orientation and angular rate. Finally, the PowerSail was assumed to be square with the length of it being a free parameter.

Constraints were imposed on both the power generation and station keeping requirements. Specifically, the energy per orbit was required to be within 5% of the previously computed value of 1545MJ and the PowerSail was required to return to the starting position and orientation after one orbit, to within 1 centimeter, and 0.1 degrees orientation. The cost function, J,

$$J = m_{sys} \tag{143}$$

was simply the total mass of the system, including the sail mass, fuel mass, and inert thruster mass (for derivation of fuel and inert mass see Section 6.6).

$$m_{sys} = A\rho_{pv} + \frac{n}{I_{sp}g}\sum \hat{F} + \frac{\beta g I_{sp}}{\eta}\left(8F_{y,amp} + 4F_{x,amp} + 4F_{c,amp}\right) \tag{144}$$

where ρ_{pv} is the PowerSail areal density, n is the total number of orbits during the PowerSail lifetime, $F_{y,amp}$ is the amplitude of the y-axis (outboard) thrusters, $F_{x,amp}$ is the amplitude of the x-axis (in-plane) thrusters, $F_{c,amp}$ is the amplitude of the center thruster, and $\hat{F}$ is the total impulse for one orbit.

Instead of writing a custom optimization code, MATLAB's constrained optimization algorithm was used. It relies on the standard Sequential Quadratic Programming approach as described in the MATLAB manuals. It should be noted that all the results here, while being mass extremum solutions, are not claimed to be globally optimal. Unfortunately, the system is sufficiently complex that a formal proof of global optimality is impossible.

The seven thruster technologies, listed in Table 6-1, were used to determine the mass optimal results of Figures 6-14 through 6-20. The x and y quantities in the (b) plots are the same as those of Eq. 41 through Eq. 43. The inertial PowerSail orientation angle, Ψ, is related to ψ and θ by

$$\Psi = \psi + \theta \tag{145}$$

While the thrust profiles for the different technologies vary, the overall PowerSail trajectory is similar in all cases. It represents a hybrid motion between the sun pointing and minimum aero solutions presented in Section 6.4. By exploiting the trade-off between pointing accuracy and fuel mass, the hybrid trajectory requires less mass than the true sun pointing or the true minimum aero solutions.

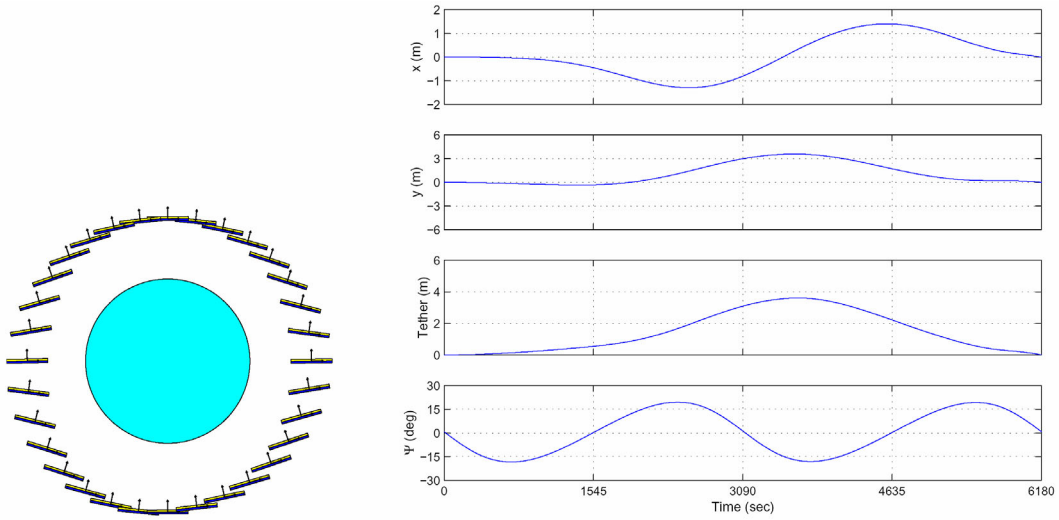

(a) trajectory

(b) x, y, tether length and inertial Ψ

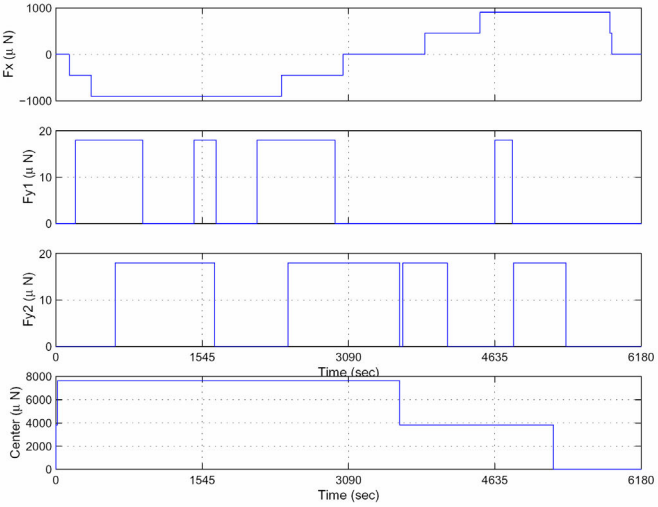

(c) thrust forces

Figure 6-14: Mass Optimal Results using Teflon™ PPT Technology

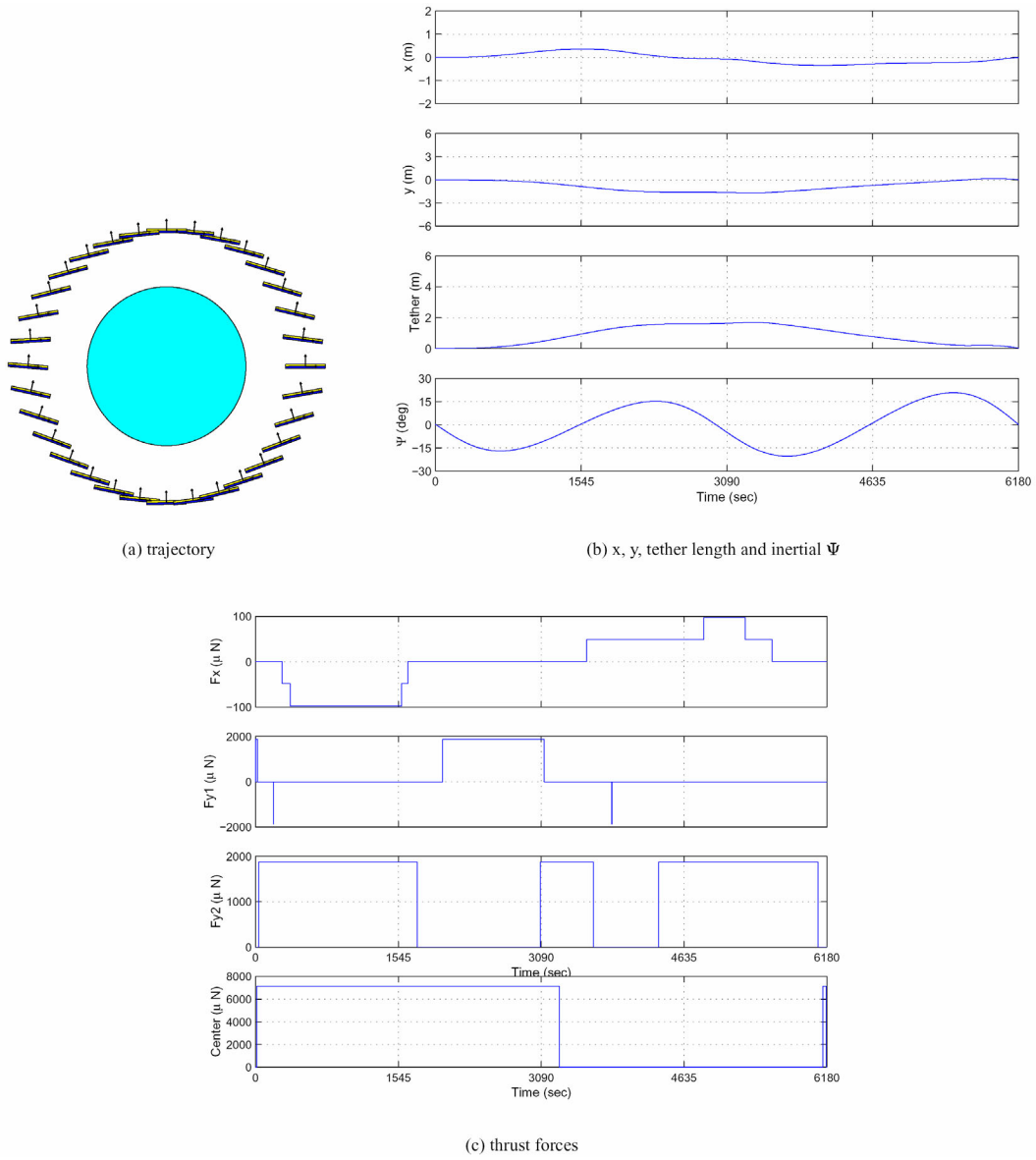

(a) trajectory

(b) x, y, tether length and inertial Ψ

(c) thrust forces

Figure 6-15: Mass Optimal Results using Hydrazine Resistojet Technology

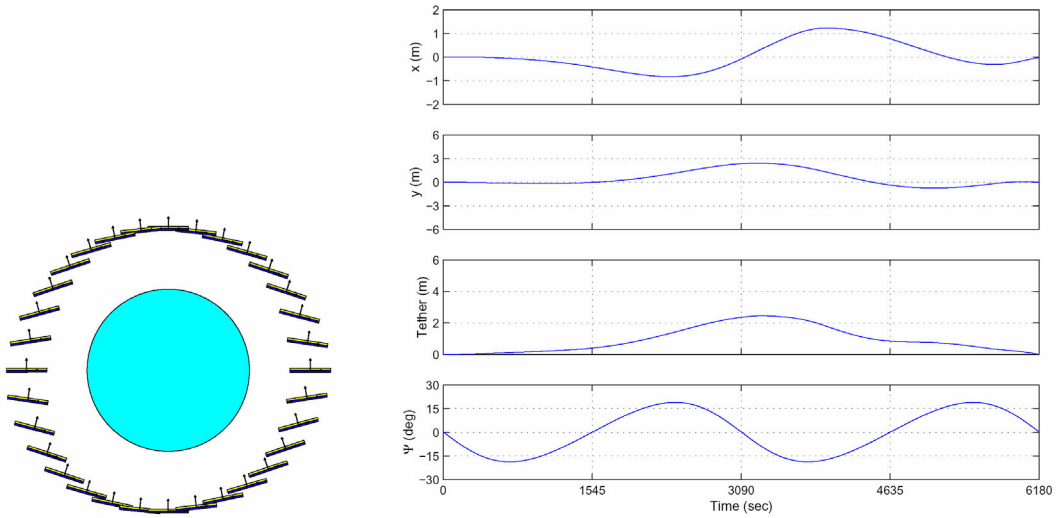

(a) trajectory

(b) x, y, tether length and inertial Ψ

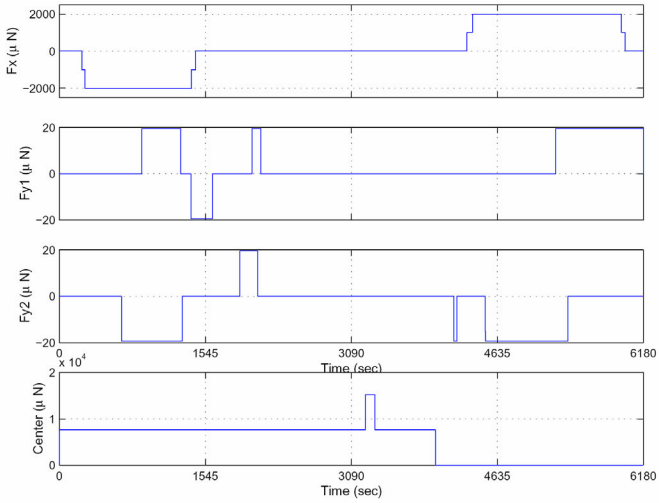

(c) thrust forces

Figure 6-16: Mass Optimal Results using Hydrazine Arcjet Thruster Technology

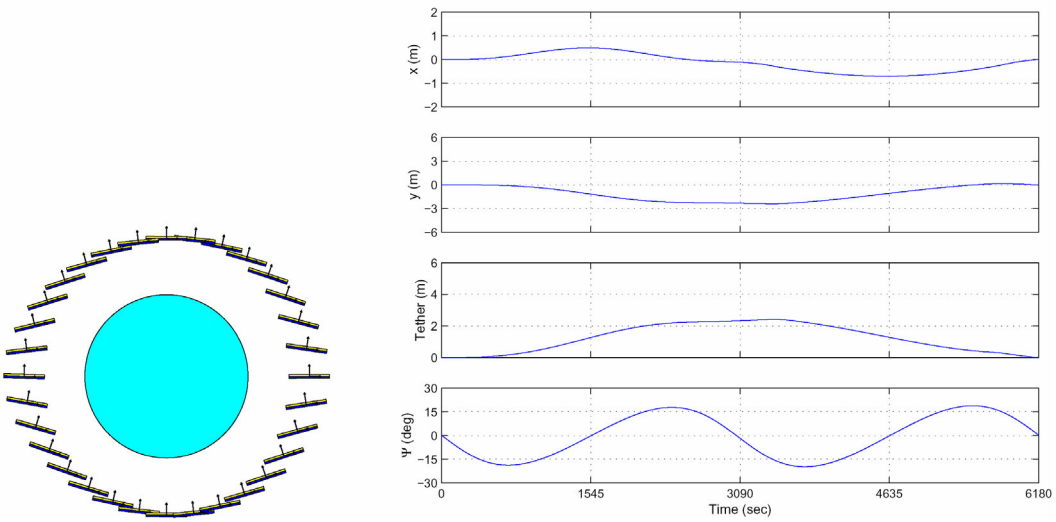

(a) trajectory

(b) x, y, tether length and inertial Ψ

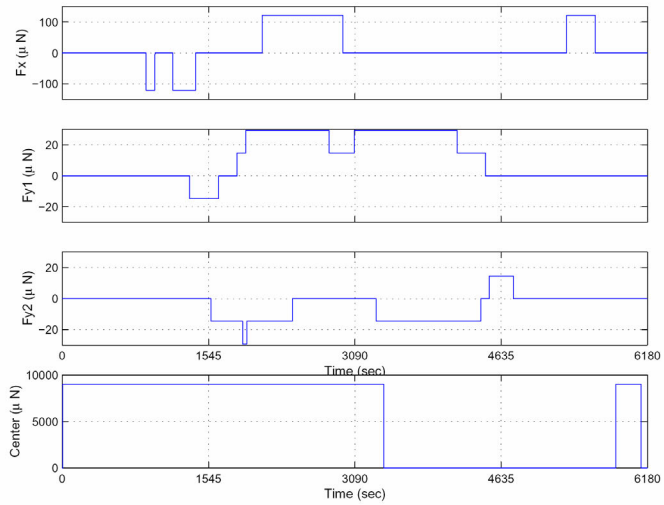

(c) thrust forces

Figure 6-17: Mass Optimal Results using Ammonia Arcjet Thruster Technology

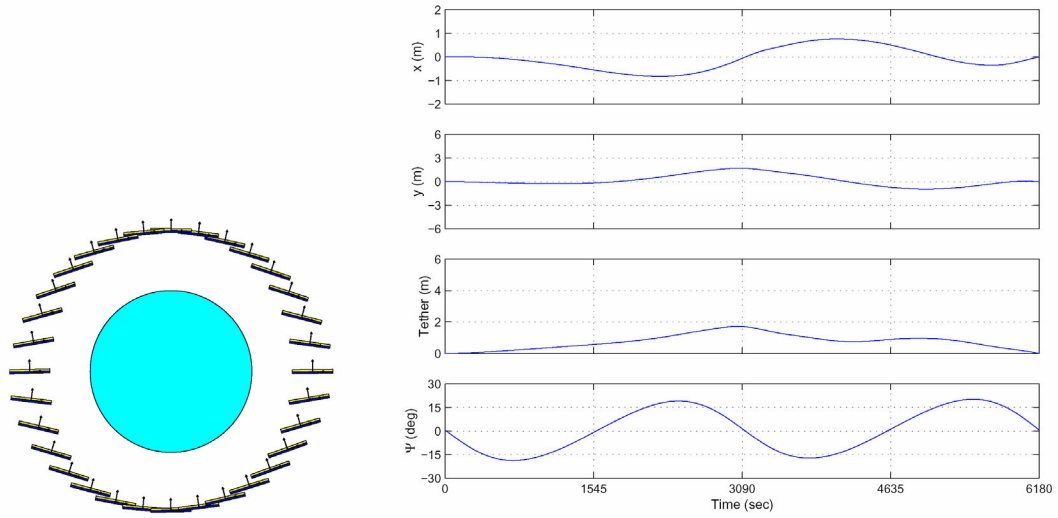

(a) trajectory

(b) x, y, tether length and inertial Ψ

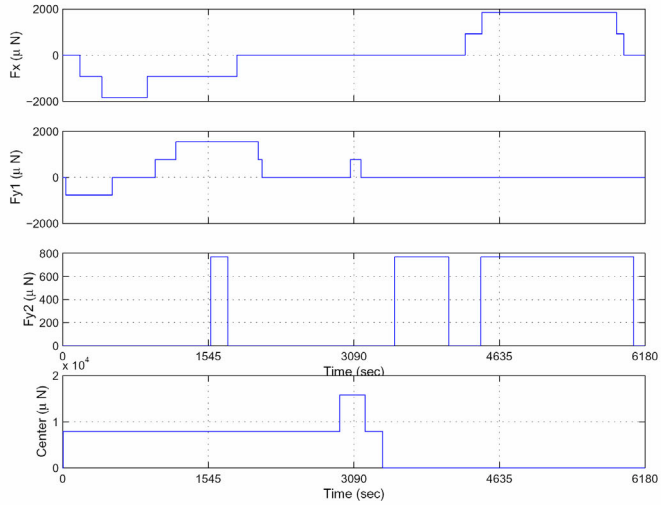

(c) thrust forces

Figure 6-18: Mass Optimal Results using Hydrogen Arcjet Technology

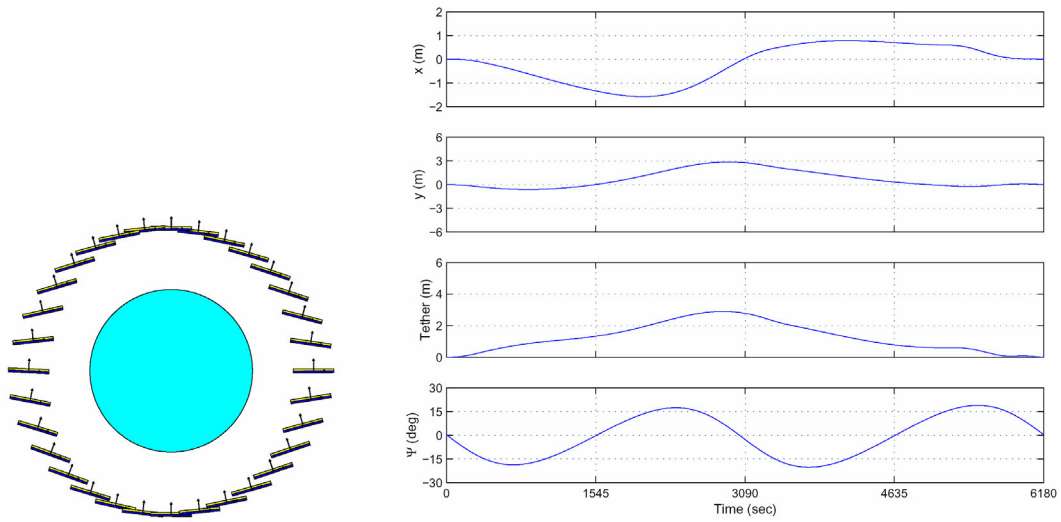

(a) trajectory

(b) x, y, tether length and inertial Ψ

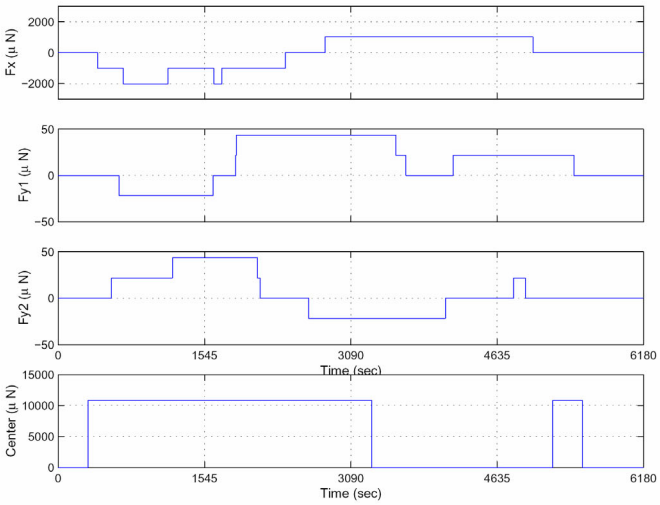

(c) thrust forces

Figure 6-19: Mass Optimal Results using Xenon Hall Thruster Technology

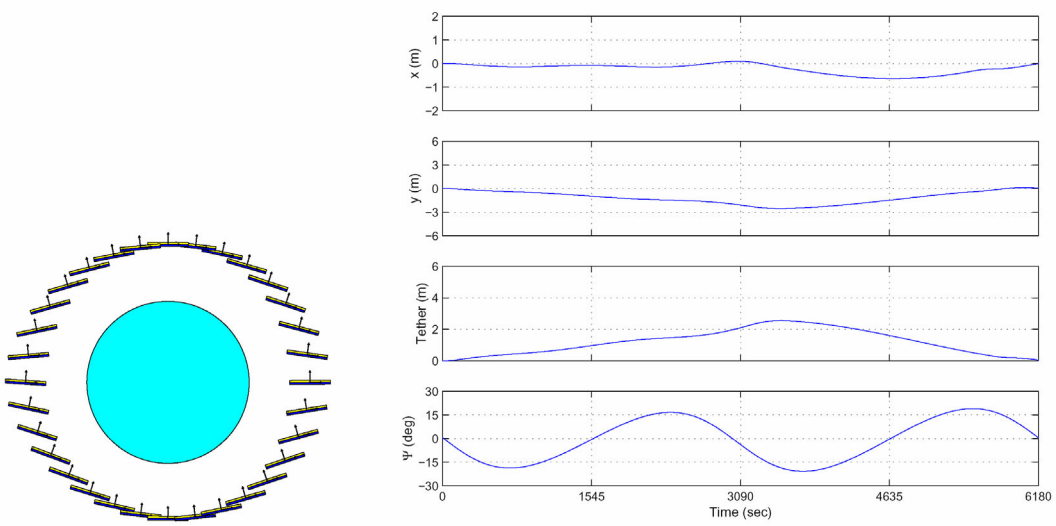

(a) trajectory

(b) x, y, tether length and inertial Ψ

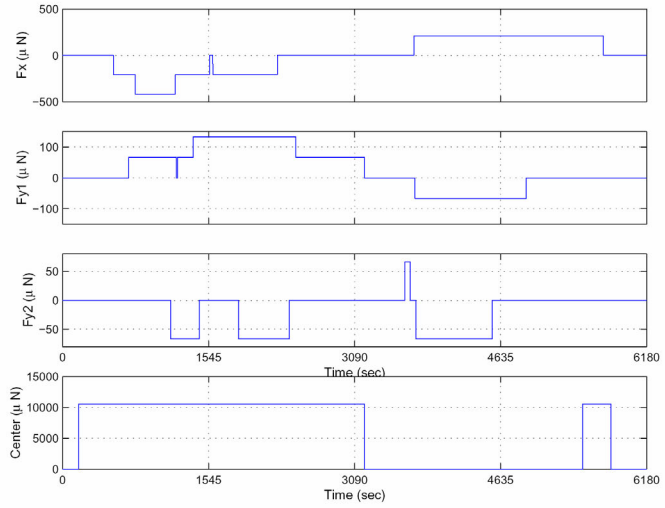

(c) thrust forces

Figure 6-20: Mass Optimal Results using Xenon Ion Thruster Technology

Table 6-5 summarizes the key mass optimal results. It is interesting to note that the PowerSail size converged to approximately the same value, independent of thruster technology. This can be explained by the tendency of the solution to favor small, and thus light, PowerSails. In all cases the pointing accuracy was allowed to slip up to the maximum allowable error in power generation, or 1468 MJ (5%).

Table 6-5: Impulse and thrust requirements from the mass optimization results

	Impulse Per Orbit (N-s)	Center Thruster Amplitude (μN)	Outboard Thruster Amplitude (μN)	In-Plane Thruster Amplitude (μN)	Sail Length (m)	Effective Pointing Time (s)
Teflon™ PPT	37.64	3814.0	18.0	452.3	41.92	3978.1
N_2H_4 Resistojet	33.53	7157.2	1896.6	48.8	41.83	3994.8
N_2H_4 Arcjet	36.67	7604.2	19.5	1003.8	41.91	3979.0
NH_3 Arcjet	33.22	9005.4	14.6	121.0	41.90	3981.6
H_2 Arcjet	37.59	7892.0	766.7	925.0	41.92	3978.3
Xe Hall	40.91	10845.0	21.8	101.3	41.89	3982.8
Xe Ion	36.32	10532.0	66.7	210.4	41.89	3984.0

6.6 Propulsion System Sizing Calculations

Based on the optimal dynamic simulation outlined in the previous section, we can calculate the required propulsion system mass, power, and overall vehicle size for a given mission. In this section of the report we will discuss the vehicle characteristics for the various propulsion technologies considered.

6.6.1 PowerSail Thruster Layout

The optimal thruster pulse generation profile constraints and assumptions were outlined previously in Section 6.5.2. These constraints can be interpreted in terms of thruster hardware and layout as detailed in Figure 6-21.

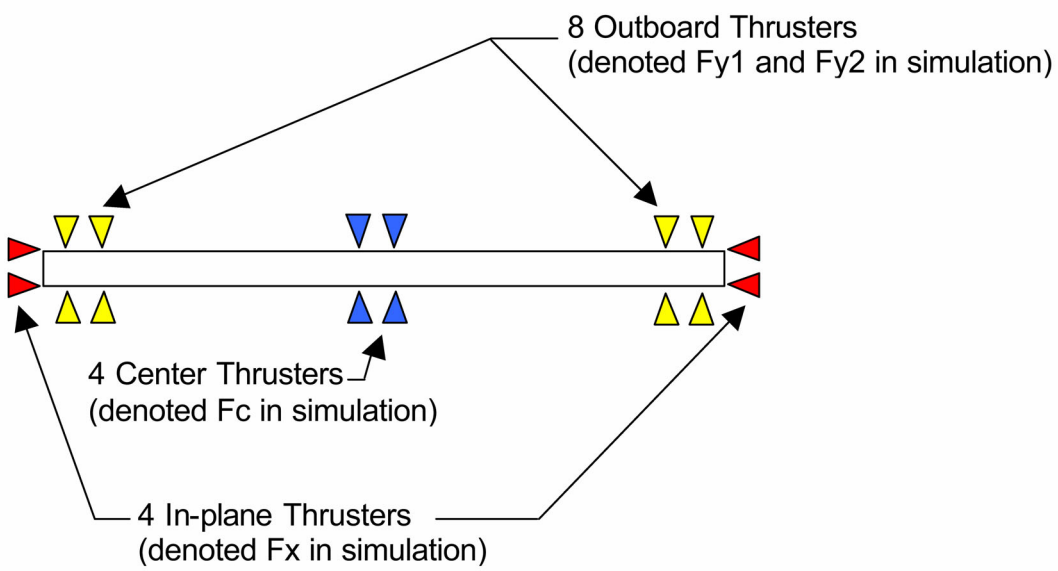

Figure 6-21: Schematic showing thruster layout implied by force constraints imposed in the dynamic simulation/optimization routine

The total number of thruster units on the vehicle amounts to sixteen. Although all sixteen thrusters are assumed to be of the same type (e.g. N_2H_4 Arcjet, Xe Ion, etc.), a variation between groups has been allowed in the optimization routine. The thruster requirements and deviations can be summarized:

- The eight outboard thrusters all have the same thrust amplitude and, hence, power requirements
- The four center thrusters all have the same thrust amplitude and, hence, power requirements
- The four in-plane thrusters all have the same thrust amplitude and, hence, power requirements
- The on-board power processing system is capable of simultaneously firing all sixteen thrusters

6.6.2 Propulsion Mass and Power Analysis

The optimization algorithm determines the thrust amplitude for each set of thrusters (outboard, center, and in-plane) as well as the total firing duration for each thruster. This information can be used to calculate the mass contribution of the propulsion system to the overall vehicle. Since this study was limited to EP devices, the propulsion system mass, m_{sys}, can be written as

$$m_{sys} = m_{fuel} + m_{inert} \tag{146}$$

where m_{fuel} is the fuel mass and m_{inert} is the dry mass, which includes the PPU as well as the thruster unit itself.

With the thrust amplitude and total firing time given for each thruster, it is straightforward to calculate the total required per-orbit impulse, $\sum \hat{F}$. Knowing $\sum \hat{F}$ and the total number of orbits in the mission, n, the mission fuel mass is calculated as

$$m_{fuel} = \frac{n\sum \hat{F}}{gI_{sp}} \tag{147}$$

The inert mass is assumed to scale proportionally with the required electrical power, or

$$m_{inert} = \beta P \tag{148}$$

where P is the electrical power demanded of the thruster and the constant of proportionality, β, has units of kg/kW. The inert mass has contributions from both the power processing hardware as well as the thruster unit itself, so β can be broken down into

$$\beta = \beta_{PPU} + \beta_T \tag{149}$$

Electrical power can be related to the thrust amplitude through a fundamental relationship according to

$$P = \frac{FgI_{sp}}{\eta} \tag{150}$$

where F is the thrust amplitude and η is the electrical efficiency of the propulsion system. With this expression we can write the inert mass in terms of the thrust

$$m_{inert} = \frac{\beta FgI_{sp}}{\eta} \tag{151}$$

Thus, when the optimization routine specifies the thrust amplitude it is implicitly fixing the thruster power as well as the required inert mass for a given thruster technology.

To calculate the total propulsion system mass contribution, we must slightly modify the inert mass expression to take into account the three sets of thrusters: outboard, center, and

in-plane. Since there are eight identical outboard thrusters, the inert mass due to the outboard thrusters can be written as

$$m_{inert} = \frac{8\beta F_{out} g I_{sp}}{\eta} \tag{152}$$

Similar expressions can be written for the four center thrusters and the four in-plane thrusters. Finally, the total propulsion system mass is given:

$$m_{sys} = \frac{n\sum \hat{F}}{gI_{sp}} + \left(8F_{out} + 4F_{in} + 4F_{center}\right)\frac{\beta g I_{sp}}{\eta} \tag{153}$$

6.6.3 Vehicle Performance Summary

The input parameters to the optimizer algorithm were

- Orbital period = 6180 sec
- Orbit radius = 7277759 m
- Sail structure areal density = 0.92 kg/m^2
- Sail vehicle aspect ratio = 1:1
- Solar energy produced per orbit must be within 5% of 1.545 x 10^9 J
- Solar cell efficiency = 15%
- Power-specific mass of PPU = β_{PPU} kg/kW
- Power-specific mass of thruster unit = β_T kg/kW
- Thruster power efficiency = η
- Thruster specific impulse = I_{sp} sec

Based on these parameters and previously discussed constraints, the optimizer was free to choose

- Thrust amplitude for eight outboard thrusters
- Thrust amplitude for four center thrusters
- Thrust amplitude for four in-plane thrusters
- Thruster firing profile (subject to pulse constraints discussed in Section 6.5.2)
- Physical size of sail array (subject to 1:1 aspect ratio requirement)

with the goal of minimizing the total vehicle mass for the given solar energy generation requirement.

Seven different thruster technologies were investigated. The resulting trajectory analyses were presented earlier in Figures 6-14 through 6-20. The corresponding propulsion system implications and overall vehicle performance are summarized in Table 6-6. A plot comparing the overall vehicle mass for the seven technologies is included as Figure 6-22.

Table 6-6: Summary of Optimizer Results for Seven Different Thruster Technologies. Data here reflect the trajectories previously presented in Figure 6-14 through Figure 6-20

	Teflon™ PPT	N_2H_4 Resistojet	N_2H_4 Arcjet	NH_3 Arcjet	H_2 Arcjet	Xe Hall	Xe Ion
I_{sp} (s)	1000	300	500	600	1000	1600	3000
β_T (kg/W)	0.12	0.002	0.0007	0.0007	0.0005	0.003	0.006
β_{PPU} (kg/W)	0.11	0.001	0.0025	0.003	0.0025	0.01	0.01
Efficiency	0.07	0.80	0.35	0.36	0.40	0.50	0.65
Number of Thrusters	16	16	16	16	16	16	16
Total Impulse per Orbit (N-s)	37.64	33.53	36.67	33.22	37.59	40.91	36.32
Number of Orbits	51030	51030	51030	51030	51030	51030	51030
Center Thrust Amplitude (mN)	3.81	7.16	7.60	9.01	7.89	10.8	10.5
Outboard Thrust Amplitude (mN)	.018	1.87	.0195	.0146	.767	.0218	.0667
In-Plane Thrust Amplitude (mN)	.452	.0488	1.00	.121	.925	.101	.210
Center Thruster Power (W)	534.5	26.3	106.6	147.2	193.6	340.4	476.9
Outboard Thruster Power (W)	2.5	6.9	0.3	0.2	18.8	0.7	3.0
In-Plane Thruster Power (W)	63.4	0.2	14.1	2.0	22.7	3.2	9.5
Fuel Mass (kg)	195.8	581.4	381.5	288.0	195.5	133.0	63.0
Inert (PPU + Thruster) Mass (kg)	554.7	0.5	1.6	2.2	3.0	17.9	31.5
Sail Mass (kg)	1616.4	1609.6	1616	1615	1616.3	1615.5	1614.1
Total Vehicle Mass (kg)	2366.9	2191.5	1999.1	1905.2	1814.9	1766.4	1708.6
Sail Edge Length (m)	41.92	41.83	41.91	41.9	41.92	41.89	41.89
Max Formation Error (m)	3.6	1.6	2.4	2.5	1.7	2.9	2.7

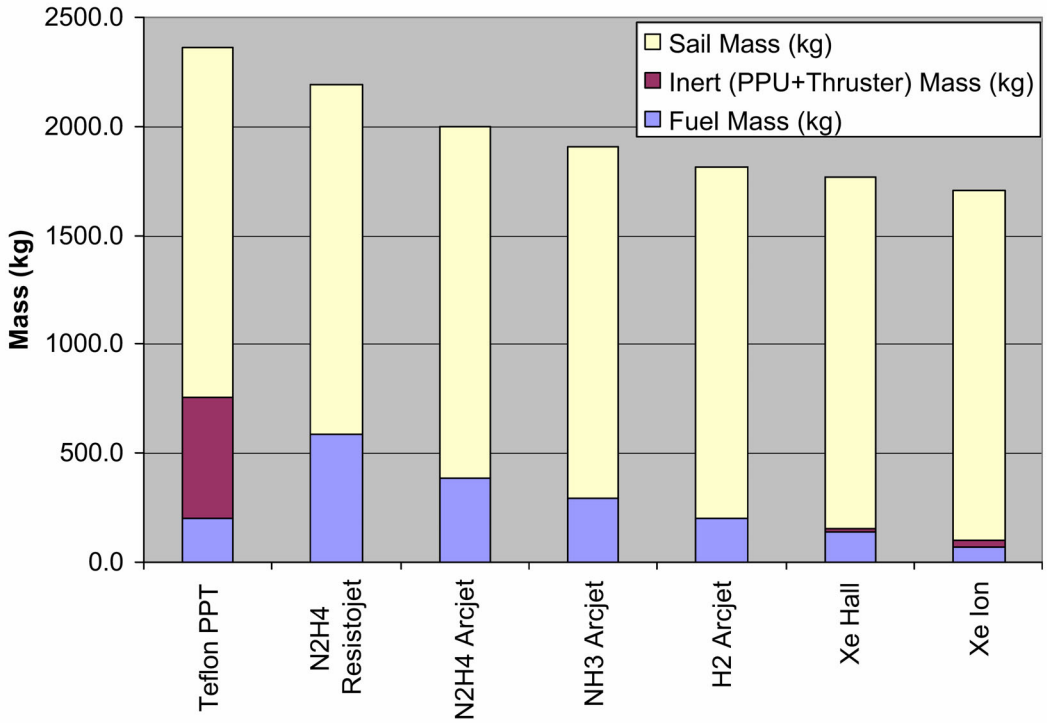

Figure 6-22: Comparison of Total Vehicle Mass for Optimized Trajectories

6.7 Closing Remarks

6.7.1 Summary

The goal of this work was to investigate practical vehicle sizing and performance requirements for a free-flying 500-kW solar array in orbital formation with a power-consuming host vehicle. To meet these requirements, the sail vehicle must employ propulsion for two functions: formation-keeping with host and ACS/Sun-pointing maneuvers. The equations of motion were developed assuming a rigid vehicle subject to gravity, aerodynamic drag, and solar pressure.

For preliminary analyses, investigators calculated the required sail size (mass), and force profiles for three pre-defined orbital trajectories: 1) minimum aerodynamic drag; 2) minimum gravity gradient torque; and 3) direct sun-pointing. In this analysis, the thrusters were assumed to have unrealistic throttleability and formation-flying constraints. The performance characteristics of a 1,000-sec-I_{sp} thruster were assumed as a candidate technology. Results indicated the best performance (lowest vehicle mass) for the direct sun-pointing trajectory, with the minimum gravity-gradient torque as the most massive vehicle. The per-orbit impulse requirements spanned 50 to 98 N-s for the three trajectories studied.

The trajectory study brought to light a design trade-space involving the overall vehicle dimensions (area) and required thruster mass. The trade-space involved balancing propulsion resources with required solar energy absorbed per-orbit. The trade is defined by competing effects concerning array sun pointing: 1) if the array normal is allowed to slip from true sun pointing then the propulsion system mass required for attitude control can be reduced; 2) if the array sun-pointing angle deviates from normal, then a larger (more massive) array area will be necessary to collect the required solar energy per-orbit. Based on the competing mass effects an optimal trajectory was pursued. The optimal trajectory depends upon thruster technology, as some thrusters will impose a greater mass expense in order to save a given amount of array area (mass) through attitude control.

Performance characteristics of real EP thrusters necessitated a different approach from the preliminary analysis. Although a generalization, it is prudent to assume that EP thrusters are not throttle-able. Thruster hardware is usually designed and optimized for a single performance point (e.g. thrust amplitude, specific impulse) or a narrow range about a fixed point. Thus, the continuously throttle-able solution from the preliminary analysis becomes a somewhat unrealistic starting point. Lessons learned from the preliminary analysis were used to estimate realistic EP thrust profiles, employing discrete thrust amplitude pulses, with the goal of achieving desired flight trajectories. It soon became apparent that the relation between the overall vehicle trajectory and the thruster pulse profile was non-intuitive.

A trajectory optimization algorithm and computer code were developed to explore the attitude control/formation-flying/thruster trade-space for realistic EP technologies. Based on defined orbit parameters, formation constraints, solar energy constraints, and thruster

limitations, the optimization routine was capable of calculating the required sail size and mass, thrust amplitude, and thruster firing profile such that the overall vehicle mass was an extremum. The vehicle was configured with eight outboard (moment-producing) thrusters, four center (no moment) thrusters, and four in-plane thrusters of the same technology, but different thrust amplitude. The tool was used to compute the trajectories and associated vehicle sizing parameters for seven canonical EP thruster technologies. The lowest vehicle mass was found to be 1708 kg for a 41.89-meter square array propelled using xenon ion thrusters in a near-sun-pointing trajectory, with the PPT being the worst performer with a vehicle mass of 2367 kg.

6.7.2 Conclusions

Although only an exploratory study, the results of this work yield the following conclusions.

- The optimized trajectory found significant propulsion mass savings over analytical design estimates. The optimization tool found a 60% savings on required per-orbit impulse for a hydrogen arcjet when compared with the 1000-s I_{sp} canonical case, reflecting an overall vehicle mass savings of 11%.
- As propulsive flexibility is made more robust, the optimization tool will exploit the added degrees-of-freedom to provide greater mass savings. The configuration documented in this report, that of 16 thrusters distributed as prescribed, likely does not represent a hard minimum vehicle mass. Adding more thrusters, more pulsing repetitions, capability to mix technologies on the same vehicle, thrust vectoring, limited throttlability, etc. are likely to provide improved mass savings.
- Propulsion savings may be possible by relaxing the formation-flying constraint. As a starting point, the work reported here constrained the sail vehicle to have zero formation error after one orbit. Trajectories calculated according to this constraint displayed a formation position error less than five meters during the orbit for all cases.
- The imposed limitation requiring identical thruster technology was overly restrictive. Examination of the optimized results indicated that the majority of the propulsive work was carried by the center thruster package, while the out-board ACS thrusters were least utilized. As such, the optimized results implied the use of unrealistic technology, such as 700-mW Hall thrusters or 500-W PPT's.
- Although not studied quantitatively, results indicate that an attractive vehicle design could consist of a Hall or ion thruster for the center package, coupled with a PPT as an out-board technology. Such a configuration may be advantageous from a vehicle deployment standpoint: the center of the sail, which will likely consist of the spacecraft bus, can house the xenon technologies and incorporate propellant storage and flow control devices, while the out-board PPT's would require only electrical connection. This would make in-space deployment of the stowed vehicle practical and avoid complicated propellant routing.

6.7.3 Suggestions for Future Work

Results of this preliminary design study naturally led to inspiration for follow-on studies. Aerophysics investigators make the following recommendations for future work.

- At the expense of computation time, an optimization tool could be modified to explore a number of different vehicle configurations with increased flexibility. Specifically, it is recommended to investigate the effects of mixed propulsion technologies on the same vehicle, limited throttleability consistent with thruster state-of-the-art, and limited thrust vectorability. It is reasonable to assume that vehicle mass reductions will arise from such studies.
- The analyses here were performed for a single canonical orbit: 900-km circular in-plane with the sun pointing vector. It is imperative to explore the behavior of different orbital regimes. For instance, as the altitude decreases the affect of atmospheric drag will become more pronounced as will the magnitude of gravity-gradient torque. The resulting optimal trajectory and propulsive needs will differ as the vehicle must counter different perturbations. Likewise, higher orbits and different inclinations will impact vehicle sizing.
- Flexible vehicle dynamics need to be incorporated into the equations of motion. Distributed mass and modal behavior will influence required per-orbit impulse as well as optimal thrust amplitudes and pulse firing history. The effects of spacecraft flexibility are not readily intuitive.

6.8 References

[1] Telephone conversation with Dr. Frank Gulczinski, AFRL Propulsion Directorate, Edwards AFB, CA, January 2001.
[2] Meink, Troy, "Powersail Program Manager," Air Force Research Laboratory, undated AFRL internal presentation, troy.meink@kirtland.af.mil, 505-846-9331.
[3] Martinez-Sanchez, M., and Pollard, J.E., "Spacecraft Electric Propulsion – An Overview," Journal of Propulsion and Power, Vol. 14, No. 5, Sept.-Oct. 1998, pp. 688-699.

AFRL-PR-ED-TR-2002-0032
Primary Distribution of this Report:

AFRL/PRSS (1 CD + 3 HC)
Dr. Frank Gulczinski
1 Ara Road
Edwards AFB CA 93524-7013

Prof. Christopher D. Hall (1 CD + 3 HC)
Virginia Polytechnic Institute & State Univ.
233 Burgess Hall
Blacksburg, VA 24061

Dr. Lyon B. King (1 CD + 5 HC)
Aerophysics, Inc.
30981 Woodbush Road
Calumet, MI 49913

Dr. Gregory Spanjers (1 CD + 3 HC)
AFRL/VSSV
3550 Aberdeen Ave SE
Kirtland AFB, NM 87117-5776

AFRL/PR Technical Library (2 CD + 1 HC)
6 Draco Drive
Edwards AFB CA 93524-7130

Chemical Propulsion Information Agency (1 CD)
Attn: Tech Lib (Dottie Becker)
10630 Little Patuxent Parkway, Suite 202
Columbia MD 21044-3200

Ranney G. Adams (1 HC)
AFRL/PROI
2 Draco Drive
Edwards AFB CA 93524-7808

Defense Technical Information Center
(1 Electronic Submission via STINT)
Attn: DTIC-ACQS (Acquisitions)
8725 John J. Kingman Road, Suite 94
Ft. Belvoir VA 22060-6218